Investigating the effects of oxygen tension and electrospun nanofibre topography on the adhesion of embryonic stem cells

Deepak Kumar

School of Postgraduate Medicine

Institute for Science and Technology in Medicine

Keele University

Thesis submitted to Keele University for the Degree of

Doctor of Philosophy

September 2013

<u>Abstract</u>

Human embryonic stem cells (hESCs) have the potential to differentiate into all cell types of the three germ layers. However, various limitations hinder their use in the clinic, including possibilities of teratoma formation, xenogenic exposure through the use of Matrigel™ and feeder layers, along with poor attachment and expansion rates and inability to transport hESCs into an *in vivo* site.

This thesis has aimed to overcome the above limitations. Electrospun nanofibrous substrates from a purely synthetic FDA approved material have been developed and investigated for the novel use in the expansion of undifferentiated hESCs. Synergistic effects between the oxygen environment and nanofibre technology were revealed which demonstrated the expansion of pluripotent hESCs in physiological normoxia (2% O_2) on these substrates, with retention of differentiation capacity. However, in hyperoxia (21% O_2), hESCs cultured on these substrates dictated embryoid body formation. A range of polymers (PCL, PLLA and PLGA) were tested (aligned and random conformations) where the optimal polymer (PCL) was further investigated at 2% O_2 at various fibre diameters to reveal its impact on hESC clonogenicity.

Exploring integrin expression levels and patterns within hESCs in 2% and 21% O_2 revealed significantly up regulated integrin's/sub-units in 2% O_2 in comparison to 21% O_2. In 2% O_2 ($\alpha V\beta 5$ and $\alpha 6$) and in 21% O_2 (CD44), specifically influenced hESC stemness and their initial attachment to Matrigel™. This data was further cross-validated by proving the adsorption of corresponding ECM proteins from MEF conditioned media to the substrates for the identified integrins/sub-units. Spectral similarities in protein adsorption

from pure proteins to conditioned media were witnessed. Critical amino acid fragments (exposed at a higher intensity) were identified on these nanofibrous substrates and thus may play a critical role for mediating hESC attachment. In conclusion, a novel substrate has been developed for the expansion of undifferentiated hESCs, which eliminates xenogenic contamination and provides a suitable carrier for transporting differentiated hESCs to a clinical setting.

Contents

List of Figures

List of Tables

Abbreviations

Ø	Diameter	**ECM**	Extracellular matrix
21% O$_2$	Physiological normoxia	**ESC**	Embryonic stem cells
2% O$_2$	Hyperoxia	**F$_C$**	Final concentration
2D	Two-dimensional	**FA**	Focal adhesion
3D	Three-dimensional	**FACS**	Flourescent Activated Cell Sorting
ALP	Alkaline phosphatase	**FAK**	Focal adhesion kinase
AP-1	Activator protein 1	**FBS**	Fetal bovine serum
bFGF	Basic fibroblastic growth factor	**FC**	Fold-change
BSA	Bovine serum albumin	**FDA**	Food and drug administration
CFUs	Colony forming units	**FESEM**	Field Emission Scanning Electron Microscopy
CHL	Chloroform	**FGF-2**	Fibroblastic growth factor-2
CM	Conditioned media	**Fn**	Fibronectin
Coll I	Collagen type I	**G**	Gauge
DCM	Dichloromethane	**GAGs**	Glycosaminoglycans
DMF	Dimethylformamide	**GAPDH**	Glyceraldehyde-3-phosphate dehydrogenase
E	Young's modulus	**GFs**	Growth factors
EBs	Embryoid bodies	**HA**	Hyaluronic acid

HIF	Hypoxia inducible factor	**PBS**	Phosphate buffer solution
hMSC	Human mesenchymal stem cells	**PC1**	Principle component 1
HSPGs	Heparin sulphate proteoglycans	**PC2**	Principle component 2
hTERT	Human telomerase reverse transcriptase	**PCA**	Principle component analysis
I_C	Initial concentration	**PCL**	Poly-ε-caprolactone
ICM	Inner cell mass	**PE-TCPS**	Oxygen plasma etched tissue culture polystyrene
IMS	Industrial methylated spirit	**PFA**	Paraformaldehyde
ILK	Interleukin kinase	**PLGA**	Poly-lactide-co-glycolic acid
IPA	isopropyl alcohol	**PLLA**	Poly-L-lactic acid
KO-SR	Knock-out serum replacement	**PS**	Penicillin and streptomycin
kV	Voltage	**RNA**	Ribonucleic acid
L-Glut	L-glutamine	**RT-PCR**	Reverse Transcriptase-polymer chain reaction
LIF	Leukemia inhibitory factor	**TA-EDTA**	Tris Acetate-Ethylenediaminetetraacetic acid
Ln	Laminin	**TCP**	Tissue culture plastic
MAPK	Mitogen-activated protein kinase	**Tof-SIMS**	Time of flight secondary ion mass spectrometry
MEFs	Mouse embryonic fibroblasts	**UV**	Ultra-violet
NEAA	Non-essential amino acid	**Vn**	Vitronectin

Publications and Presentations

Patents

<u>Kumar D</u>, Yang Y and Forsyth NR. Stem Cell Culture Method: UK Patent # GB1214704.7; filed August 2012.

Kumar D, Yang Y and Forsyth NR. Stem Cell Culture Method: US Patent # US13/800325; filed March 2013.

Associated research publications

<u>Kumar D</u>, Wimpenny I, Dale T, Yang Y and Forsyth NR. Self-Renewal of Human Embryonic Stem Cells using Nanofibres as Non-Biological Supports. (Submitted)

<u>Kumar D</u>, Gupta S, Yang Y and Forsyth NR. $\alpha V\beta 5$, $\alpha 6$ and CD44 are Oxygen-Regulated Human Embryonic Stem Cell Attachment Factors. (Submitted)

<u>Kumar D</u>, Roach P, Forsyth NR and Yang Y. Study of Adsorbed Proteins on Nanofibrous Substrates. (In Preparation)

Non-associated research publications

Pijanka JK, <u>Kumar D</u>, Dale T, Yousef I, Parkes G, Untereiner V, Yang Y, Dumas P, Collins D, Manfait M, Sockalingum GD, Forsyth NR and Sule-Suso J. Vibrational Spectroscopy Differentiates between Multipotent and Pluripotent Stem Cells. Analyst (2010), 135: 3126-3132.

<u>Kumar D</u>, Gittings JP, Turner IG, Bowen CR, Bastida-Hidalgo A and Cartmell SH. Polarization of Hydroxyapatite: Influence on Osteoblast Cell Proliferation. Acta Biomaterialia (2009), 6: 1549-1554.

Fouriki A, <u>Kumar D</u>, Forsyth NR and Dobson J. Nanomagnetic Gene Transfection for Non-Viral Gene Delivery in Human Embryonic Stem Cells. (Accepted; Gene Therapy).

<u>Kumar D</u>, Rutter AV, Pijanka JK, Sandt C, Cinque G, Dumas P, Yang Y, Forsyth NR and Sule-Suso J. Lipids as a Potential Human Embryonic Stem Cell Biomarker for Cell Differentiation. (In Preparation)

Akram KM, <u>Kumar D</u>, Spiteri MA and Forsyth NR. Expansion of Bone Marrow Derived Mesenchymal Stem Cells in Hypoxia Enhances their Differentiation when Cultured in Normoxia. (In Preparation).

Published poster presentations

<u>Kumar D</u>, Roach P, Forsyth NR and Yang Y. Study of Adsorbed Proteins to Nanofibrous Substrates. TERMIS World Congress, Vienna (September 2012).

<u>Kumar D</u>, Gupta S, Yang Y and Forsyth NR. αVβ5, α6 and CD44 are Oxygen-Regulated Human Embryonic Stem Cell Attachment Factors. BIRAX Conference Israel (2011)

<u>Kumar D</u>, Gupta S, Yang Y and Forsyth NR. Integrin Expression and Reliance are Oxygen Concentration Dependant in Human Embryonic Stem Cells. European Cells and Materials (TCES Leeds, 2011), 22 (3): 31.

<u>Kumar D</u>, Wilson SL, Forsyth NR and Yang Y. Investigating the Relationship between Surface Properties of Polymers and Protein Adsorption. European Cells and Materials (TCES Manchester, 2011), 22 (2): 60.

<u>Kumar D</u>, Gupta, Wilson SL, Forsyth NR and Yang Y. Investigating the Relationship between Surface Topography of Polymers and Protein Adsorption. (ExperTissues, Portugal; 2010)

Conference Oral Presentations

<u>Kumar D</u>, Forsyth NR and Yang L. Intervertebral Disc Tissue Engineering through Design of Injectable Scaffolds and Physiologically Informed Bioreactors. TERMIS World Congress, Vienna (September 2012).

Acknowledgements

*Thank you to His Holiness "**Shri Ashutosh Maharaaj**", for his blessings*

"Dedicated to my granddad Late Mohinder Pal"

A deep hearted thank you to both of my supervisors without whom this thesis would not have been possible. I feel very lucky to have had a supervisor like Dr Nick Forsyth who has guided me constantly throughout my PhD, pushed me too boundaries which I never thought I could reach and for constantly giving me the drive to push myself to the extremes. I feel like I have learned so much from you; skills which will "no doubt" be useful for the rest of my career. Also, a thank you to Dr Ying Yang for her useful contributions and lifting my spirits up during the low points. The classic phrase of "I believe this should happen" always managed to convince me that an experiment must work and it was "my bad" for not making it happen. Ying you have truly challenged my stamina and patience. I would also like to thank Dr Paul Roach for a collaboration that has resulted in valuable data. More importantly, for his unlimited availability, support and encouragement when I needed to "hang tough". Paul, you have a massive heart and will always value your support and good nature. A big "gracias" to Dr Josep Sule-Suso who has been a great character; I always enjoy having our awesome "non-work related convo's" and looking at your holiday photo's with a cuppa!!

Just as importantly, I would like to thank the greatest parents in the world. This thesis and achievement is dedicated to you. I will always appreciate and never forget the sacrifice, continuous support (in everything and anything I can possibly think of, and more), encouragement and the pillar of strength that you have been for more. You have definitely raised the bar for being amazing parents – which I feel I will never be able to achieve.

Mum-Star, your constant words of "you can always do better", comparisons to others and constantly challenging me, have all no doubt contributed to achieving this thesis. Thanks Supz for taking care of everything whilst I have been trying to get through this; knowing that you had everything under control back home gave me the peace of mind to carry on. Thanks for your sacrifice; part of this achievement is defo down to you (*hurry up and become a Lyer…. I mean a Lawyer*). Thanks Raj (aka Pinky) for your contributions; you may be bigger than me, but I defo have the bigger brains, Boom!! Also thank you to Ashok (Godfather, *you defo have swagger like a Godfather, which I still need to work on, classy!!*), Asha, Rakesh, Ravi (*Beast in body and mind*) and Ramma, who have all made priceless contributions.

Good work by the BRO-TEAM. Firstly Sid (*Soul bro who's a pro*), Meeta and Calvin "Klein". Am privileged to have the most amazing mate and bro in the world. An abso legend who ticks all the boxes that I have ever wanted in a bro. "Bro's 4 life" is a solid statement. Thanks W*h*omps, nice 1 blud for your priceless help, support and words of wisdom when the going got tough. You have contributed in helping me power through this bizzle ("*wiggle wiggle wiggle, yeah*"). Thanks to all the other boys in the team, Jizzatastic Jazz, DJ Shayan, Mo-Star, Manu, Jamie (Dodga), Shiraz, Indi and Si. Nights out have always been "memories", no matter what life has thrown at us……….Brrraaapppppp!!!

A special thanks to the Cypriat Villager-Hari; I don't have the words to thank you enough for everything that you have done for me over the last few years – you have a massive heart. You are a total pillar of strength and a legend. A big hug to Sammy (aka Blonde Kutti) and Angeliki, we have truly powered through stuff as a team, lifting each other up through high's and lows. Nice work Sammy with the random raving in labs, courtesy of

"High achievement always takes place in the framework of high expectation"

Chapter 1

1. Introduction

1.1 Overview of Stem Cells

Currently there is high interest and research into the unspecialised cells known as stem cells for use in tissue engineering and regenerative medicine applications. These cells can be used individually by injecting them into defect (injury) sites or can be incorporated into tissue engineering strategies and constructs to repair or regenerate tissue *in vitro* or *in vivo* [Finkemeier, 2002].

A stem cell has three important properties;

- **Self-renewal**: via symmetrical division (where a parental cell divides to give two daughter cells that retain the potentiality of its parental cell known as mitosis; this increases the pool of stem cells), or by asymmetric division (whereby a stem cell divides to give one daughter cell that retains its stem cell properties and another daughter cell which commits to a differentiation lineage by becoming a progenitor cell) [Howell and Yoder, 2003; Trounson, 2006; Wagers and Weissman, 2004].

- **Differentiation capacity**: the ability to differentiate into a specialised mature cell type. Stem cells can be further classified depending on their differentiation capacity in terms of the various specialised cells/tissues/organs that they can form and can be termed as either totipotent, pluripotent or multipotent (for definitions, see Table 1.1) [Howell and Yoder, 2003].

- ***In vivo* reconstitution of a given tissue:** Stem cells should able to divide symmetrically to maintain a population of stem cells and differentiate into the cells required to generate the tissue in which they are situated [Howell and Yoder, 2003].

Chapter 1

The stem cell niche plays an important part in maintaining the undifferentiated state of a stem cell and can be defined as the 3D microenvironment which controls gene expression and the properties of stem cells through signalling molecules, inter-cellular contact and stem cell- extracellular matrix (ECM) interactions. The ECM is the chemical and mechanical structure required for development and for responses to (patho)-physiological signals. Stiffness and composition of the ECM considerably influence cell behaviour [Kruegel and Miosge, 2010]. Cells are sensitive to applied mechanical forces as well as the mechanical properties of its environment such as elasticity which is directly affected by the composition of ECM (as structural proteins such as collagen provide strength to tissues, whereas elastin and proteoglycans provide matrix resiliency). Substrate stiffness strongly influences several factors such as how strongly cells can adhere to a substrate, the amount of force they can exert, the degree of spreading, the rate of proliferation (which has known to be faster on stiffer substrates compared to softer ones), and cell differentiation. For example; stiffer substrates have demonstrated to induce differentiation of hMSCs towards myocytes and osteoblasts whereas softer substrates induced their differentiation to neurons [Engler *et al.*, 2006]. On softer substrates, hESCs enhanced their attachment and proliferation rate whereas stiffer substrates induced their differentiation towards an osteogenic lineage [Evans *et al.*, 2009].

Furthermore, the stem cell niche also influences "stem cell plasticity/stem cell fate" (flexibility to differentiate into mature cell types giving rise to cell types of the certain microenvironments in which they have been placed) and exerts restrictions on its differentiation capabilities [Bajada *et al.*, 2008b].

Chapter 1

Table 1.1 Stem cells with varying potency and the locations where they can be found [Wagers and Weissman, 2004]

Level of Potency	Definition	Example of Source
Totipotent	Able to give rise to all embryonic and extra-embryonic cell types	Zygote (Oocyte)
Pluripotent	Able to differentiate into all cell types of the embryo apart from placental cells	Inner cell mass (ICM) of a blastocyst
Multipotent	Ability to differentiate into a few specialised cell lineages	Marrow Stroma

1.1.1 Different Types of Stem Cells

Stem cells can be broadly classified into two types; embryonic stem cells (ESCs) and adult stem cells (ASCs). ESCs are pluripotent which enables them to give rise to all specialised, mature cell types of the three somatic germ layers (Ectoderm, Endoderm and Mesoderm) but not the extraembryonic tissues. ASCs are traditionally considered to be multipotent and have less plasticity in comparison to ESCs. However, this dogma has recently been questioned where current literature states that ASCs may actually have a greater plasticity than originally thought. It has been demonstrated that ASCs are able to differentiate into other cell types rather than the tissue from which it originates from, in response to its surrounding microenvironment [Bajada *et al.*, 2008a]. For example, neural stem cells which traditionally were thought to only differentiate into various nerve cells in the adult brain, have now also been shown to differentiate into hematopoietic cells [Lakshmipathy and Verfaillie, 2005]. Another example includes, human neuronal stem cells co-cultured with muscle cells resulting in neuronal stem cell differentiation into skeletal muscle [Galli *et al.*, 2000]. Bone marrow stromal cells have been demonstrated differentiation towards lung, liver and gut tissues [Jiang *et al.*, 2002]. Possibility of greater plasticity of ASCs has triggered a keen interest by stem cell biologists due to their great therapeutic potential.

Chapter 1

Various types of ASCs exist including: Amniotic-fluid derived stem cells (AFDSCs), umbilical cord derived stem cells (UCDSCs; derived from the cord lining or cord blood), fat-derived stem cells and bone marrow derived mesenchymal stem cells (BM-MSCs). Their characteristics and properties are described briefly in Table 1.2.

Table 1.2 Different sources for attaining ASCs and their plasticity

Different types of ASCs	Location	Differentiation Capacity
Tissue -specific stem cells	Within specific tissues and organs such as adipose	Able to differentiate into the mature cell type of the tissue/organ it is located within. Eg. Cardiac stem cells support myocardial regeneration [Beltrami *et al.*, 2003] and limbal stem cells support cornea regeneration [Dua and Azuara-Blanco, 2000].
Haematopoietic stem cells	Bone marrow	Able to differentiate into all lineages of mature blood cell types and blood components [Spangrude *et al.*, 1988].
Amniotic fluid derived stem cells	Amniotic fluid	Multipotent stem cells which also express some ESC markers. Demonstrated differentiation towards functional cells of each of the three embryonic germ layers [De Coppi *et al.*, 2007].
Umbilical cord/placental tissue derived syem cells	Umbilical cord	Source for both pluripotent stem cells (from umbilical cord blood) [Kogler *et al.*, 2005] and mulitpotent stem cells (umbilical cord matrix) [Mitchell *et al.*, 2003].
Adipose-derived stem cells	Fat tissue	Ability to differentiate into chondrocytes [Erickson *et al.*, 2002], osteocytes [Halvorsen *et al.*, 2001], adipocytes, hepatocytes [Seo *et al.*, 2005] and neurogenic lineages [Safford *et al.*, 2002].
Mesenchymal stem cells	Bone Marrow	Mesenchymal lineages including; skeletal muscle, bone, cartilage, tendon, fat [Pittenger *et al.*, 1999].

Chapter 1

ASCs with typical multipotent characteristics include; haematopoietic stem cells (HSCs; able to differentiate to give rise to all mature blood cell types including vessels) and mesenchymal stem cells (MSCs) [Trounson, 2006]. MSCs can be sourced from the bone marrow and extracted via the iliac crest, for instance. Within bone marrow stromal cells; a subpopulation of approximately $0.001 - 0.01\%$ are multipotent MSCs (first isolated by Friedenstein and collegaues in the 1960s) [Friedenstein *et al.*, 1987].

hMSCs can be separated from the rest of the bone marrow which contains HSCs and non-adherent cells by their adherent properties . During *in vitro* culture, hMSCs expand with a fibroblastic-like morphology and demonstrate the ability to produce colony forming units (CFU), which are a typical feature of undifferentiated stem cell expansion. The surface antigen expression profile of hMSCs include; SH2, SH3, $CD29^+$, $CD44^+$, $CD71^+$, $CD90^+$, $CD106^+$, $CD120a^+$, $CD124^+$, STRO-1^+, VCAM-1^+, $CD14^-$, $CD34^-$ and $CD45^-$ [Pittenger *et al.*, 1999; Young and Black, 2004].

hMSCs are also immune-privileged [Rose and Oreffo, 2002] demonstrated by their ability to inhibit critical immune effector cells such as $CD4^+$, $CD8^+$, NK cells, B cells and monocytes during culture in combination with transforming growth factor (TGF-β), hepatocyte-growth factor (HGF), prostaglandin (PG)E_2 and interferon-gamma (IFN-γ) [Krampera *et al.*, 2006].

Chapter 1

1.2 Human Embryonic Stem Cells

1.2.1 Derivation & Isolation of Embryonic Stem Cells

When the male gamete (sperm cell) fertilises the female gamete (ovum) this produces a diploid zygote cell, which is the earliest developmental stage of the embryo. At this stage and up to the eight-cell stage of the morula it is possible to produce an entire organism including the placenta as the cells are totipotent and thus can differentiate into any cell type. After this stage, ongoing development results in the formation of a pre-implantation blastocyst; comprised of an outer layer of trophoblast cells and an inner cell mass (ICM) of undifferentiated cells from which ESCs are isolated between day 3-5. Characteristics of cells from ICM explants plated out onto tissue culture plastic (TCP) and cultured *in vitro* have a rounded morphology and expand as tightly packed adherent colonies [Thomson *et al.*, 1998].
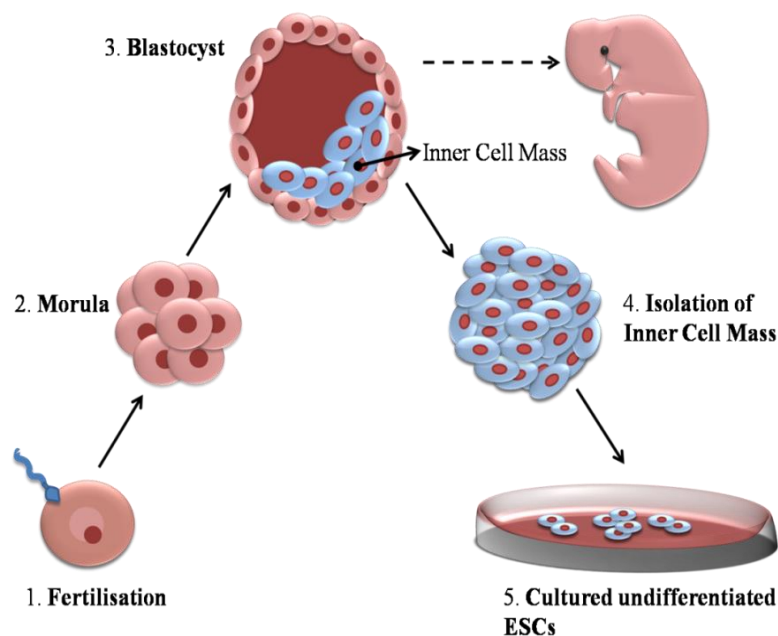
Figure 1.1 Process involved in the derivation and isolation of pluripotent ESCs from the inner cell mass (ICM) of a blastocyst. Adapted from Wobus *et al.*, 2005.

Chapter 1

The ability to isolate and culture undifferentiated hESCs *in vitro*, is a recent development and the key milestones associated with ESC culture development are summarised in Figure 1.2. However, several ethical concerns still surround the use of ESCs where several countries do not permit embryo research (Austria, Denmark, Poland, Slovakia, Malta and France where as some countries permit embryo research under specific legislation (Finland, Belgium, Spain and UK).

Chapter 1

1981
The isolation of pluripotent mouse ES lines from blastocysts using both feeder layers (MEFs; Axelrod et al., 1984) and embryonic carcinoma cell conditioned media. These cells were shown to maintain a normal karyotype.

2001:
An establishment of approximately 70 hESC lines using MEFs as feeder layers.

2004:
22 cell lines listed in the NIH register propagated in vitro

1967-1970
Established embryonic cell lines were first derived from mouse teratocarcinoma's

(Gearhart and Mintz., 1974)

1998:
First successful isolation of human embryonic stem cells from the inner cell mass (ICM) of a blastocyst using MEFs as a feeder layer (Thomson et al., 1998).

2001:
Use of Matrigel™ in hESC culture (Xu et al., 2001)

2005:
Use of serum-free media in parallel with Matrigel™ for hESC culture. (Xu et al., 2005)

Figure 1.2 Timeline illustrating the essential milestones during embryonic stem cell culture development [Axelrod, 1984; Thomson *et al.*, 1998; Gearhart and Mintz., 1974; Xu *et al.*, 2001; Xu *et al.*, 2005].

Chapter 1

1.2.2 Embryonic Stem Cell Characteristics

ESCs display unlimited self-renew and are immortal *in vitro.* This is attributed to ESCs having high telomerase activity (a ribonucleoprotein enzyme which maintains telomere length by adding repeats to chromosome ends), providing long-term proliferative potential [Thomson *et al.*, 1998] and preventing senescence, which usually occurs during tissue culture after a population doubling between 50-80 [Odorico *et al.*, 2001]. During expansion *in vitro*, ESCs have a high nucleus to cytoplasmic ratio with prominent nucleoli [Thomson *et al.*, 1998]. Furthermore, as pluripotent hESCs proliferate (population doubling time of 36 hours) [Amit *et al.*, 2000], they form flat, compact colonies that are tightly adherent (more so in hESCs, relative to mouse embryonic stem cells; mESCs), whereas differentiated ESCs aggregate together in suspension to form embryoid bodies (EBs) *in vitro* or teratoma's *in vivo*, resulting in tumorigenicity [Thomson *et al.*, 1998].

1.2.2.1 Plasticity of Embryonic Stem Cells

ESCs are pluripotent with the potential to differentiate into all mature cell types of the 3 somatic germ layers; endoderm, ectoderm and mesoderm (Figure 1.3), including the male and female germ cells [Thomson *et al.*, 1998] with the exception of placental cells *in vitro.* Therefore, the use of ESCs have great potential for a wide range of therapeutic applications as they provide an unlimited source of several different cell types for tissue replacement and regeneration [Xu *et al.*, 2001]. Certain growth factors can direct the differentiation of hESCs into specific germ layers; for example endoderm lineages can be stimulated using hepatocyte growth factor, mesoderm lineages can be encouraged using BMP-4 and TGF-β and ectoderm lineages using nerve growth factor and retinoic acid [Trounson, 2006].

Chapter 1

During embryo development ESCs within the ICM of a blastocyst spontaneously differentiate and give rise to the entire organism. Theoretically, isolated ESCs should have the same plasticity *in vitro*; however establishing supportive chemical cues and environment is crucial in directing their differentiation to become functional, specialised cell types. Examples of *in vitro* differentiation of hESCs include; oligodendrocytes, (induced using bFGF, epidermal GF and retinoic acid, [Nistor *et al.*, 2005], the haematopoietic lineage (using a cocktail of haematopoietic cytokines SCF, Flt3L, IL-3, IL-6, G-CSF and BMP-4 [Chadwick *et al.*, 2003]), cardiomyocytes (when co-cultured with mouse visceral endoderm gave rise to beating heart muscle colonies that expressed cardiomyocyte markers, α-myosin heavy chain and cardiac troponins) and hepatocytes (which expressed markers, albumin, α-1-anti-trypsin and cytokeratin 8 and 18) [Mummery *et al.*, 2003]. Examples of *in vitro* hESC differentiation into mesodermal lineages include: chondrogenesis (confirmed by expression of proteoglycans, Col2a1, Sox9 and Col10a1) [Koay *et al.*, 2007], osteogenesis (confirmed by expression of osteoblastic markers; alkaline phosphatase, osteocalcin and collagen type II) [Karner *et al.*, 2007] and adipogenesis (confirmed by expression of Adiponectin, Leptin, Adipophilin and Perilipin) [Olivier *et al.*, 2006]. hESCs were cultured in relevant chemical media for each of the lineages.
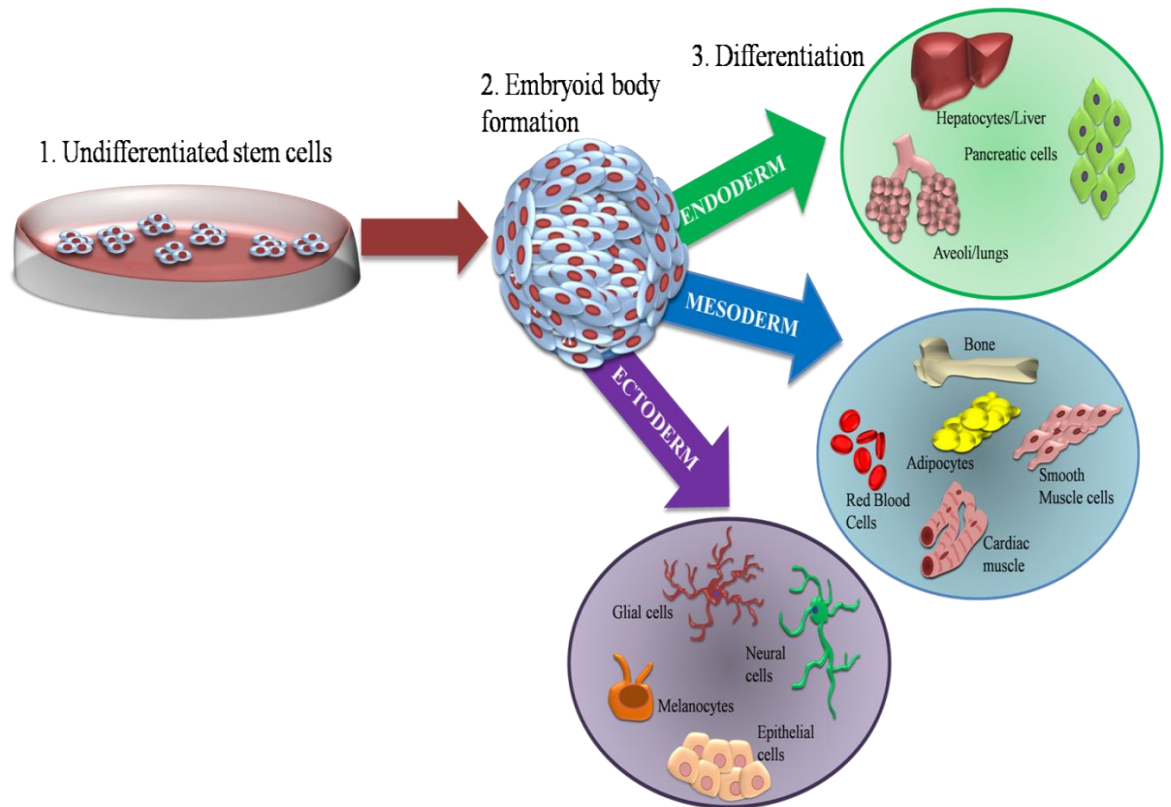
Figure 1.3 *In vitro* differentiation capacity of ESCs into specialised cell types of the three somatic germ layers; Ectoderm, Endoderm and Mesoderm.

1.2.2.2 Embryonic Stem Cell Molecular Markers

Surface antigens which are frequently employed to determine hESC 'stemness' include stage specific embryonic surface antigens (SSEA)-3, SSEA-4 and high molecular weight glycoproteins TRA-1-60 and TRA-1-81. However, mESCs express SSEA-1 (hESCs do not) and not the SSEA-3/SSEA-4 antigens and also require leukemia inhibitory factor (LIF; a soluble glycoprotein belonging to the interleukin-6 family of cytokines that activates the gp130 signalling pathway) in their media during pluripotent proliferation. High alkaline phosphatase activity is also demonstrated by hESCs as well as the expression of the transcriptional factors; Oct 3/4 (POU5-F1), Nanog and SOX-2 [Thomson *et al.*, 1998].

Chapter 1

1.2.3 In Vitro Culture Methods

Current techniques for culturing pluripotent hESCs *in vitro* can involve either direct or indirect feeder layer methods. However the underlying mechanisms which support their proliferation in an undifferentiated state remain largely unresolved.

1.2.3.1 Feeder Method

The feeder method involves the co-culture of hESCs with a layer of mitotically inactivated mouse embryonic fibroblasts (MEFs). Recent modifications to this include the use of alternative feeder layers such as; human embryonic fibroblasts, adult Fallopian tube epithelium [Richards *et al.*, 2002] or human foreskin fibroblasts (with the ability to expand up to 42 passages) [Amit *et al.*, 2003], human muscle or skin and postnatal mitotically inactivated human bone marrow stromal cells [Conley *et al.*, 2004]. All of which claim to support the expansion of undifferentiated hESCs with retained morphology and expression of pluripotent hESC markers [Conley *et al.*, 2004].

1.2.3.2 Feeder-Free Method

The feeder-free method uses pre hESC-conditioned media from MEFs (where cytokines and other growth factors are secreted) and is further supplemented with basic fibroblastic growth factor (bFGF; known to enhance cloning efficiency during hESC expansion *in vitro*) [Odorico *et al.*, 2001], in combination with a biological substrate such as Matrigel^{TM} [Thomson *et al.*, 1998; Xu *et al.*, 2001]. This method supported the expansion of undifferentiated hESCs *in vitro* for up to 130 population doublings [Xu *et al.*, 2001] with karyotype and phenotype characteristic retention and gave rise to more tightly packed colonies in comparison to MEF feeder layers.

Chapter 1

Matrigel^{TM} is a commercially available, loosely defined gel, sourced from Engelbreth-Holm-Swarm tumours. Matrigel^{TM} is comprised of extracellular matrix (ECM) proteins including; laminen-111, collagen IV, heparin sulphate proteoglycans, entactin/nidogen, fibronectin, growth factors, matrix-degrading enzymes and their inhibitors; and other proteins yet to be defined [Meng *et al.*, 2010; Xu *et al.*, 2001]. Matrigel^{TM} functions to artificially mimic the ESC ECM niche environment and provides the required chemical cues during for the expansion of hESCs in a pluripotent state, whilst inhibiting differentiation. Recent improvements related to this method have included eliminating animal based serum and replacing it with Knock-out™ serum replacement; whose components are kept confidential but is known to contain better-defined growth supplements [Price *et al.*, 1998]. Further developments to completely eliminate any xenogenic contaminations have included designing a medium which is totally serum and xeno–free; TeSR contains bFGF, TGF β1, Human Insulin, Human Holo-Transferrin, Human Serum Albumin and Glutathione in DMEM/F12 and retain the undifferentiated state of hESCs when used in combination with Matrigel™ [Ludwig *et al.*, 2006]. Despite various recent modifications to enhance hESC scale-up *in vitro* whilst retaining their pluripotency, feeder layers (MEFs) and Matrigel™ still provides the best performance and are the conventional methods for hESC expansion [Fadeev and Melkoumian, 2011].

Other limitations associated with the current technique of culturing hESCs using Matrigel^{TM} include; batch to batch variability of MEFs, xenogenic contamination and expression of foreign oligosaccharide residues, and issues associated with scale-up [Meng *et al.*, 2010]. Feeder layers also carry the risk of retroviral infections [Braam *et al.*, 2008; Martin *et al.*, 2005]. Sialic acid (Neu5Gc) has been identified on the surface of hESCs; this

Chapter 1

molecule is not of human origin and therefore may potentially elicit an immune response during transplantation. Originally it had been speculated that the Neu5Gc molecule was derived from MEFs but now its origin appears to have been from serum replacement [Mallon *et al.*, 2006].

The underlying mechanisms associated with Matrigel™ which support the attachment and undifferentiated expansion of hESCs are yet to be fully defined. Investigating these pathways would be important to help in understanding the associated pathways and proteins and perhaps mimic this phenomenon by using novel substrates that would eliminate the use of xenogenic materials and increase the efficiency of hESC numbers during routine culture.

Chapter 1

1.3 Integrins

1.3.1 Structure and Function

Integrins are heterodimeric, transmembrane glycoproteins situated in the plasma membrane of a cell. There are 18 α-subunits and 8 β-subunits, which are able to construct 24 distinct heterodimer arrangements. An individual receptor is a combination of an α-subunit and a β-subunit (non-covalently linked) and each unique integrin heterodimer is able to recognise and connect to a specific ECM ligand and determines subsequent signal transduction [Gao *et al.*, 2010; Humphries *et al.*, 2006; Hynes, 2002; Wiesner *et al.*, 2005; Wong and Bernstein, 2010]. For example; the β_1 subunit is able to form heterodimers with at least 12 distinct α chains and these integrins have been identified on cells derived from all three somatic germ layers. The β subunits can be further classified into three sub-categories which are β_1, β_2 and β_3 sub-units; however it is the β_1 sub-units in combination with a variety of interacting proteins (such as Talin and α-actinin) which primarily mediate the connection between the cytoplasm of a cell and its ECM. β-tails are also vital in promoting subcellular localisation, the activation of signalling pathways and more importantly in regulating the affinity of integrins towards ECM-ligands. Integrin function is further strengthened by the α-subunits which support integrin regulation [Liu *et al.*, 2000; Meng *et al.*, 2010].

A large section of the integrin sub-units are situated in the ECM region and are globular in shape, whereas the cytoplasmic domains are shorter and in the shape of a tail. The β sub-unit tails act to transduce signals to the cell [Wiesner *et al.*, 2005]. During the change from an "inactive state" to an "active state" of an integrin, conformational changes occur upon binding of the integrin to its corresponding ECM ligand; these conformational changes are

Chapter 1

largely regulated by the intramolecular interaction between α and β cytoplasmic domains [Schwartz, 2001]. Basically in a low affinity state, the tail of an integrin is in a closed form and the ECM section is bent; upon activation the integrins have a high affinity for their corresponding ligand and is characterised by a dissociated tail and erect ECM region (Figure 1.4) [Hynes, 2002].
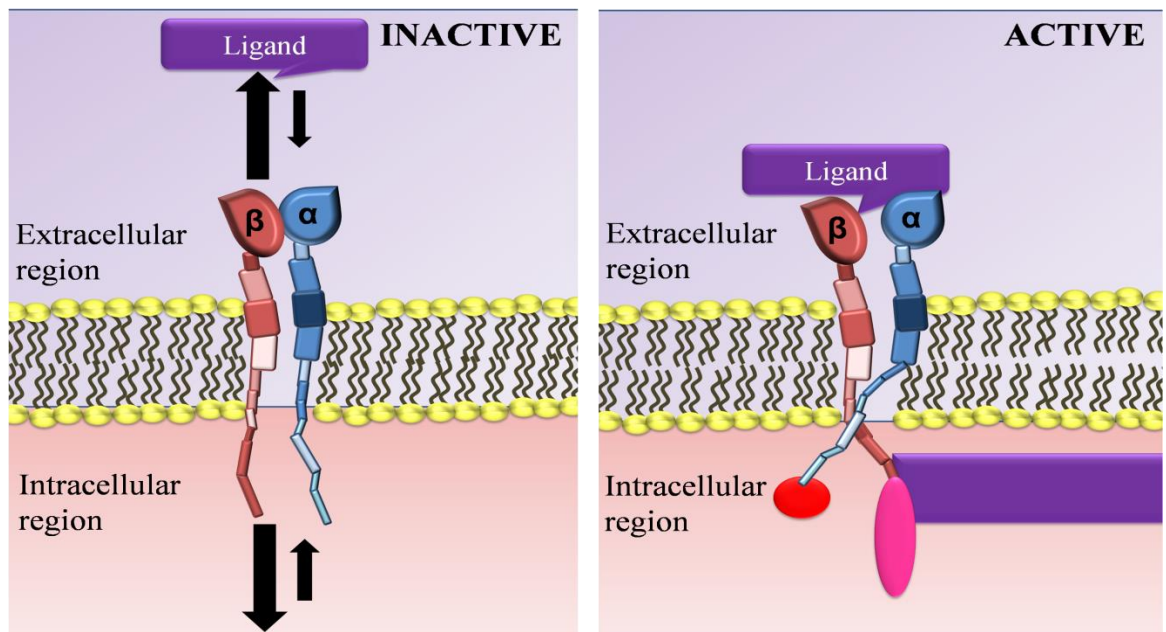
Figure 1.4 Structure of an integrin, demonstrating both α and β sub-units during an "inactive" and "active" state. Adapted from Humphries *et al*., 2006.

The primary biological function of integrins is to provide a mechanically sound interaction between the cell and its surrounding ECM by specifically binding to basement membrane proteins [Wiesner *et al.*, 2005]. Other integrin functions include; facilitating cell-cell and cell-ECM interaction and aiding in various cell activities. These include: the initial settlement of cells to their niche, mediating bidirectional signalling and exchange of vital information between the cells' cytoskeleton and its surrounding ECM effectively, retaining

Chapter 1

the cell-niche environment (regulation of matrix secretion and degradation) and also the advancement in the architecture of the cell-niche [Ellis and Tanentzapf, 2010]. As a result, integrins are able to detect physical and chemical changes in the ECM and transmit external environmental signals to intracellular regions of the cell or vice versa, triggering a cascade of intracellular pathways impacting cell motility, behaviour, morphology, proliferation and differentiation. However, binding of integrins to soluble ECM ligands or their overexpression can also have a negative effect resulting in the inhibition of proliferation leading to apoptosis [Wiesner *et al.*, 2005].

In some cases, deactivation of integrins is also important; particularly during mitosis where a cell needs to lose its adhesiveness to divide and also during cell migration where integrins within cells require deactivation in areas where they have already adhered and be activated in sites where adhesion needs to take place to permit cell movement within an ECM environment.

1.3.2 Bidirectional Signalling and Signalling Pathways

Bidirectional signalling of integrins permits "inside-out" and "outside-in" signalling within cells. "Inside-out" signalling are the signalling mechanisms which regulate components related to integrin-ECM ligand binding activities and encourage adhesion [Coppolino and Dedhar, 2000]. Integrin activity is affected by two main mechanisms; changes in avidity and changes in affinity. Changes in avidity (multiple integrin interactions resulting in combined strength) is associated with the re-arrangement of integrins across the plasma membrane. When integrins group together they form a cluster known as focal adhesion points resulting in an attraction of matrix adhesion proteins towards these integrin clusters

and providing a strong connection between the cell and ECM ligand sites. Several clusters can result in multiple interactions with ECM ligands as well as permitting rebinding activities [Coppolino and Dedhar, 2000]. However, ECM proteins are also dynamic and are constantly changing resulting in changes in integrin activity. Phosphorylation (addition of PO_4^{3-} to a protein), GTP-GDP and phospholipid metabolism are all known to also enhance integrin avidity. Changes in affinity are also known to have an impact on integrin activity. During its "inactive form", integrins are expressed on the cell surface; they have a low binding efficiency to their corresponding ligands as they are in a low affinity state. The activation of an integrin to a "high affinity state" is attributed to intracellular signals and agonists within the cell which require energy and result in the conformational change of an integrin within the cytoplasmic region through to the extracellular protein binding region allowing the receptor to bind to its corresponding protein.

"Outside-in" signalling is crucial in determining cell fate/survival; the absence of appropriate integrin-ECM interaction results in cell apoptosis (programmed cell death) in adherent cell types. Furthermore, "outside in" signalling of integrins allows the transduction of signals which stimulate cytoskeletal re-organisation and expression of specific genes [Liu *et al.*, 2000]. Soluble factors and ECM proteins situated within the ECM transduce biochemical signals to the cells via integrins which influence cellular processes such as promotion of cell proliferation and inhibition of cell apoptosis as well as activation of a number of growth factor pathways such as Platelet derived growth factor (PDGF; [Sundberg and Rubin, 1996]), Vascular endothelial growth factor (VEGF; [Wang *et al.*, 2006]) and Epidermal growth factor (EGF; [Moro *et al.*, 1998]). Self-phosphorylation of growth factors can also lead to a cascade of signalling events resulting in an alternative route to integrin activation. Intracellular biochemical signals activated as a

Chapter 1

result of integrin activation are known to cause elevation of intracellular calcium, activation of the N_α/H anti-porter, phosphorylation of cytoplasmic proteins, accumulation of GTP-bound $P21^{ras}$ and phosphoinositide 3-OH kinase. This further triggers a network of signalling pathways essentially through the MAPK (Mitogen-activated protein kinase) pathway involving the Cyclins, Cyclin-Dependent Kinases and cell cycle inhibitors which regulate cell cycle progression and encourage cell adhesion. Cell survival has also been demonstrated to be influenced by a key molecule (bcl-2) whose expression is upregulated through integrin $\alpha5\beta1$ (fibronectin receptor) signalling; this protein interacts with BAX (promotes cell apoptosis) and the ratio between these two molecules is crucial in determining cell-survival [Coppolino and Dedhar, 2000; Zhang *et al.*, 1995].

1.3.3 Integrin-related Proteins

The exact mechanisms associated with the transduction of information from cytoplasmic integrin regions to intracellular molecules are yet to be fully defined. However, two other types of proteins identified within the membrane-region forming direct contacts with integrins are; integrin associated protein (IAP; CD47, a member of the immunoglobulin superfamily) (with a size of 46kDa) is known to be an important factor for regulating calcium influx in endothelial cells during $\alpha V\beta3$ attachment to fibronectin or vitronectin. The other types of proteins are CD9, CD63 and CD81 (which belong to the transmembrane-4 superfamily); these have also shown to have an effect on intracellular calcium and have been suggested to function as ion channels [Schwartz, 2001].

Important intracellular proteins essential for integrin function include interacting adaptor (also referred as effector) proteins. Integrins lack enzymatic activity and it is therefore

essential for integrins to associate with these proteins to activate and transmit a signal, in either direction [Liu *et al.*, 2000]. Specifically, the cytoplasmic region of the integrin binds directly to the cytoskeletal associated adaptor proteins and completes the physical connection pathway which ultimately targets the actin cytoskeleton region of a cell [Wiesner *et al.*, 2005]. Examples of effector proteins include: α-actinin, Filamin, Focal Adhesion Kinase (FAK), Paxillin, Talin, Vinculin and others whose structure and function are stated in Table 1.3. [Liu *et al.*, 2000].

A plaque of these adaptor proteins combine to form a focal adhesion (FA) complex where each individual protein has specific binding properties. The FA complex permits the connection between the ECM and cytoskeleton of a cell to transmit vital signals; acting as contacts, these allow the attachment of actin filaments (also referred to as filamentous actin; F-actin) to the membrane region of a cell (Figure 1.5). Actin filaments are a network of stress fibres which complete the physical connection between the cell and its ECM. Once a connection is made, actin filaments are able to control cell retraction and cell body stiffness; actin filaments are able to create tension which affects the assembly and organisation of the ECM which ultimately influences cell behaviour such as proliferation and differentiation [Schoenwaelder and Burridge, 1999]. Actin filaments also permit the protrusion of cell membranes allowing the formation of features such as lamellipodia and filopodia. These are generated by an extensively dense, branched network of actin filaments against the cell membrane which occurs by an autocatalytic process using the seven-polypeptide Arp 2/3 complex [Le Clainche and Carlier, 2008]. Fibrillar adhesions also have a similar role but are particularly formed by cells that bind to fibronectin through the α5β1 receptor; this mediates the organisation of ECM fibronectin fibrils in a parallel direction to the actin stress fibres [Danen *et al.*, 2002].

Chapter 1
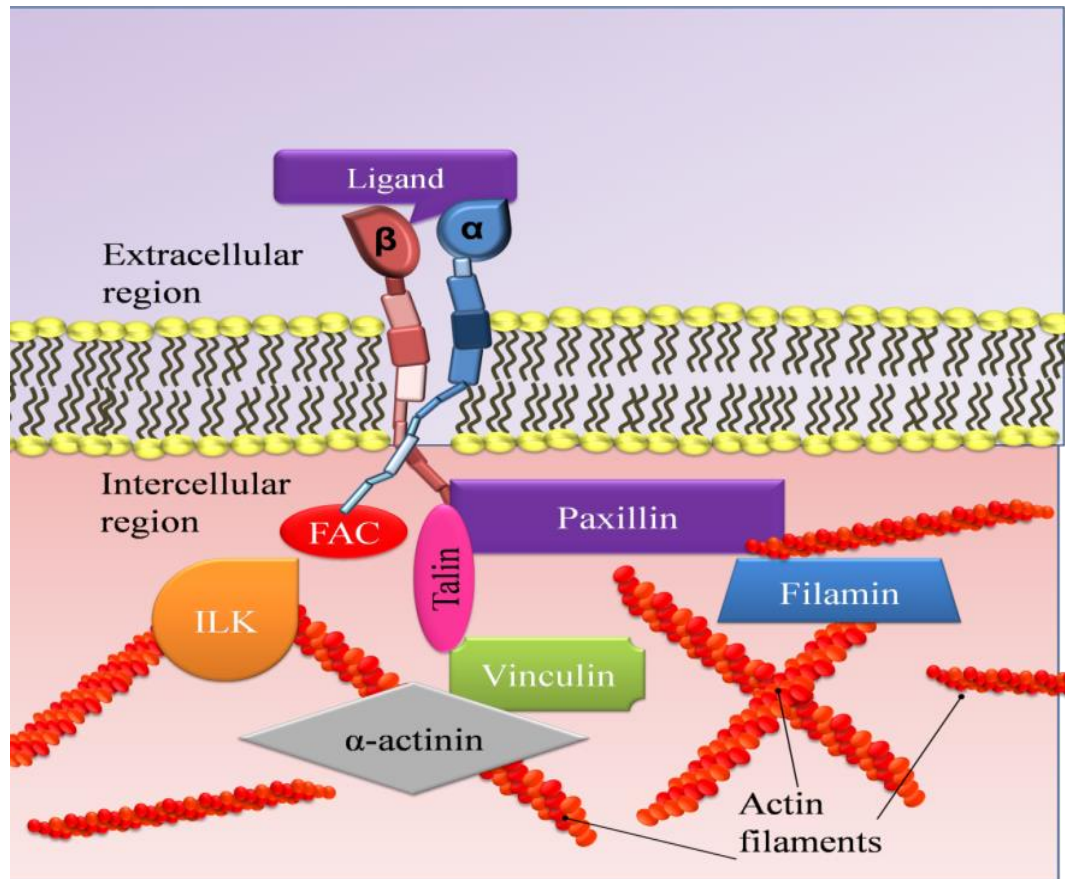
Figure 1.5 Essential intracellular proteins which mediate integrin interaction. Adapted from Humphries *et al*., 2006.

1.3.4 Factors Affecting Integrin Expression

There are several factors that can determine the activation and expression of integrins including the availability of ECM ligands, the ability of integrins to recognise corresponding ECM ligands, matrix stiffness, mechanotransduction and oxygen concentration [Forsyth *et al.*, 2008; Millward-Sadler and Salter, 2004]. The overall effect of these parameters affects specific cell types differently. These parameters may also play an important role in mediating the expansion of hESCs both *in vivo* and *in vitro*; any incremental changes can lead to changes in integrin expression subsequently determining the adhesion, proliferation and pluripotency of hESCs [Forsyth and McWhir, 2008].

Chapter 1

Table 1.3 Structure and function of integrin binding adaptor proteins.

Integrin Binding Proteins	Structure and Function	Reference
α-actinin	A modular protein which has the ability to bind and cross-link F-actin. Also has an additional number of binding partners which involve actin-binding proteins such as vinculin, zyxin and p85 subunit of phosphatidylinositol-3-kinase (PI3K). α-actinin is able to co-localise with integrins within focal adhesion complexes as well as along cytoskeletal stress fibres (actin filaments).	[Otey *et al.*, 1990]
Filamin	Has a size of 280 kDa and is comprised of 24-immunoglobulin-like repeats; Filamin interacts with a number of signalling proteins and is able to bind to F-actin Binding sites for Actin are situated in the N-terminal region. Filamin localises to the cortical region of the actin cytoskeleton and any mechanical stress encourages the localisation of Filamin towards β1 which stimulates the recruitment of F-actin.	[van der Flier and Sonnenberg, 2001]
Focal Adhesion Kinase (FAK)	Also referred as pp125^{FAK} is a tyrosine kinase but functions in non-specific binding. Due to lack of enzymatic activity within integrins, FAKs function as enzymes which transfer a phosphate group from ATP to a tyrosine residue in a protein resulting in tyrosine phosphorylation of Paxillin, Talin and Tenascin which is vital for the transduction of signalling.	[Liu *et al.*, 2000; Parsons, 2003; Schaller *et al.*, 1995]
Interleukin Kinase (ILK)	ILK is another non-receptor serine/threonine kinase which binds to crucial adaptor proteins such as Paxillin to connect to the β-tails of an integrin.	[Schlaepfer and Hunter, 1996]
Paxillin	Paxillin mediates matrix adhesion assembly, the turnover of matrix and matrix signalling and is the only protein known to have the ability to bind to the α4 sub-unit.	[Schaller *et al.*, 1995]
Talin	Has a size of 270 kDa and plays a key role in integrin activation and initiates matrix adhesion formation by connecting integrin receptors to the actin cytoskeleton (F-actin) via the formation of focal complexes. The head region of Talin contains a binding site for FAK and PIP$_2$.A reduction in the expression of Talin has been proven to disrupt the expression of integrins on the cell surface resulting in the prevention of creating focal adhesion complexes.	[Goldmann, 2000; Horwitz *et al.*, 1986; Liu *et al.*, 2000]
Vinculin	An actin binding protein which promotes and stabilises the clustering of integrins.	[Franco *et al.*, 2004]

Chapter 1

1.3.5 Embryonic Stem Cell Associated Integrins

The difficulty in expanding large numbers of hESCs *in vitro*, is attributed to the lack of understanding of the key mechanisms which promote the adhesion and expansion of hESCs whilst retaining their pluripotency. As mentioned earlier, the current standard method for culturing hESCs *in vitro* is using Matrigel[TM]; this permits good initial recovery and attachment of hESCs and retains their undifferentiated state with a typical morphology. Although the exact composition of Matrigel[TM] is unknown, the crucial proteins which are known to play an important role in hESC adhesion and pluripotent expansion have been identified as; Laminin, Fibronectin, Vitronectin, Collagen IV and Heparin Sulphate Proteoglycans. However, the concentration of these proteins in respect to each other varies and whether or not this influences hESC adhesion is yet to be investigated.

Partial elucidation of proteins in Matrigel[TM] has encouraged the identification of some of the important corresponding integrins expressed on the surface of hESCs. These integrins permit the successful connection resulting in their ability to adhere to ECM proteins, attach and proliferate in a typical pluripotent manner by forming colony-forming units (Young and Carpenter 2001). This results in "inside-out" integrin signalling where integrin-mediated signalling determines the type of ECM protein secreted and control how they are organised in the ECM binding surface of cells to encourage pluripotent expansion [Streuli and Akhtar, 2009]. Therefore, understanding the hESC integrin profile will help improve current technology by creating novel substrates that would promote hESC adhesion via those integrins resulting in an increased yield of initial hESC adhesion and allowing an efficient expansion rate of undifferentiated cells. With sufficient numbers this would permit the use of hESCs for clinical trials [Fadeev and Melkoumian, 2011].

Chapter 1

1.3.6 ECM Proteins and Corresponding Integrin Interactions Mediating hESC Activity Using Matrigel^{TM} and Feeder Cells

1.3.6.1 Laminin

During embryonic development, Laminin is the first basement membrane (BM) component of the ECM to be laid down [Mostafavi-Pour *et al.*, 2012]. BM's function as structural barriers and act as substrates for cellular behaviours including; cell polarity, proliferation, differentiation, migration and chemotaxis [Poschl *et al.*, 2004]. Therefore, BMs allow the isolation of cells whilst at the same time connect them to their interstitial matrix. Examples of BM's include: perlecan, collagen IV and nidogen [Kruegel and Miosge, 2010].

Laminin is a heterotrimeric glycoprotein with three chains consisting of α, β and γ which can able to give rise to 16 different isoform types of laminin, which all help regulate tissue structure and the behaviour of cells [Kruegel and Miosge, 2010]. During embryonic development, the key laminin isoforms that are involved include laminin-111 and laminin-511, which are also expressed by hESC lines; although on Matrigel™ substrate, laminin-111 is the isoform that is present [Rodin *et al.*, 2012]. However, *in vitro* investigations have also shown the ability of recombinant laminin-511 to promote hESC self-renewal and to be more effective in mediating hESC adhesion, expressing standard hESC markers, maintaining a reasonable proliferation rate, and retention of pluripotency (up to 20 passages) relative to other laminin isoforms such as laminin-111 and laminin-332. Furthermore, the extensive use of laminin-511 has included its ability to support derivation of new hESC lines simply by plating ICM's onto laminin-511 which permitted ICM attachment and the outgrowth of hESCs [Azarin and Palecek, 2010].

Chapter 1

Recent investigations have confirmed the ability of laminin to support hESC growth similar to Matrigel™ during *in vitro* culture [Young and Carpentar, 2002]. Thus, laminin is considered to be an essential protein in promoting cell adhesion, migration, spreading and stimulating the proliferation of hESCs whilst retaining their undifferentiated state [Mostafavi-Pour *et al.*, 2012]. Many interacting integrin receptors for laminin have been identified and include: α1β1, α2β1, α2β2, α3β1, α6β1, α6β4, α7β1, α9β1, α10β1 and αVβ1; these are able to give rise to heterodimers specific for adhesion to other ECM proteins including fibronectin, vitronectin and collagen IV [Prowse *et al.*, 2011].

However, for laminin, α6β1 is considered to play a crucial role in hESC adhesion and is a highly expressed surface receptor [Humphries *et al.*, 2006; Kruegel and Miosge, 2010; Young and Carpentar, 2002]. Specifically, there are two isoforms of the α6 sub-unit, α6A and α6B with the differences visible in the cytoplasmic domains but in undifferentiated hESCs the α6B isoform is expressed.

Chapter 1

1.3.6.2 Fibronectin

Fibronectin is an omnipresent, structural glycoprotein with a high molecular weight, consisting of peptide sub-units which comprise three types of repeats including type I, II and III. Fibronectin contains binding sites for various ECM proteins including: collagen, fibrin, fibronectin itself and heparin. Functions of fibronectin include; organising the ECM, therefore it plays a vital role in matrix assembly, cell adhesion, spreading, migration, morphology and organisation of the cytoskeleton. Within the cell, fibronectin is initially synthesised as a monomer but is instantly dimerised inside the endoplasmic reticulum and secreted into the ECM as a disulphide-bonded dimer in an inactive form; upon binding to its interacting integrin ($\alpha5\beta1$) [Mostafavi-Pour *et al.*, 2012], this extends the fibronectin dimer via the RGD (Arg-Gly-Asp) peptide binding sequence [Coppolino and Dedhar, 2000] resulting in its activation and subsequent fibrillar network formation [Labat-Robert, 2012]. Furthermore, out of the 24 integrin heterodimers, 8 of these integrins have been identified to be able to bind to the RGD peptide sequence [Labat-Robert, 2012].

During hESC culture, fibronectin is secreted by feeder cells (MEFs) into ES conditioned media but is also present as a component of Matrigel^{TM}; hESCs cultured on Matrigel™ in combination with ESC conditioned media express corresponding interacting integrins for fibronectin, specifically $\alpha5\beta1$.

1.3.6.3 Vitronectin

Vitronectin (molecular weight of ~ 75kDa) is a multi-functional glycoprotein and can be found in blood, plasma (concentration of 200µg/ml) and ECM; it has the ability to bind and anchor onto proteins such as glycosaminoglycans (GAGs), collagen, plasminogen as

Chapter 1

well as the urokinase receptor. Major biological functions of vitronectin include: fibrinolysis, hemostasis, immune defence and more relevant functions with respect to cell behaviour. These include; cell adhesion, spreading, ECM anchoring (to collagen and GAGs), proliferation, proteolytic degradation of matrix and cell migration when coupled with interacting cell integrins and growth factors, which together have a synergistic effect on cell growth [Schvartz *et al.*, 1999].

Cell adhesion, spreading and migration are primarily mediated via the RGD peptide within vitronectin; *in vitro* the RGD peptide has demonstrated its ability to bind to and interact with several integrins such as; αVβ3, αVβ5, αVβ1, αVβ6, and αVβ8 resulting in subsequent protein phosphorylation triggering the activation of the MAPK pathway [Braam *et al.*, 2008; Schvartz *et al.*, 1999]. However, recent studies have reported the αVβ5 vitronectin receptor to be important in mediating hESC adhesion and pluripotent expansion when cultured using Matrigel^{TM} or Vitronectin substrates [Braam *et al.*, 2008]

Chapter 1

1.3.6.4 Collagen IV

Collagen IV is another type of BM protein that is present in all BMs including Matrigel™ [Poschl *et al.*, 2004]. It is comprised of 6 different alpha chains that are able to assemble into 3 different heterotrimers. Collagen IV is unique compared to other types of collagen. As a basement membrane, collagen IV has an important role in mediating cell adhesion, migration and differentiation by acting as a scaffold which provides mechanical stability, structural integrity and central cohesiveness to BMs in situations where greater mechanical stability is required and there is an increase in mechanical forces [Poschl *et al.*, 2004]. The network of collagen IV fibres functions as a foundation scaffold with the ability to form a complex arrangement by the incorporation of other components such as Laminin, Nidogen-1 and 2 (mediate the formation of ternary complexes between Laminin and collagen IV *in vitro*) and Perlecan. Together, this combination of proteins produces a highly supramolecular architecture that form sheet-like BM complex structures [Poschl *et al.*, 2004].

Collagen IV contains binding sites for numerous cell types including: platelets, hepatocytes, keratinocytes, endothelial/pancreatic cells and hESCs [Kruegel and Miosge, 2010]. There are many interacting integrins that can bind to collagen IV including; α1β1, α2β1, α3β1, α6β1, α10β1, α11β1 and αVβ5 [Kruegel and Miosge, 2010]. However, the collagen receptor identified in playing a major role in adhesion of hESCs to Matrigel™ specifically includes α2β1 [Mostafavi-Pour *et al.*, 2012] and α9β1, which is a receptor not only for collagen IV but also laminin and VCAM-1 [Lee *et al.*, 2010].

Chapter 1

1.3.6.5 Heparin Sulphate Proteoglycans

Heparin sulphate protegolycans (HSPGs) are cell surface and ECM proteins; containing a core protein they are surrounded by covalently linked glycosaminoglycan (GAG) chains. Based on the core protein of HSPGs, they can be classified into 3 types; perlecan, glypican (disulfide-stabilised globular core protein linked to the plasma membrane) and syndecan (transmembrane protein which can also bind chondroitin sulphate), the latter two having a greater importance in cell surface HSPGs [Lin, 2004]. HSPGs are able to incorporate into a network of other BM proteins including Laminin and Collagen IV. Other critical functions of HSPGs in relation to BMs include; retaining BM integrity, BM filtration functions and the ability of BMs to lock storage of growth factors [Poschl *et al.*, 2004]. HSPGs are able to manage GFs, but also function as GFs themselves and more importantly, they are able to facilitate the interaction of GFs with the extracellular matrix [Symes *et al.*, 2010]. HSPGs play an important role in regulating the formation of signalling pathways such as Wnt, Hedgehog, TGF-β and specifically bFGF. bFGF receptor activation is known to mediate hESC pluripotency and is also strongly linked with integrin signalling pathways [Braam *et al.*, 2008].

Chapter 1

Table 1.4 Summary of the critical integrins and interactive ECM ligands which promote the adhesion and undifferentiated expansion of hESCs [Meng *et al.*, 2010; Mostafavi-Pour *et al.*, 2012 Rowland *et al.*, 2010]

Integrin	Integrin Function	Corresponding ECM Protein (Ligand)	Reference
α6β1	Maintain hESC stemness	Laminin	Meng *et al.*, 2010, Mostafavi-Pour *et al.*, 2012.
α5β1	Maintain hESC stemness	Fibronectin	Rowland *et al.*, 2010, Mostafavi-Pour *et al.*, 2012.
αVβ5	Mediates hESC adhesion and maintenance of pluripotency	Vitronectin	Rowland *et al.*, 2010
α2β1	Major role in hESC adhesion to Matrigel™	Collagen IV	Meng *et al.*, 2010

In summary, numerous ECM proteins are present in Matrigel^{TM} and are also secreted by hESCs. These proteins play a crucial role in mediating hESC attachment and proliferation when cultured *in vitro* (Figure 1.6). There are various integrin receptors located on the membrane of hESCs which mediate the connection to these proteins and support the bi-directional talk between the cytoplasmic region of a cell and its extracellular matrix. The critical integrins that have been identified in mediating hESC attachment and proliferation whilst retaining pluripotency are summarised in Table 1.4. Furthermore, the impact of ECM protein availability, concentration and corresponding hESC surface integrin expression on hESC differentiation is not fully understood and yet to be fully elucidated. This would help to determine the exact integrin-protein interactions which induce hESC differentiation. However, the key interactions involved in hESC adhesion have partially been identified.

Chapter 1
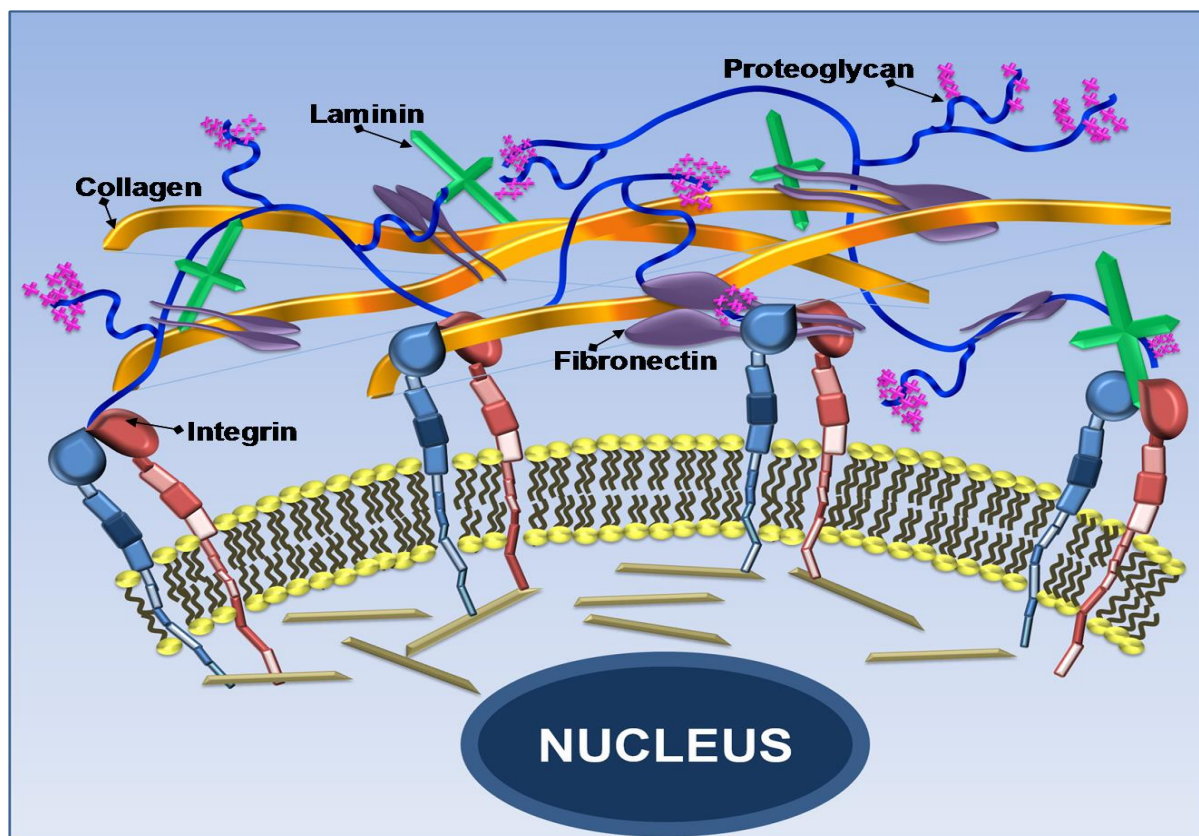
Figure 1.6 Schematic representing the connection between ECM proteins and intracellular components proteins through integrins. Adapted from Humphries *et al*., 2006.

1.4 Physiological Normoxia and Intracellular Pathways for Embryonic Stem Cells

Several factors can affect the expression of integrins and growth factors including; chemical cues, mechanotransduction, the substrate on which cells are cultured, ECM proteins and oxygen concentration. As a result, integrins and growth factors ultimately affect the intracellular pathways, which in turn influence pluripotency and differentiation of hESCs. The dominating signalling cascades that are involved in controlling differentiation of hESCs include; bone morphogenetic, Wnt, Hedgehog and Notch [Zachar *et al.*, 2010].

Chapter 1

One essential component of the stem cell microenvironment is the oxygen concentration [Csete, 2005], which also plays a central role in oxidative metabolism, cell signal transduction pathways as well as tissue and organ morphogenesis [De Filippis and Delia, 2011]. Various stem cells have performed better during expansion in *in vitro* physiological normoxic (also referred as hypoxia; defined as low oxygen levels; 2% - 8% O_2) culture conditions in comparison to hyperoxia (21% O_2) and have particularly shown to retain their stemness and undifferentiated state [Szablowska-Gadomska *et al.*, 2011; Zuk *et al.*, 2002]. Examples include; Hematopoietic stem cells (HSCs) which were shown to express a significantly greater number of long-term colony initiating cells (LTC-ICS), relative to HSCs cultured in 21% O_2 [Ivanović *et al.*, 2000]. The bone marrow is also a physiologically normoxic environment, hence mimicking this environment *in vitro* further supported an increase in the number and frequency of colony forming units (CFU) of undifferentiated hMSCs [Grayson *et al.*, 2006], amongst other beneficial changes, summarised in Table 1.6.

The oxygen environment has also shown to have an influence on the intracellular pathways of hESCs. Oxygen is known to function as a signalling, bioactive molecule in conjunction with other regulatory factors [Zachar *et al.*, 2010] which can determine hESC survival, proliferation and differentiation, by providing a metabolic substrate for cells in a 3D spatial environment [Griffith and Swartz, 2006]. As mentioned earlier, hESCs are derived from the ICM of a blastocyst; the blastocyst is surrounded by a trophoblast shell which excludes oxygenated maternal blood, hence forming an hypoxic environment until vascularisation occurs at a later stage [Rodesch *et al.*, 1992]. Furthermore, the oxygen environment within the uterine environment is between 2.5% - 5% O_2, to which human embryos are exposed to

and experience a physiological normoxic environment [Chen *et al.*, 2010; Szablowska-Gadomska *et al.*, 2011]. Therefore, hypoxia is typically considered to be the physiological norm for hESCs and thus creating a hypoxic environment *in vitro* would be beneficial to mimic this physiological environment [Chen *et al.*, 2010].

Recent studies have demonstrated that the effects of physiological normoxia on *in vitro* culture of hESCs improves their ability to retain typical undifferentiated morphological characteristics effectively (appear significantly smaller and less granular relative to hESCs cultured in 21% O_2 [Forsyth *et al.*, 2006], for longer periods of time [Zachar *et al.*, 2010]. hESCs at 5% O_2, have shown stimulated proliferation, enhanced phenotypic characteristics, a greater capacity to differentiate into all 3 germ layers and many other encouraging changes summarised in Table 1.5). Essentially, hESCs cultured in physiological normoxia maintain their pluripotency [Forsyth *et al.*, 2008] and demonstrate an enhanced expression of pluripotent markers including Oct-3/4, Nanog and Notch-1(heavily involved in hESC differentiation) [Zachar *et al.*, 2010], due to physiological normoxia activating signalling pathways such as FGF, TGF-β/GMP in hESCs as well as increased expression of P-Smad 2/3 [Chen *et al.*, 2010]. Up regulation of Nanog, significantly increases hESC proliferation by binding to interacting regions of CDK6 and CDC25A, which are important cell cycle molecules [Forristal *et al.*, 2010]. Transcriptional fingerprint analysis has demonstrated the up regulation of 302 genes and the down regulation of 56 genes in hESCs cultured in physiological normoxia [Forsyth *et al.*, 2008]. Furthermore, oxygen levels of 20% O_2 causes the down regulation of LEFTY2 in comparison to hESCs cultured in physiological normoxia; LEFTY2 is a key gene which prevents the spontaneous differentiation of hESCs along mesoderm and endoderm lineages

Chapter 1

and its down regulation causes the destabilisation of a network of genes that maintain ES pluripotency [Westfall *et al.*, 2008]. However, oxygen concentrations any lower than 1% O_2 decrease the proliferation rate of hESCs but still retain their pluripotent state; this suggests the apparent ability of oxygen to modulate proliferation and quiescence of stem cells [Ezashi *et al.*, 2005; Mohyeldin *et al.*, 2010].

Recently, pluripotency of hESCs has been proven to be primarily regulated by a family of hypoxia inducible factors (HIFs) which can be expressed by decreasing the oxygen environment, but can also be activated by various growth factors, cytokines, vascular hormones and viral proteins [Szablowska-Gadomska *et al.*, 2011]. HIFs are heterodimeric, environment sensing [Mohyeldin *et al.*, 2010], transcriptional factors and are comprised of α and β sub-units. There are three oxygen dependant isoforms of the α-subunit which are HIF-1α (120 kDa), HIF-2α (EPASI) and HIF-3α; these can bind to two types of β sub-units which are HIF-1β and HIF-2β [Forristal *et al.*, 2010; Szablowska-Gadomska *et al.*, 2011]. The expression of HIFs influences the promotion and suppression of several genes that are associated with cell survival, oxygen homeostasis, cell proliferation, angiogenesis, glucose metabolism and cell apoptosis [Szablowska-Gadomska *et al.*, 2011]. Specifically, this is mediated by the direct interaction of HIFs with other important transcriptional factors that have a critical function in several cellular processes including mediating Notch signalling by binding to its intracellular domain which contribute in maintaining pluripotency. These include; NF-kB, Activator protein-1 (AP-1), p53 and c-Myc. NF-kB has known to play an important role in inflammatory response and the immune system, AP-1 has an involvement in proliferation and cell apoptosis; c-Myc is known to mediate cell growth, proliferation,

Chapter 1

promotion of angiogenesis and the inhibition of cell differentiation [Szablowska-Gadomska *et al.*, 2011].

HIF-A has been recognised as the main oxygen sensing sub-unit controlling glycolytic genes [Forristal *et al.*, 2010]. In 21% O_2 proteosomal degradation (through the 26S proteasome) of HIF-1α occurs, whereas in physiological normoxia (2% O_2) HIF-1α in combination with HIF-2α and HIF-1β expression, activates the expression of several hESC pluripotent markers [Szablowska-Gadomska *et al.*, 2011]. The stable presence of HIF-1 supported by physiological normoxia (2% O_2) contributes to maintaining the undifferentiated phenotype of hESCs [Zachar *et al.*, 2010]; blockage of prolyl hydroxylation proteins (PHD) and factor inhibiting factor (FHIF) which further stabilises HIF-α and initiates activation of nuclear localisation signals (NLSs), particularly the C-terminal section of the transactivation domain (TAD) causing the dimerization of HIF-α with HIF-β and the translocation of HIF-1α into the nucleus resulting in subsequent activation of more than 60 genes all of which are particularly involved in glycolysis, angiogenesis and cell cycle and survival [Szablowska-Gadomska *et al.*, 2011]. However, in hyperoxia (21% O_2), PHDs are activated causing subsequent proteosomal degradation of HIFs, which is further mediated by the Von Hippel-Lindau (VHL) protein preventing its translocation and activation of several genes [Forristal *et al.*, 2010].

Chapter 1

Table 1.5 Effects of physiological normoxia (2% O_2) on hESCs and hMSCs cultured *in vitro*.

hESC Activity *in vitro*
Maintain pluripotency [Forsyth *et al.*, 2008]
Minimise spontaneous differentiation [Ezashi *et al.*, 2005; Forristal *et al.*, 2010; Forsyth *et al.*, 2008]
Improve establishment of mouse ESCs [Wang *et al.*, 2006]
Enhance clonal recovery (reported to have a 6-fold increase in 2% O_2, relative to 21 % O_2) [Forsyth *et al.*, 2006]
Reduce Chromosomal abnormalities [Forristal *et al.*, 2010; Forsyth *et al.*, 2008]
Decreased morphological differentiation phenotype [Ma *et al.*, 2009]
Produce lower amounts of chorionic Gonadotropin and progesterone [Ezashi *et al.*, 2005]
Enhanced EB formation as a result of down regulation in the expression of SOX-17, Desmin, GATA4, Brachyury and cdx2 [Chen *et al.*, 2010].
Direct ESC differentiation [Bauwens *et al.*, 2005]
Enhanced proliferation demonstrated by significantly larger colonies [Ezashi *et al.*, 2005]
Enhanced differentiation into skeletal lineages such as Osteogenesis [Zachar *et al.*, 2010]
hMSC Activity *in vitro*
Greater colony forming unit potential [Ren *et al.*, 2006]
Faster and prolonged proliferation [Ren *et al.*, 2006]
Maintenance of undifferentiated state [D'Ippolito *et al.*, 2004]

Essentially, HIF-1α plays a crucial role in the initial adaptation of cells to the physiological normoxic environment; as HIF-1α is only applicable for a short term [Zachar *et al.*, 2010], its expression is lost after 48 hours and instead HIF-3α is expressed and transferred to the nucleus. Upon entering the nucleus, this activates the up regulation of HIF-2α; the expression of HIF-2α results in the up regulation of crucial transcriptional factors such as

Chapter 1

Oct-3/4 (POU5-F1), Sox-2, SSEA-4 and Nanog, all of which maintain the pluripotency of

hESCs [Ezashi *et al.*, 2005; Szablowska-Gadomska *et al.*, 2011]. However, there are

concerns involved in attempting to mimic the hypoxic environment for cells *in vitro*. Issues

include the speculation of reoxygenation which can occur when attempting to create a

constant hypoxic environment. It is apparent that reoxygenation triggers the generation of

reactive oxygen species and the up regulation of a number of genes which have subsequent

deleterious effects, such as DNA damage [Mohyeldin *et al.*, 2010; Zachar *et al.*, 2010].

1.5 ECM Proteins for *In Vitro* hESC Expansion

The realisation of many limitations associated with the *in vitro* expansion of hESCs using

Matrigel™ has driven researchers to explore other alternatives. Partial elucidation of the

composition of Matrigel™ has identified the presence of various ECM proteins including

fibronectin, laminin and collagen. This has encouraged the investigation of the ability of

various ECM proteins to support the *in vitro* expansion of undifferentiated hESCs. ECM

proteins investigated have included: vitronectin, fibronectin, laminin, collagen type I and

IV and hyaluronic acid; a summary of various studies is shown in Table 1.6. These

proteins have been coated onto typical tissue culture plastic surfaces and cultured with

MEF-conditioned media or more defined ESC media's that are commercially available.

Despite extensive research suggesting the possible use of ECM proteins for the *in vitro*

expansion of hESCs, the scale up of hESCs using ECM proteins as their growth substrates

is not as straightforward, as previously thought. Limitations associated with using

recombinant proteins include; highly expensive to produce and purify, batch-to-batch

variability, issues of coating during an aseptic environment, the possibility of degradation

Chapter 1

and denaturation once dehydrated, an undefined thickness threshold to provide similar attachment and proliferation to Matrigel^{TM} and the inefficiency in protein coating as more than 50% remains in the solution. As a result of these limitations, Matrigel^{TM} still remains the gold standard and desirable substrate to culture and expand undifferentiated hESCs *in vitro* [Jones *et al.*, 2010].

Chapter 1

Table 1.6 A summary of studies which have investigated the potential of purified ECM proteins as substrates for the attachment and expansion of human embryonic stem cells during *in vitro* culture.

ECM Protein Substrate	Substrate details	hESC Line	Observations	Reference
Collagen Type I	Biomatrix (10 µg/cm^2)	H1 and H9	hESCs expanded on Collagen I substrate with conditioned media from human embryonic germ-cell-derived cells had a population doubling time similar to hESCs expanded on Matrigel^{TM} with ES conditioned media. hESC expressed typical pluripotent markers (Oct-4, Nanog and Tra-1-60)	[Jones *et al.*, 2010]
	Substrate coating on flask	HUES-1 and SHEF-1	hESCs were expanded with KO-DMEM/SR and defined media (HESF8). Both media's in combination with Type I Collagen substrate demonstrated stable expression of pluripotent markers (Oct-3/4, Nanog, SSEA-1 and 3) as well as maintaining their differentiation capacity	[Furue *et al.*, 2008]
Collagen Type IV	Substrate coating onto 96-well plate	HUES-1, HES2, HESC-NL3	Supported undifferentiated expansion of hESCs with MEF conditioned media, however in defined media (mTESR) proliferation was not as effective	[Braam *et al.*, 2008]
Vitronectin	Human purified and Recombinant Vitronectin coating onto 96-well plate	HUES-1, HES2, HESC-NL3	hESCs were expanded on Vitronectin with mTESR-1 media or MEF-conditioned media; mTESR-1 supported better hESC growth with retained pluripotency; although in both media's, vitronectin supported the greatest proliferation of hESCs, in comparison to laminin + entactin, collagen IV and fibronectin	[Braam *et al.*, 2008]

Chapter 1

	Substrate coating	hES1	hESCs were cultured in combination with StemPro media	[Prowse et al., 2011]
	Substrate coating	H9	Good proliferation and retained pluripotency	[Rowland et al., 2010]
Laminin	Various recombinant laminins (511, 411, 332, 211 and 111)	KhES-1, KhES-2 and KhES-3	hESCs were cultured with MEF conditioned media and observed a inconsistent cell attachment with laminin 332 showing better results.	[Miyazaki et al., 2008]
	Laminin 511 coating	HS420, HS207, HS401	Good attachment and proliferation with retention of pluripotency.	[Rodin et al., 2012]
	Substrate coating	H1 and h9	hESCs expanded with MEF conditioned media. hESCs maintained a normal karyotype, stable proliferation rate and high telomerase activity. Expressed Oct-4, hTERT, ALP and surface markers such as SSEA-4, Tra 1-60 and Tra 1-81	[Xu et al., 2001]
. Laminin + Entactin	Substrate coating onto 96-well plate	HUES-1, HES2, HESC-NL3	Supported the proliferation of undifferentiated hESCs; however proliferation activity was the lowest on this substrate, relative to Collagen IV, Vitronectin, Fibronectin and Matrigel^{TM}	[Braam et al., 2008]
Fibronectin	Human plasma fibronectin (Fn) coating	HUES-1	Supported hESC colony expansion with retained pluripotency when expanded in MEF-conditioned media. Proliferation rate was lower in comparison to hESCs grown on collagen IV and vitronectin.	[Braam et al., 2008]
	Three types of fibronectin investigated: bovine Fn (bovine, human plasma and human cellular),	I-3, I-6 and H9	hESCs cultured on all 3 types of fibronectin coated substrates with media (plus 15% SR and a combination of TGF-β1, LiF and bFGF were suitable for the undifferentiated hESC proliferation for more than 50 passages.	[Amit et al., 2004]

Chapter 1

Hyaluronic Acid (HA) and dextran hydrogels	3D Hydrogel, modified with photoinitiator groups and photoinitiator cross-linked by UV curing for 10 mins HA hydrogels (Ø 3 mm and 2 mm thickness)	H1, H9 and H13	hESCs were encapsulated into HA hydrogel and cultured in MEF conditioned ES media. hESCs retained their metabolic activity, supported their proliferation whilst retaining their pluripotency and capacity to differentiate for up to 20 days in culture. Dextran hydrogels supported EB formation instead.	[Gerecht *et al.*, 2007]
Hyaluronic Acid surface functionalised with ECM proteins/peptides	Layer-by-layer self-assembled surface of HA functionalised with various ECM proteins using a cross-linking agent	MEL1 and MEL2	hESC attachment observations after 2 hours showed no attachment of hESCs to HA without any biofunctionalisation of proteins to its surface and that functionalization of recombinant Fn to HA enhanced hESC attachment. hESCs were cultured on these substrates using defined culture media.	[Doran *et al.*, 2010]
E-cadherin	Human E-cadherin coating	H1 and H9	hESCs maintained a typical morphology and retained a similar proliferation rate to hESCs grown on Matrigel^{TM}	[Nagaoka *et al.*, 2010]

Chapter 1

1.6 Tissue Engineering and Regenerative Medicine Strategies

Major limitations of Matrigel^{TM} include batch-to-batch variability, reproducibility, scale-up issues, xenogenic contaminations (such as Neu5Gc and lactate dehydrogenase elevating virus; LDEV) [Nagaoka *et al.*, 2010] and cost cause great concern for their clinical therapeutic use [Li *et al.*, 2010]. In addition to the limitations of using ECM proteins as alternatives, this has driven researchers to attempt to overcome these limitations and increase their applicability for clinical therapeutics. Currently, there are four main therapeutic approaches using stem cells: direct administration of adult stem cells (currently in clinical use), regeneration by stimulation of endogenous stem cells, implantation of differentiated stem cells and tissue engineering [Polak and Bishop, 2006]. Improved scale up of hESCs would have many beneficial implications such as the *in vivo* clinical application use with the elimination of any xenogenic contact and applications relating to tissue engineering and regenerative medicine applications.

The ultimate goal of regenerative medicine and tissue engineering is "to replace or regenerate cells, tissues or organs, to restore, improve or create normal function" [Mason and Dunnill, 2008]. This field is highly interdisciplinary and applies the knowledge and principles of engineering, materials science, medicine, biology and life science towards the development of biological substitutes. A tissue engineering strategy involves a combinatory use of cells, engineering materials and biochemical factors; [Agarwal *et al.*, 2008; Godier *et al.*, 2008; Liao *et al.*, 2008]. The native stem cell ECM is an environmental structure to anchor and support cells and provides a template for tissue growth in 3D [Polak and Bishop, 2006]. It is made of several fibrous proteins such as collagen, fibronectin, glycoproteins, proteoglycans, growth factors, bioactive molecules

Chapter 1

that maintain cell adhesion and growth [Ramakrishna *et al.*, 2006] including chemical ligands which are able to interact with surface receptors on cells with mechanical stability [Toh *et al.*, 2006] Biomaterial scaffolds are temporary, artificial substrates which fundamentally aim to provide a 3D environment (physically, chemically and biologically) [Slaughter *et al.*, 2009] to mimic this native ECM. Fundamental aims of scaffolds are to support and encourage cell proliferation and differentiation, allow the isolation and expansion of cells, function as a drug delivery system, growth factor delivery systems and to maintain the spatial environment to encourage the regeneration of tissue [Rose and Oreffo, 2002]. The more similar the structure and the ability of the scaffold to mimic the extracellular matrix, the better the end result of tissue engineering and its function. Specific to hESCs, biomaterials endeavour to simulate the stem cell microenvironment and niche which would hope to help maintain the typical stem cell phenotype expression whilst also retaining their plasticity and differentiation function by providing the appropriate biochemical signals.

Incorporating the use of biomaterial scaffolds with stem cell therapy would provide the ability to expand a sufficient number of undifferentiated hESCs in a shorter time period. hESCs would be suitable for clinical therapies and expand with a greater homogeneity of undifferentiated hESCs that can be directed to differentiate into various specialised cell/tissue lineages. More importantly, scaffolds would able to act as a portable carrier to permit in vivo transplantation for the use of hESCs in *in vivo* clinical implantations. [Higuchi *et al.*, 2012]

Chapter 1

The composition, topography and architecture of scaffolds allow cellular interaction and can influence behaviour and even modify the response of cells [Howard *et al.*, 2008]. Scaffolds must have several important characteristics which enable them to function appropriately. Essentially, a scaffold must be "biocompatible" and hence must not elicit a host response and be non-toxic to the cell [Rose and Oreffo, 2002; Slaughter *et al.*, 2009]. Therefore, many substrates are fabricated from materials that are already FDA approved, which permits their use for in vivo implantation [Rose and Oreffo, 2002]. "Biodegradability", is also an important consideration; a substrates main function would be to act as a carrier for implantation of expanded stem cells to an in vivo injured site. Upon arrival, the rate of scaffold breakdown should correlate with sufficient amount of matrix deposition. If the degradation rate is too slow, this will impede neotissue formation, on the contrary, if the degradation rate is too fast this reduces the mechanical properties of the scaffold which are important for the initial support to cells. Furthermore, degraded by-products via hydrolysis must be non-toxic to the cells or the host whilst *in vivo* implantation and biodegradability of substrate prevents the need for secondary surgical intervention [Sill and von Recum, 2008]. A scaffold must also be "bioactive", which allows a better interaction with the biological environment and is able to support cellular functions [Sill and von Recum, 2008]. Furthermore, the ease of a scaffold to be easily processed into complicated shapes with appropriate porosity is also essential [Gunatillake and Adhikari, 2003].

Chapter 1

1.6.1 Naturally-derived Polymer Scaffolds

Polymers are a primary choice for biomaterials as they possess functional properties and flexibility in design. Broadly, there are two types of polymers which are natural and synthetic polymers; naturally-derived polymers include popular examples such as collagen, gelatin, chitin, chitosan and cellulose. Advantages of using natural polymers includes: precise mimicking of the native ECM structure, available recognition sites which provide multiple cell attachment opportunities and therefore giving the substrate good adhesion properties which support subsequent cell growth and better interaction between the substrate and cells due to the bioactive nature of the substrate. Natural polymer hydrogels are also biocompatible, allow cell dependant degradability, inherent cellular interaction and eliminate the limitations of 2D flat culture using tissue culture plastic surfaces [Higuchi *et al.*, 2012]. However, limitations associated with the use of natural polymers as scaffolds includes: the dangers of eliciting an immune response, batch to batch variability with a limited range of mechanical properties, rapid degradation rate and weak mechanical properties (though these limitations can be overcome by cross-linking), lack of consistency and structural malleability [Polak and Bishop, 2006].

Currently, there are a limited number of studies which have investigated the use of natural polymer scaffolds to support the expansion of hESCs. A 3D porous chitosan scaffold (Ø 13 mm and 2mm thickness, with 95% porosity and 65% average pore size) with mechanical properties (compressive E of 8.1 MPa and tensile E of 0.8 MPa) has been reported to support the expansion of hESCs *in vitro* where hESCs retained their pluripotency (confirmed by ALP and SSEA-4 expression) and retained typical hESC morphology. Further investigations included *in vivo* transplantation into an immunodeficient mouse

where observations included hESCs populating the scaffold. Pluripotency was not maintained for longer than 30 days [Li *et al.*, 2009].

Complex investigations have included the fabrication of hydrogels. Hydrogels are 3D networks formed from hydrophilic homopolymers, copolymers or macromers cross-linked to form insoluble polymer matrices [Slaughter *et al.*, 2009]. Properties such as biocompatibility, flexible method of formation, anticipated physical characteristics, the provision of structural integrity to tissue constructs, the essential structural and compositional similarities to ECM and an extensive framework which provides cellular proliferation and survival [Slaughter *et al.*, 2009] makes them the ideal candidates for hESCs. Hydrogels fabricated from natural polymers have been demonstrated to successfully culture stem cells [Benoit *et al.*, 2008; Brännvall *et al.*, 2007] although issues exist in terms of controlling mechanical and degradation properties, which could be eliminated using synthetic hydrogels due to superior control over chemical composition and architecture. Hydrogels have the potential to mimic the 3D environment that hESCs are exposed to including: biological, chemical, physical and mechanical cues during embryogenesis, within the inner cell mass whilst embedded in a 3D matrix, which controls their self-renewal and differentiation. hESCs have been encapsulated within calcium alginate hydrogels and expanded in typical hESC media; it was apparent that after 260 days of culture, hESCs retained their pluripotency (expression of Oct-4, Nanog and SSEA-4) with the capacity to differentiate into all three germ layers. Furthermore hESCs were arranged in typical closely packed colonies. This study showed promising results and eliminated any xenogenic contamination [Siti-Ismail *et al.*, 2008]. Hyaluronic acid (HA) hydrogels (Ø 3 mm and 2 mm thickness) fabricated by UV cross-linking were

demonstrated to support the expansion of undifferentiated hESCs for up to 20 days in culture, while dextran hydrogels caused EB formation and subsequent differentiation [Gerecht *et al.*, 2007]. Biofunctionality of HA with ECM proteins/peptides, especially fibronectin improved and enhanced initial hESC attachment rates [Doran *et al.*, 2010].

1.6.2 Synthetic Polymer Scaffolds

Synthetic polymers are man-made polymers that have great potential in tissue engineering due to biodegradation and mechanical property [Dhandayuthapani *et al.*, 2011]. Several advantages of using synthetic polymers for scaffolds include biocompatibility, their chemistry being versatile, able to incorporate mimicking biological properties and the ability to tailor scaffolds' mechanical properties (including porosity, spatial arrangement, strength and degradation rate to suit various applications) [Polak and Bishop, 2006]. Synthetic polymers are also cheaper, can be produced in large uniform numbers with a long shelf life, can be designed to show similar physicochemical and mechanical properties to biological tissue with reproducible mechanical properties such as tensile strength and elastic modulus. With regards to hESCs, synthetic polymers can contribute to the development of feeder-free cultures with the ability to offer reproducible culture conditions. Furthermore, they can minimise the cost of hESC expansion and eliminate their contact with xenogenic contaminants. These contributions as a result of utlilising synthetic polymers for stem cell culture would increase the potential clinical applications of differentiated hESCs [Higuchi *et al.*, 2012].

However, synthetic polymers lack biological function and require physical or chemical modification for cells to function appropriately. An example of simple modifications has

Chapter 1

included treatment of typical polystyrene flasks including, plasma etching and plasma-deposited gradients of octadiene to acrylic acid which have demonstrated to support the expansion of ESCs whilst retaining pluripotency. The same modification technique has been used for modification of the surface chemistry of scaffolds (via charged gas plasma polymerisation deposition) which allows the ability to enhance the adherence properties of cells to a scaffold [Howard *et al.*, 2008]. However, although synthetic polymers such as (polyethylene glycol) PEG/PLGA have properties such as the ease to control and reproduce, the surfaces have to be modified to enhance cell adhesion as they lack biological signalling in comparison to natural polymers [Godier *et al.*, 2008]. As a result, more complex modifications have included the biofunctionalisation of synthetic materials using ECM/natural proteins; for example, ECM molecules/peptides have been deposited onto various substrates including Hyaluronic acid and chitosan using methods such as layer-by-layer self-assembly and covalent bonding to enhance ESC adhesion properties. [Derda *et al.*, 2007; Doran *et al.*, 2010; Nur-E-Kamal *et al.*, 2006]. A summary of various synthetic polymer substrates that have demonstrated to show the ability to expand undifferentiated hESCs are stated in Table 1.7. However, limitations associated with many of these substrates include: flat 2D surfaces such as oxygen plasma treatment to typical tissue culture plastic surfaces, which do not fully mimic the typical 3D ECM structure and environment; there is batch to batch variability with limited mechanical properties, many of the polymers are not FDA approved (such as PMVE-Alt-Ma and PGSA) and the possibility of causing genotoxicity through UV photo cross-linked curing polymers [Brafman *et al.*, 2010; Irwin *et al.*, 2011].

Chapter 1

Table 1.7 A summary of synthetic substrates used to culture and expand, undifferentiated

hESCs.

Synthetic Substrates	Scaffold Properties	hESC Line	Observations	Reference
Oxygen plasma etched tissue culture polystyrene	2D synthetic culture surface stable at room temperature for atleast a year.	HUES7 and NOTT1	hESCs cultured with MEF conditioned media and retained typical hESC morphology for up to 10-14 passages. Expressed typical pluripotent markers (Oct-4, TRA1-60 and SSEA-4).	[Mahlstedt *et al.*, 2010]
Poly(ethylene terephthalate) PET	Porous membranes. 1-4 x 10^6 pores/cm^2 (0.291-0.345 GPa).	Information not available	Pore density of 4 x 10^6 supported the greatest number of hESC colonies, increased cell proliferation and maintained uniform and undifferentiated hESCs.	[Lee *et al.*, 2011]
Poly(ethylene terephthalate) PET	Porous membranes with different pore sizes (1, 3 and 8 μm).	CHA-hESC3	Feeder layers at the bottom of the trans-well inserts whilst hESCs were seeded on top of the porous membranes. 3 μm pore size demonstrated optimal results with greatest number of hESC colonies formed, prevented direct interaction with feeder cells and helped retain undifferentiated state for up to 25 passages.	[Kim *et al.*, 2007]
Amino-propylmethacrylate hydrochloride (APMAA$_m$)	Hydrogel photointiated using UV light.	H1 and H9	In combination with chemically defined media (mTESR1). hESCs demonstrated pluripotent expansion similar to hESCs expanded on Matrigel^{TM} for over	[Irwin *et al.*, 2011]

Chapter 1

			20 passages.	
PLGA/PLA	Porous sponges, fabricated via salt leaching with dimensions; 5 x 4 x 1 mm^3 coated with either Matrigel^{TM} or fibronectin [50 μg/ml] for 1 hour at room temperature. Pore size 250-500μm.	H9	hESC expanded in media with various growth factors (TGF-β1, Activin-A, Insulin-like growth factor and retinoic acid) specific for various differentiation lineages such as neural tissues and cartilage. Showed good attachment and 2-week survival of differentiated EBs	[Levenberg *et al.*, 2003]
Poly (methyl vinyl ether-Alt-maleic anhydride) PMVE-Alt-MA	Various polymers including PMVE-Alt-MA were deposited onto acrylamide gel coated slides in a spot (Ø150 – 200 μm)	HUES1 HUES9	1 x 10^6 cells seeded per array slide (10-20 cells/polymer spot) and cultured. Supported long-term proliferation and self-renewal of hESCs (Oct-4 and Sox-2) with differentiation capacity to form all 3 germ layers	[Brafman *et al.*, 2010]
Poly(glycerolco-sebacate)-acrylate PGSA	PGSA polymerisation using a photoinitiator and UV. Macropore size (~85-86 μM) and Youngs modulus (42.3-59.9 kPa)	H9 and H13	Encapsulated hESCs within PGSA scaffolds demonstrated organisation into colonies within the macropores after 1 day of culture. After 7 days, cells proliferated and formed EBs where cells expressed markers for all 3 germ layers	[Gerecht *et al.*, 2007]
Poly [2-(methacryloyl oxy) ethyl dimethyl-(3-sulfopropyl) ammonium hydroxide] PMEDSAH	PMEDSAH coated onto typical tissue culture plastic dishes	BG01 and H9	hESCs cultured long-term up to passage 15 with defined media including Stem-Pro and mTeSR. hESCs stained positive for pluripotent markers and all 3 germ layers	[Ross *et al.*, 2012]

Chapter 1

Many FDA approved, biodegradable synthetic polymers are used in tissue engineering and belong to the polyester family [Gunatillake and Adhikari, 2003]; popular examples include: poly-lactic acid (PLA), poly-glycolic acid (PGA), poly-lactic-co-glycolic acid (PLGA) and poly-ε-caprolactone (PCL). PLA, PGA and PLGA are poly-α-hydroxy acids that have bulk degradation properties and thus are able to breakdown by hydrolysis of ester linkages which results in non-toxic by-products that can be resorbed through the metabolic pathways and thus do not elicit an immune response. For example; PGA breaks down into glycolic acid (a natural metabolite) and PLA degrades into lactic acid which enters the tricarboxylic acid cycle and excreted as water and carbon dioxide [Gunatillake and Adhikari, 2003; Howard *et al.*, 2008].

PLA has two isoforms, "D" and "L"; PDLA has a higher degradation rate than PLLA, although PLLA has better biocompatibility. However, as PGA is more hydrophilic, it has a faster degradation rate (*in vivo* and *in vitro*) than PLA resulting in subsequent lower mechanical strength than PLA. A combined polymer of PGA and PLA results in poly-lactide-co-glycolic acid (PLGA) and has a degradation rate which can be manipulated depending on the ratio between PLA and PGA. On the other hand, PCL has a much slower degradation rate than both PGA and PLA as a result of being more hydrophobic. Degradation rates of commonly used synthetic biodegradable polymers are stated in Table 1.8

Chapter 1

Table 1.8 Molecular structure and properties of commonly used synthetic biodegradable polymers in tissue engineering [Gunatillake and Adhikari, 2003].

Biodegradable polymer	Properties	Degradation rate (months)	Molecular structure
Poly Glycolic acid (PGA)	• Rigid thermoplastic material • High crystallinity (46-50 %) • Glass Transition temperature = 36 °C • Melting temperature = 225 °C • Approximate strength 7.0 GPa • Degradation products into glycolic acid • Tensile modulus: 6-7 GPa • Tensile strength: 60-100 MPa	6-12	$\left[O-CH_2-\overset{\overset{\displaystyle O}{\|}}{C} \right]_n$
Poly-L-Lactic Acid (PLA)	• Semi-crystalline solid • Melting temperature 173 – 178 °C • Glass transition temperature 60-65 °C • Approximate strength 2.7 GPa • Degradation products into lactic acid • Tensile modulus: 3-4 GPa • Tensile strength: 50-70 MPa	>24	$\left[O-\underset{\underset{\displaystyle CH_3}{\|}}{CH}-\overset{\overset{\displaystyle O}{\|}}{C} \right]_n$
Poly-ε-caprolactone (PCL)	• Semi-crystalline • Glass transition temperature = - 60 °C • Low melting temperature 59 – 64 °C • Approximate strength 0.4 GPa. • Degradation product in caproic acid • Tensile modulus: 200-400 MPa • Tensile strength: 20-42 MPa	>24	$\left[O-(CH_2)_5-\overset{\overset{\displaystyle O}{\|}}{C} \right]_n$

Limitations concerning the use of biodegradable synthetic polymers are that they have weak mechanical properties, batch to batch variability, lack biomimetic function and thus do not have recognisable attachment sites for cells. The natural ECM environment is hydrophilic in nature with a 3D network of nanofibres at the micro- and nano-scale [Slaughter *et al.*, 2009] and therefore it is important for the polymer substrates to support cell attachment, proliferation and differentiation and enhance their biocompatibility for these cell activities. As mentioned previously, many studies have attempted to enhance the

adhesive properties of substrates, either by surface treatment, e.g. altering the surface energy properties via presenting charged particles or by functionalising natural ECM proteins to synthetic substrates which provide recognisable attachment sites for cells.

1.6.3 Protein Adsorption

It is important to select the appropriate polymer to function as a tissue engineering scaffold or substrate which makes it highly biocompatible and thus support activities such as cell attachment. Cell attachment and interaction to a biomaterial and its biocompatibility is a subsequent result of protein adsorption (process where molecules adhere to a solid surface) [Kasemo, 2002] to the surface of a biomaterial which is a fundamental process taking place during the initial stages of implantation *in vivo* [Kasemo, 1998]. The surface of an implant/scaffold is a dynamic area where protein adsorption activity is continuously changing. Initially, highly abundant serum proteins with low molecular weight adhere to the surface and are gradually replaced by less abundant, high molecular weight, cell adhesive proteins such as fibronectin with time; this is known as the Vroman effect [Vroman, 1962] (shown in Figure 1.7). The ability of proteins to adsorb to substrate surfaces from media is highly dependent on its wettability (which can be evaluated by contact angle. Contact angle is defined as the angle of liquid to a solid in the presence of gas; [Roach, 2005]), which is ultimately dependant on numerous factors including: surface chemistry, [Roach *et al.*, 2005; Roach *et al.*, 2006] shape, charge, topography [Roach *et al.*, 2006], surface roughness and surface energy; changes in these factors can enhance protein adsorption which subsequently influence cell behaviour such as adhesion and proliferation [Roach *et al.*, 2005]. These physical and chemical modifications of the surface can have an influence in the quantity, density, conformation and orientation of the

adsorbed proteins [Taborelli *et al.*, 1995]. Adsorption of proteins to substrates occurs through various interactions including; van der Waals, hydrophobic and electrostatic interactions, and hydrogen bonding [Roach *et al.*, 2005]. If the surface is hydrophobic (non-wettable and opposes contact with water due to cohesive forces causing the liquid to ball up), it produces a less water dense region with an open hydrogen-bonded network and has a pure water adhesion tension (τ^o) of <30 dyn/cm [Vogler, 1998]. Adsorption of proteins is even more energetically favourable on hydrophobic surfaces compared to hydrophilic (wettable surface; a dense water region that has a pure water adhesion tension (τ^o) of >30 dyn/cm; [Vogler, 1998] surfaces) and also bind more stubbornly [Roach *et al.*, 2005].

Contact angle is a method through which wettability of a material substrate can be characterised. A high water contact angle ($\geq 90^o$) means that water is unable to spread over a surface and therefore is defined as hydrophobic. Whereas on hydrophilic surfaces, water is able to spread over its surface resulting in a high solid water interface and a contact angle of $\leq 90^o$ [Roach, 2005]. Furthermore, it has been demonstrated that measuring the water contact angle from a direction perpendicular to the anisotropic topography of grooves is a more accurate indicator of water contact angle as supposed to taking a measurement from a parallel direction [McHale *et al.*, 2004; Yang *et al.*, 2009]. Generally cells prefer a substrate which is neither too hydrophobic nor too hydrophilic and thus have moderate wettability [Horbett *et al.*, 1985; van Wachem *et al.*, 1987]. Furthermore different cells prefer a different surface type in terms of wettability. For example, endothelial cells prefer a surface with a contact angle of 70° [Zhu *et al.*, 2002] whereas chondrocytes prefer a surface with a contact angle of 76°. It was apparent that reducing the

Chapter 1

water contact angle to 65° (increasing the hydrophilicity) resulted in decreased attachment

and proliferation of chondrocytes [Ma, 2003]. In agreement, it has also been stated that

hydrophobic materials with a $\tau^o < 30$ dyn/cm permit good cell attachment. The relationship

between contact angle and water adhesion tension τ^o is summarised in Table 1.9.
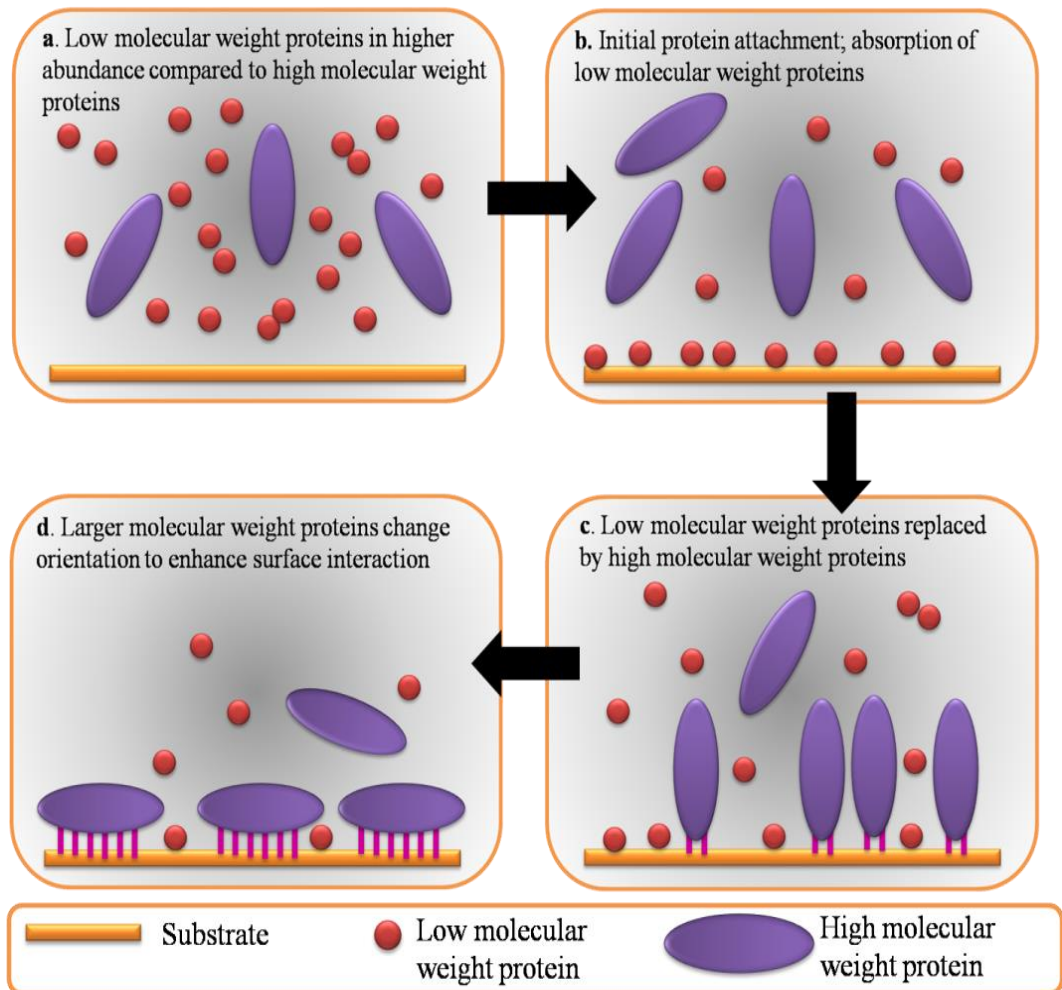
Figure 1.7 A schematic describing the Vroman effect. Adapted from Roach *et al*., 2006.

Chapter 1

Table 1.9 Relationship between wettability dictating parameters; contact angle and adhesion tension [Ma *et al.*, 2007].

Wettability	Contact Angle (θ)	Water Adhesion Tension (τ^o)
Hydrophobic	High contact angle ($\geq 90^o$)	Low adhesion tension (<30 dyn/cm)
Hydrophilic	Low contact angle ($\leq 90^o$)	High adhesion tension (>30 dyn/cm)

Proteins are amphipathic in nature as they have hydrophobic residues in the interior and hydrophilic polar and charged amino acids in the exterior. Each protein has a unique primary structure (made up of an amino acid sequence) and can directly affect the interaction of the protein with the surface. There are 20 amino acids and each amino acid differs in its chemical nature in terms of its side chain which give rise to various physicochemical properties, which also play a role in the overall properties of the protein itself. Charged amino acids are hydrophilic and are usually located on the outside of proteins and hence are available for direct interaction with surfaces [Dee *et al.*, 2003; Patthy, 1999]. Charge and the distribution of charge on these proteins can also affect the ability of protein adsorption. In addition, size of the protein can also play a major role, where larger molecules have a greater number of contact sites with the surface; molecules close to their isoelectric point (the pH at which the molecule exhibits zero charge) also adsorb more willingly as at this point there is reduced electrostatic repulsion between uncharged adsorbing molecules. This also permits a greater number of proteins to bind [Dee *et al.*, 2003]. Conformational changes of proteins also lead to alterations in the protein structure resulting in a change in the charge of amino acids; unfolding of proteins reveals more sites available for surface attachment/contact and so substrates which induce

and enhance the rate of unfolding can result in greater surface adhesion of proteins [Roach *et al.*, 2006]. Furthermore, proteins that are able to unfold better and expose more sites for attachment to surfaces are those which have an unstable structural stability due to less intramolecular cross-linking which allows greater and more ease of unfolding. As a consequence of protein unfolding this can change the type of amino acids exposed on the protein surface such as unveiling hydrophobic amino acids to the protein surface for interaction with a surface [Dee *et al.*, 2003].

As well as protein properties, the properties of the biomaterial surfaces are also just as important. Surface properties can be generalised broadly into three categories; electrical, chemical and geometric. Surface potential of the biomaterial can determine counter-ions from the electrolyte solution attracted to the surface; this also results in isotropically dispersed water molecules to become ordered [Dee *et al.*, 2003]. The overall result is combinatory of water ions, molecules and net surface charge which regulate interaction with proteins. For example, it has been demonstrated that polarised hydroxyapatite scaffolds enhanced MC3T3 cell proliferation in comparison to non-polarised scaffolds [Kumar *et al.*, 2010]. Chemical composition of the surface depicts the available functional species for interaction with proteins. For example, metallic biomaterials whose surfaces are oxidised expose metal and oxygen ions, as do ceramics and glass; polymer materials have functional groups present such as amino, carbonyl, carboxyl and aromatic groups. The presence of particular functional groups can determine the affinity of specific proteins or even a specific region of a protein to a biomaterial surface. Topographical features such as nanofibres expose a greater surface area for the adsorption of proteins [Roach *et al.*, 2006; Scopelliti *et al.*, 2010]; this can result in an increase of a local protein concentration at the

Chapter 1

biomaterial surface up to 1,000 times greater than in the bulk solution. Furthermore it has been demonstrated that introducing topography through increasing surface curvature on smaller substrates at the nano-scale, increased affinity of BSA and fibrinogen and lowered their saturation constants. Additionally, wettability also had an effect on protein adsorption ability; on flat surfaces BSA adsorbed in greater quantities on hydrophilic surfaces in comparison to hydrophobic surfaces [Roach *et al.*, 2006].

1.6.4 Nanotechnology

Nanotechnology is a field that has become popular and gained keen interest by many researchers from many fields. It was first introduced by Richard Feynman in 1959 who defined nanotechnology as "the understanding and control of matter at dimensions of 1-100nm (in at least one of their dimensions) where unique phenomena allow novel applications". The development of materials, devices and constructs within this size range is also regarded as nanotechnology [Khademhosseini *et al.*, 2007]. Fabrication approaches of nano-scale materials and devices are possible via two routes which are commonly known as top-down and bottom-down approaches. Nanostructures fabricated from a build-up of atoms or molecules in a controlled manner generally are considered as the bottom-up approach, whereas top-down approaches utilise micro-technologies to fabricate these nanostructures [Khademhosseini *et al.*, 2007]. Nanotechnology has an important role in numerous applications including: energy storage, healthcare, biotechnology, environmental engineering, and defense and security [Ramakrishna *et al.*, 2006].

Chapter 1

1.6.4.1 Applications of Nanotechnology in Tissue Engineering and Human Embryonic

Stem cells

Nanotechnology in tissue engineering aims to create structures at the atomic and molecular levels with a size range of 10-500 nm [Prabhakaran *et al.*, 2012]. The natural 3D stem cell niche and ECM at the nano-scale level is very dynamic and has a complex mixture of pores, pits and a network of intricate nanofibres composed from various structural proteins including collagen fibrils which all provide fundamental cues at the cellular level that support and regulate various cell functions and activity as a consequence of topographical features [Prabhakaran *et al.*, 2012].

Cells are highly sensitive to the local nanoscale ECM patterns and topography and can probe these features using their filopodia which can strongly encourage the retention of cell shape or induce changes resulting in subsequent differentiation via cytoskeletal arrangement modification [Howard *et al.*, 2008; Prabhakaran *et al.*, 2012; Stevens and George, 2005]. Typically, cells are tens of micrometers in diameter but have components such as cytoskeletal elements and transmembrane proteins that are nano-sized. Furthermore, it has been stated that stem cells have the ability to react with features as small as 5 nm and thus are highly sensitive to nanotopography [Biggs *et al.*, 2010]. Anisotropic topography is also considered important at the nanoscale level in ECM where cells in tissues such as nerve, cardiac and tendon require to be highly organised which directs secreted ECM and tissues structure organisation from nanoscale through to macroscale levels [Lim and Mao, 2009]. With relevance to tissue engineering applications, this architecture provides an important model for the design of artificial synthetic scaffolds which can support, instruct and guide the behaviour of cells [Liao *et al.*, 2008; Stevens and George, 2005].

Chapter 1

Nanotechnology enables to provide artificial templates which are able to mimic the architecture and topographical structure of the native ECM as closely and accurately as possible. This enables the expectation of a cell response and behaviour to be similar to as it would react or perform *in vivo,* in its natural environment. Scaffolds fabricated with a nanotexture such as nanofibres, whose topography can also be controlled are able to mimic this natural ECM architecture and provide a high surface area to volume ratio with a microporous structure [Vasita and Katti, 2006]. This has known to enhance cell adhesion and biomimetic properties, in turn attract stem cells, support stem cell activities such as proliferation, differentiation and also provide appropriate functioning of tissues (Figure 1.8) [Liao *et al.*, 2008; Prabhakaran *et al.*, 2012]. Various techniques are available to fabricate nanofibres including template synthesis, drawing, self-assembly, phase separation and electrospinning; the pros and cons of these methods are summarised in Table 1.10.

Chapter 1
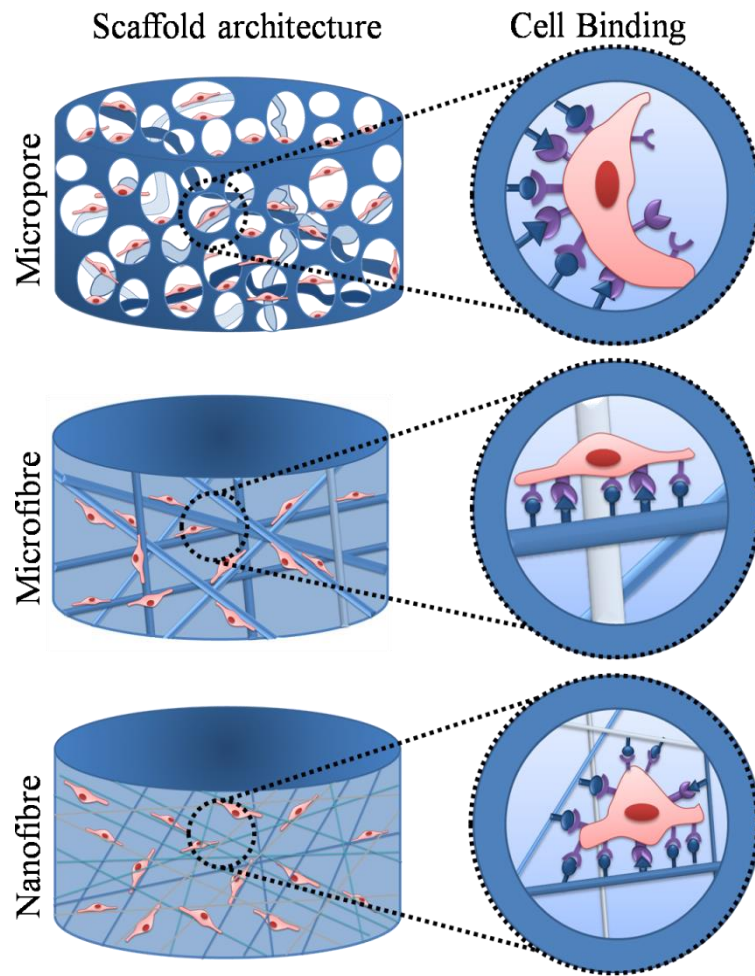
Figure 1.8 Nano-scale topography and architecture influence on cell attachment abilities. Adapted from Stevens and George., 2005.

Chapter 1

Table 1.10 Available techniques for fabricating nanofibrous substrates [Ramakrishna *et al.*, 2005].

Nanofibre Fabrication Technology	Description of Technique	Reference
Self-Assembly	**Method**: Autonomous organisation of individual constituents in an organised structure or pattern without human intervention. This occurs through non-covalent forces such as hydrogen bonding, electrostatic forces, or hydrophobic forces. **Advantages**: Extremely fine nanofibres. **Disadvantages**: Limited amphiphilic materials, random/very short nanofibres and questionable ability for large-scale production of consistent fibre dimensions.	[Liao *et al.*, 2008; Prabhakaran *et al.*, 2012]
Phase Separation	**Method:** Two different phases of materials are combined and mixed together; after solidification process of this mixture the removal of one phase (solvent) leaves the remaining phase material with pores. **Advantages**: Simple set-up polymer adjustable properties which allows a production of microporous substrates only. **Disadvantages**: Time consuming, only applicable to a limited number of polymers that produces inconsistent fibre dimensions. Usually used for the production of microfibrous substrates.	[Ma and Zhang, 1999]
Template Synthesis	**Method:** Template with certain dimensions used through which a material is extruded into another non-interacting material. **Advantages**: Able to produce fibres with variable length and size from a variety of polymers **Disadvantages:** A complicated process that has the inability to produce fibres that are continuous and feasible for small scale production	[Feng *et al.*, 2002]
Drawing	**Method**: Micropipette used to extrude out a fibre from a polymer droplet **Advantages:** A simple set-up which allows the production of fine fibres possible **Disadvantages:** Can only use viscoelastic materials, which are able to resist shear stresses applied on the material. Inconsistent production of fibres	[Nain *et al.*, 2006]
Electrospinning	**Method:** Use of an electrode which polarises a polymer solution drawn through a needle and deposited onto an oppositely polarised or ground electrode collector. **Advantages:** Simple system, versatile, affordable and cost-effective. Long fibres can be fabricated from various materials including natural, synthetic and composite polymers from nano to micro-scale. Precise control of fibre diameter and allows large-scale production of tissue engineering scaffolds on an industrial level. **Disadvantages:** fibre production rate, although considered to be faster than other production methods mentioned above. Difficult to control steadiness of the jet causing subsequent changes in fibre morphology	[Prabhakaran *et al.*, 2012] [Ramakrishna *et al.*, 2005]

Chapter 1

1.7 Electrospinning

Nanofibres have great implications for tissue engineering, in both research and industrial settings. Specifically, electrospinning has attracted great attention by the regenerative medicine field, in both academia and industry due to its unique ability to generate nanofibres from a variety of materials (including synthetic biodegradable and natural polymers). Electrospinning has the ability to form various fibrous structures that are able to provide an excellent supportive, framework for stem cell adhesion, proliferation and differentiation [Prabhakaran *et al.*, 2012; Ramakrishna *et al.*, 2006]. Other benefits of electrospinning include: high production rate of nanofibrous substrates, can be fabricated to fill any anatomical defect shape, a simple set-up and versatile procedure, architecture provides appropriate mechanical properties to support various cell activities, formation of highly porous mesh', production of fibres from micro to nano-scales and their large surface area to volume ratio (100 m^2/g). High surface area to volume ratio provides the ability to enhance protein adsorption activity onto the surface of these nanofibrous substrates causing subsequent enhancement in cell adhesion properties thus providing an availability of recognition sites for cells to attach, spread and expand.

1.7.1 Electrospinning Method

The electrospinning process utilises a polymer solution which is charged up using high voltage electrodes which allows the polymer to be drawn from a needle (nozzle) and is accelerated towards an oppositely charged or grounded collecting substrate [Toh *et al.*, 2006]. During flight from the needle to the collector, the intensity of the electric field pulls the polymer solution by forming a Taylor cone from the needle. Once the electric field over powers the surface tension of the polymer, this results in the formation of an instable

Chapter 1

jet which during flight undergoes whipping and solvent evaporation causing the deposition of finer fibres on the collecting substrate [Toh *et al.*, 2006]. A schematic of a basic electrospinning set-up is shown in Figure 1.9.
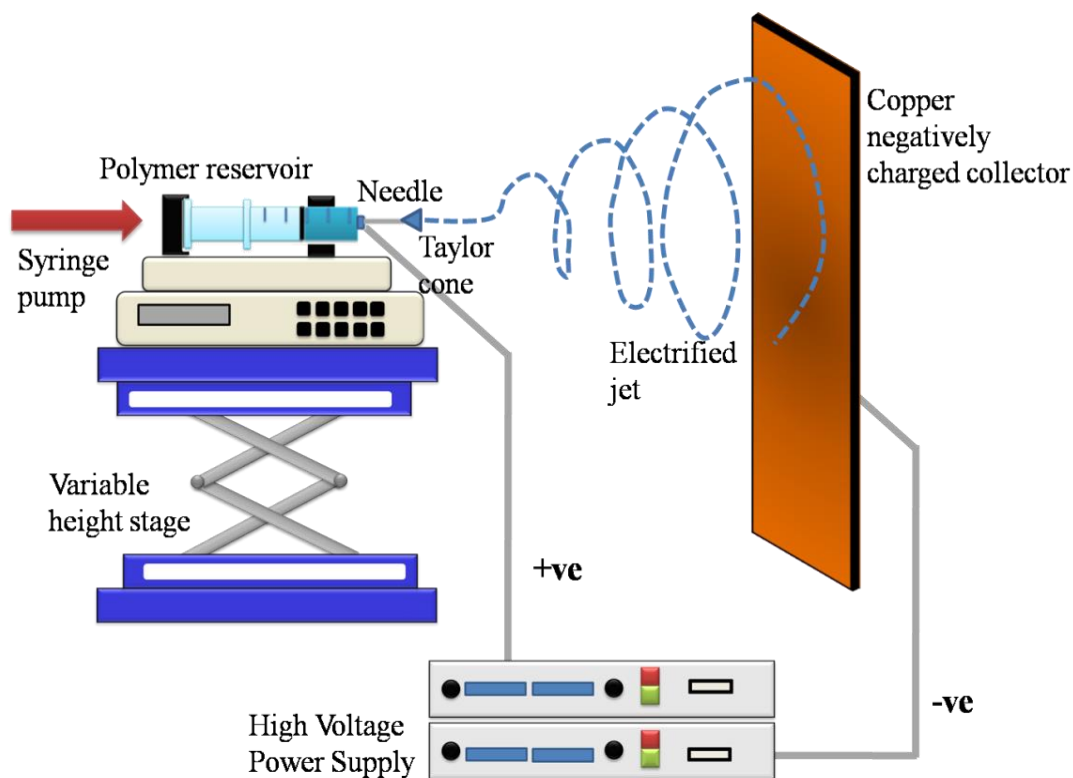
Figure 1.9 A schematic of a basic electrospinning set-up. Adapted from Ramakrishna *et al*., 2006.

1.7.2 Electrospinning Parameters

Properties of electrospun nanofibres such as fibre diameter and morphology can be controlled by manipulating a range of electrospinning parameters, broadly categorised as solution, operating and environmental parameters.

Chapter 1

1.7.2.1 Polymer solution Parameters

These parameters are perhaps the most important and have a significant effect and influence on the overall electrospinning system. Polymer solution parameters can have a direct influence on the morphology of the nanofibres.

1.7.2.1.1 Viscosity, Concentration, Surface Tension and Solution Conductivity

Higher the number of monomers (single unit) within a polymer results in a higher molecular weight (M_w) and length of the polymer. Increasing the M_w and length causes a subsequent increase in viscosity due to an increase in the number of entanglements between the polymer chains. It is a necessity for the polymer solution to be of adequate M_w and sufficient viscosity, otherwise upon exposure to an intense electric field, if there are not enough entanglements between the molecule chains to resist the electrostatic repulsion force, this results in the extrusion jet to break up and not maintain a continuous jet resulting in the formation of shorter length fibres with inconsistency in fibre diameter and beaded morphology. Extreme consequences would result in electrospraying with little or no deposition of fibres on the collector [Sill and von Recum, 2008].

Alternatively, the polymer concentration can also increase the viscosity; this enables greater entanglements between the polymer chains within the solution which during electrospinning prevents the jet breaking up and remains continuously intact. The concentration of a polymer at lower M_w can determine the spinnability of the solution as well as the viscosity and surface tension [Sill and von Recum, 2008]. For example,

Chapter 1

changing the polymer concentration of PCL ($M_w = 80,000$) from 13% to 10% resulted in change in fibre morphology from uniform fibres to beaded fibres [Lee *et al.*, 2003].

On the contrary, if the viscosity of the polymer is too high, this increases the number of polymer chain entanglements to such an extent that it becomes difficult to produce a high enough electric field intensity that overcomes the surface tension causing prevention of the polymer solution to be drawn out of the needle tip. However, suitable viscosity is desirable, as when charge is applied to the solution this results in more polymer chain entanglements and thus is able to extrude better as well as allowing distribution of solvent molecules amongst the polymer chains thus presenting a lower surface tension [Ramakrishna *et al.*, 2005]. Furthermore, it has been demonstrated that increasing the viscosity or concentration subsequently increases the fibre diameter as a result of increased number of entanglements giving a greater resistance to the polymer solution to be stretched by the electrostatic force. As viscosity can be increased as a result of an increase in concentration, this can decrease the amount of bending instability thus reducing the polymer path to the collector [Greiner and Wendorff, 2007].

Electrospinning is initiated if the charged jet of polymer solution is greater than its surface attractive force to the surface of the capillary; this is referred to as surface tension. Depending on polymer solution properties, surface tension can sometimes cause the jet to form beads in within the nanofibres. This is a result of surface tension which aims to decrease the surface area per unit mass of a fluid. Bead-like fibres form in situations where the polymer solution is of a low viscosity, or where there a high number of solvent molecules that are free to move and have not been distributed well over the entangled

Chapter 1

polymer molecules. These solvent molecules instead prefer to congregate together and adapt a spherical shape due to surface tension [Ramakrishna *et al.*, 2005]. On the hand, where the viscosity of the polymer solution is higher, there is better distribution of the solvent molecules amongst the polymer molecule chains and thus during extrusion force, this reduces the chances of the solvent molecules accumulating together thus preventing the increase in surface tension. Surface tension can also be decreased by using a solvent with appropriate properties.

Polymer solution is able to be drawn out during electrospinning as a result of charges at the surface repelling each other. Therefore, increasing the charge number carried by the jet causes a subsequent increase in its conductivity. The incorporation of additional ions to the polymer solution through salts or a polyelectrolyte provide increased solution conductivity which permits a better extrusion force, resulting in much smoother, thinner fibres and prevention beaded morphology which occur due to insufficient stretching of the polymer solution [Keun Kwon *et al.*, 2005; Zuo *et al.*, 2005]. Furthermore, this also decreases the critical voltage at which the jet needs to be initiated and electrospun. However, increasing solution conductivity can result in bending instability of the jet giving rise to a larger fibre deposition area on the collector. Bending stability increases the pathway of the jet resulting in fibres with a smaller diameter [Zuo *et al.*, 2005]. Various solvents are used to increase conductivity [Fong *et al.*, 1999] including: dimethylformamide (1.090 mS/m), methanol (0.1207 mS/m) and ethanol (0.0554 mS/m).

Solvent properties can also have an impact on the production of nanofibres via electrospinning. An important property is the dielectric constant which is the ratio of the

permittivity of a substance to the permittivity of free space. An increase in dielectric constant can increase the electric flux density in the substance and can prevent the formation of beads. Addtionally, it can also encourage the reduction in fibre diameter. However, at the same time increasing dielectric property increases bending instability, the jet pathway and thus resulting in a greater deposition area of the fibres on the collector [Zuo *et al.*, 2005]. For example, dimethylformamide has a high dielectric constant (36.71) in comparison to acetic acid (6.15) and chloroform (4.80) [Ramakrishna *et al.*, 2005].

1.7.2.2 Processing Parameters

Electrospinning has many processing parameters which are important to control and can influence the characteristics of the fibres produced.

1.7.2.2.1 Voltage

The polymer solution jet is initiated by the voltage supply which stimulates the charges present in the solution; by the use of an external electric field this results in the electrostatic repulsion force to become greater than the solutions surface tension. Whether positive or negative, an applied high voltage causes the drop of polymer solution located at the needle tip to stretch and distort into a shape referred to as the Taylor cone, once the electrospinning jet has been established. A sufficient and adequate voltage supply will provide a stable Taylor cone and the electrostatic repulsion forces in the jet then become greater than the viscoelastic force and surface tension resulting in the ejection of the polymer solution from the Taylor cone [Taylor, 1964]. Increasing the voltage increases the amount of charge, which subsequently provides a faster ejection of the polymer solution from the needle tip. However, increasing the voltage can also unstable and reduce the

Chapter 1

Taylor cone. Increased voltage and the resultant electric field both have an effect on the stretching and speed of the jet which in turn has an influence on fibre morphology, as a result of voltage increasing the energy carried by the charge which provides a greater columbic repulsive forces in the jet and a more intense electric field due to a greater potential difference [Beachley and Wen, 2009].

At higher voltages, the polymer jet undergoes greater stretching, subsequently resulting in a reduction in fibre diameter and accelerated solvent evaporation giving rise to drier fibres. This is particularly the case with low viscosity polymers where secondary jets are visible resulting in thinner fibres. Alternatively, thinner fibres can be generated by reducing the voltage which causes deceleration of the jet and thus increasing the jet path flight time; an increase in jet path time allows the polymer jet to stretch and elongate for a longer time and thus giving rise to fibres with a reduced fibre diameter [Beachley and Wen, 2009]. However, high voltages on high viscosity polymers increases the bending instability due to the movement of the Taylor cone into the needle resulting in greater bead density within fibres which can at extremely high voltages even merge together and produce thicker beads; as voltage can directly have an effect on the shape of the Taylor cone this can therefore dictate the morphology of the electrospun fibres. Other effects of increasing voltage also include the electrostatic field encouraging a more ordered alignment of the polymer molecules causing changes in crystallinity properties of the formulated polymer fibres on the collector. Electric field induced through applied voltage effects are sinusoidal and hence there is an optimum range for a specific polymer solvent system, which above or below this optimum range can result in beaded fibres [Sill and von Recum, 2008].

Chapter 1

1.7.2.2.2 Flow Rate

Flow rate is defined as the volume of polymer solution which passes through the needle per unit time. It is imperative to identify and match the correct voltage and flow rate to maintain a stable Taylor cone throughout the process. However, should the flow rate be increased with a constant voltage this can result in thicker fibres or greater bead size due to a greater volume of polymer solution being extruded from the needle tip at one time [Ramakrishna *et al.*, 2005]. It is generally preferred to keep the flow rate slow to allow sufficient evaporation of the solvents and increases the jet pathway time to obtain drier fibres [Greiner and Wendorff, 2007; Sill and von Recum, 2008].
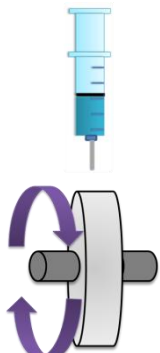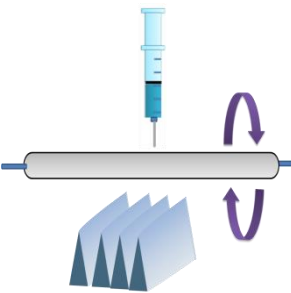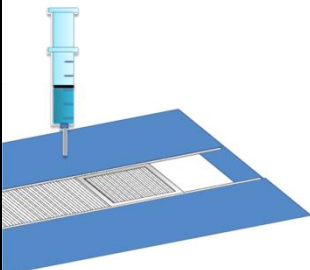
1.7.2.2.3 Working Distance

Working distance is defined as the jet pathway distance from the needle tip to the collector; this also has a direct effect on the jet pathway time as well as the strength of the electric field. Increasing the working distance subsequently increases the jet pathway time as well as decreasing the electric field strength. On the contrary, decreasing the working distance reduces the jet pathway but also increases the electric field intensity which accelerates the jet (allowing less time for solvent evaporation). Therefore, it is apparent that either decreasing the working distance or increasing the voltage both has the same effect which is to increase the strength of the electric field [Ramakrishna *et al.*, 2005]. Working distance can influence the diameter of the fibres; fibre diameter can be decreased by increasing the polymer jet pathway which increases the time for it to be stretched and elongated before deposition onto the collector [Beachley and Wen, 2009].

Chapter 1

1.7.2.2.4 Effect of Collector

Electrospun fibres are deposited onto a collector which is either oppositely charged to the ejection site at the needle tip or is grounded. The collector is electrically conductive and is usually covered with aluminium foil to maintain a potential difference. Furthermore, conductive collectors allow charge dissipation thus yielding a greater number of fibres closer together rather a non-conducting collector where charge accumulates causing repulsion of fibres resulting in a lower yield of fibres [Ramakrishna *et al.*, 2005]. The type of collector can determine the type of fibres attained; a simple change such as a static collector versus a moving collector can have dramatic effects. Generally, a static collector allows the production of random nanofibres whereas moving collectors allow the production of aligned nanofibres that are also drier as rotation increases evaporation time. There are various methods by which aligned nanofibres can be attained including: rotating mandrel, knife-edge disk, auxillary electrode and parallel conducting collector; these techniques are summarised in Table 1.11

Chapter 1

Table 1.11 A summary of various modified methods of electrospinning to attain aligned nanofibrous substrates.

Method	Schematic	Description	Reference
Rotating mandrel		A simple set-up where a mandrel is attached to a motor which allows rotation at high speed (1000 rpm) resulting in the accumulation of fibres around the circumference. A large area of aligned fibres can be fabricated and the degree of alignment can varied depending on rotation speed	[Ashammakhi *et al.*, 2009; Boland *et al.*, 2004; Matthews *et al.*, 2002]
Disc collector		A simple set-up where a rotating disc with a small deposition area is used. Allows the fabrication of highly aligned fibres. However, difficult to maintain high alignment of fibres as deposition becomes thicker. Only a small area of deposition.	[Zussman *et al.*, 2003]
Rotating tube collector with knife-edge electrodes		Knife-edged blades attached to a negative high electrode and a rotating mandrel directly in front is used to attain highly aligned nanofibres which cover the whole mandrel. This allows a thicker layer of aligned fibres and the rotating tube has to be of small diameter.	[Teo and Ramakrishna, 2006]
Parallel conducting collector		A static simple set-up where two parallel conducting electrodes are placed with a gap between them. This allows easy fabrication of highly aligned fibres which can also be transferrable to another substrate. However, limitations of this method include a limit in the length of the aligned fibres	[Ashammakhi *et al.*, 2009; Teo and Ramakrishna, 2005]

Chapter 1

1.7.2.3 Environmental Parameters

Polymer solution and processing parameters have the greatest impact and effect on fibre morphology and diameter; however, environmental parameters can also have an influence. Environmental parameters include: humidity, temperature, type of atmosphere and pressure; these have been summarised in Table 1.12.

Table 1.12 A summary of environmental parameters that have an impact on the electrospinning process. Adapted from [Ramakrishna *et al.*, 2005]

Environmental Parameter	Effects on Electrospinning Process
Humidity	Determines amount of water that condenses onto the polymer fibre surfaces which can disrupt the rate of solvent evaporation. High humidity results in slower evaporation of the solvent whereas low humidity would speed up evaporation thus providing drier fibres.
Temperature	Two major effects can occur as a result of increased temperature; evaporation rate of solvent is increased thus producing drier and more uniform fibres, and also reduces the viscosity of the polymer solution which is able to provide a greater extrusion force as the polymer molecules are more mobile thus allowing the jet to stretch greater resulting in thinner fibres.
Type of atmosphere	Air is made of various gases including oxygen and nitrogen which can also influence the electrospinning process. The electric field has an effect on the gases themselves; an example is Helium which can breakdown under high electrostatic fields allowing the process to proceed.
Pressure	The correct pressure is also important during electrospinning; if the surrounding pressure of the jet is lower than the atmosphere pressure this will cause the solution to be unstable and just seep out without proper jet initiation.

1.7.3 Applications of Electrospun Nanofibre Scaffolds with Stem cells

Many studies have investigated the ability to expand and culture various stem cells on synthetic polymer electrospun nanofibrous substrates. Aligned electrospun nanofibres fabricated from polymers such as PLLA, PLAGA, PCL and PCL/collagen blends have all demonstrated to induce the differentiation of neural stem cells towards nerve cells.

Chapter 1

Alignment and topography are particularly important parameters for the application of neural tissue engineering where the anisotropic organisation of the fibres encourages and increases neurite outgrowth in the direction parallel to the fibres when compared to random nanofibres and controls (flat surfaces without topography) Other factors which were also identified to increase neurite outgrowth in terms of topography included fibres with a narrower diameter and increased anisotropy of fibres which also resulted in increased cell attachment and differentiation [Schnell *et al.*, 2007]. Human cord-blood derived somatic stem cells have also been cultured on electrospun PCL random nanofibres; in this study stem cells were successfully differentiated *in vitro* towards hepatocyte-like cells using inducing factor media for 6 weeks. Typical endoderm hepatic markers (albumin, glycogen storage and α-fetoprotein) were expressed positively via immunostaining expression markers were positively stained via immunostaining [Hashemi *et al.*, 2009].

hMSCs are a popular source of stem cells due to their potential to differentiate into various skeletal lineages, availability and immunoprivilige [Rose and Oreffo, 2002]. Introducing topography via electrospun nanofibres from various polymer including: PLDLA, PLGA, PCL and poly vinyl alchohol induced the differentiation of hMSCs towards osteogenesis, chondrogenesis and adipogenesis after 21 days of culture in relevant chemical supplements. Histological staining via von kossa and alizarin red (bone), alcian blue (cartilage) and oil red O (fat) confirmed hMSC differentiation which was cross-vailidated by PCR analysis of specific markers for each tissue type [Li *et al.*, 2005; Wimpenny *et al.*, 2010].

Chapter 1

Current limitations associated with stem cells include; efficiency of expansion and adequate numbers suitable for clinical therapeutic use. To overcome this limitation, many researchers have attempted to expand stem cells using nanofibrous substrates. Bone marrow-derived hematopoietic stem cells have non-adherent properties and their current conventional culture methods have several limitations including maintaining cell localisation. The use of electrospun nanofibres have displayed promising results to overcome these limitations where collagen I blended PLGA nanofibres were able to significantly increase stem cell capture and enhance their proliferation activity [Ma *et al.*, 2008]. Undifferentiated umbilical cord stem cells have successfully been expanded on electrospun polyethersulfone (PES) nanofibres (Ø 627 nm). PES is generally hydrophobic and thus through surface treatment and collagen grafting, this improved its biocompatibility resulting in subsequent provision of attachment sites to enhance cell adhesion. This resulted in cell attachment and infiltration of the stem cells into the scaffold whilst retaining its typical cell phenotype morphology [Shabani *et al.*, 2009].

Electrospun, ultra-fine fibres (Ø 500-800nm) fabricated from PLGA with a tensile modulus of 323.145 MPa and an ultimate tensile stress of 22.67 MPa had a similar morphology to fibres found in the natural ECM. This substrate supported the successful adhesion and proliferation of hMSCs (up to day 10), whilst maintaining their typical phenotypic morphology and multipotency [Li *et al.*, 2002]. hMSCs can also expand whilst retaining their stemness on electrospun silk fibroin–based fibre matrices (Ø 700 nm). These fibres demonstrated suitable biocompatibility adequate to support hMSC adhesion and proliferation up to 14 days of culture [Jin *et al.*, 2004]. However, many of the above studies have investigated hMSCs that have been already recovered from bone marrow aspirate, isolated and expanded on TCP before seeding and culturing onto alternative

Chapter 1

substrates such as electrospun nanofibres. An improved one-step direct method of hMSC recovery and isolation from bone marrow aspirate has been successfully performed by our research group, previously. Here, bone marrow aspirate was directly seeded onto electrospun PLDLA (Ø 478 – 645 nm), PLGA (Ø 96.3 – 2000 nm) and PCL (Ø 222 – 275 nm) nano to sub-micron fibre scaffolds in both aligned and random conformations and expanded for 3 weeks in either 2% or 21% O_2 to recover undifferentiated hMSCs. Results demonstrated, overall a greater number of hMSC colony recovery in 2% O_2 rather than 21% O_2, on all substrates. Furthermore, aligned nanofibres supported greater hMSC colony recovery relative to their random counterparts; overall, PLGA and PCL aligned substrates which also had the smallest fibre diameter provided the best performance [Wimpenny *et al.*, 2010]. Early adhesive efficiency of hMSCs has also been enhanced through nanotopography on collagen-coated P(LLA-CL) electrospun nanofibres, where topography demonstrated to significantly improve hMSC attachment after 30 minutes of seeding onto the substrates, relative to flat collagen or gelatin coated coverslips [Chan *et al.*, 2009]. Thus, it is apparent that topography (such as aligned nanofibres) is not only effective for inducing the differentiation of stem cells towards various lineages but can also enhance stem cell adhesion and proliferative properties whilst retaining their stemness. Additionally, it appears that fibre diameter also influences the adhesion and expansion ability of stem cells, where the narrower fibres are accurately mimicking the native ECM nanofibrils.

With regards to embryonic stem cells, a limited number of investigations have explored the ability of electrospun nanofibrous scaffolds to support their activity including attachment, proliferation and differentiation and hence is still a very much unexplored area. Perhaps, the reason for this is due to various complications associated with the complex

Chapter 1

conventional culture of expanding ESCs and the partial understanding of the exact mechanisms associated with controlling embryonic stem cell behaviour. For this reason, many studies have found it easier to differentiate embryonic stem cells towards countless lineages, as they have potential to transform into specialised cell types of all three germ layers. For example, PLLA nanofibres were able to successfully differentiate mESCs towards the osteogenic lineage and expressed bone specific markers such as calcium and osteocalcin [Smith *et al.*, 2009]. Considerable attention has been given to the application of electrospun nanofibres for nerve regeneration, as electrospinning provides the ability to generate nanofibres with great degree of anisotropy and alignment which provides topographical cues to induce and direct the differentiation of ESCs towards nerve cells [Prabhakaran *et al.*, 2012]. Electrospun polyurethane nanofibrous scaffolds (150 μm thickness, 84 % porosity and 360 nm fibre Ø) supported the initial adhesion and undifferentiated expansion of hESCs, which were then differentiated towards neurones by culturing in neurobasal A basal media supplemented with 1% B27, 1% N2, epidermal growth factor (EGF) and bFGF for up to 47 days [Carlberg *et al.*, 2009]. Similarly, neurospheres generated from hESCs were cultured onto PLDLA electrospun nanofibrous 3D scaffolds (thin structures of 2-3 fibre thickness; thick structures of >10 fibre thickness); observations here included enhanced neuron growth on the thicker scaffolds relative to thinner scaffolds. Cells had a typical morphology for neuronal cells and followed fibre orientation [Yla-Outinen *et al.*, 2010]. Due to the difficulty of hESCs adhering to synthetic substrates, alternative methods have included inducing embryoid body formation and then seeding these embryoid bodies onto electrospun nanofibrous substrates in combination with biochemical cues to induce their differentiation into specific lineages. Examples include electropsun nanofibre scaffolds from PLA which supported the differentiation of hESC-derived EB cells in the presence of osteogenic media towards osteogenesis and

implanted subcutaneously to the back of immunodeficient mice for 5 weeks. Observations included discrete mineralisation expression of typical bone markers including osteocalcin [Bielby *et al.*, 2004]. PCL aligned and random electrospun nanofibres have successfully supported the differentiation of hESC-derived EBs into neural progenitors in the presence of neurobasal media (supplemented with B27); aligned nanofibres particularly enhanced the neurite outgrowth which was directed parallel to the orientation of the nanofibres [Xie *et al.*, 2009].

However, there are a limited number of studies that have attempted to culture and expand undifferentiated embryonic stem cells (mouse and human origin) on electrospun synthetic nanofibrous substrates, specifically of human origin. A few attempts have been made using synthetic biodegradable polymers such as PCL, polyurethane and polyamide. Furthermore, composite polymers where natural polymers such as collagen and gelatin have been electrospun with synthetic polymers such as PCL have successfully enhanced the adhesion properties of the nanofibres resulting in attachment and expansion of undifferentiated ESCs. It has also been identified that the geometry and topography of the electrospun nanofibres alone was sufficient to support of significantly larger colonies of undifferentiated ESCs in comparison to controls such as glass coverlips and relative polymer films [Nur-E-Kamal *et al.*, 2006]. A summary of studies which have attempted to culture ESCs on electrospun nanofibrous substrates is stated in Table 1.13.

Chapter 1

Table 1.13 A summary of electrospun nanorfibrous substrates fabricated from various synthetic polymers to culture, expand and differentiate embryonic stem cells.

Synthetic Nanofibrous Substrates	Substrate properties	hESC Line	Observations	Reference
Polyurethane	150 µm thickness Exhibited high porosity 84 % Pore size 5-6 and 1 µm Fibre Ø 360 nm	SA002	Undifferentiated hESCs were cultured and expanded on scaffolds (in hESC media for 5-7 days) and then induced to differentiate (using neurobasal media supplemented with 1 % B27 and 1 % N2) towards neurones for up to 47 days. Differentiation confirmed by positive immunostaining of dopaminergic tyrosine hydroxylase	[Carlberg *et al.*, 2009]
PCL	Random and aligned nanofibres on coverslips Fibre Ø 250 nm	mESCs	ESCs induced to form embryoid bodies which were seeded onto the nanofibrous substrates and induced to differentiate towards neurons using retinoic acid and neural basal media. After 14 days expression of neuron marker Tuj1 was visible. Direct seeding of ESCs without forming EBs displayed that using retinoic acid and culturing in neural basal media with B27 supplement ESCs formed aggregates on both aligned and random nanofibrous substrates	[Xie *et al.*, 2009]
PCL/collagen and PCL/gelatin	Random topography nanofibrous substrates. PCL/collagen (Ø 275 nm) and PCL/gelatin (Ø 283 nm) fibre diameters	HES3	hESCs were grown in the presence of MEFs. Larger hESC colonies were supported on both substrates with increased cell growth by 47.58% and 40.18% for (PCL/collagen and PCL /gelatin, respectively) in comparison to their control (hESCs on MEFs only). Colonies generated on substrates retained stemness characteristics. On aligned substrates cell migrated away from the EB an along the axis of the aligned fibres	[Gauthaman *et al.*, 2009]
PCL and calcium deficient hydroxyapatite	Electrospun nanohybrid mats (non-woven architecture) 2 and 55 wt.% of calcium hydroxyapatite content	mESCs	mESC response to nanohybrid PCL and calcium deficient hydroxyapatite substrates and neat PCL was evaluated. mESCs were able to adhere (although 45 % efficiency relative to control), expand in an undifferentiated, pluripotent state (Nanog and β-Tubilin) in a typical way	[Bianco *et al.*, 2009]

	Average fibre size 1.5 m, porosity 80-90 % and specific surface area $16m^2g^{-1}$			
PCL	Thickness of scaffold 200 µm. Porosity of ~ 88 %, Pore size 30 µm and average fibre diameter 691 nm	mESCs	mESCs differentiated towards adipogenesis using a 3D culture system. mESCs seeded into PCL matrices. mESCs seeded into PCL matrices sealed into transwell inserts with membrane removed and expanded for 2 days before 4-day treatment with RA, insulin and T_3 induction. Upon inducing differentiation morphology changed from fibroblastic to a spherical with evidence of lipid accumulation (Oil-red-O-staining) with confirmation using PPAR-γ marker. Migration and penetration of differentiated mESCs 40 µm deep into substrate	[Kang *et al.*, 2007]
Polyamide	A 3D Ultra-thin nanofibrous substrate	mESCs	Ultra-web nanofibrous substrates fabricated from polyamide demonstrated to support the expansion of significantly larger colonies of undifferentiated mESCs compared to glass coverslips and relative polymer film controls.	[Nur-E-Kamal *et al.*, 2006]

Despite the recent attempt to culture and expand hESCs on synthetic nanofibrous substrates; the use of purely synthetic FDA approved polymers such as PCL, PLGA and PLLA electrospun into aligned and random conformations are yet to be investigated with the combined effects of oxygen tension on the attachment and expansion of hESCs.

Chapter 1

1.8 Thesis Aims and Objectives

Electrospinning offers great potential in the field of tissue engineering to generate nano-scale scaffolds for many applications. By merging biomaterial technology with embryonic stem cell biology this may drive their potential use in clinical therapeutics by enhancing and improving the expansion capabilities of hESCs by the elimination of current associated limitations including retaining pluripotency, slow expansion rate and the use of xenogenic agents in culture.

The aims of this thesis are to:

- Develop a synthetic substrate of electrospun nanofibrous scaffolds from FDA approved polymers with different topographical conformations.

- Investigate the potential of these substrates to support the attachment and undifferentiated expansion and differentiation capacity of hESCs in combination with different oxygen tension exposures to identify the optimal materials related and culture environment related parameters suitable for hESC expansion.

- Characterise the underlying integrin mechanisms within hESCs that regulates their attachment to electrospun nanofibrous substrates.

- Identify proteins in relatively undefined ESC media which specifically interact with electrospun nanofibrous substrates and encourage their attachment.

Chapter 2

2. Materials and Methods

2.1 Electrospinning and Scaffold Fabrication

2.1.1 Electrospinning Set-up

All electrospinning was performed within a fume cupboard in accordance with local Health and Safety regulations and included interlocks and a voltage dissipater. The fundamental components of the electrospinner included, two high voltage power supplies (HVPS; Spellman HV, Pulborough, UK) which were connected in master-slave configuration (allowing an adjustment of voltage between $0 - 60kV$ and current between $0 - 5mA$); a calibrated syringe pump (KR Analytical, Sandbach, UK) to which a glass syringe with a stainless steel needle is attached and a negatively charged copper collection plate. An image of the electrospinning equipment is shown in Figure 2.1

2.1.2 Preparation of Polymer solutions

Electrospinning polymer solutions were prepared from Poly-L-lactic acid (PLA), poly-l,d lactic-glycolic acid (96L/4D; L:G 80/20 PLGA; Purac BV, Netherlands) and Poly-ε-caprolactone (PCL, Mw 80,000), purchased from Sigma, Poole, UK; Purac BV, Netherlands and Sigma, Poole, UK, respectively. Polymer solutions were prepared by initially dissolving each polymer (w/v) in chloroform (CHL) or dichloromethane (DCM) followed by the addition of electric charge using dimethylformamide (DMF). A summary of the concentration of polymer solutions and the solvents used to make those solutions are stated in Table 2.1. Outline of experiments performed using each of the polymers is briefly described in Figure 2.2.

Chapter 2
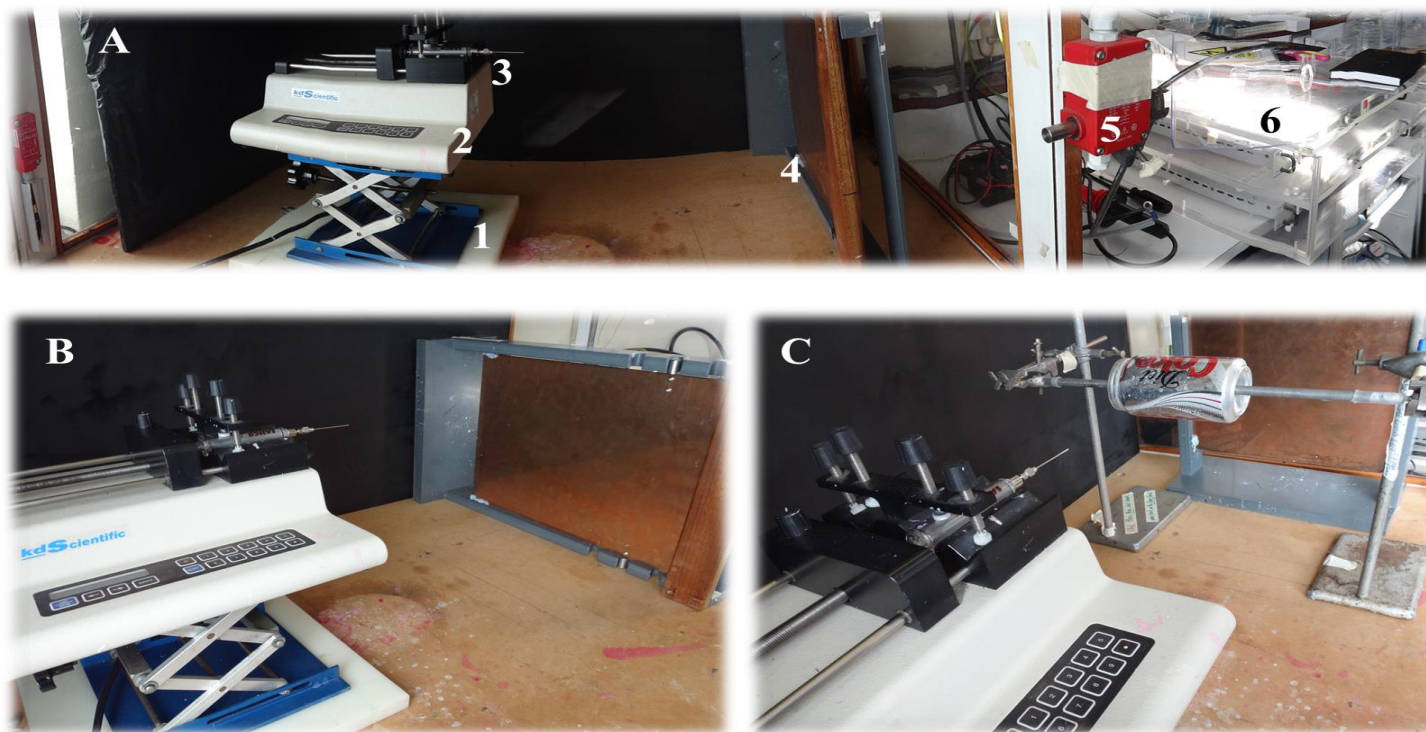
Figure 2.1 Image of the electrospinning set-up. (A) Showing the basic components of the electrospinner; (1) Adjusting platform, (2) Syringe pump, (3) Glass syringe with metal needle attached, (4) Copper plate collector, (5) Safety interlock and (6) External high voltage power supply; (B) Illustrates the electrospinning set-up for attaining random electrospun fibres and (C) demonstrates the rotating mandrel set-up for attaining aligned electrospun fibres.

Chapter 2

Table 2.1 Polymer solutions and the concentration at which they were prepared using solvents at specific ratios.

Polymer Solution	Solvent	Ratio
12.5% PCL	CHL and DMF	7:3
15% PCL	DCM and DMF	7:3
2% PLGA	CHL and DMF	7:3
7% PLLA	CHL and DMF	9:1

PCL   PLGA   PLLA

12.5 % PCL:
Optimisation of preferential material for hESC CFU expansion

Optimisation of preferential material for hESC CFU expansion

Optimisation of preferential material for hESC CFU expansion

12.5 % PCL:
Antibody αVβ5 blocked hESCs cultured on nanofibrous substrates

12.5 % PCL:
RT-PCR analysis of pluripotent markers and germ layer markers

12.5 % PCL:
Immunostaining and histology of pluripotent and differentiation markers respectively

15 % and 20 % PCL:
The effect of fiber diameter on the expansion of hESC CFUs

Figure 2.2 Flow diagram representing the experiments performed with each electrospun polymer solution.

Chapter 2

2.1.3 Fabrication of Random Electrospun Fibres

Electrospun random fibres were attained using the basic set-up as shown in Figure 2.1A and B. Polymer solutions were loaded into the glass syringe and spun using the parameters stated in Table 2.2. The copper plate was pre-covered with aluminium foil; 24 mm x 24 mm glass coverslips were attached to the collector directly opposite the syringe and fibres were spun and collected onto these coverslips.

Table 2.2 Electrospinning parameters used to attain random fibres for each polymer type

Polymer	Parameter			
	Needle	Flow Rate ml/min	Working Distance (cm)	Voltage (kV)
12.5% PCL	22G	0.01	15	4
15% PCL	18G	0.025	15	5
2% PLGA	22G	0.01	20	4
7% PLLA	18G	0.025	15	6

2.1.4 Fabrication of Aligned Electrospun Fibres

Electrospun aligned fibres were fabricated using the rotating mandrel method and the parameters for each polymer as stated in Table 2.3. This required a brief modification to the basic set-up as demonstrated in Figure 2.1C. A 10 mm aluminium rod functioned as an axle for the mandrel; the mandrel itself was a drink can (22 cm aluminium), sealed drum (0.95 mm diameter to ensure a firm fixation to the aluminium axle) which was drilled in the centre at both ends of the drum and fixated over the axle. A motor was connected to the axle using a modified plastic eppendorf and parafilm to ensure a tight, firm fit preventing the axle from slipping from the axle connector. A DC sourced voltage transformer with variable voltage (3-12 volts) was connected to the motor with *ca.* 5,250 rpm. The distal end

of the axle was firmly fixed using another eppendorf attached with a small hole in the conical end held in place with a smooth metal needle, preventing low friction during rotation of the mandrel. Finally, the whole rotating mandrel was held together and fixed in position using clamp stands.

Table 2.3 Electrospinning parameters used to attain aligned fibres for each polymer type.

Polymer	Parameter			
	Needle	**Flow Rate ml/min**	**Working Distance (cm)**	**Voltage (kV)**
12.5% PCL	22G	0.01	20	4.5
15% PCL	18G	0.025	20	6
2% PLGA	22G	0.01	20	3.5
7% PLLA	18G	0.025	20	7

2.1.5 Reinforcement of Electrospun Fibrous Scaffolds

Electrospun fibrous scaffold attachment on glass coverslips was further reinforced with silicone rubber strips (Silex Ltd, Borden, UK). These strips were adhered using silicone glue (RS Scientific, Corby, UK). Scaffolds were allowed to dry for 3-4 hours before sterilisation and cell seeding.

2.1.6 Sterilisation Process of Electrospun Fibrous Scaffolds

All electrospun fibrous scaffolds and controls were sterilised by immersion in 70% industrial methylated spirit (IMS) for at least one hour. After this, IMS was aspirated off

Chapter 2

and the scaffolds were air-dried in non-adherent petri dishes for one hour (Sterilin, Newport, UK).

2.2 Human Embryonic Stem Cell Culture

All experiments carried out in this thesis used human embryonic stem cells which were cultured using the feeder-free method as described below. Specifically, the cell line Sheffield 1 (SHEF1) was used for all experiments in this thesis

2.2.1 Extraction and Isolation of Mouse Embryonic Fibroblasts

Female mice at day 12.5-13.5 of pregnancy were first sacrificed before having the abdomen area sterilised using 70% ethanol and dissection performed using tools pre-swabbed in ethanol. Briefly, skin was removed from the stomach and an incision was made across the body (proximal to the legs) ensuring to slice on the skin layer. The skin layer was pulled back and a "V" shape cut was made towards the head in order to expose the internal regions. The uterine horn was removed with the filled purple sacs attached, and was cut open in order to detach the embryo's using sterile blunt forceps. After removing the heads, the bodies were placed in tubes containing Phosphate Buffer Saline (PBS) and Penicillin and Streptomycin (PS).

Within a sterile biological safety cabinet the embryos were removed from PBS + PS and placed onto a sterile petri dish lid. The viscera (red matter) was removed and the remaining material washed with a series of three PBS wash bath's in petri dishes. Each embryo was placed into a bijou containing 1% Trypsin and EDTA solution and incubated at 37 ºC for 5

minutes, vortexed and placed into the incubator at 37 ℃ for 5 minutes again. After vortexing, 3 ml of MEF medium (DMEM, 10% Fetal Bovine Serum, 1% L-Glutamine and 1% Non-essential amino acids) was added and the top 3 ml were removed and plated into a T_{75} flask with 12-15 ml of MEF media. Flasks were placed in incubators (37 ℃) overnight, after which a media change was performed.

MEFs were allowed to expand with a MEF media change every 3-4 days until a confluent monolayer of cells was achieved. MEFs were then trypsinised and cryopreserved in freeze media (90 % FBS + 10 % DMSO) until required. Briefly, a flask of cells were spun down to a pellet, resuspended in 1 ml of freeze media, transferred to cryovials and stored in a Mr Frosty overnight at -80 ℃ before storing in liquid nitrogen.

2.2.2 Conditioning Embryonic Stem Cell Media using Mouse Embryonic Fibroblasts

MEFs were resuscitated and expanded using MEF media until 50% confluence, after which point hESC media was conditioned. This comprised Knock-out DMEM (Gibco-Invitrogen, Paisley, UK) supplemented with 20% Knock-out Serum Replacement (Gibco-Invitrogen, UK), 1% L-glut (Lonza, Slough, UK), 1% NEAA (Lonza, Slough, UK), 4 ng/ml basic fibroblastic growth factor (bFGF; Lonza, Slough, UK) and 0.1 mM $\beta-$mercaptoethanol (Gibco-Invitrogen, UK). hESC media was conditioned overnight, collected, further supplemented with 4 ng/ml of bFGF, and sterile filtered (Millipore, Watford, UK) before use [Xu *et al.*, 2001].

2.2.3 Expansion of Human Embryonic Stem Cell Line SHEF 1

hESCs (SHEF 1) were resuscitated (Passage 32) and cultured on Matrigel™ coated flasks (BD Biosciences, Oxford, UK) and hESC conditioned culture media prepared as described previously and above in section 2.1.2 [Forsyth *et al.*, 2008]. T_{25} Flasks were coated with Matrigel™ (thawed from -20 ° C to -4 ° C) diluted at 1:100 using KO-DMEM and chilled stripettes (Gibco-Invitrogen, UK) for 1 hour at room temperature and then aspirated off. Media was changed daily and hESCs were generally passaged at a ratio of 1:2 every two-three days after reaching 90% confluence using a brief 0.25% Trypsin/EDTA treatment [Xu *et al.*, 2001]

hESCs were cultured and expanded in two different oxygen tensions; 2% O_2 (using a modular modification of a Galaxy R^+ incubator; RS Biotech, Irvine, UK, and 21% O_2 (Heraeus Cytoperm 2 incubator; Thermo Electron Corporation, UK).

2.3 Human Embryonic Stem Cell Culture on Electrospun Fibres

Electrospun scaffolds and controls (positive control; Matrigel™ coated coverslips and negative control; non-coated coverslips) were placed in non-adherent petri dishes (60 mm diameter; Corning, UK) and seeded with hESCs (SHEF 1, Passage 42-56), cultured and expanded in either 2% O_2 or 21% O_2 conditions. Cell density was 1700 cells/cm^2 per scaffold/control sample; this was determined to be the optimum by an experiment performed examining hESC Colony forming units (CFU) on Matrigel™ during a three week time period of culture at different seeding densities. hESCs were seeded in 500 μl of MEF conditioned hESC media, which was pipetted directly onto the nanofibre scaffold or

control coverslips. All samples were incubated in their relevant oxygen levels (2% O_2 or

21% O_2) overnight, after which, each petri dish was flooded with 6 ml of MEF-conditioned

hESC media and colonies were recovered over a 21 day period without a change of media.

For each sample type (controls and scaffolds), at each oxygen tension, n=3 (three

replicates) in 3 experimental repeats, unless stated otherwise.

2.3.1 Pluripotent Colony-Forming Unit Assay

An essential characteristic of stem cells expanding whilst maintaining their stemness is

their ability to expand as colonies. A stem cell colony is an indication that a stem cell is

able to self-renew whilst maintaining its undifferentiated state and expand in a tightly

packed homogenous cluster [Thomson *et al.*, 1998].

2.3.1.1 Giemsa Staining

After 21 days of culture, formed hESC CFUs on electrospun fibrous scaffolds and

Matrigel^{TM} substrates were washed twice with PBS, fixed in 95% methanol for 10 minutes

and immersed in 100% Giemsa stain (Catalogue # G5637; Sigma-Aldrich, Gillingham,

UK) and placed on a shaker (at low speed) for 30 minutes. All samples were washed

thoroughly with water to remove background staining. Samples were then subsequently

air-dried and colonies visually recorded by placing a dot with a marker pen on the

underside of the glass coverslip.

2.3.1.2 Alkaline Phosphatase Staining

hESCs were expanded at different cell densities (0, 1, 10, 100, 1000 and 10 000 cells/well),

in 6-well plates coated with Matrigel^{TM}, in either 2% O_2 or 21% O_2 for 21 days using

MEF-conditioned media. hESCs were washed once with PBS and fixed in 4% paraformaldehyde (prepared in PBS) for 1-2 minutes (any longer causes deactivation of alkaline phosphatase within the cells). Fixed hESCs were further rinsed using Tris-buffered Saline Tween-20; TBST) rinse buffer and treated with 500 µl/sample of alkaline phosphatase staining solution prepared using three components; Fast Red Violet, Naphthol AS-B1 Phosphate (4 mg/ml) in 2-Amino-2-methyl-1,3-propanediol buffer (AMPD; 2 mol/L at pH 9.5) and distilled water at a ratio of 2:1:1 as per manufacturer's instructions (Millipore, Catalogue # SCR004). Samples were incubated in the dark at room temperature for 15 minutes, washed with rinse buffer and stored in PBS for optical microscopy imaging.

2.3.2 Embryoid Body Formation

hESCs were expanded in a T_{25} flask until confluence, trypsinised and seeded into a non-adherent 60 mm petri dish. hESCs were flooded in with 10 ml of ES conditioned media and incubated overnight in order to allow hESCs to aggregate together. hESC aggregates and media were collected and transferred into a centrifuge tube and allowed to stand for 10 minutes; ES conditioned media was removed carefully and replaced with 10 ml of basic media composed of; DMEM, 10% FBS, % L-glut and 1% NEAA. Aggregates and media were transferred into a non-adherent petri dish and incubated for 5 days without changing media. After 5 days, EBs were transferred into gelatin coated adherent petri dishes with fresh spontaneous differentiation media. After 21 days of expansion, media was removed and EBs fixed in 10% Formalin for 10 minutes before being immersed in 100% Giemsa stain for 30 minutes. EBs were washed thoroughly with water to remove background staining and air-dried before imaging.

2.3.3 Differentiation of Human Embryonic Stem Cells

For all differentiation studies, hESCs were cultured for a period of 21 days on electrospun PCL nanofibre substrates and Matrigel^{TM} coated glass coverslips, in physiological normoxia (2% O_2); hESC colonies were then induced to differentiate into specialised mesodermal germ layer lineages (Adipogenesis, Chondrogenesis and Osteogenesis) using chemical cues in the form of supplemented media for respective differentiation lineages, for a further 21 days in physiological normoxic (2% O_2) conditions. MEF-conditioned media was removed from all samples, washed with PBS and immersed in corresponding differentiating media's where media changes took place every three days.

2.3.3.1 Spontaneous Differentiation

Spontaneous differentiation media was composed of knock-out DMEM, 10% FBS, 1% L-Glut, 1% NEAA and 0.1 mM β-mercaptoethanol.

2.3.3.1.1 RT-PCR

After 21 days of hESC culture on electrospun nanofibre substrates and Matrigel^{TM} controls, in physiological normoxic conditions and spontaneous differentiation media; cell lysis was performed *in situ* at 0, 5, 10 and 20 days of culture in spontaneous media for subsequent RNA extraction. Cell lysates were prepared and homogenised as per manufacturer's protocol (RNeasy, Qiagen, Crawley, UK). Briefly, cells were lysed in 350μl RLT buffer (prepared in 70% ethanol) and 10 μl/ml of β-mercaptoethanol, centrifuged for 2 minutes at full power and stored at -80 °C until RNA extraction is required.

2.3.3.1.2 RNA Extraction and Quantification

Cell lysates were removed from -80 °C and thawed on ice. Lysates volume samples underwent a series of centrifugation steps and washes in RW^1 and RPE buffer, and water as provided by the RNAeasy Mini Kit (Qiagen, Crawley) according to manufacturer's instructions. Samples placed in eppendorfs were centrifuged and homogenised for 7 seconds (at full speed), immersed in 350 μl of 70% ethanol and transferred to RNeasy mini spin columns. Samples were again centrifuged for a further 15 seconds (at full speed, 4 °C) and the supernatant discarded. 700 μl of RW^1 buffer was added to samples and centrifuged (full speed for15 seconds). RW^1 buffer was removed and samples centrifuged with RPE buffer (500 μl, 15 seconds at full power); this step was repeated twice. Second time, samples were centrifuged for 2 minutes at full power and then transferred to sterile eppendorfs, where 10 μl of H_2O was added to the centre of the RNeasy mini spin column and allowed to soak through for 1 minute before centrifugation (full speed, 1 minute). 10 μl H_2O containing RNA was extracted and replaced within RNeasy mini spin column to be centrifuged for a final time (full speed, 1 minute). Finally, eppendorfs, with pure RNA content were labelled appropriately and ready for quantification using the Nanodrop spectrophotometer (ND1000; Thermo Scientific, Dorset, UK).

2.3.3.1.3 One-Step Reverse Transcriptase Polymer Chain Reaction

RT-PCR analysis was performed on RNA samples for hESCs cultured on all substrate types (Matrigel^{TM} coated glass coverslips, PCL Aligned nanofibres and PCL Random nanofibres) at all time points (0, 5, 10, 20 days), in physiological normoxic conditions (2% O_2). All RNA samples were used at a working concentration of 5 ng/ μl and one-step RT-

Chapter 2

PCR was performed using the SuperScript® III One-Step RT-PCR system with Platinum® *Taq* DNA Polymerase (Invitrogen, Paisley, UK) according to manufacturer's instructions.

Briefly all primers were designed using the Primer3 Freeware [Rozen and Skaletsky, 1999], primer sequences and the annealing temperatures for each gene are stated in Table 2.4. Mastermix solutions were prepared which included; 6.25 μl of 2X reaction mix, 1 μl Forward primer (10 μM), 1 μl Reverse primer (10 μM), 3 μl of DNA/RNA free water and 0.25 μl of SuperScript III RT/Platinum *Taq* High Fidelity Enzyme, per 1 μl of sample. All RT-PCR reactions consisted of 50 °C for 30 minutes, 94 °C for 2 minutes, 30 cycles: 94 °C for 15 seconds, primer specific annealing temperature (Table 2.4) for 30 seconds, and 68 °C for one minute followed by a final extension of 68 °C for 5 minutes.

GAPDH (a gene which codes for glyceraldehyde-3-phosphate dehydrogenase) was the housekeeping gene used alongside the genes of interest; POU5-F1 (pluripotency of hESCs), hTERT (Catalytic unit of telomerase), SOX-1 (mesodermal germ layer), ACTC-1 (Cardiac actinin; Endodermal germ layer) [Wong and Bernstein, 2010] and AFP (Ectodermal germ layer) [Abeyta *et al.*, 2004; Osafune *et al.*, 2008]. GAPDH was selected as previous reports indicate that reducing oxygen tensions do not affect its expression [Barber *et al.*, 2005].

Chapter 2

Table 2.4 One-Step RT-PCR. Gene type investigated and their forward and reverse primers plus annealing temperatures.

Gene Type	Forward Primer	Reverse Primer	Annealing Temperature (ºC)
GAPDH (Housekeeping gene)	5'TGAAGGTCGGAGT CAACGGATTTGGT'3	5'CATGTGGGCCATGA GGTCCAC CAC'3	56
POU5F1	5'GCAATTTGCCAAG CTCCTGAAGCAG'3	5'CATAGC CTGGGGTACCAAAAT GGGG'3	56
hTERT	5'GCAGCTCCCATTTC ATCAGC'3	5'CAGGATGGTCTTGA AGTCTG'3	58
SOX-1	5'CCAGGAGAACCCC AAGA GGC'3	5'CGGCCAGCGAGTAC TTGTCC'3	56
ACTC-1	5'CATCCTGACCCT GAAGTATCCCATC'3	5'CCCTCATAGATGGG GACATTGT GAG'3	56
AFP	5'CAGAAAAATGGCA GCCACAGC'3	5'TGGCAGCATTTCTCC AACAGG'3	54

2.3.3.1.4 Electrophoresis Gel

Gel electrophoresis was performed to confirm PCR product amplification. Agarose gel (Catalogue # BP1356; Fisher Scientific, USA) was prepared at 2% by dissolving the powder in 1X Tris Acetate-Ethylenediaminetetraacetic acid (TA-EDTA; catalogue # T9650-4L; Sigma-Aldrich, UK) at high heat. Agarose gel was further supplemented with 6.25 μl Ethidium Bromide (E1510-10 ml; Sigma-Aldrich, UK) and poured into a tray with a gel comb. Gel was allowed to set for 45 minutes after which the set gel was placed into the electrophoresis chamber containing 1X TA-EDTA buffer. 6 μl of PCR product were loaded with 2 μl of loading buffer and 5 μl of DNA ladder was also loaded along with a blank control (water plus loading buffer). Gel was run for 45 minutes at 100 V on constant mode from negative to positive. After completion of electrophoresis, gel was transferred to Genesnap where images were taken using a UV camera.

2.3.3.2 Mesodermal Germ Layer Lineage Differentiation

2.3.3.2.1 Adipogenic Differentiation

Adipogenic differentiation media was composed of DMEM supplemented with; 2% FBS, 1% L-Glut, 1% NEAA, 0.5 mM Dexamethasone, 60 mM Indomethacin, 10 μg/ml Insulin and 0.5 mM Isobutylmethylxanthine [Pittenger *et al.*, 1999].

2.3.3.2.2 Chondrogenic Differentiation

Chondrogenic differentiation media was comprised of supplementing DMEM/F12 with; 1% L-Glut, 1% NEAA, 1% Sodium Pyruvate, 1% Insulin Transferin Sodium Selenite, 50 μg/ml Ascorbic acid, 50 μg/ml L-proline, 0.1 μM Dexamethasone, 10 ng/ml of Transforming growth factor (Peprotech, London, UK) [Mackay *et al.*, 1998].

2.3.3.2.3 Osteogenic Differentiation

Osteogenic differentiation media consisted of: DMEM with 2% FBS, 1% L-Glut, 1% NEAA, 0.1 μM Dexamethasone, 10 mM β−Glycerophosphate and 50 μM Ascorbic acid-2-phosphate [Jaiswal *et al.*, 1997].

2.3.3.3 Histological Evaluation

After 21 days of culturing hESC CFU's on PCL electrospun nanofibre scaffolds and Matrigel^{TM} using chemically induced differentiation media in hypoxic conditions; media was removed from all samples, washed with PBS and fixed with 10% Formalin for 10 minutes. Samples were then histologically stained in correspondence to each lineage investigated using the following stains:

2.3.3.3.1 Oil Red O Staining of Lipids

Samples were rinsed in distilled H_2O and then in 60% isopropyl alcohol (IPA) before being stained with 0.18% Oil red 'O' (Sigma, UK) prepared in 60% IPA for 10 minutes [Pittenger *et al.*, 1999]. Samples were rinsed in tap water to remove residual stains and air-dried; lipids secreted appeared red.

2.3.3.3.2 Alcian Blue Staining of Glycosaminoglycans

0.1% Alcian Blue GX was prepared at pH 1.5 using 3% Acetic acid [Pittenger *et al.*, 1999]. Samples were immersed in the stain overnight at room temperature, after which they were rinsed in distilled water 3X in order to remove excess stain. GAGs secreted via hESCs differentiated into chondrocytes appeared blue.

2.3.3.3.3 Alizarin Red Staining of Ca^{2+} ions

Alizarin Red stain was prepared at 1% in distilled H_2O and paper filtered before use [Pittenger *et al.*, 1999]. Samples were washed once with PBS, once with distilled H_2O and treated with 200 μl of Alizarin Red solution for 5 minutes at room temperature. Stain was removed and samples washed 3X with distilled H_2O. Secreted calcium ions representing inorganic bone matrix secretion activity of an osteoblast appeared red.

Light microscopy was performed on all histologically stained samples using a bright field Nikon Eclipse TS-100 light microscope equipped with a Canon EOS 400D digital SLR camera. Representative images were taken of various samples at x10, x20 and x40 magnifications in different areas of the samples.

Chapter 2

2.4 Antibody Blocking of Human Embryonic Stem Cell Receptors

Monoclonal antibodies specific to integrin's/sub-units were used in adhesion blocking experiments as well as characterising and quantifying these receptors in hESCs cultured in either 2% O_2 (physiological normoxia) or 21% O_2 (hyperoxia).

2.4.1 *In silico* Microarray Analysis of hESCs Integrin Expression

Sample file output for hESCs (cell lines; H1, H9, and RH1) cultured on Matrigel[TM] until 90% confluence was generated for both 21% O_2 and 2% O_2 cultured cells as previously described (Forsyth *et al.*, 2008). Data was then sorted by gene name, relative expression values of <10 removed, and multiple probe hits deleted after generating averaged values.

2.4.2 Antibody Blocking of Integrins and Surface Adhesion Molecules

2.4.2.1 Matrigel™

hESCs (SHEF 1) used for these experiments were cultured and expanded in either; 2% O_2 or 21% O_2 from P 34 to P 62. hESCs were pre-treated with blocking antibodies raised against integrin sub-units; anti-integrin αV (R & D Biosystems, Abingdon, UK), anti-integrin αVβ5 (Chemicon International, Watford, UK), anti-integrin β5 (R & D Biosystems, Abingdon, UK) anti-integrin αE (Lifespan Bioscience, Nottingham UK), anti-integrin α6 (Autogen Bioclear, Calne, UK) and anti-CD44 (HCAM) (Santa Cruz Biotechnology, Heidelberg, Germany). hESCs were incubated with either 0, 1 or 25 μg/ml concentrations of antibody (in PBS) in either 2% O_2 or 21% O_2 at 37°C for 30 minutes in KO-DMEM. Cells were then re-plated into Matrigel[TM] coated 6-well plates at a density of 4 x 10^5 cells per well and incubated at either physiological normoxia (2% O_2) or hyperoxia (21% O_2) for 24 hours [Meng *et al.*, 2010; Paikal *et al.*, 2000].

2.4.2.2 Electrospun Nanofibrous Substrates

hESCs (SHEF 1) were cultured and expanded in 2% O_2 from P 42 to P 46. hESCs were trypsinised and treated with primary antibody anti-αVβ5 at 25 µg/ml concentration and KO-DMEM for one hour at 37 ºC in hypoxia. The control groups were hESCs without any primary antibody anti-αVβ5 treatment. Cells were then resuspended in 500 µl of MEF-conditioned media and seeded onto pre-sterilised PCL electrospun nanofibrous substrates (PCL; Aligned and Random) and Matrigel™ glass coverslip controls at a concentration 1700 cells/cm^2 and incubated overnight at 37 ºC physiological normoxia. Substrates were then flooded with MEF-conditioned media and continued to be cultured for 21 days in physiological normoxia.

2.4.2.3 Quantification of Cell Number Post-Antibody Treatment

After 24 hours, cells were trypsinised and counts recorded with a haemocytometer. Cell viability was determined by staining hESCs with Trypan Blue at a 1:1 ratio with cell solution.

2.4.3 Immunoflourescent Staining

2.4.3.1 αVβ5 Integrin and CD44 Expression in hESCs

hESCs were cultured and expanded on Matrigel™ coated 24 – well plates to approximately 70% confluence in both oxygen concentrations (21% O_2 or 2% O_2). Cells were fixed using 4% paraformaldehyde (in PBS) for 40 minutes at room temperature and non-specific proteins were blocked with 3% bovine serum albumin (BSA; Gibco) for 1 hour at room temperature. Primary antibody treatment included; anti-integrin αVβ5 and anti-CD44 at 50

µg/ml concentration for one hour at 37 ℃ in corresponding oxygen environments (2% O_2 or 21% O_2). After treatment, cells were washed with PBS and visualised using a secondary antibody treatment with donkey anti-human IgG at 5 µg/ml for 2 hours at room temperature whilst wrapped in foil.

2.4.3.2 Pluripotent hESC Markers on Matrigel™ and Electrospun Nanofibre Substrates

hESCs were cultured and expanded on Matrigel™ coated 24 well plates and PCL electrospun nanofibres (Aligned and Random), in 2% O_2 for a period of 21 days in MEF-conditioned media. Media was removed, washed with PBS and fixed in 4% PFA (in PBS) for 40 minutes at room temperature. Cells were treated with 0.5% Triton-X for 5 minutes at room temperature, washed twice with PBS and non-specific proteins were blocked using 3% BSA for 1 hour at room temperature. hESC colonies were then incubated with 1 µg/ 100 µl working solution of primary anti-human monoclonal antibodies; mouse anti-alkaline phosphatase, mouse anti-SSEA-1, mouse SSEA-4, goat anti-Nanog and goat anti-Oct-3/4 overnight at 2-8 ℃. hESCs were washed three times with PBS; antibodies Nanog and Oct 3/4 were treated using secondary antibody donkey anti-goat IgG (NL003; R & D Biosystems); alkaline phosphatase and SSEA-4 were using secondary antibody; donkey anti-mouse IgG (NL557; R & D Biosystems) at 5 µg/ml for two hours at room temperature.

All immunostained samples were further counterstained with DAPI (1:500, prepared in PBS (Sigma, UK) in order to visualise nuclei of cells and imaged using a fluorescent microscope (Nikon TZ1; Leica, Germany).

Chapter 2

2.4.3.3 Flourescent Activated Cell Sorting (FACS)

hESCs expanded in 2% O_2 or 21% O_2, were trypsinised off Matrigel™ coated flasks and resuspended to a cell density concentration of 100 000 cells/sample. At this density, hESCs were washed with PBS, centrifuged at 1200 rpm for 3 minutes and fixed in 4% paraformaldehyde (prepared in PBS) for 30 minutes at room temperature. Cells were washed twice in FACS buffer (0.5% FBS in PBS) and centrifuged before resuspending allocated samples for their primary antibody treatment in; 100 µl of 5 µg/10^6 cells for αVβ5 antibody solution and 100 µl of 1.5 µg/10^6 cells for CD44. Incubation period was for 2 hours at room temperature after which point, cells were micro-centrifuged, primary antibody solutions were removed, cells washed with FACS buffer and resuspended in secondary antibody; goat anti-mouse IgG secondary antibody (NL557; R&D Biosystems) at 5 µg/ml for a further 2 hours at room temperature and wrapped in foil. Cells were then washed in FACS buffer and transferred into FACS tubes. Samples were analysed on a FACSort flow cytometer (Beckton, Dickinson, Oxfordshire, UK). Data analysis was perfomed with the CellQuest Software package (BD Biosciences, UK).

2.5 Materials Related Characterising Techniques

2.5.1 Field Emission Scanning Electron Microscopy

Field Emission Scanning Electron Microscopy (FESEM) samples were coated with gold using an Emscope 200 (Emscope, UK) sputter coater for two minutes prior to analysis. Samples were analysed using a Hitachi F4500, (Hitachi, UK) FESEM. FESEM images of electrospun fibres were analysed using Image J. Image J was calibrated according to the image magnification and the diameters of individual fibres were measured. Two separate fibre sub-samples were examined in a minimum of 3 different areas. Once the data for the

measurements was collected for each polymer/orientation, the average fibre diameter and standard deviations were calculated. 50-70 fibre diameter readings were taken for each substrate.

2.5.2 Water Contact Angle analysis

Determining the wettability of a substrate is important in terms of identifying its biocompatibility. Hydrophobic materials have high contact angles resulting in less wettability due to minimal spreading of the water droplet; in comparison to hydrophilic materials that have a low contact angle, demonstrating greater wettability as a result of spreading of the water droplet over time. In order to characterise the wettability of the electrospun fibrous substrates, contact angle measurements were taken using the sessile drop technique. Firstly, using a Hamilton syringe (Precision sampling corp. USA), 10 µl of ultra-pure H_2O was placed onto substrates from a vertical distance of 5 mm. Conditions were set to 22 ℃ and 35 % humidity before placing a droplet onto the substrate and imaged after 20 seconds using a CCD camera (XC-ST50CE, Sony, Japan) (Figure 2.3). Images were taken of 3 separate regions for each of the 3 samples of a substrate type. All electrospun fibrous substrates fabricated were compared to a blank glass coverslip control. The 'LBADSA' Image J plug-in [Stalder *et al.*, 2006] was used to analyse the images in terms of its contact angle.
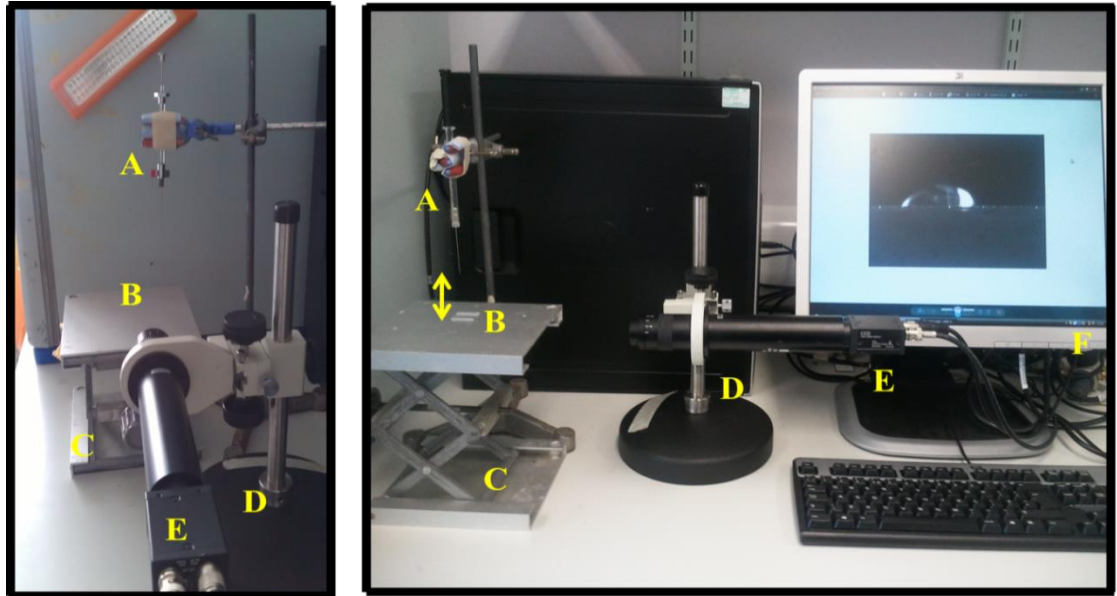
Figure 2.3 Photograph illustrating the contact angle set-up. (A) Hamilton syringe, (B) Substrate, (C) Adjusting platform, (D) Long working distance microscope is connected to a precision x,y translation stage, (E) CCD camera (Nikon, Japan) and (F) Image analysis system

2.5.3 Time of Flight Secondary Ion Mass Spectrometry

Time of flight secondary ion mass spectrometry (Tof-SIMS) consists of a liquid metal (LMIG) ion gun for spectroscopy and imaging purposes at a spatial resolution of closer to one micron during mode of operation in order to acquire high mass resolution data. Tof mass analyser has a mass resolution in excess of 7,000. The Tof-SIMS instrument is shown in Figure 2.4.

Figure 2.4 Photograph illustrating the Tof-SIMS instrument set-up. *Courtesy of Dr David Scurr, Nottingham University.*

2.5.3.1 Sample Preparation

PCL was electrospun into both aligned and random conformations at various different fibre diameters onto 13 mm circular glass coverslips. Parameters used to fabricate both random and aligned nanofibres are stated in Tables 2.2 and 2.3, respectively.

2.5.3.2 Protein Adsorption to Substrates Experiment

All substrates were placed into a 24 well plate, sterilised using UV for 90 seconds. Four different protein solutions; Collagen I (Rat tail; 3.4mg/ml BD Biosciences), Fibronectin (Human plasma 0.1% solution; Sigma, UK, 088K7537), and Laminin (Natural mouse; Invitrogen, 23017-015) and Vitronectin (Human plasma; Sigma-Aldrich, V8379) were prepared at 50 µg/ml in PBS, as well as MEF-conditioned hESC media. 50 µl of each prepared protein solution and MEF-conditioned media was placed onto separate samples and incubated at 2% O_2 for 2 hours. Protein/media supernatant was collected (leaving a

negligible volume to prevent the disruption of the adsorbed protein layer meniscus) into eppendorfs and stored at 2-8 ℃, for protein quantification later. Substrates were rinsed with 50 µl of PBS three times and then 50 µl of ultrapure distilled water also three times (to remove salts from PBS) and then allowed to air dry. Samples were transported to Nottingham University in order to be analysed using ToF-SIMS.

2.5.3.3 Specimen Analysis Using Tof-SIMS

All samples were stored in nitrogen prior to sample loading into the Tof-SIMS specimen chamber for analysis. Sample analysis was conducted on a Tof-SIMS IV (ION-TOF GmbH of Műnster), with data acquisition and analysis performed using Surface-lab 6 (IONTOF GmbH) software. A primary ion source (Bi_3^+) of 25 kV was established using a Bismuth liquid metal ion gun (LMIG) and a raster in random mode with a resolution of 256 x 256. Positive and negative ion Tof-SIMS spectra were acquired over an area of 500 × 500 µm and a pulsed electron flood gun (20 eV) was used for charge neutralisation for all samples in this study. Principle component analysis was performed using The Unscrambler.

2.5.4 Nano Orange® Flourometric Assay

The NanoOrange® assay (Molecular probes, N6666) is highly sensitive and allows the detection and quantification of proteins within solution between 10 ng/ml and 10 µg/ml. In aqueous solution the surfactant dye molecule is non-fluorescent but once bound to proteins, the surfactant dye is able to fluoresce at excitation peak 470 nm and emission peak 570 nm [Jones *et al.*, 2010; Roach, 2005]. Protein/media supernatants were collected after incubation on electrospun nanofibrous substrates (12.5% PCL-Aligned, 12.5% PCL-

Chapter 2

Random; 15% PCL-Aligned, 15% PCL-Random) and controls (blank glass coverslip), in physiological normoxia for 2 hours at 37 ℃, as stated above in section 2.5.3.2. 100 μl of each sample (including standards) was plated into eppendorfs to which 100 μl of 1X NanoOrange working solution (prepared using 1X NanoOrange solution reagent diluted 500-fold into a 1X protein quantification diluent which was further prepared by diluting 10-fold in distilled water). Samples were then heated at 95℃ for 10 minutes and then allowed to cool down for a further 20 minutes. Finally, samples were analysed using a fluorescent plate reader. 485/590 nm (excitation/emission). Standard curve calibration plots were produced for protein concentration of each protein type investigated (collagen I, fibronectin, laminin, vitronectin), except MEF-conditioned media, for which a BSA standard curve was formulated. All samples were conducted in triplicates and the plots attained are demonstrated in Figures 2.6 to 2.10.
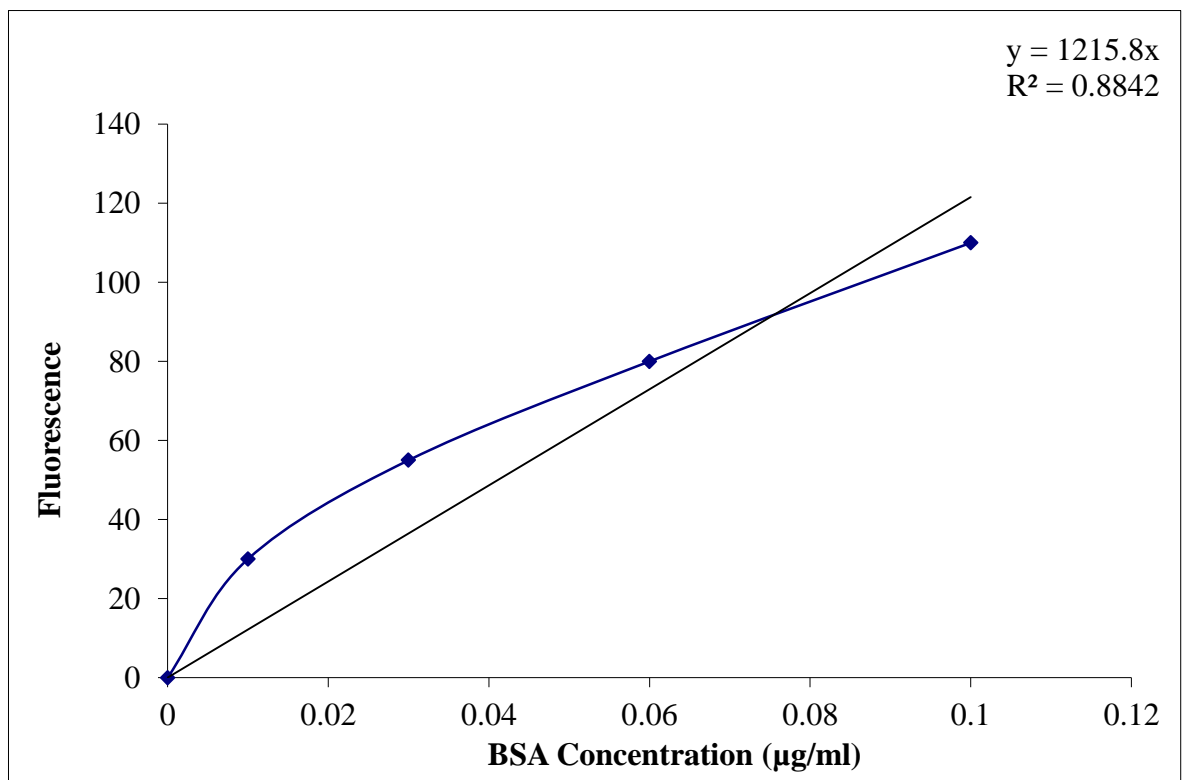
Figure 2.5 Typical standard curve performed using dilutions of BSA ranging from 0 to 0.1 μg/ml.
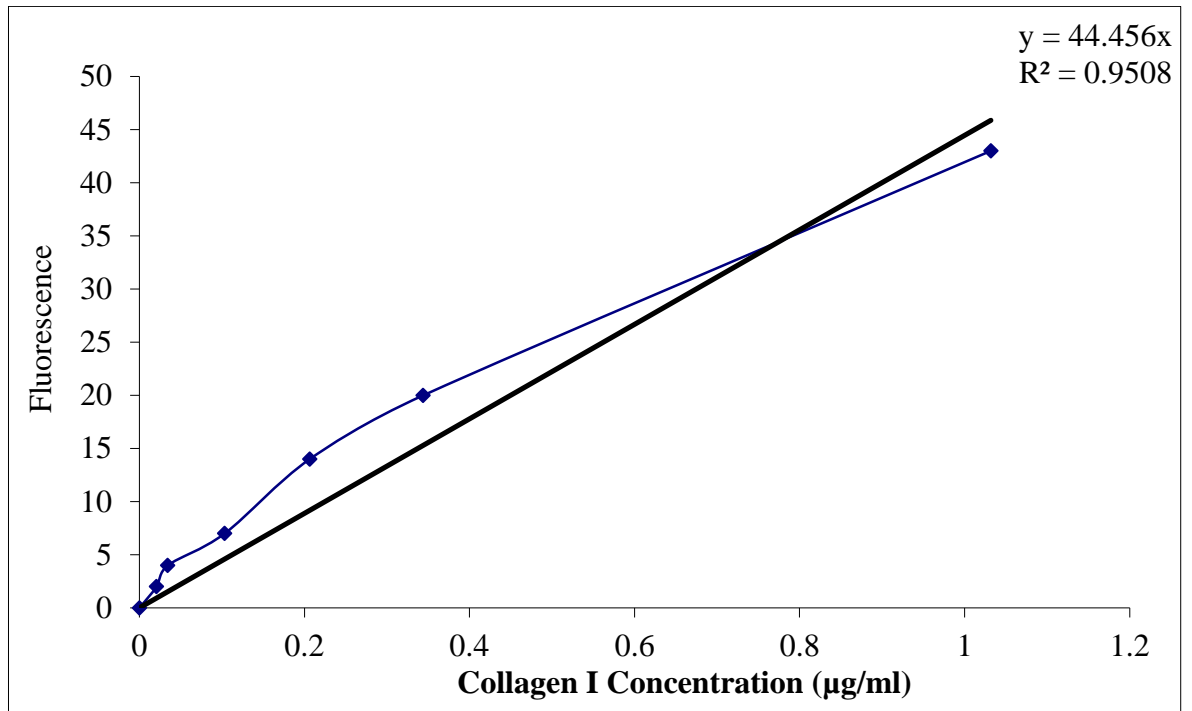
Figure 2.6 Typical standard curve performed using dilutions of Collagen I protein ranging

from 0 to 0.35 µg/ml.
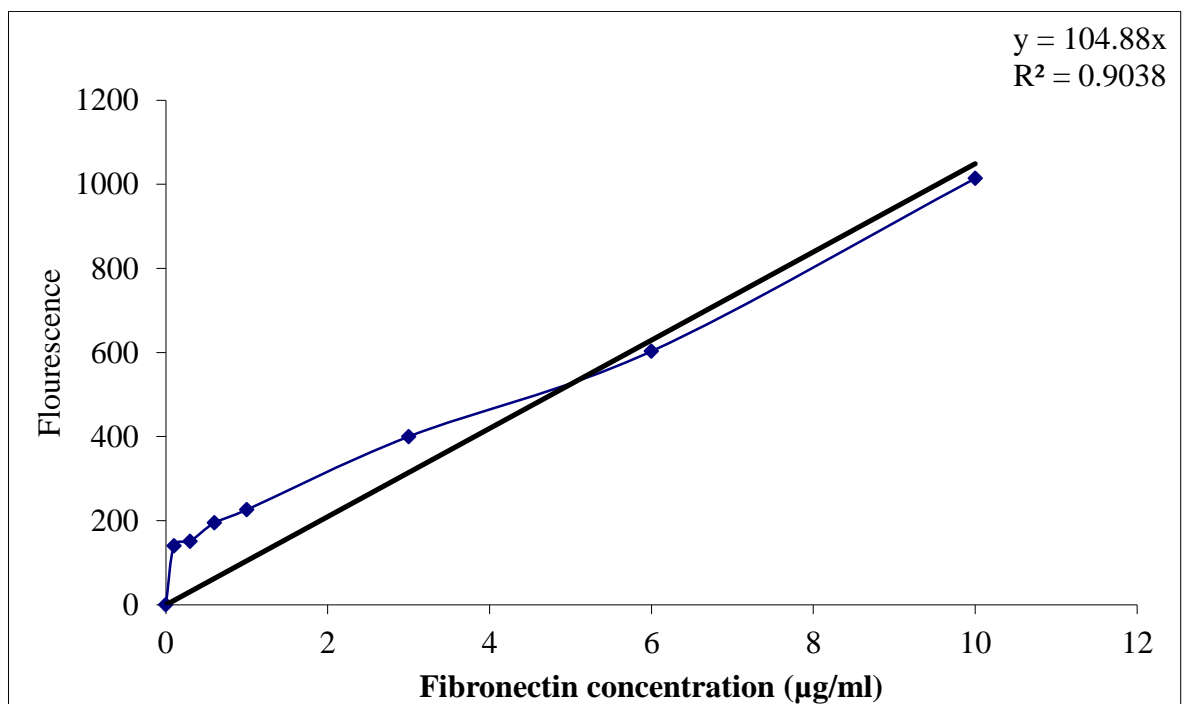
Figure 2.7 Typical standard curve performed using dilutions of Fibronectin protein ranging

from 0 to 10 µg/ml.
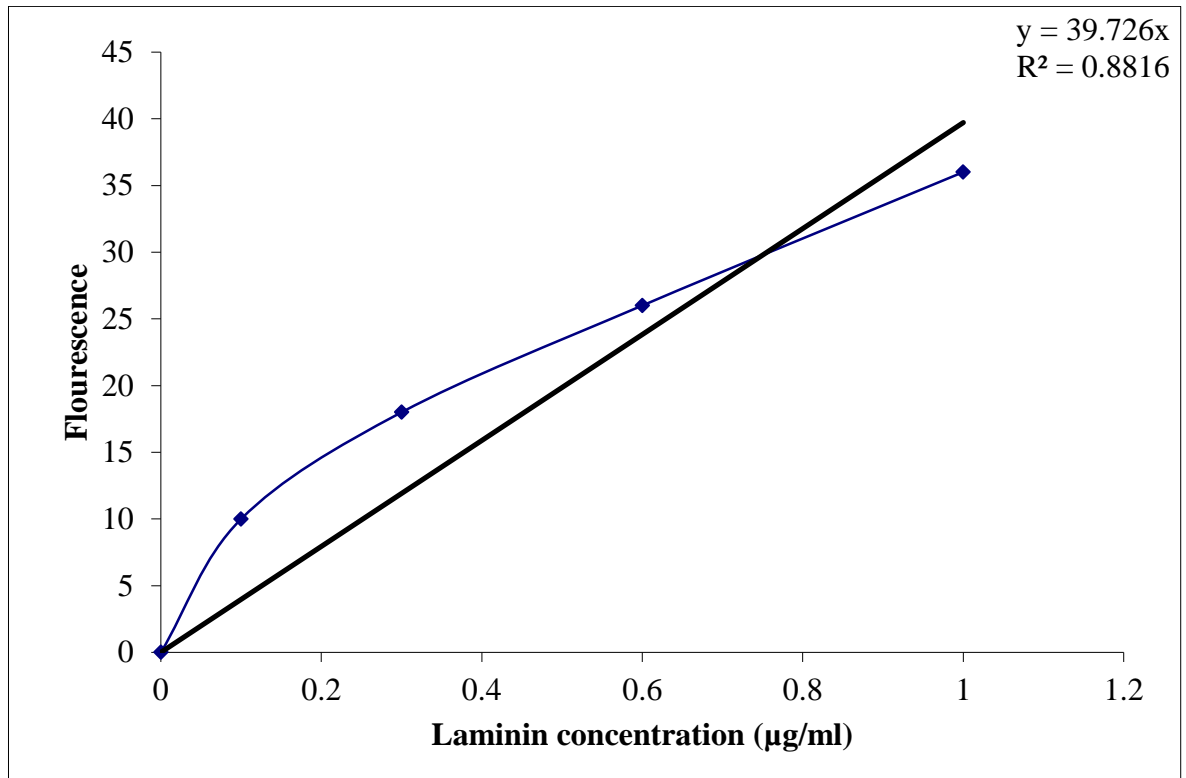
Figure 2.8 Typical standard curve performed using dilutions of Laminin protein ranging
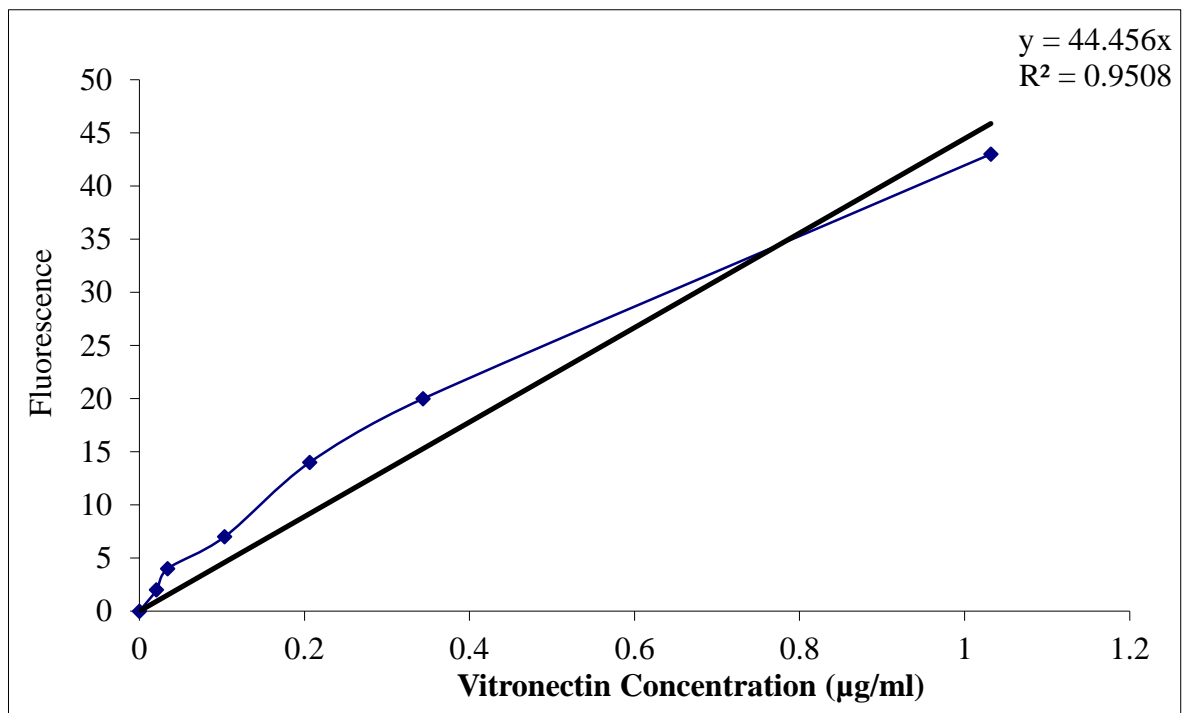
from 0 to 1 µg/ml.

Figure 2.9 Typical standard curve performed using dilutions of Vitronectin protein ranging

from 0 to 1 µg/ml.

Chapter 2

2.6 Statistical Analysis

Error bars on graphs indicate standard deviations (SD). Data were tested for normality and a 1-way ANOVA/Kruskall Wallis test or a 2-way ANOVA test was performed followed by an appropriate post hoc test (Tukey's or Dunns, respectively) to determine the origins of significance. In this study significance levels are indicated according to the legend $p < 0.05^*$, $p < 0.01^{**}$ and $p < 0.001^{***}$.

Chapter 3

3. Self-Renewal of hESCs on Electrospun Nanofibrous Substrates

3.1 Introduction

Current methodology for expansion of hESCs is largely reliant on either the mitotically-inactivated feeder cell method (using direct co-culture with embryonic or adult fibroblasts), or the feeder-free method, which utilises feeder cell, pre-conditioned media and a biological substrate, such as Matrigel^{TM} [Thomson *et al.*, 1998; Xu *et al.*, 2001]. The inherent limitation of the Matrigel^{TM}-based feeder-free method is that it is unsuitable for incorporation into hESC-based clinical trials due to the risk of xenocontamination alongside the batch to batch variability of MEFs used to condition hESC media and the presence of a nonhuman sialic acid (Neu5Gc). Furthermore, Matrigel^{TM} limits hESC expansion to a two dimensional (2D) environment with subsequent interventions required prior to transplantation. Hence, innovative and novel tissue engineering strategies are urgently required to provide the opportunity of incorporating hESCs with synthetic, biomimetic substrates (scaffolds), with the potential to act as three dimensional (3D) carriers to facilitate ready transplantation into *in vivo* target sites and eliminate any xenogenic contaminations.

Cells are sensitive to nano-scale topography [Toh *et al.*, 2006]. A common method used for fabricating nano-scale tissue engineering scaffolds is electrospinning. Electrospinning provides the opportunity to produce nanofibrous scaffolds, of tailored dimensions, that are able to mimic the nano-architecture of native extracellular matrix [Matthews *et al.*, 2002]. Nanofibres also provide a high surface area to volume ratio and high surface roughness resulting in an effective environment for cell adhesion due to increased focal adhesion

contact between the cells and the surrounding fibres [Agarwal *et al.*, 2008; Yang *et al.*, 2005; Zhang *et al.*, 2005]. This is an indication of effective interaction between the cell and the surrounding artificial ECM, which results in the potential transmission of guidance cues to the cells. Electrospun fibre meshes generally have poor mechanical strength, but are highly flexible, which can result in an environment where cells produce fewer stress fibres [Galbraith and Sheetz, 1998]. An involvement of nanotopographical features in the maintenance of undifferentiated ESCs has been previously proposed [Jacobson *et al.*, 2001].

Previous reports have detailed the biocompatibility of electrospun nanofibre scaffolds to support the attachment, proliferation and differentiation of human bone marrow-derived mesenchymal stem cells (hMSC), cord blood-derived somatic stem cells, neural stem cells**,** and haematopoietic stem cells [Bini *et al.*, 2006; Chan *et al.*, 2009; Hashemi *et al.*, 2009; Ma *et al.*, 2008; Schnell *et al.*, 2007; Shih *et al.*, 2006]. Many of these researchers used synthetic polymers such as PCL, poly-L-lactide acid (PLLA), poly(lactic-co-glycolic acid) (PLGA), as they are FDA approved and their bulk degradation properties are well characterised [Ramakrishna *et al.*, 2005]. Recent observations have demonstrated aligned and random nanofibre scaffolds, fabricated using PCL, PLGA and poly-L/D-lactide acid (PLDLA) to function as a suitable, alternative substrate for the isolation and expansion of hMSCs directly from bone marrow aspirate while maintaining their multipotent state [Wimpenny *et al.*, 2010].

Chapter 3

Currently, studies performed regarding the culture and differentiation of hESCs on electrospun nanofibres is limited. However, recent attempts have included the differentiation of murine ESCs into mature neural cells using retinoic acid, via an embryoid body (EB) stage, when cultured on electrospun, oriented PCL nanofibre scaffolds [Xie *et al.*, 2009]. Unfortunately, differentiation through the EB stage results in spontaneous differentiation and a heterogeneous population, hence only a small population of the specialised cell type of interest can be recovered. Attempts to culture hESCs on electrospun nanofibres have included: the use of composite polymer substrates such as PCL/collagen and PCL/gelatin; however hESCs co-cultured with MEFs on these substrates was the only method by which pluripotency could be maintained. Attempts have been made to culture hESCs on electrospun nanofibres from a purely synthetic material such as FDA-approved Polyurethane. In this case, neuronal differentiation was explored of hESCs cultured on polyurethane nanofibres in combination with .neuronal differentiation inducing media [Carlberg *et al.*, 2009].

Though recent attempts have been made to culture hESCs on electrospun nanofibres, it is clear that hESCs display poor attachment to synthetic materials and subsequent proliferation is limited. Furthermore, expansion of pluripotent hESCs on purely synthetic nanofibres without the co-culture of MEFs still appears to be impossible and a challenging task. In this chapter, the use of electrospun nanofibres from FDA approved synthetic polymers are investigated for roles in encouraging the attachment and pluripotent expansion of hESCs without the use of Matrigel™. Furthermore, it is well documented that the use of physiological normoxia (2% O_2) is thought to be a better environment for culturing hESCs. Hypoxia inducible factors (HIFs) are known to be expressed by

decreasing the oxygen environment; these are heterodimeric, environment sensing transcriptional factors and are comprised of α and β sub-units. The expression of HIFs influences the promotion and suppression of several genes that are associated with various cell activities. Investigations have revealed that hESCs cultured in physiological normoxia (2% O_2) increases their clonogenicity whilst maintaining their undifferentiated state, amongst others (see section 1.4). This study investigates the synergistic effect of both nanofibre topography and physiological normoxic conditions for increased attachment and enhanced hESC expansion in an undifferentiated state. The final outcome would be to replace the conventional substrate (Matrigel™) with electrospun nanofibres for expansion of pluripotent hESCs without their exposure to xenogenic contaminations in identified optimal conditions.

3.2 Aims and Objectives

Several studies have documented the use of electrospun nanofibres in the support of activity of various stem cells including recovery, proliferation and differentiation into multiple lineages. An additional stem cell type which could also be supported by electrospun nanofibre scaffolds may include hESCs. Furthermore, by combining the effects of nanofibre topography (which mimics the topographical structure of native ECM at the nanoscale) and physiological normoxia (2% O_2; suggested to enhance clonogenicity and retain pluripotency), it can be hypothesised that a novel, synthetic substrate may support the attachment and expansion of hESCs, though pending optimisation of several materials related and culture conditions.

Chapter 3

The aims of this chapter were as follows:

- To optimise and characterise electrospun nanofibrous (<500 nm) and sub-micron fibrous substrates from three FDA approved synthetic polymers (PCL, PLGA and PLLA) in both aligned and random conformations.

- Optimise materials related parameters (polymer type, fibre diameter and fibre orientation) in order to identify electrospun nanofibrous substrate to support hESC colony forming unit ability.

- Compare the effects between physiological normoxia (2% O_2) and hyperoxia (21% O_2) in combination with electrospun nanofibrous substrates on hESC expansion.

- Characterise the undifferentiated state and pluripotential differentiation capacity of hESCs recovered on electrospun nanofibrous substrates.

Chapter 3

3.3 Materials and Methods

All nanofibrous substrates were fabricated using electrospinning. Aligned fibres were attained using the rotating mandrel technique, whereas random fibres were produced using the static copper plate collector. The operating parameters used to attain both aligned and random fibres onto glass coverslips are stated in (Table 2.2-2.3, Chapter 2, section 2.1.3). Electrospun fibres on glass coverslips were further reinforced using silicone rubber strips and silicone glue to prevent their detachment whilst immersed in media. All electrospun fibrous substrates were sterilised using 70% IMS for at least 1 hour.

Fibre morphology, orientation and diameter were characterised using field emission scanning electron microscopy (FESEM). Surface properties were characterised in terms of wettability using water contact angle analysis.

hESCs were cultured and expanded on Matrigel™ in physiological normoxia (2% O_2) and hyperoxia (21% O_2) using MEF conditioned ESC media and seeded onto electrospun fibrous substrates at passage 35-42. hESC CFU recovery and hESC morphology within those colonies on electrospun fibrous substrates after 21 days of expansion in MEF conditioned ESC media was evaluated using Giemsa staining. Furthermore, the undifferentiated state of hESCs recovered on optimal (PCL) nanofibrous substrates in optimal oxygen conditions for 21 days was evaluated using immunoflourescent staining for pluripotent markers as well as Alkaline phosphatase staining. In addition the pluripotential differentiation capacity was investigated using RT-PCR.

<u>**3.4 Results**</u>

3.4.1 Characterisation of Optimised Electrospun Fibrous Substrates

Electrospinning is a versatile technique with several parameters that require optimisation to attain non-beaded and uniform nanofibres with the required diameter. Preliminary experiments included optimising polymer concentration of each polymer (PCL, PLGA and PLLA) in both aligned and random conformations to prevent the formation of beads and to provide consistency in fibre diameter. Linear and uniform electrospun fibres were achieved with concentrations of 12.5%, 2% and 7% for PCL, PLGA and PLLA respectively. The optimised concentration for each polymer was then electrospun at various working distances (10 cm, 15 cm and 20 cm), voltage (4 kV, 6 kV and 8 kV) and needle gauges (18G, 20G and 22G); for both aligned and random fibres deposited onto glass coverslips. The final parameters used to attain both aligned and random electrospun fibres from all 3 polymers are stated in Table 2.2-2.3 (Chapter 2, section 2.1.3) Visualisation of the electrospun fibres using optical microscopy as shown in Figure 3.1 demonstrates the precise anisotropic direction of the aligned electrospun fibres and the complete disorganisation of the random electrospun fibres; whilst attaining linear fibres without beading.

Chapter 3
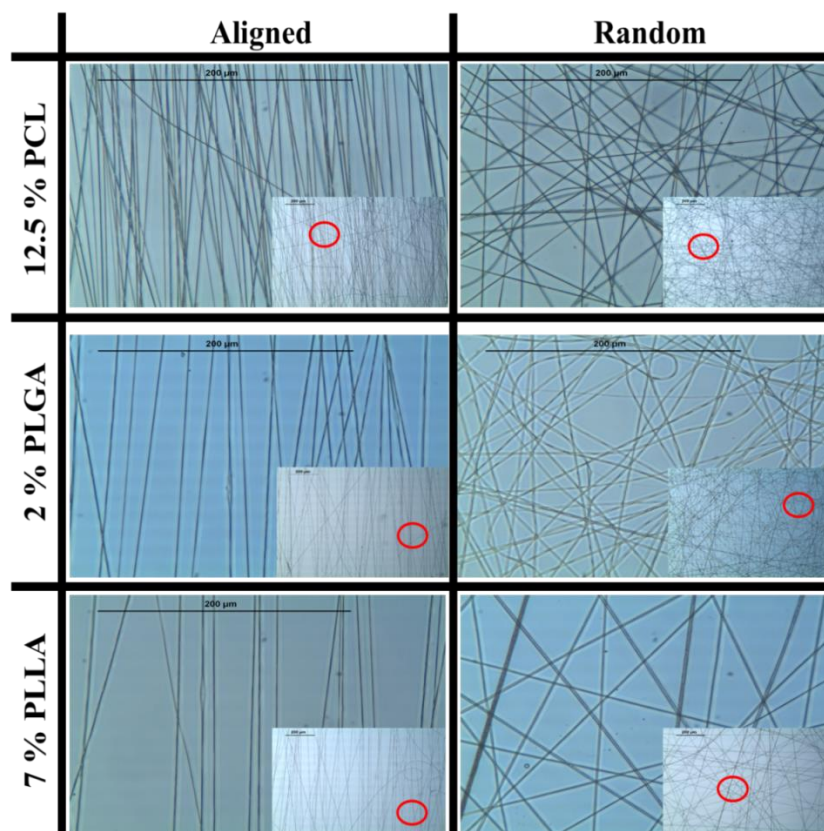
Figure 3.1 Optical microscopy images of optimised electropsun fibrous scaffolds fabricated from 12.5% PCL, 7% PLGA and 2% PLLA in both aligned and random conformations. Red circle indicates the area magnified. Scale bar = 200 μm.

To define the exact diameter of electrospun fibres and to visualise fibre morphology and overall surface topography, FESEM was performed (Figure 3.2). FESEM images allowed the direct analysis of fibre diameter; results demonstrated that PCL nanofibres had a smaller fibre diameter (aligned, 280 nm; random 318 nm) in comparison to PLLA (aligned 2506 nm; random, 1028 nm) and PLGA (aligned, 769 nm; random 1229 nm) fibres. Furthermore, significant differences were apparent in the fibre diameters between aligned and random conformations within each polymer type when electrospun with the same concentration of the solution (Figure 3.3). Specifically, PCL-aligned nanofibres had a

significantly smaller fibre diameter in comparison to PCL-random nanofibres ($p < 0.01$); PLGA-A sub-micron fibres had a significantly greater fibre diameter in comparision to PLGA-R ($p < 0.001$) and PLLA-A sub-micron fibres also had a significantly greater fibre diameter when compared to the diameter of PLLA-R ($p < 0.001$) counterparts.
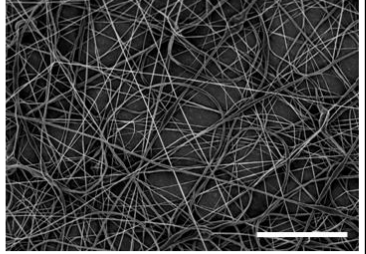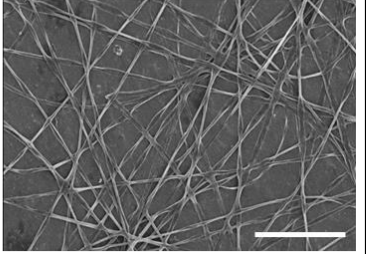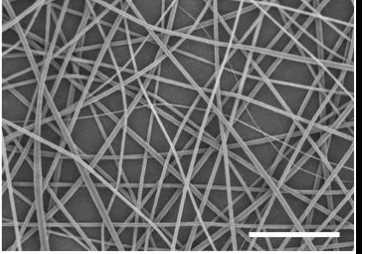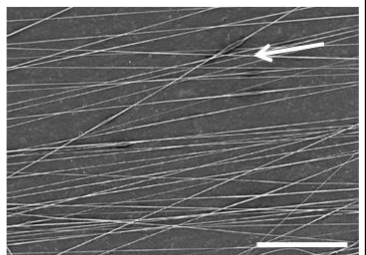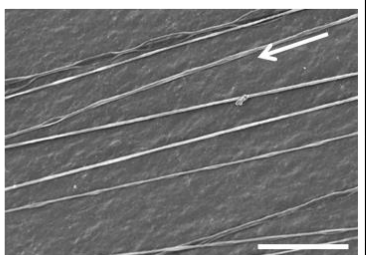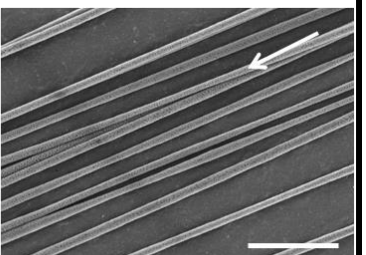
	12.5% PCL	2% PLGA	7% PLLA
Random			
	318 ± 151 nm	1229 ± 507 nm	1028 ± 271 nm
Aligned			
	280 ± 122 nm	769 ± 225 nm	2506 ± 565 nm

Figure 3.2 FESEM images of electrospun fibrous substrates fabricated from: PCL, PLGA and PLLA, in both random and aligned conformations. Electrospun fibre diameters are presented under each image. An arrow indicates the predominant direction of aligned fibres. Scale bar = 3 μm.
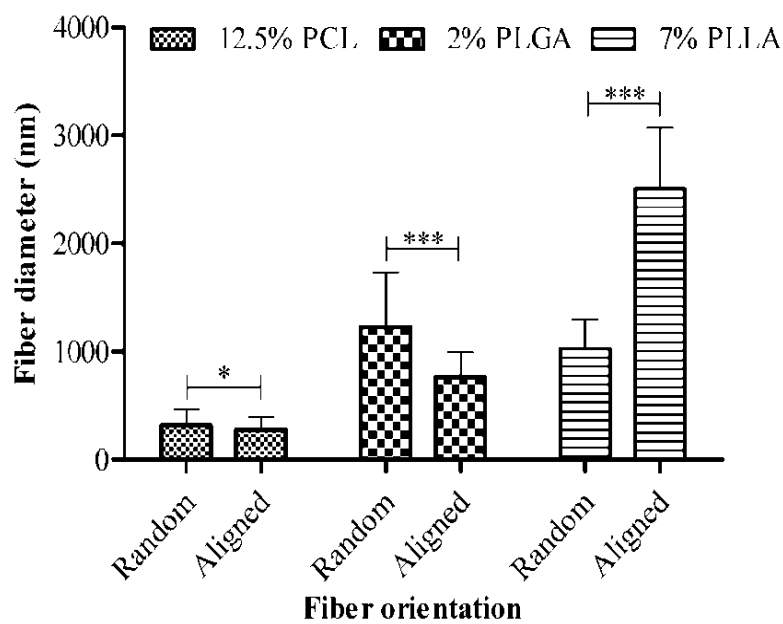
Figure 3.3 Graph representing the average fibre diameters of both aligned and random electrospun fibres made from PCL, PLGA and PLLA. Values indicate mean fibre diameter and standard deviation of $n=20$; $*p < 0.05$, $***p < 0.001$.

Chapter 3

Surface roughness can be affected by several parameters including; polymer chemistry, fibre morphology, fibre diameter, and topography, and this can affect the biocompatibility and the wettability of a substrate which ultimately affects cell adhesion and proliferation. Wettability was evaluated using the water contact angle analysis method for all optimised electrospun fibrous substrates (PCL-A, PCL-R, PLGA-A, PLGA-R, PLLA-A and PLLA-R) as well as a blank glass coverslip onto which the electrospun fibres were electrospun. Briefly, the water contact angle is measured by calculating the droplet angle made tangent to the liquid surface with the solid at the three phase boundary measured through the liquid, using image J, as shown in Figure 3.4A (Roach thesis; 2005)

Water contact angle analysis demonstrated that PCL nanofibres (aligned, 83°; random, 81.5°) were marginally more hydrophobic in comparison to fibres fabricated from PLGA (aligned, 79°; random, 77°) and PLLA (aligned, 77°; random, 79°) in both aligned and random conformations. PLGA and PLLA substrates had similar contact angle measurements, as shown in Figure 3.4B and 3.5. Interestingly Matrigel^TM (61°) and glass (65°) contact angle measurements were significantly more hydrophilic in comparison to all polymer contact angle measurements.
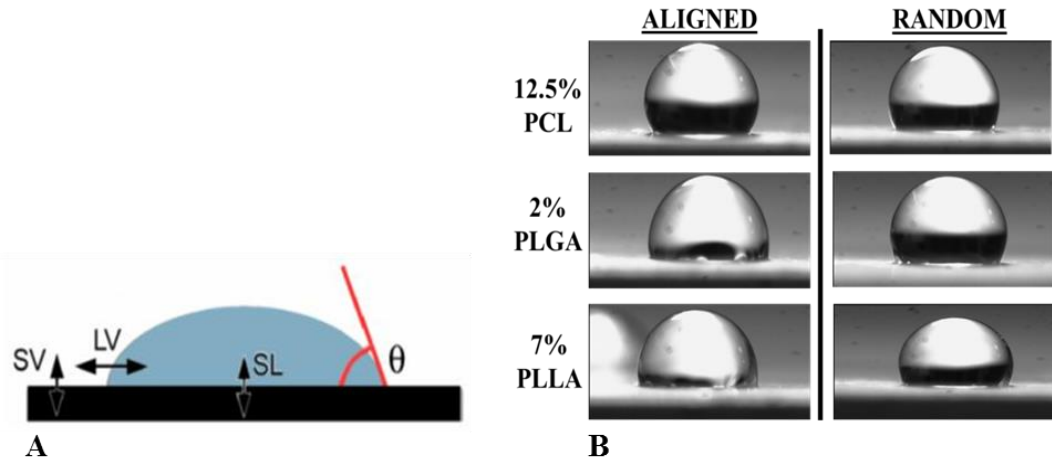
Figure 3.4 (A) Method of calculating water contact angle [Roach, 2005]. Various forces act at a solid-liquid interface (SV, solid-vapour; LV, liquid-vapour and SL, solid-liquid); these energetics dictate the droplet shape and thus wettable nature of the substrate. The angle contact angle made between the solid and liquid phase can be calculated using Image J. (B) Images representing water contact angles on electrospun fibrous substrates in both aligned and random conformations fabricated from: 12.5% PCL, 2% PLGA and 7% PLLA.
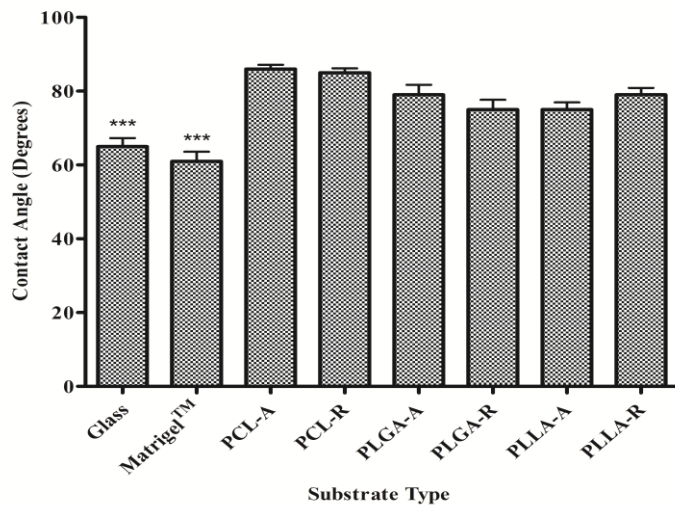
Figure 3.5 Water contact angle analysis. Graph representing the water contact angle measurement for both aligned and random electrospun fibrous substrates fabricated from: 12.5% PCL, 2% PLGA and 7% PLLA as well as naked glass and Matrigel[TM]. Values indicate mean contact angle measurement and standard deviation of $n=3$, ***$p < 0.001$.

3.4.2 Optimisation of hESC Seeding Density

Before seeding human embryonic stem cells onto electrospun fibrous substrates it was important to optimise the seeding density at which the greatest number of hESC-CFUs could be recovered without the formation of a complete monolayer and the merging of colonies into each other after 21 days of culture with ES maintenance media in both physiological normoxia (2% O_2) and hyperoxia (21% O_2). A typical characteristic feature of hESC expansion in an undifferentiated state is their ability to form tightly adherent, compact colonies; the most vigorous environment to test the clonogenicity of hESCs, is to allow hESC expansion in ES conditioned media for 21 days with minimal disturbance.

Matrigel™ coated 6-well plates were seeded with hESCs at 6 different seeding densities which were; 0, 1, 10, 100, 1000 and 10 000 cells per well resuspended in 500 µl of ES conditioned media and further immersed in 6 ml of ES conditioned media. After 21 days, hESC CFUs were fixed and Giemsa stained for colony morphological visualisation as well as morphological evaluation of single hESCs within a colony (Figure 3.6A). Results clearly demonstrated that in both 2% O_2 and 21% O_2 the greatest number of CFUs were formed when seeding hESCs at a density of 1000 cells (Figure 3.6B). For seeding densities; 100 and 1000 cells/well, a significantly greater number of hESC-CFUs were recovered in physiological normoxia (2% O_2) relative to hyperoxia (21% O_2), confirming that 2% O_2 enhances the clonogenicity of hESCs, as demonstrated in Figure 3.6A.

Furthermore, hESC CFUs produced were stained for alkaline phosphatase in order to evaluate their undifferentiated state. Pluripotent hESCs express alkaline phosphatase (ALP); as confirmed in Figure 3.6. A difference in stain intensity was noted as a

consequence of the change in oxygen environment in which the hESCs were cultured. It was clear that in physiological normoxia (2% O_2) hESC CFUs expressed a greater intensity of ALP when compared to colonies expanded in hyperoxia (21 % O_2).
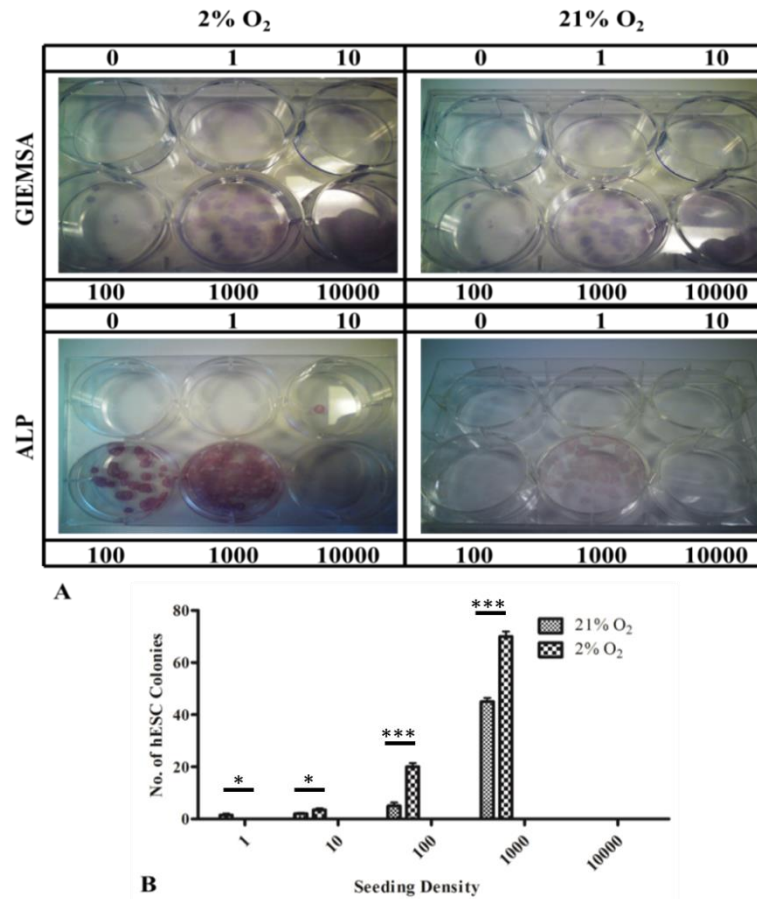
Figure 3.6 (A) Optimisation of hESC seeding density to form CFUs on Matrigel™ coated 6-well plates, cultured for 21 days with ES conditioned media and in physiological normoxia (2% O_2) and hyperoxia (21% O_2) stained using Giemsa and Alkaline phosphatase. (B) Quantification of Giemsa stained hESC colony count on Matrigel™ when seeded at different seeding densities (0, 1, 10, 100, 1000 and 10 000 cells/ well) and cultured with ES conditioned media in physiological normoxia (2% O_2) and hyperoxia (21% O_2) for 21 days. Values indicate mean number of forming units and standard deviation of n=3, ***$p < 0.001$.

Chapter 3

3.4.3 Characterisation and Quantification of hESC CFUs on Electrospun Fibrous Substrates in 2% O_2 and 21% O_2.

To investigate the ability of electrospun fibrous substrates to support hESC expansion, electrospun fibrous substrates (aligned and random) fabricated from PCL, PLGA and PLLA and controls (positive control; Matrigel™ coated glass coverslip and negative control; non-Matrigel™ coated glass coverslip) were seeded with 1000 cells per scaffold/control. hESCs seeded on substrates were cultured in both; physiological normoxia (2% O_2) and hyperoxia (21% O_2) for 21 days. All substrates investigated were fixed and Giemsa stained; hESC-CFUs were only found to be present on positive controls with no colony recovery activity occurring on all electrospun fibrous substrates, regardless of oxygen environment in which they were cultured.

The seeding density was increased to 10 000 cells/substrate (1700 cells/cm^2) and all electrospun fibrous substrates including controls were seeded with hESCs and cultured in both oxygen environments (2% O_2 and 21% O_2) for 21 days. After fixing, Giemsa staining revealed the presence of hESC colonies on electrospun fibrous substrates. However, the oxygen environment highly influenced and determined whether or not hESCs were able to form colonies. As demonstrated in Figure 3.7, it was clear that physiological normoxia (2% O_2) supported the expansion of tightly adherent, compact hESC colonies; broadly similar colony morphology was demonstrated on both PCL-Aligned and PCL-Random nanofibrous substrates (Figure 3.7C and Figure 3.7E, as an example) to the positive (Matrigel™) control (Figure 3.7A).

Chapter 3

In hyperoxia (21% O_2), despite maintaining all other conditions constant and only changing the oxygen environment, all electrospun fibrous substrates supported tightly packed, dense, adherent bodies of cells which resembled an adherent embryoid body (EB), to an extent, formation as demonstrated by PCL-Aligned (Figure 3.7D) and PCL-Random (Figure 3.7F) nanofibrous substrates, as an example. EB formation is typically induced by culturing hESCs on a substrate which prevents their initial attachment forcing them to group together into a clump of cells subsequently resulting in their spontaneous differentiation. Subsequently these EBs may be able to attach to a previously non-permissive substrate as the expression of surface receptors changes with accompanying differentiation state. Characteristically, EBs have an "egg-like" morphology as demonstrated in Figure 3.7B; this feature appears similar to the cluster of hESCs formed on the same electrospun nanofibrous substrates but when cultured in hyperoxia (21 % O_2) suggesting that these are also EBs that have formed.

Chapter 3
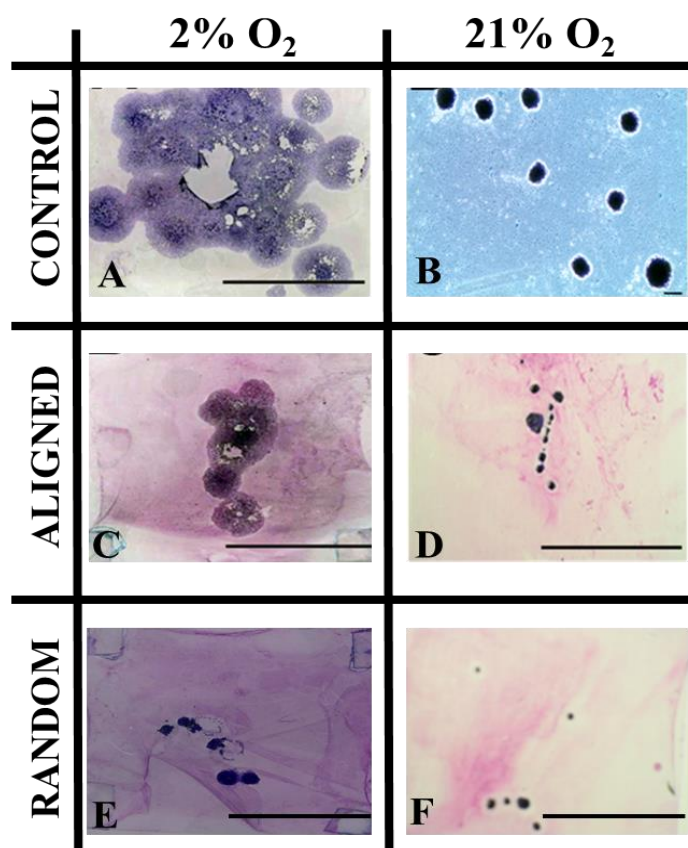
Figure 3.7 Macroscopic evaluation of hESC expansion. Photographs of hESC expansion cultured in different oxygen environments: hESC-CFU formation in physiological normoxia (2% O_2) on, (A) Matrigel™, (C) 12.5% PCL aligned nanofibrous substrate and (E) 12.5% PCL random nanofibrous substrate, whereas in hyperoxia (21% O_2) hESC-embryoid body formation on (B) gelatin, (D) 12.5% PCL aligned nanofibrous substrate and (F) 12.5% PCL random nanofibrous substrate. hESCs were cultured up to 21 days using ES conditioned media. (Scale bar = 12 mm for A and C-D but 200 μm for B)

Evaluating the morphology of CFUs (microscopically) on electrospun fibrous substrates in physiological normoxia (2% O_2) demonstrated similar morphology to hESCs expanded on Matrigel™. As expected, no colonies were visualised on a negative control (Figure 3.8A) but Matrigel™ substrates supported hESC-CFU formation in both 2% O_2 (Figure 3.8B) and 21% O_2. All colonies formed on all electropsun fibrous substrates (Figure 3.8C-F) in 2

Chapter 3

% O_2 displayed hESC morphology similar to that seen in recovered colonies on Matrigel™ control; however, hESC colonies recovered on PCL-Random (Figure 3.8C) appear to be more dense and compact when compared to its aligned counterpart (Figure 3.8D)
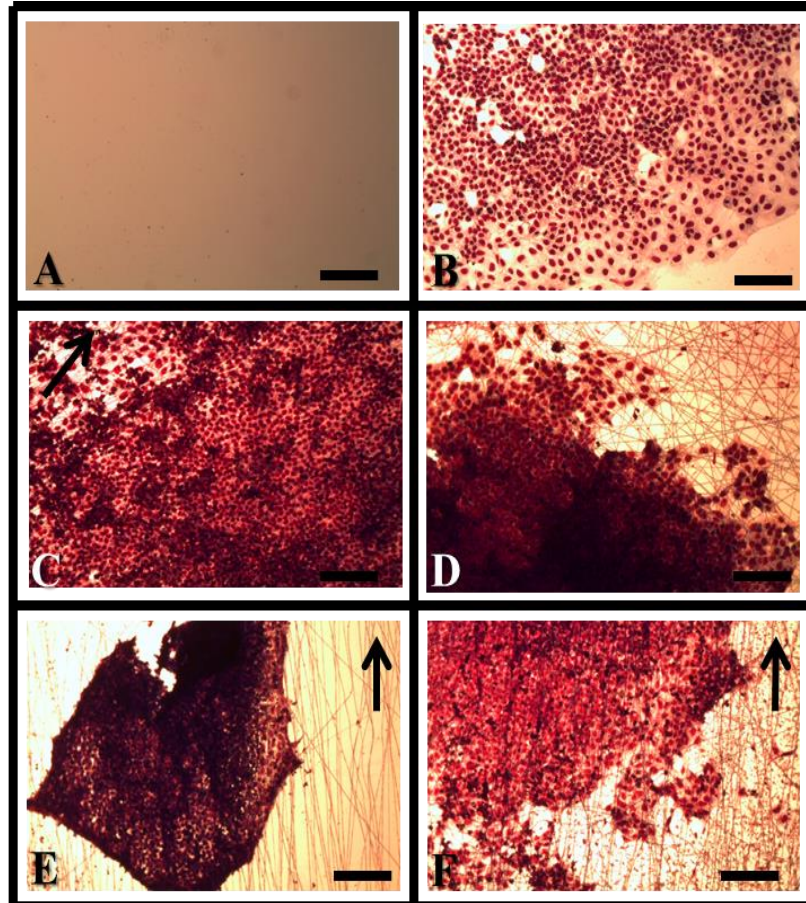
Figure 3.8 hESC morphology within a colony formed under physiological normoxia (2% O_2) on: (A) negative control (non-Matrigel™ coated glass coverslip; no colony formation), (B) positive control (Matrigel™ coated glass coverslip), (C) 12.5% PCL aligned nanofibrous substrate, (D) 12.5% PCL random nanofibrous substrate, (E) 2% PLGA aligned fibrous substrate and (F) 7% PLLA aligned fibrous substrate. hESC-CFUs were expanded for 21 days in ES conditioned media, fixed and Giemsa stained. Arrows indicate the predominant direction of the aligned fibres. Scale bar = 200 µm.

Chapter 3

Quantification of colony forming units (CFU's) demonstratesd that as anticipated, the Matrigel™-coated glass coverslips yielded significantly more hESC colonies than any other surface in both 2% O_2 (5.9 CFUs) and 21% O_2 (2 CFUs) conditions (Figure 3.9A). PCL nanofibrous substrates proved to be the most efficient polymer for the adherance and expansion of hESCs, particularly PCL-A (2.2 CFUs). However, it was strongly evident that the attachment of hESCs and their subsequent expansion into colonies was only possible in physiological normoxia (2% O_2), as confirmed by colony appearance as well as the morphology of single hESCs within these formed colonies. The frequency of colony formation was broadly similar for PLGA (aligned, 0.5 CFUs; random, 0 CFUs) and PLLA (aligned, 0.2 CFUs; random, 0 CFUs) electrospun fibrous substrates irrespective of fibre orienatation; however PCL-A provided a 2-fold increase over its PCL-R counterpart (Figure 3.9A).

The overall schema of colony formation and expansion in 2% O_2 was as follows: positive control (5.9 CFUs) > PCL-A (2.2 CFUs) > PCL-R (1.2 CFUs) > PLGA-A (0.5 CFUs) > PLLA-A (0.2 CFUs) > PLGA-R (0 CFUs) = PLGA-R (0 CFUs). Interestingly, the isolation and expansion of hESC colonies could be performed on all aligned electrospun fibrous substrates and that irrespective of polymer, aligned electrospun fibres were preferable to their random counterparts. There was a significantly greater number of hESC CFUs on both PLGA-A and PLLA-A over their random counterparts ($F_{(6,112)}$ = 9.07, p< 0.001); however, their was no significant difference found between orientation of PCL nanofibres.

Chapter 3

In 21% O_2, recovery of hESC colonies on electrospun fibrous substrates was not apparent but instead the attachment of tight, darkly stained, clusters of cells which had a morphological appearance similar to the mature EBs formed on gelatin-coated substrates (Figure 3.7B). The greatest number of these EB-like (EBL) cell clusters was seen on PCL nanofibres (aligned, 3 EBLs; random 3.8 EBLs) in comparison to all other polymer types. In particular, PCL-A supported the greatest number of EBL clusters with significantly greater number of EBL clusters than PLGA-A ($F_{(5, 96)} = 4.30$, p< 0.05). EBL clusters were not observed on Matrigel™-coated coverslips in 21% O_2 but instead the formation of an average of 2 CFU's; however in 2% O_2 a significantly greater of number of hESC CFUs were recovered relative to 21% O_2 on Matrigel™-coated coverslips ($F_{(1, 112)} = 10.28$, p< 0.05) (Figure 3.9A). Overall schema for EBL clusters formation in 21% O_2 was as follows: PCL-R (3.8) > PCL-A (3)> PLLA-R (1)> PLLA- A (0.8), PLGA-R (0) and PLGA-A (0) (Figure 3.9B).
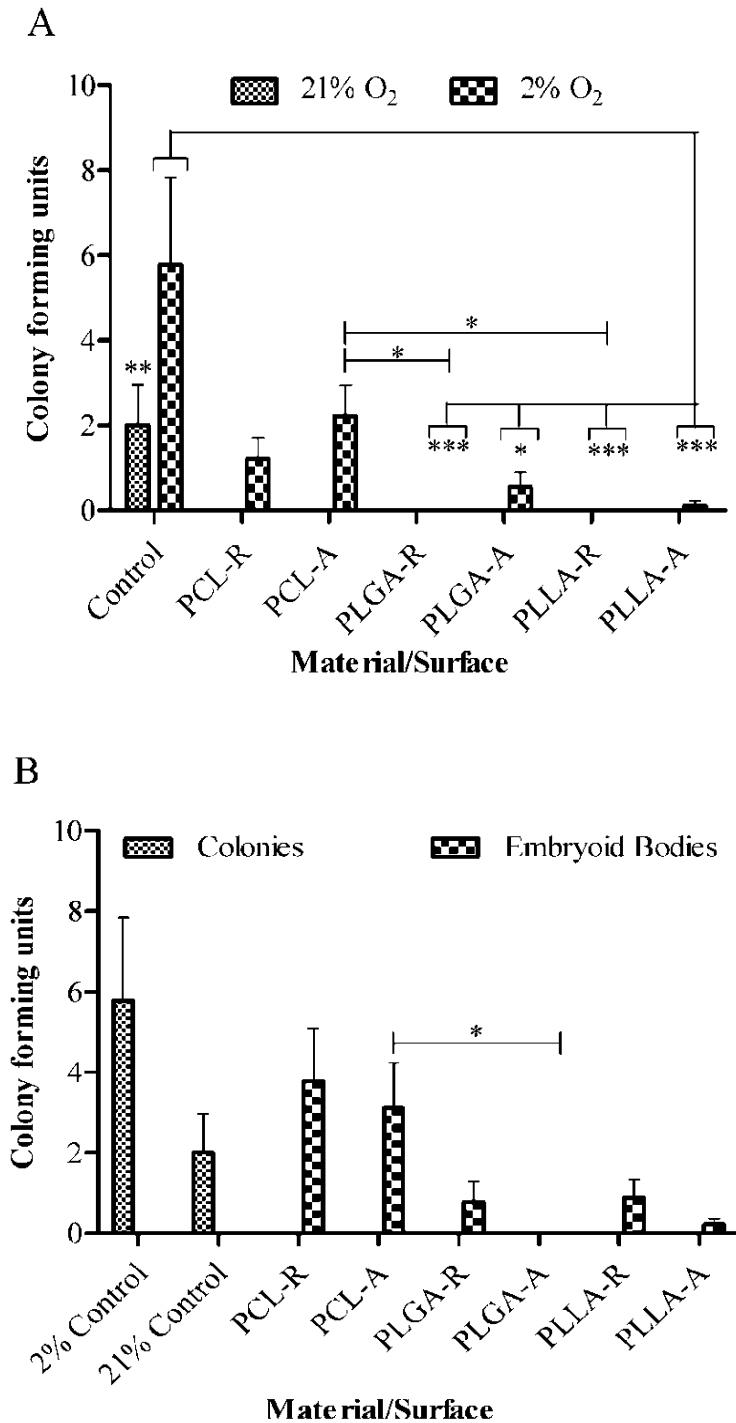
Figure 3.9 (A) Quantification of CFUs on control (Matrigel™) and electrospun fibrous substrates under physiological normoxia (2%); (B) Embryoid body like clusters formed on fibrous surfaces in hyperoxia (21%). Values indicate mean number of forming units and standard deviation of $n=9$; $*p < 0.05$, $**p < 0.01$, $***p < 0.001$.

Chapter 3

Evaluation of the effect of electrospun fibrous substrates on the expansion of hESC CFUs in 2% O_2 with regards to colony size was also investigated. Results demonstrated that, as anticipated significantly ($p < 0.001$) larger sized colonies were recovered on Matrigel™ (5 mm) relative to all electrospun fibrous substrates after 21 days of culture with ES conditioned media (Figure 3.10). Interestingly, amongst the electrospun fibrous substrates, PCL nanofibres appeared to be the overall preferential polymer type and in particular PCL-A (2.5 mm) gave rise to significantly ($p < 0.001$) larger sized colonies in comparison to PLGA-R (0 mm), PLGA-A (0.5 mm), PLLA-R (0 mm) and PLLA-A (0.2 mm). In summary of these results it appears that overall PCL appeared to be the preferential polymer type in comparison to PLLA and PLGA for hESC colony formation and expansion in 2% O_2 and EBL formation and expansion in 21% O_2.
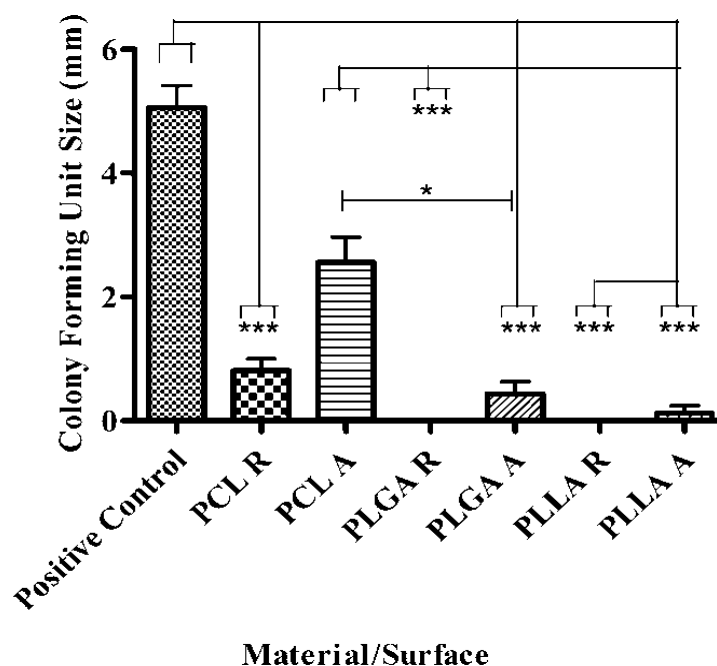
Figure 3.10 Quantification of colony size of ES colonies formed on positive control and electrospun fibrous substrates in physiological normoxia (2% O_2). Values indicate mean colony size and standard deviation of $n=9$; *$p < 0.05$, ***$p < 0.001$.

Chapter 3

3.4.4 Pluripotency of hESCs Cultured on Electrospun Nanofibrous Substrates

Using the conventional method of culturing hESCs *in vitro*, hESCs express pluripotent markers such as Alkaline Phosphatase (ALP), Nanog and Oct-3/4, where the former is a cytoplasmic marker and the latter two are intra-nuclear markers. Therefore it was important to investigate the pluripotency of hESCs cultured on Matrigel™ and PCL nanofibrous substrates (aligned and random) for 21 days with ES conditioned media in physiological normoxia (2% O_2). As expected, results demonstrated that the expansion of hESC CFUs on Matrigel™ remained undifferentiated and expressed pluripotent markers: ALP, Nanog and Oct-3/4, as shown in Figure 3.11.
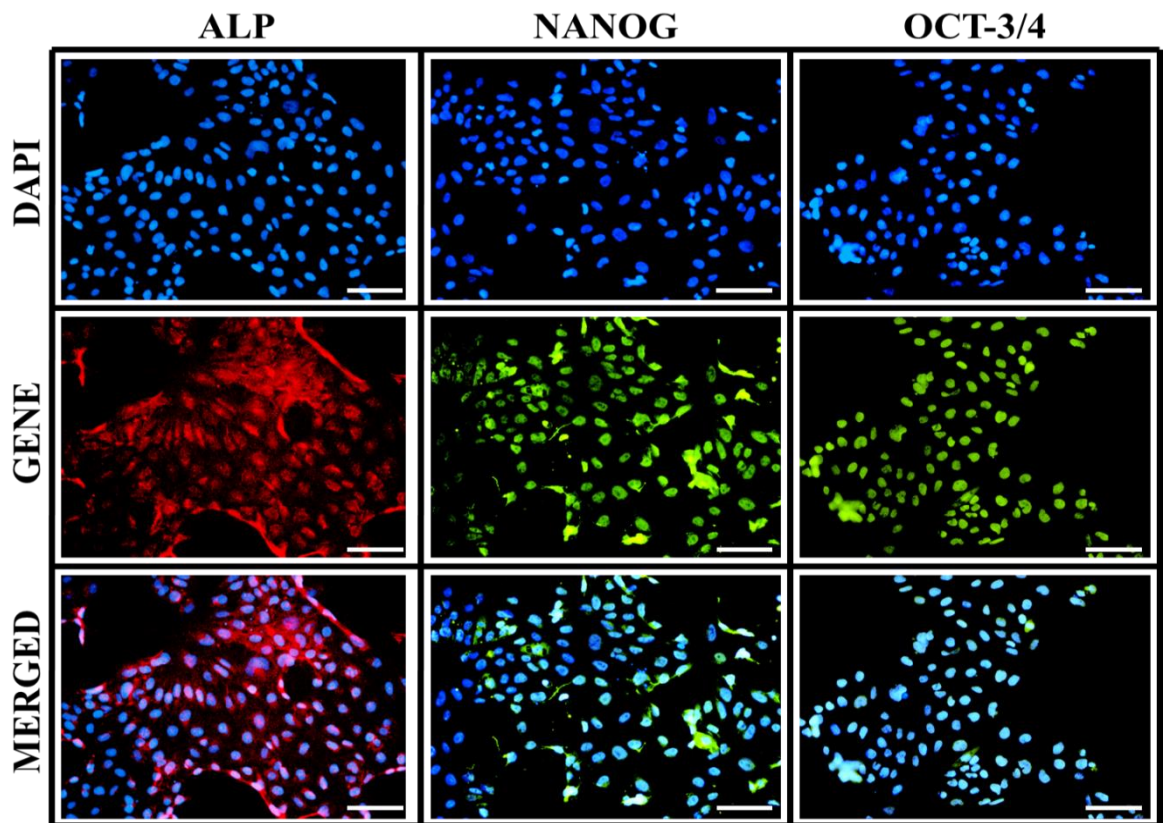
Figure 3.11 Representative immunostained images of pluripotent gene expression (alkaline phosphatase, Nanog and Oct-3/4) in hESCs cultured on Matrigel™ in physiological normoxia (2% O_2) for 21 days with ES conditioned media. Scale Bar = 200 μm.

Chapter 3

Despite colony morphology similarities it was important to confirm expression of pluripotency markers. PCL nanofibrous substrates were selected for pluripotency characterisation. hESCs-CFUs expanded in 2% O_2, for 21 days with ES conditioned media on both PCL-aligned and PCL-random nanofibres expressed pluripotent markers: ALP (Figure 3.12), Nanog (Figure 3.13) and Oct-3/4 (Figure 3.14) as confirmed via immunostaining. Expression was similar on both aligned and random PCL nanofibrous substrates for ALP, Nanog and Oct-3/4 markers.
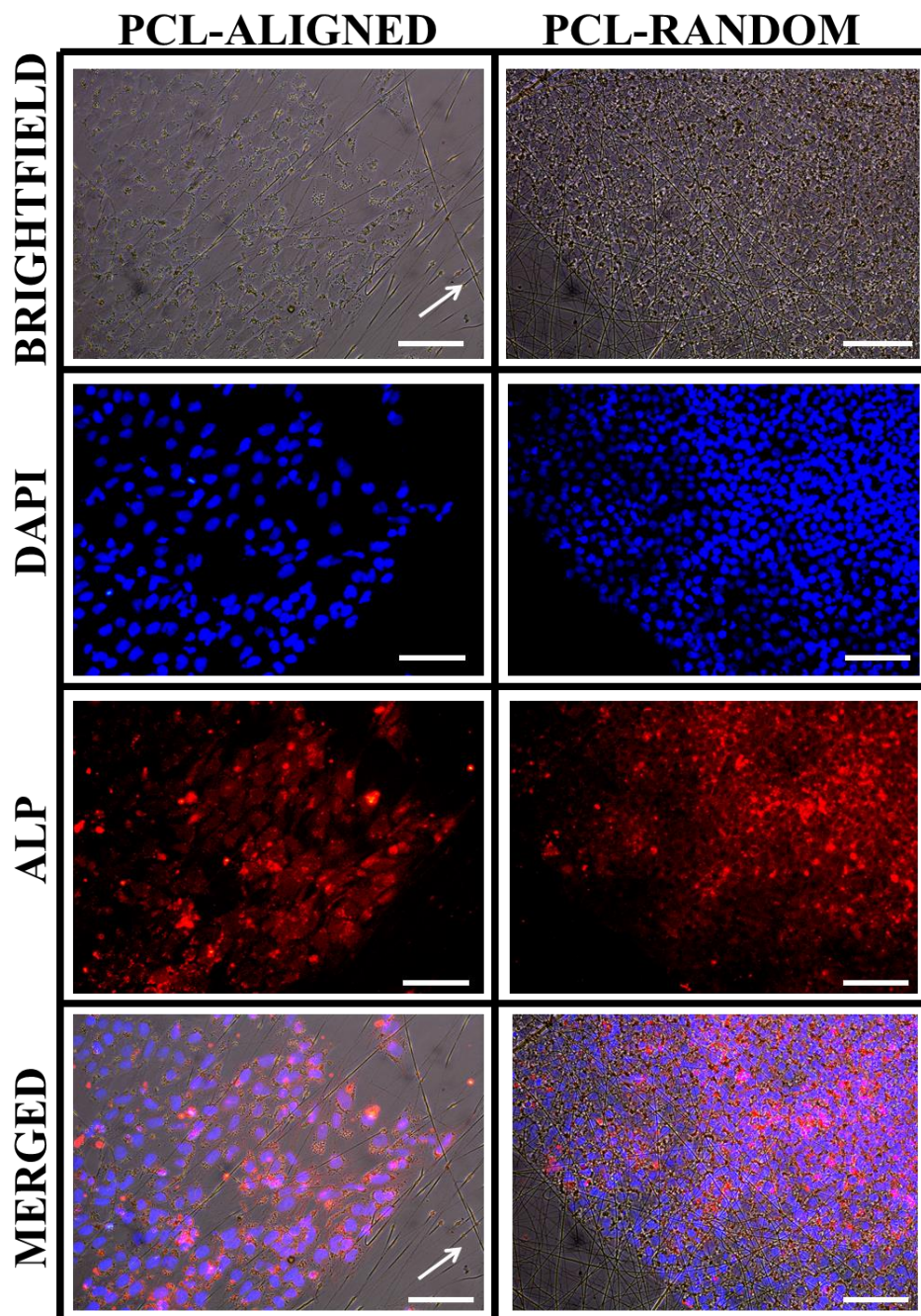
Figure 3.12 Representative immunostained images of alkaline phosphatase expression in hESCs cultured on electrospun nanofibrous substrates; PCL-random and PCL-aligned in physiological normoxia (2% O_2) for 21 days. An arrow indicates the predominant direction of aligned fibres. Scale Bar = 200 μm.
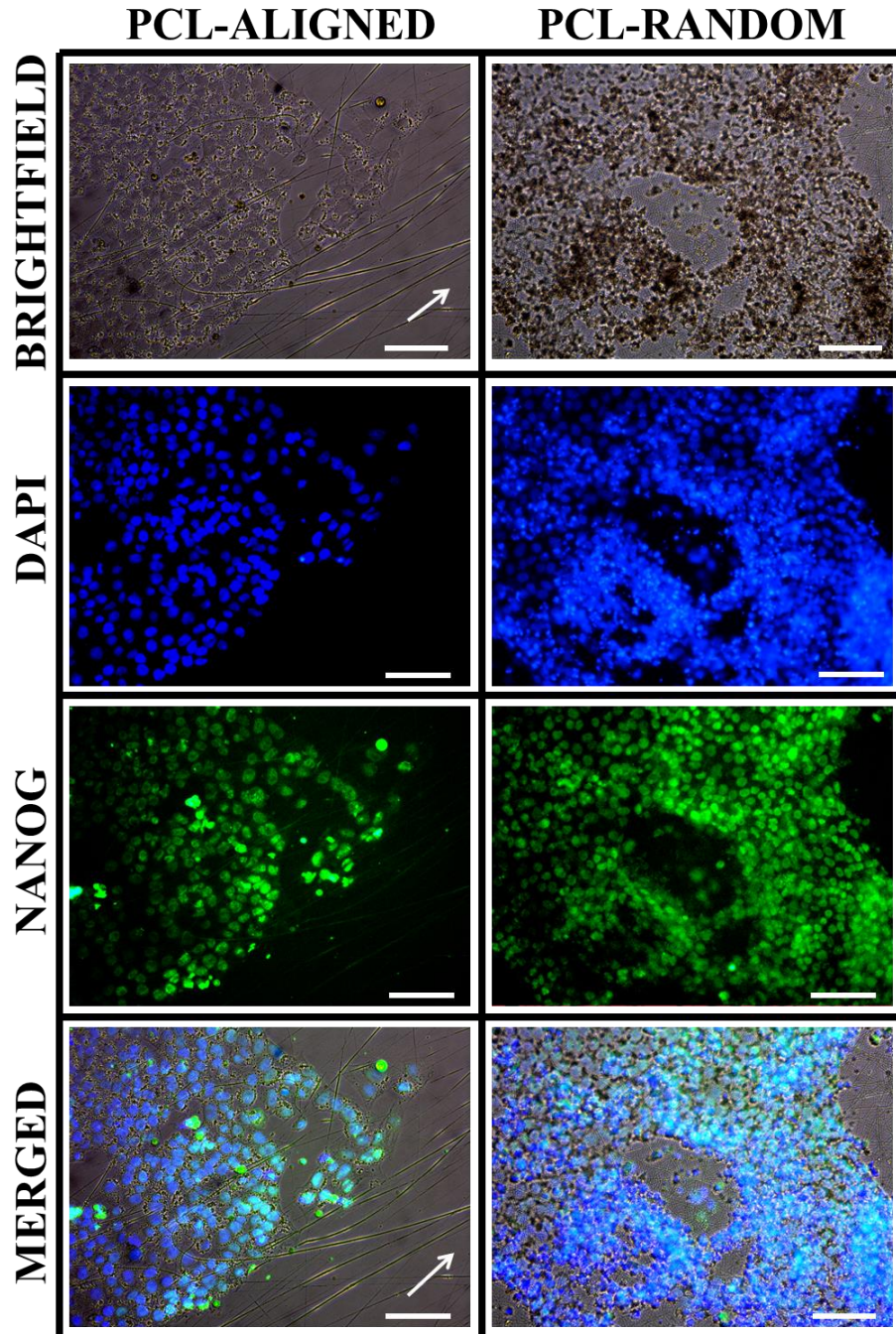
Figure 3.13 Representative immunostained images of Nanog expression in hESCs cultured on electrospun nanofibrous substrates; PCL-random and PCL-aligned in physiological normoxia (2% O_2) for 3 weeks. An arrow indicates the predominant direction of aligned fibres. Scale Bar = 200 µm.
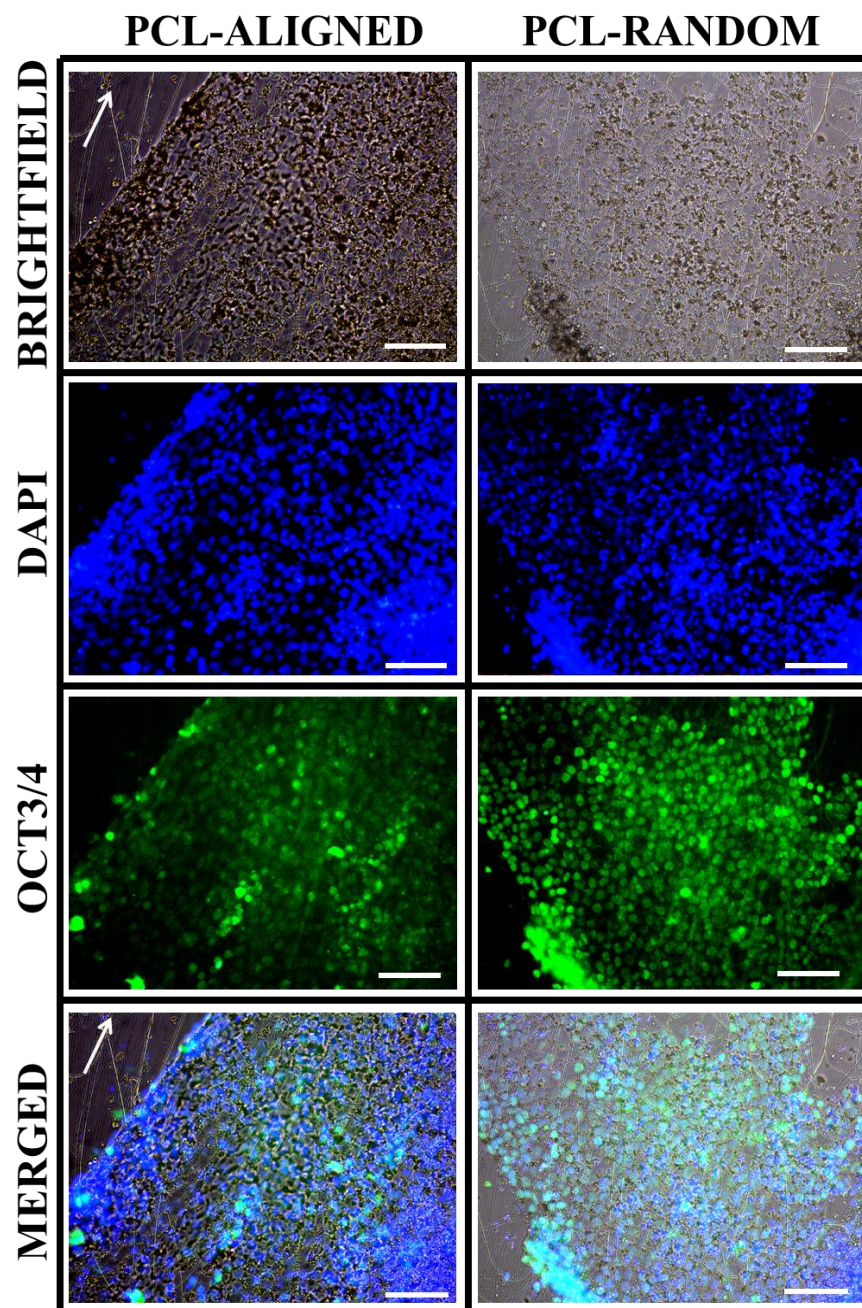
Figure 314 Representative immunostained images of Oct-3/4 expression in hESCs cultured on electrospun nanofibrous substrates; PCL-random and PCL-aligned in physiological normoxia (2% O_2) for 3 weeks. An arrow indicates the predominant direction of aligned fibres. Scale Bar = 200 μm.

Chapter 3

3.4.5 Differentiation Capacity of hESCs on Electrospun Nanofibrous Substrates

Though hESCs expanded on both PCL-aligned and PCL-random nanofibrous substrates with ES conditioned media in 2% O_2 for 21 days expressed all typical undifferentiated markers (ALP, Nanog and Oct-3/4), as confirmed by immunostaining; the pluripotential differentiation capacity of these hESCs remained unconfirmed. hESCs are theoretically able to differentiate into cells of all three somatic germ layers (Ectoderm, Endoderm, and Mesoderm).

Following recovery, hESC colonies on Matrigel™ and PCL (aligned and random) in 2% O_2 were transferred into spontaneous differentiation media for a further 20 days. Optical images in Figure 3.15 demonstrate that hESC-CFUs cultured in spontaneous differentiation media begin to spontaneously differentiate into heterogeneous, random morphology populations with loss of hESC characteristics such as a high nucleus to cytoplasmic ratio. At day 21 of hESCs cultured in spontaneous differentiation media, cells appear much larger and different in shape on all three substrates: Matrigel™, PCL-A and PCL-R nanofibrous substrates. As expected, differentiating hESCs begin to migrate out of their colonies and become more spaced out, particularly on PCL-A and PCL-R nanofibrous substrates demonstrated in Figure 3.15.
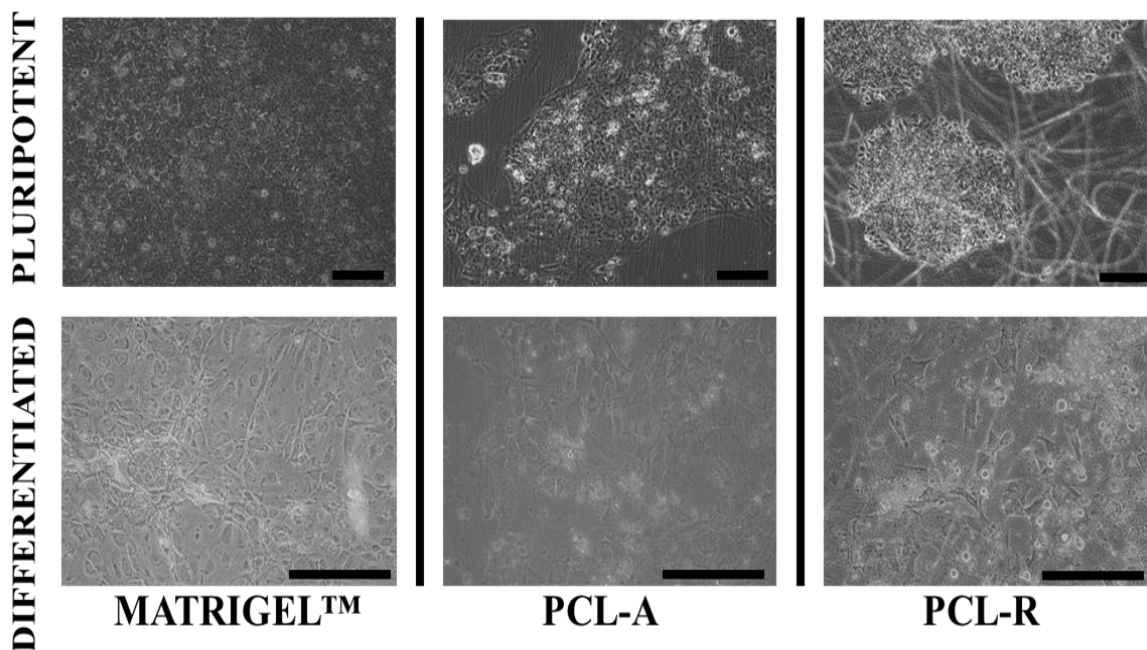
Figure 3.15 Representative optical microscopy images of hESC CFUs (expanded for 21 days with ES conditioned media) and spontaneously differentiated hESC-CFUs for a further 21 days using spontaneously differentiating media, formed on Matrigel™, PCL aligned and PCL random nanofibrous substrates in physiological normoxia (2% O_2). Scale bar = 200 μm.

Gene expression analysis of spontaneously differentiated hESC demonstrated that gradual down regulation of POU5F1 (Oct-3/4) and human Telomerase reverse transcriptase (hTERT, associated with telomere lengthening resulting in immortaility of hESCs) was immediately apparent on Matrigel™-coated and PCL-A coated coverslips and less so on PCL-R (Figure 3.16). The retention of pluripotential differentiation capacity was evidenced by the expression of transcription factors associated with the three germ layers; ectoderm (SOX1), endoderm (AFP), and mesoderm (ACTC1). SOX1 and ACTC1. However, there were slight differences in expression witnessed dependent on the substrate on which hESCs were cultured. SOX-1 expression was visible from day 0 to day 10 on Matrigel™,

whereas on PCL-R and PCL-A expression was evident from day 0 to day 20, although this was weaker expression compared to SOX-1 expression in hESCs cultured on Matrigel™. AFP expression was visible up to day 5 on Matrigel™ and up to day 10 for both PCL-A and PCL-R substrates. ACTC-1 expression was strong and visible from day 0 to day 20 on all three substrates (Matrigel™, PCL-A and PCL-R)
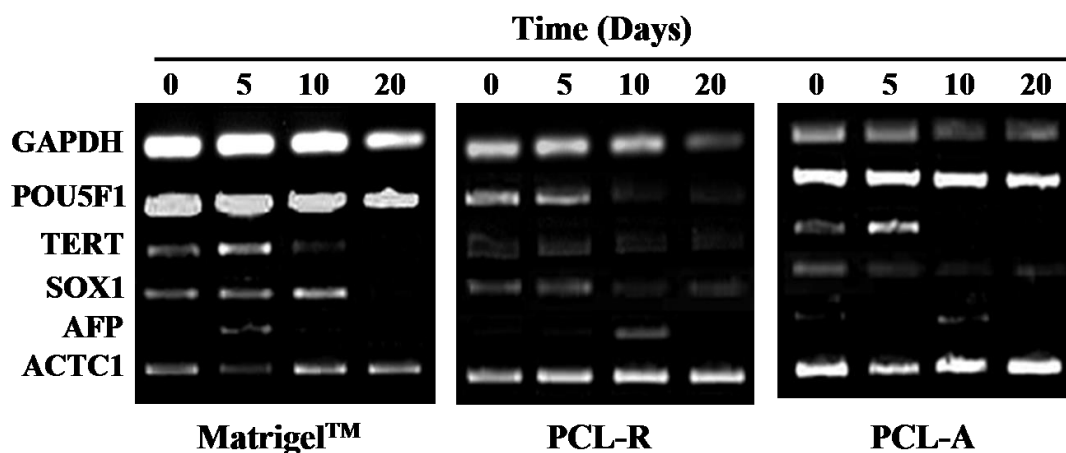
Figure 3.16 RT-PCR ran on 2% Agarose Gel electrophoresis to evidently illustrate the presence and expression levels of various genes, on both PCL aligned and random nanofibrous substrates including positive control (Matrigel™). Qualitative gene expression was investigated at different time points during spontaneous differentiation. Genes investigated include: GAPDH (housekeeping gene), POU5F1 (pluripotent marker), TERT (immortality marker) SOX1 (ectoderm germ layer), ACTC1 (mesoderm germ layer) and AFP (endoderm germ layer).

Having identified the differentiation capacity of hESCs towards all three somatic germ layers (ectoderm, endoderm and mesoderm) on PCL electrospun nanofibrous substrates in physiological normoxia (2% O_2), the ability of hESCs to differentiate further into the

mesoderm lineage to become specialised cells of the skeletal lineages was also investigated on Matrigel™, PCL aligned and PCL random nanofibrous substrates. Expanded hESC-CFUs on all three substrates for 21 days in physiological normoxia (2% O_2) were differentiated into adipogenic, chondrogenic and osteogenic lineages using respective differentiation media's for a further 21 days. Differentiated hESCs on all three substrates were fixed and stained using corresponding differentiation media's; lipids (adipose tissue) were stained using oil red O, sulphated glycosaminoglycans (GAGs; cartilage tissue) were stained using alcian blue and calcium ions (bone tissue) were stained using alizarin red (Figure 3.17). Observations revealed that undifferentiated hESCs on all three substrates were negative for all three stains. All three substrates stained positive for lipids (indicated by red stain); greatest intensity of the stain was observed on Matrigel™ in comparison to PCL nanofibrous substrates (aligned and random). Chondrogenic differentiation of hESCs was evaluated by staining sulphated GAGs; though all three substrates stained positive for sulphated GAGs (indicated by blue stain), it was apparent that the nanofibres enhanced chondrogenic differentiation indicated by a greater secretion of GAGs in comparison to Matrigel™. Evaluation of hESC osteogenic differentiation was demonstrated by positive staining for secreted calcium ions (indicated by red stain). Despite similar intensity of staining on all three substrates, there was a visible difference in organisation of secreted calcium ions in the matrix; on PCL random nanofibres calcium ions were gathered in large rounded clumps in comparison to PCL aligned nanofibres where calcium ions within the secreted matrix were aligned parallel to the direction of the nanofibres.
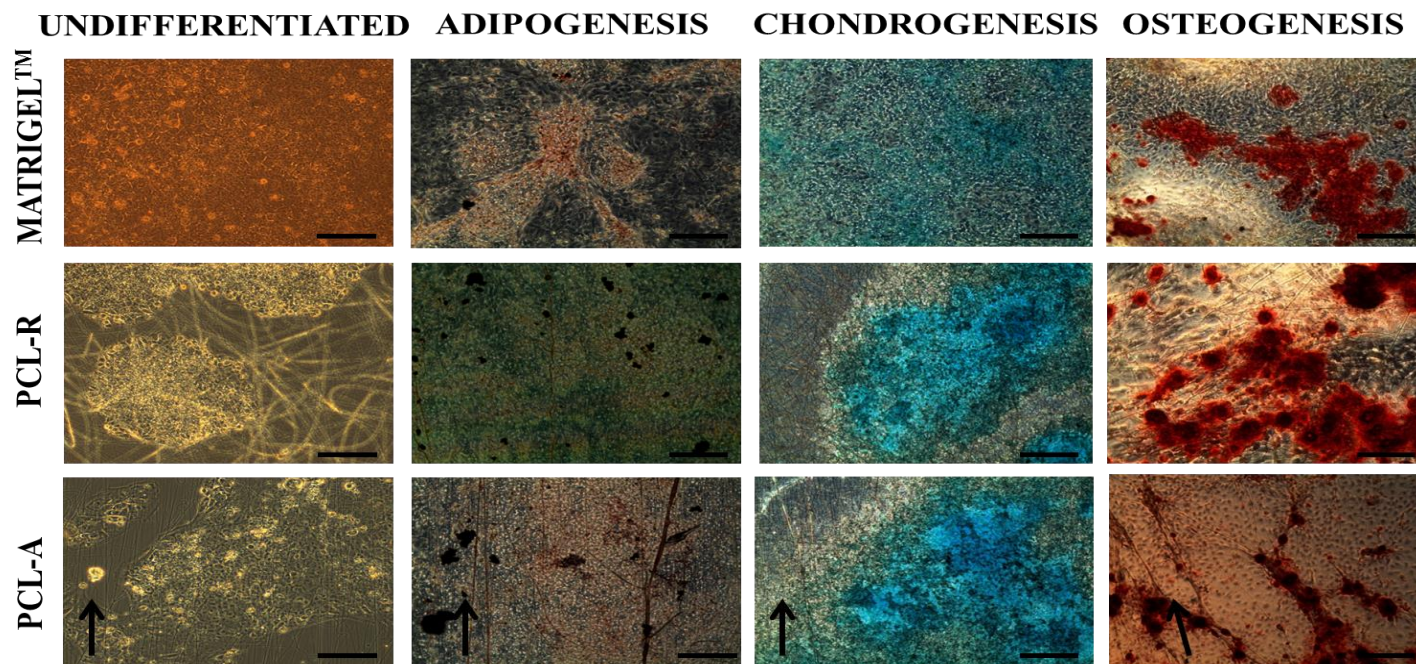
Figure 3.17 Representative optical images of respective histology stains of differentiated hESC CFUs into skeletal lineages. hESCs were expanded on PCL aligned and random nanofibrous substrates using ES maintenance media for 21 days in physiological normoxia (2% O_2); media was then switched to differentiation media specific for adipogenesis, chondrogenesis and osteogenesis for a further 21 days. Differentiated hESCs were fixed and stained for lipids (adipose tissue), sulphated glycosaminoglycans (cartilage tissue) and calcium ions (bone tissue) using relevant histological stains. Scale bar = 200 µm.

Chapter 3

3.4.6 The effect of Fibre Diameter on the Recovery and Expansion of hESC-CFUs in Physiological Normoxia (2% O_2)

It has recently been documented that fibre diameter can influence the ability of cells to adhere, proliferate and differentiate [Badami *et al.*, 2006]; however trends that occur are specific to both cell type and the substrate properties. PCL-A and PCL-R nanofibrous substrates were fabricated with two different fibre diameters for each fibre orientation. FESEM visualisation shows fibre morphology of the non-beaded PCL nanofibres as well as the difference in fibre diameter (Figure 3.18). FESEM also further permitted fibre diameter analysis; in both cases for aligned and random nanofibres, the larger diameter nanofibres (PCL-A, 521 nm; PCL-R, 660 nm) were significantly (p < 0.01) greater than their smaller counterparts (PCL-A, 280 nm; PCL-R, 318 nm) as evaluated in Figure 3.19.
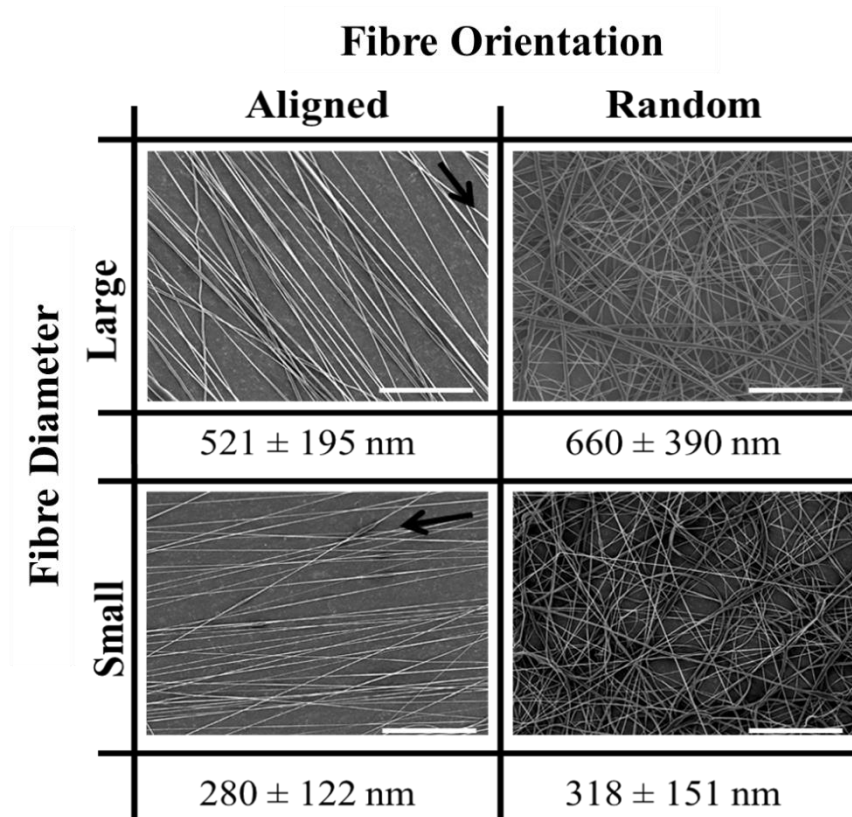
Figure 3.18 Scanning Electron Microscopy images of electrospun PCL nanofibrous substrates (Aligned and Random) with varying fibre diameter. Scale Bar = 3 μm.

Chapter 3
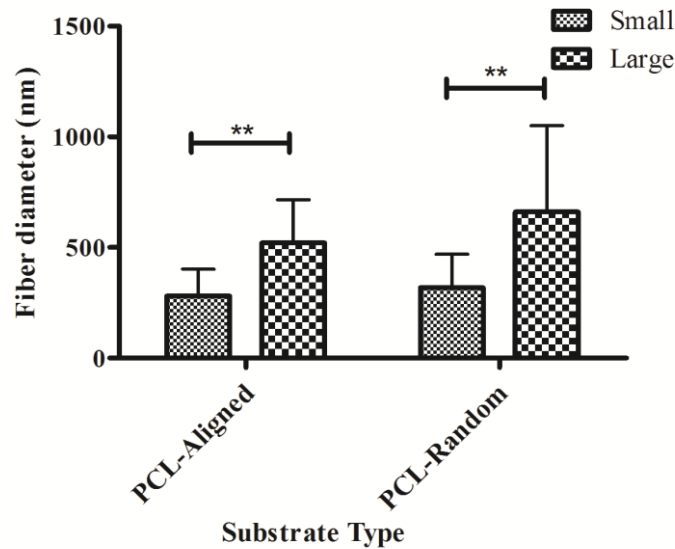
Figure 3.19 Graph representing the average fibre diameters of both aligned and random electrospun nanofibres fabricated from PCL with varying fibre diameter. Values indicate mean fibre diameter and standard deviation of n=20; $**p < 0.01$,

hESCs were cultured on PCL-A and PCL-R nanofibrous substrates with large diameters (-A = 521 nm and –R= 660 nm) and small diameters (-A = 280 nm and –R = 318 nm) with ES conditioned media in physiological normoxia for 21 days. Giemsa staining of recovered colonies revealed as anticipated Matrigel™ surfaces to support significantly greater number of hESC CFUs than any nanofibrous substrate regardless of fibre orientation and diameter. Amongst the nanofibrous substrates, the smaller diameter nanofibres for both PCL-A and PCL-R recovered a greater number of hESC colonies compared to their larger diameter counterparts (Figure 3.20A). Morphological evaluation of recovered hESC colonies on each substrate was also visualised shown in Figure 3.20B.

Chapter 3
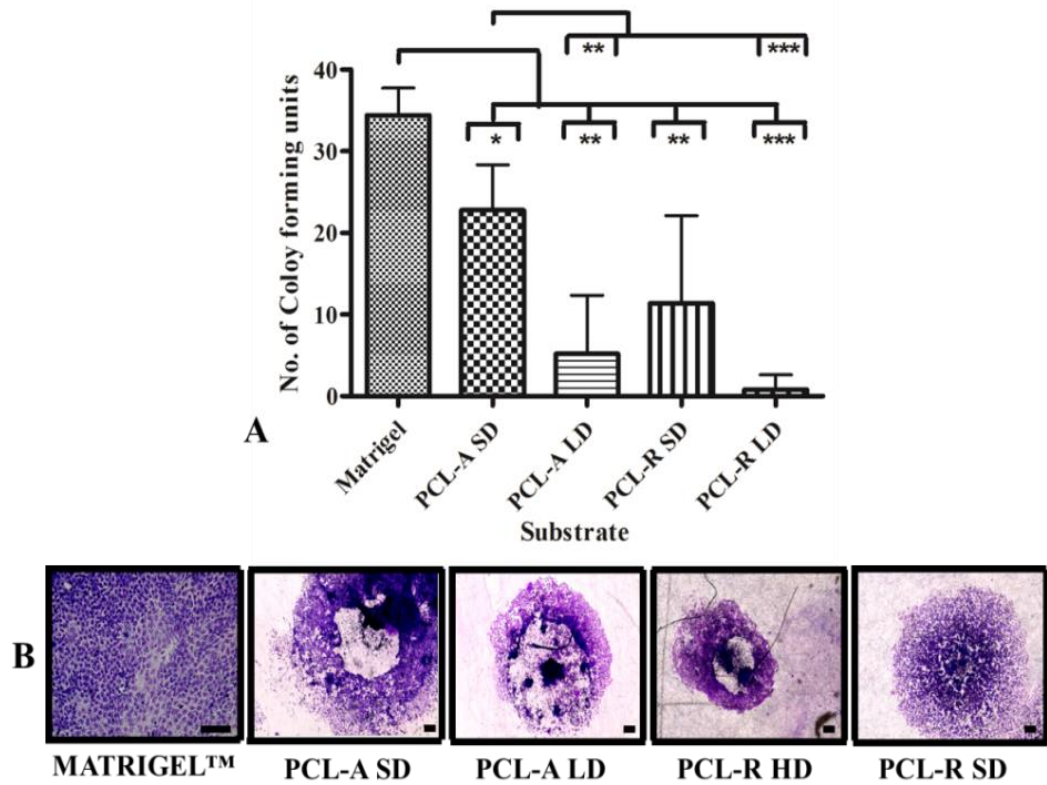
Figure 3.20 Relationship between PCL aligned and random nanofibrous substrates at various diameters and hESC CFU ability. (A) Quantitative analysis of the number of hESC colonies formed on Matrigel™ PCL nanofibres where SD denotes for "small diameter (Ø 280-318 nm)" and LD stands for "large diameter (Ø 521-660 nm)". (B) Representative optical microscopy images of Giemsa stained optical microscopy images of hESC colonies on the various substrates investigated. Scale bar = 200 µm.

Chapter 3

3.5 Discussion

A novel substrate and culture conditions for hESCs have been identified and developed with the capacity to support the culture and expansion of hESCs whilst retaining their undifferentiated state, with scaleable opportunities sufficient for clinical therapies. However, the effectiveness of the substrate to support the expansion of hESCs is very much reliant on the oxygen environment. The novelty of the findings in this chapter demonstrates the synergistic effect of nanofibre and oxygen environment. In combination they eliminate the use of Matrigel™ preventing xenocontamination exposure as well as providing basic foundations for a potential transportable and a transplantable substrate for the use of hESC-derived differentiated cells in clinical therapeutics including tissue engineering and regenerative medicine applications.

hESCs expanded on electrospun fibrous substrates fabricated from FDA approved polymers (PCL, PLGA and PLLA) in both aligned and random conformations demonstrated their suitability for CFU expansion. PCL was then further exemplified as supportive of hESC culture through hESC morphology, CFU morphology, pluripotentcy marker expression, germ layer gene expression, and mesodermal differentiation capacity. However, this phenomenon was apparent in physiological normoxia (2% O_2) only. These unique findings demonstrate several advantages over current attempts to culture hESCs on nanofibrous substrates; where many studies have shown to be reliant on either co-culture of MEFs (feeder layers) or the use of composite polymers (natural and synthetic) to encourage hESCs to recognise attachment sites for adhesion with the compromise of losing hESC pluripotency. This chapter is the first to demonstrate the use of purely synthetic polymers in both aligned and random conformations, in combination with the effects of

lower oxygen concentrations on the expansion of undifferentiated hESCs. However, limitations associated with this substrate include the lack of 3D structure (at the cellular level) of the substrate and the importance in maintaining the nano-architectural feature (at the cellular level) within a 3D construct.

Of the polymers tested, PCL supported the recovery of the greatest number of hESC colonies. Colony Size, morphology, pluripotency and differentiation capacity were very similar between electrospun PCL nanofibres and positive controls (Matrigel™). The largest CFUs were observed on Matrigel™-coated and PCL-A nanofibre-coated coverslips. PCL belongs to the aliphatic polyester group of polymers and is considered to be semi-crystalline with resorbable properties permitting a slow degradation rate as a result of its chemically stable and hydrophobic nature [Barnes *et al.*, 2007; Kweon *et al.*, 2003]. This data therefore suggests that degree of hydrophobicity and alignment may be suitable characteristics for hESC culture. PCL has FDA approval for use in medical devices due to its ready biodegradability into non-toxic by-products and its *in vitro* and *in vivo* biocompatibility. Previous cell-based studies have shown that electrospun PCL nanofibrous scaffolds can support numerous cell types including skeletal muscle cells [Choi *et al.*, 2008], schwann cells [Schnell *et al.*, 2007], fibroblasts [Chong *et al.*, 2007], bone marrow derived-MSCs [Li *et al.*, 2005], human cord-blood derived somatic stem cells [Hashemi *et al.*, 2009], mouse ESCs [Xie *et al.*, 2009] and hESCs [Gauthaman *et al.*, 2009].

Chapter 3

The architectural structure of the extracellular matrix includes a network of nano- and micro fibres made up of structural, basement membrane proteins such as collagen and laminin. The attempt to mimic this native ECM architecture using synthetic electrospun nanofibres has encouraged the attachment and expansion of undifferentiated hESCs. This has been particularly demonstrated by the retention of the typical hESC morphology as small rounded cells with a high nucleus to cytoplasmic ratio, and the maintainance of the characteristic feature of expanding in tightly adherent, compact colonies, between the expanded hESCs on PCL (aligned and random) nanofibrous substrates and Matrigel™. These observations were corroborated with the expression of pluripotent gene markers including Alkaline phosphatase, Oct-3/4 and Nanog at similar intensities between PCL and Matrigel™. Evaluation of the differentiation capacity of expanded hESCs on PCL substrates validated their ability to express gene markers for all three somatic germ layers (Ectoderm, Endoderm and Mesoderm).

Wettability of the nanofibrous substrates was investigated using water contact angle analysis. Wettability can be affected by many factors including polymer chemistry, surface roughness, and topography. Increasing the hydrophilic nature of a substrate would result in greater wettability and increased adsorption of proteins from media with subsequent increase in cell attachment. Hence, increasing the hydrophilic nature of a substrate as demonstrated by a previous study where natural polymers (collagen and gelatin) were incorporated into PCL to fabricate nanofibrous substrates for culturing hESCs, improved their biocompatibility and thus cell affinity resulting in their attachment and proliferation. Water contact angle analysis demonstrated that all nanofibrous substrates investigated in this chapter had insignificant differences in terms of wettability regardless of polymer type

and orientation, although PCL is generally considered more hydrophobic in nature relative to PLGA and PLLA.

Topography is also considered to have strong effects on cell activity [Badami *et al.*, 2006], as it provides physical guidance, which is able to mimic native fibrillar ECM proteins, a key component of the stem cell niche [Ravichandran *et al.*, 2009]. Cell adherence has been demonstrated to be directly under the influence of nanotopography (nanofibres) rather than the chemistry of the polymer itself [Schindler *et al.*, 2005]. This was also demonstrated by preliminary data which revealed that polymer films (acting as a material control) fabricated from PCL, PLGA and PLLA, supported embryoid body-like cluster formation and no CFU's, regardless of oxygen concentration. However, further work would be required to fully confirm this statement. Many studies have demonstrated the ability of electrospun nanofibrous substrates in combination with chemical cues to induce the differentiation of stem cells such as hMSCs/ESCs and other stem cells towards skeletal lineages such as adipose, bone and cartilage tissue [Bielby *et al.*, 2004; Li *et al.*, 2005; Smith *et al.*, 2009; Wimpenny *et al.*, 2010; Xie *et al.*, 2009]which were confirmed by typical histological stains for specific ECM proteins and RT-PCR for transcriptional markers up regulated for each lineage. Furthermore, the substrates used in this chapter (electrospun PCL aligned and random nanofibrous substrates) supported hESC differentiation towards adipogenic, chondrogenic and osteogenic lineages as confirmed by histological stains for lipids, GAGs and calcium ions, respectively. Furthermore topography has also demonstrated to support the expansion of stem cells in an undifferentiated state; ESCs and hMSCs have been previously reported to expand on electrospun nanofibrous substrates while retaining their stemness, which further supports the data from this chapter [Chan *et al.*, 2009; Jin *et al.*,

2004; Li *et al.*, 2005; Nur-E-Kamal *et al.*, 2006]. However, in all of these cases, ESCs were reliant upon co-culture with other cells such as feeder layers or the combination of natural polymers electrospun with the synthetic polymer. None of these studies investigated the effects of purely synthetic polymers without the use of feeder layers for the attachment and expansion of undifferentiated hESCs. Nanofibres have an increased surface area to volume ratio which increases the number of focal adhesions sites a cell can form with numerous surrounding nanofibres. Increase in anisotropy is known to further increase the number of focal adhesion contacts from the cells to the surrounding fibres which may be the reason why aligned nanofibres support larger and greater number of CFU's [Yang *et al.*, 2005]. Anisotropy has shown to be particularly important during neural stem cell differentiation towards functional nerve cells with increased neurite outgrowth on aligned nanofibres and enhanced differentiation of hMSCs into mesoderm lineages [Pittenger *et al.*, 1999; Schnell *et al.*, 2007]. Findings from this chapter further demonstrate that anisotropy also plays an important role in stimulating cell proliferation of hESCs during culture in physiological normoxia (2% O_2).

It is important to note that different cell types behave differently and may prefer a certain type of substrate, dependant on hydrophilicity, topography and stiffness. PCL has modest bulk mechanical properties with a tensile modulus of 200-400MPa. When compared to other polymers used in this chapter (PLLA, up to 3-4 GPa; PGA, up to 6-7 GPa) , it is evident that PCL is less stiff and thus hESCs in particular may prefer a softer substrate for attachment and expansion [Mano *et al.*, 2004]. Extensive studies investigating the relationship between stem cell fate and the stiffness of substrate matrix have demonstrated that with changing substrate modulus, hMSCs and ESCs can differentiate into various

Chapter 3

lineages including bone, muscle and brain [Li *et al.*, 2011]. Furthermore, softer hydrogels with a lower modulus increased the proliferation rate of hESCs [Lee *et al.*, 2010], which also lies in agreement with observations by [Evans *et al.*, 2009], where polydimethlysiloxane substrates with varying stiffness demonstrated to influence ESC proliferation and differentiation; in this study softer substrates enhanced cell attachment and proliferation rate whereas stiffer substrates induced their differentiation towards an osteogenic lineage [Evans *et al.*, 2009].

The impact of fibre diameter on cell activities including attachment and proliferation with various other cell types but not hESCs [Badami *et al.*, 2006]. A study by Kwon *et al.*, 2005 described how fibres with a smaller diameter supported greater attachment and proliferation of human umbilical vein endothelial cells (HUVEC) [Keun Kwon *et al.*, 2005]. However, speculation still remains with regards to whether or not this is a generic trend or is influenced by several other factors including; degree of hydrophilicity, the cell type and the substrate stiffness. Nonetheless, data from this chapter supports the findings from [Keun Kwon *et al.*, 2005]. PCL nanofibres were the thinnest fibres; Ø 280 nm and Ø 318 nm for PCL-aligned and PCL-random, respectively; these fibres supported the greatest number of hESC-CFUs in contract to PLLA-A which were the thickest fibres (2506 nm) but yielded the smallest number of CFUs. These observations were further corroborated with colony size analysis which demonstrated that thinner nanofibres (PCL-aligned and PCL-random) supported greater proliferation represented by the formation of much larger colonies relative to thicker fibres such as PLLA-A. In depth investigations into the effect of fibre diameter on hESC expansion included electrospinning the preferential material PCL with tailored fibre diameters. Results demonstrated a similar trend where thinner fibres supported the greatest number of hESC-CFUs.

Chapter 3

A similar trend was also determined by a previous study using hMSCs where nanofibrous scaffolds fabricated from 0.5% PLGA and 10% PCL had fibre diameters <280 nm but supported the greatest number of colonies in both physiological normoxia (2% O_2) and hyperoxia (21% O_2) (A combination of hMSC and hESC CFU recovery as a result of fibre diameter is demonstrated in Figure 3.21A). These observations have broad agreement across the field where fibre diameters of <500 nm generally promote cell adhesion and encourage greater cell attachment due to increased surface area to volume ratio with an associated increase in the probability of focal adhesion sites available for cell attachment [Ma *et al.*, 2008; Ravichandran *et al.*, 2009]. Fibre diameter may therefore play a pivotal role of more importance than the chemistry of the polymer itself (as preliminary data showed that polymer films supported the formation of embryoid body-like clusters rather than CFUs'). Furthermore, by tailoring the diameter of fibres electrospun from PLGA and PLLA, which under performed in comparison to PCL could enhance hESC CFU ability. Analysis of data also revealed the direct influence of fibre diameter on the size of CFUs recovered regardless of polymer chemistry. As shown in Figure 3.21, decreasing fibre diameter also resulted in an increase in colony size
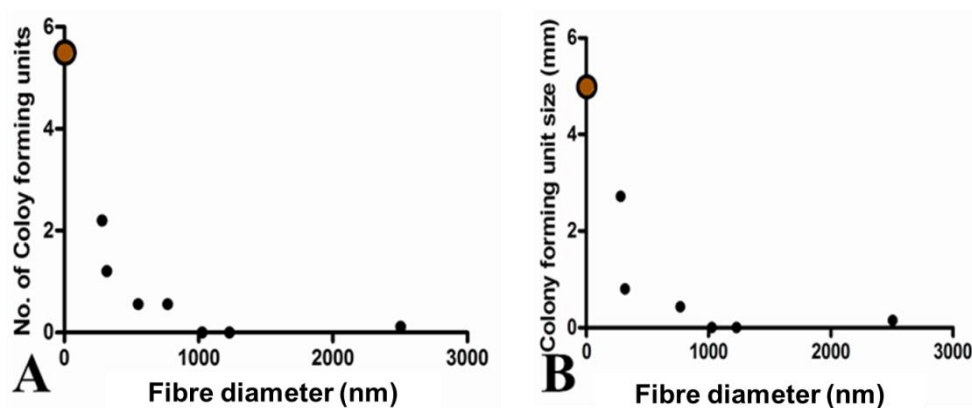
Figure 3.21 Graphs representing relationship between hESC and hMSC CFU phenomenon and fibre diameter; (A) number of colonies formed on various fibre diameters and (B) CFU size

influenced by fibre diameter on which they were cultured. Red circles indicate Matrigel^{TM} control values.

The biocompatibility of a substrate dictates its ability to support cell activity such as attachment, proliferation and differentiation. In particular, the surface interface of the substrate is a dynamic environment and upon contact with biological fluid or media (during *in vitro* culture) initiates the adsorption of proteins to its surface and subsequent cell attachment. Protein adsorption is thus dependant on the availability of functional groups on the substrate, the polarity of the functional groups on the substrate as well as protein characteristics and their conformational changes. ECM proteins such as fibronectin, laminin and collagen IV are known to exist abundantly in hESC cultures; this leads to the speculation that there is a possibility in the difference of concentration of these proteins adsorbing to the various substrates investigated in this chapter resulting in a difference in cell attachment. Furthermore, the potential of PCL nanofibres to adsorb these ECM proteins and in turn for these proteins to have a high affinity for this substrate in an active conformational state result in more effective cell attachment in comparison to PLGA and PLLA. Physical entrapment of a greater number of proteins within thinner nanofibrous substrates may also enhance the concentration of crucial ECM proteins being present on PCL substrates allowing increased availability of recognised attachment sites for corresponding membrane receptors situated on hESCs. However, further investigations would be required to validate this hypothesis.

It has been reported that selective adsorption of key ECM proteins on nanofibrous substrates can alter hESC cytoskeletal morphology on the fibres, consequently resulting in

the activation of Rac-AKT-JNK signalling pathways which maintain stem cell pluripotency [Nur-E-Kamal *et al.*, 2006]. However, this cross-talk between cells and its surrounding ECM occurs through membrane receptors known as integrins, which permits the initial attachment of cells to their ECM and can influence several cellular activities. Integrins are able to interact with corresponding ECM ligands (such as fibronectin and laminin) that are initially adsorbed onto synthetic substrates depending on their conformation shape which determines their affinity for integrins. Additionally, integrins also become activated by ECM proteins permitting their initial adhesion and proliferation. As the results of this chapter have revealed a synergistic effect on hESC colony formation through combining physiological normoxia (2% O_2) and nanofibrous substrate; this leads to the hypothesis that there may be a difference in integrin expression pattern dependant on the oxygen environment in which hESCs have been cultured which permits hESC attachment and proliferation on nanofibrous substrates to form undifferentiated hESC colonies under 2% O_2 and EB-like structures under 21% O_2.

3.6 Conclusion

A novel substrate for hESC expansion in the form of electrospun nanofibrous substrates fabricated from purely synthetic, FDA approved polymers demonstrated the ability to support the attachment and expansion of hESCs whilst retaining their undifferentiated state. However, a synergistic effect was apparent between nanofibres and oxygen concentration which supported this phenomenon; this was apparent in physiological normoxia (2% O_2) only, as in 21% O_2 hESCs demonstrated the expansion of embryoid bodies instead. As expected, Matrigel™ supported the greatest recovery of hESC colonies but the preferential synthetic material for hESC expansion in either oxygen environment

Chapter 3

was PCL. Furthermore, aligned nanofibrous substrates significantly performed better over their random counterparts as demonstrated by CFU numbers and size. Overall, amongst the electrospun fibrous substrates, PCL-aligned significantly provided the optimal results. Characterisation of hESC expansion on optimal substrates (PCL nanofibres) in optimal oxygen conditions (2% O_2) indicated that hESCs expressed undifferentiated markers such as alkaline phosphatase, Oct-3/4 and Nanog as well as hESCs cultured on Matrigel™. Additionally, pluripotential differentiation capacity evaluation of hESCs expanded on PCL nanofibrous substrates demonstrated the ability of expanded hESC colonies to express SOX1 (ectoderm germ layer), AFP (endoderm germ layer) and ACTC1 (mesoderm germ layer). Investigating the relationship between fibre diameter and expansion of hESC-CFUs in optimal conditions such as PCL-nanofibrous substrates and 2% O_2 indicated that by tailoring fibres to a thinner diameter from Ø 521 – 660 nm to Ø 280 – 318 nm significantly increased the number of recovered hESC-CFUs.

Chapter 4

4. Identification of Adhesion Determining Molecules in hESCs

4.1 Introduction

The previous chapter demonstrated the ability of FDA approved synthetic substrates to support the attachment, and expansion of hESCs in a defined environment dependent upon polymer type, fibre orientation, fibre diameter, and oxygen environment. The optimal conditions were identified as a PCL substrate, in aligned conformation, with fibre diameter in the range of 280 nm and physiological normoxic conditions (2% O_2) for the expansion of undifferentiated hESCs with typical morphological characteristics, retention of pluripotential markers and differentiation capacity. However, these yielded a lower number of colonies in comparison to the conventional Matrigel^{TM} method, which remains as the optimal method for the expansion of undifferentiated hESCs *in vitro*. Minimal research has been performed to investigate the exact mechanisms which dictate the specificity of hESCs to adhere to substrates such as Matrigel^{TM}.

Matrigel^{TM} is comprised of extracellular matrix (ECM) proteins including laminin-111, collagen IV, heparin sulphate proteoglycans, entactin, fibronectin, growth factors, matrix-degrading enzymes and their inhibitors; and other undefined components [Xu *et al.*, 2001]. Thus, Matrigel^{TM} is a broad-range substrate which, alongside medium provided components (i.e. FGF2), provides essential cues for hESC *in vitro* expansion. The ECM attachment of hESCs is primarily mediated by integrins (heterodimeric, transmembrane glycoproteins) and other surface receptors [Humphries *et al.*, 2006]. Broadly, integrin functions include mediating cell-cell and cell-ECM interactions and bidirectional signalling between the cytoskeleton and ECM. As a result, integrins can detect and

transmit physical and chemical changes in the ECM to the intracellular regions of the cell or *vice versa*, triggering a cascade of intracellular pathways. The integrin family is comprised of 18 α-subunits and 8 β-subunits, with 24 recognised distinct heterodimer arrangements each with a specific set of functions [Humphries *et al.*, 2006; Hynes, 2002; Wong and Bernstein, 2010]. For example, the β_1 subunit can heterodimerise with, minimally, 12 distinct α chains to form integrin dimers found on cell types representative of the three germ layers [Meng *et al.*, 2010].

ECM proteins which are essential for hESC adhesion and pluripotency retention have been identified as laminin-111, collagen IV, fibronectin and vitronectin [Prowse *et al.*, 2011]. Laminin, a key developmental, structural ECM protein, is an essential component of virtually all basement membranes [Cooper *et al.*, 1991]. Critical roles of laminin include the mediation of cell adhesion, cell spreading, cell migration and proliferation. There are many associated integrin receptors for laminin including; α1β1, α2β1 and α3β1. α6β1 is considered to be specific to laminin while the $\alpha6_B\beta1$ variant is expressed by pluripotent hESCs [Cooper *et al.*, 1991]. Integrin subunits and heterodimers detected on the surface of hESCs include α2, α3, α5, α6, α11, β1 and αVβ5. These subunits can heterodimerise to form receptors specific to fibronectin (α5β1), vitronectin (αVβ5), collagen and laminin (α2β1) and laminin-111 (α6β1) Furthermore, α9β1 (integrin receptor for collagen, laminin and VCAM1) has also been recognised as an essential mediator for maintaining hESC pluripotency [Lee *et al.*, 2010]. Fibronectin, bound by the α5β1 heterodimer, is one of the major substrate proteins found within MEF-conditioned media [Braam *et al.*, 2008]. A recent study demonstrated that antibody-directed blockage of the α5β1 heterodimer impacted hESC attachment across a range of defined substrate coatings including collagen

Chapter 4

IV, laminin and entactin, when cultured with MEF-conditioned media, suggesting that

fibronectin is secreted by feeder cells which adsorbs onto surfaces thus promoting hESC

adherence [Braam *et al.*, 2008]. In defined media (mTeSR1), blocking α5β1 had no effect

on hESC attachment to a vitronectin-coated substrate but hindered adhesion to all other

ECM protein substrates (laminin, entactin, and collagen IV), suggesting that hESC

substrate adhesion via αVβ5 is adequate for expansion of hESCs when cultured using

defined media [Braam *et al.*, 2008].

The oxygen environment has a direct influence on the intracellular pathways of stem cells,

specifically hESCs. This occurs by a combinatory effect of oxygen (a bioactive signalling

molecule) and other regulatory factors (integrins) that can influence a change in hESC

activities including survival, proliferation and differentiation [Zachar *et al.*, 2010]. hESCs

are exposed to a physiological normoxic (2% O_2) environment *in vivo* where the ICM of a

blastocyst (from which they are derived) is surrounded by a trophoblast shell that prevents

their exposure to oxygenated material blood. The pluripotency of hESCs has been proven

to be primarily regulated by these hypoxia inducible factors (HIFs) which are expressed in

decreased oxygen environments. HIFs are heterodimeric, environment sensing [Mohyeldin

et al., 2010], transcriptional factors and are comprised of α and β sub-units. There are three

oxygen dependant isoforms of the α-subunit which are HIF-1α (120 kDa), HIF-2α (EPASI)

and HIF-3α; these can bind to two types of β sub-units which are HIF-1β and HIF-2β.

[Forristal *et al.*, 2010; Szablowska-Gadomska *et al.*, 2011]. The expression of HIFs have

known to have a direct influence on the up regulation and down regulation of several genes

that are associated with cell survival, proliferation, angiogenesis, glucose metabolism and

cell apoptosis [Szablowska-Gadomska *et al.*, 2011]. Furthermore, previous studies on the

effects of reduced oxygen on hESC culture have demonstrated enhanced clonogenicity, decreased *in vitro* spontaneous differentiation, maintenance of pluripotency for prolonged periods, reduced chromosomal aberration frequency, improved consistency of embryoid body formation, significant transcriptional alterations, and permissive single-cell derived progenitor isolation [Ezashi *et al.*, 2005; Forsyth *et al.*, 2008; Forsyth *et al.*, 2006; Hewitt *et al.*, 2006; Westfall *et al.*, 2008]. Further details of the effects of hypoxia on hESCs can be found in section 1.4, Chapter 1.

Though recent attempts have been made to identify the critical interactions between hESC integrins and corresponding ECM adhesion proteins the key interactions remain to be fully elucidated and as a result Matrigel^{TM} still remains the gold standard for *in vitro* hESC expansion despite mediocre attachment, inconsistent proliferation and limitations including xenogenic contaminations. In this study, a detailed investigation is performed to determine the effects of a reduced oxygen environment on hESC integrin expression, seeking to understand and identify the mechanisms of action and critical interactions associated between specific integrins and ECM proteins with defined culture parameters which permit hESC attachment and undifferentiated expansion. These findings could help to drive the future development of novel substrates designed to improve the yield of hESC attachment, improve expansion efficiency, help retain a more homogenous population of undifferentiated hESCs, eliminate scale-up issues resulting in the elimination of Matrigel^{TM} and xenogenic contaminations. This would result in key implications of hESCs for clinical application coupled to *in vivo* post-transplantation modelling.

Chapter 4

4.2 Aims and Objectives

The oxygen environment can influence the attachment and proliferation of hESCs. Furthermore, reduced oxygen concentrations enhance hESC clonogenicity, minimise spontaneous differentiation, maintain pluripotency for prolonged *in vitro* cultures and reduce chromosomal aberrations. It can be hypothesised that due to improved clonogenicity as a result of change in oxygen environment, this suggests a potential for altered integrin expression resulting in enhanced colony formation through improved hESC attachment and expansion on Matrigel™.

The aims of this chapter were as follows:

- To evaluate the up regulation and down regulation of integrins between hESCs cultured in both physiological normoxia (2% O_2) and hyperoxia (21% O_2)

- To identify the critical oxygen responsive integrins within hESCs cultured in both physiological normoxia (2% O_2) and hyperoxia (21% O_2)

- Select the significant oxygen responsive integrins in hESCs and investigate their importance on cell attachment via antibody blocking adhesion assays.

- Characterise and quantify the expression of significant oxygen responsive integrins in hESCs cultured in both physiological normoxia (2% O_2) and hyperoxia (21% O_2)

- To investigate the effect of blocking the αVβ5 integrin receptor in hESCs on their ability to adhere to nanofibrous substrates when cultured in physiological normoxia

4.3 Materials and Methods

Microarrays are a powerful, efficient technique which provides the ability to identify and quantify expression patterns of hundreds and thousands of genes in a short period, in parallel. DNA microarrays utilise cDNA or oligonucleotides as gene probes where amplified cDNA fragments in a high density pattern are identified on solid surface such as glass. [Kothapalli *et al.*, 2002] Previous *in silico* Microarray experiments performed by our research group on hESCs cultured in both physiological normoxia (2% O_2) and hyperoxia (21% O_2) were reanalysed and statistically evaluated to identify oxygen-responsive integrin sub-units and determine changes in their expression levels.

Integrin adhesion blocking assays were performed to investigate the effect of blocking significantly expressed integrins/sub-units on hESC attachment after 24 hours on Matrigel^{TM}, cultured in either 2% O_2 or 21% O_2; the methodology is summarised in Figure 4.1 below. **A detailed protocol is stated in Section 2.4.2, Chapter 2**.
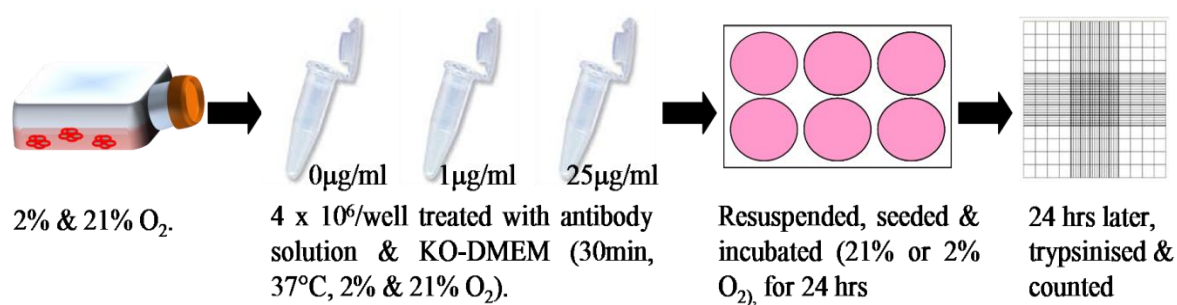
Figure 4.1 Schematic demonstrating the protocol used for antibody blocking of hESCs for cell adhesion investigations.

Chapter 4

Immunocytochemistry analysis was used to visualise αVβ5 and CD44 expression and monitor changes in expression levels. hESCs cultured in both 2% and 21% O_2 were fixed, BSA blocked and treated with primary antibodies specific to αVβ5 and CD44 receptors at 50 µg/ml concentration for 24 hours and then treated with secondary antibody and counterstained with DAPI. Immunocytochemistry was used to characterise the expression of markers associated with pluripotency (Oct 3/4, Nanog, Alkaline Phosphatase and SSEA-4) of hESCs after being blocked with αVβ5 and CD44 at 50 µg/ml for 24 hours in the relevant oxygen environments (2% O_2 and 21% O_2). A fluorescent microscope was then used to detect and visualise these fluorescently tagged markers within hESCs. **Detailed protocol is stated in Section 2.4.3, Chapter 2**

Fluorescent-activated cell sorting (FACS) allows the quantification of cells that specifically express surface antigens that are recognised specifically by a fluorescently-tagged antibody. FACS was used to quantify the expression of αVβ5 and CD44 in hESCs cultured in both physiological normoxia (2% O_2) and hyperoxia (21% O_2). **Detailed protocol is described in Section 2.4.3.3, Chapter 2**.

hESCs were treated with and without anti-αVβ5 antibody solution before seeding and culturing them onto Matrigel™ and nanofibrous substrates (PCL aligned and random) in physiological normoxia for 21 days. Colonies were fixed and stained with Giemsa and counted for quantification.

Chapter 4

4.4 Results

4.4.1 In Silico Micro Array Analysis

Previous reports have detailed widespread transcriptional alterations as a consequence of culturing hESCs in reduced oxygen environments [Forsyth *et al.*, 2006; Westfall *et al.*, 2008]. The data set obtained previously by Forsyth et al was re-analysed to determine the integrin sub-units expression level in hESCs. Three hESC lines (H1, H9 and RH1) were investigated. Though these cell lines are different to the cell line used in this thesis (SHEF 1), it has been reported that most hESC cell lines show broad equivalence of transcriptional protein expression and phosphorylation sites [Phanstiel *et al.,* 2012]. Analysis of data revealed that integrin sub-units: β3 binding protein, β1 binding protein 1, β4 binding protein, α5, α6, α8, α9, αD, αE, αV, β1 and β5 were all expressed significantly higher in hESCs cultured in physiological normoxia (2% O_2) when compared to hyperoxia (21% O_2) as shown in Figure 4.1. Analysis of data revealed that the following integrin sub-units were expressed significantly higher in physiological normoxia (2% O_2) relative to 21% O_2: β1 binding protein 1 ($p < 7$ x 10^{-3}), αE ($p < 3$ x 10^{-4}), β3 binding protein ($p < 3$ x 10^{-3}), α6 ($p < 2$ x 10^{-4}), αV ($p < 1.5$ x 10^{-4}), β5 ($p < 1$ x 10^{-3}), α9 ($p < 0.01$), β4-binding protein ($p < 0.02$), β1, ($p < 0.03$), α5 ($p < 0.04$) and αD ($p < 0.05$), , and. However, the order of relative intensity fold-change (FC) of these integrins with significance in 2% O_2 over 21% O_2 culture was; αD (2.25 FC), αV (1.64 FC), α9 (1.54 FC), α5 (1.36 FC), α6 and αE (1.31 FC), β4 binding protein (1.26 FC), , β1 and β1 binding protein 1 (1.20 FC), β5 (1.16 FC) and β3 binding protein (1.09 FC), as shown in Table 4.1

Chapter 4

Hyaluronic acid associated gene expression was also analysed in hESCs cultured in both physiological normoxia (2% O_2) and hyperoxia (21% O_2); these were investigated as Hyaluronic acid (HA) is known to promote hESC proliferation and associated intracellular pathways [Bourguignon *et al.*, 2008; Gerecht *et al.*, 2007] Significantly higher levels of expression were noted in 2% O_2 cultured hESCs relative to hESCs cultured in 21% O_2 for; Hyaluronan-mediated motility receptor, RHAMM (1.43 FC), Hyaluronoglucosaminidase (1.25 FC) and Hyaluronan and proteoglycan link protein-3 (0.90 FC), as stated in Table 4.1

Chapter 4

Table 4.1 Expression units (relative) from microarray analysis for all integrins expressed in hESCs cultured in physiological normoxia (2% O$_2$) and hyperoxia (21% O$_2$). F/C indicates Fold Change (2% O$_2$/21% O$_2$) Integrins expressed significantly higher in hESCs cultured in 2% O$_2$ relative to 21% O$_2$ are highlighted in bold.

Gene Symbol (Gene Name)	2% O$_2$	21% O$_2$	P Value	Fold Change
ITGB1BP2 (Integrin beta 1 binding protein 2)	16.25	11.79	0.14	1.38
AaeL-AAEL007077 (Integrin beta 1 binding protein 1)	**212.15**	**177.21**	**7x10^{-3}**	**1.20**
ITGB1BP3 (Integrin beta 1 binding protein 3)	496.54	544.12	0.47	1.10
ITGB3BP (Integrin beta 3 binding protein)	**595.30**	**545.43**	**3 x10^{-3}**	**1.09**
LOC658655 (Integrin beta 4 binding protein)	**1354.68**	**1074.23**	**0.02**	**1.26**
ITGA1 (Integrin alpha 1)	25.87	27.10	0.77	1.05
ITGA10 (Integrin alpha 10)	39.93	34.89	0.43	1.14
ITGA11 (Integrin alpha 11)	88.46	91.98	0.65	1.04
ITGA2 (Integrin alpha 2)	21.55	28.47	0.24	1.32
ITGA2B (Integrin alpha 2b)	64.27	67.22	0.63	1.05
ITGA4 (Integrin alpha 4)	23.37	18.80	0.35	1.24
ITGA5 (Integrin, alpha 5)	**182.51**	**134.33**	**0.04**	**1.36**
ITGA6 (Integrin alpha 6)	**1229.82**	**938.91**	**2 x10^{-4}**	**1.31**
ITGA7 (Integrin alpha 7)	163.05	117.39	0.24	1.39
ITGA8 (Integrin alpha 8)	34.53	43.15	0.09	1.25
ITGA9 (Integrin alpha 9)	**43.93**	**28.54**	**0.01**	**1.54**
ITGAD (Integrin alpha D)	**25.82**	**11.50**	**0.05**	**2.25**
ITGAE (Integrin alpha E)	**553.67**	**423.84**	**3 x10^{-4}**	**1.31**

ITGA11 (Integrin L)	16.06	15.69	0.88	1.02
ITGAM (Integrin alpha M)	21.03	19.04	0.48	1.11
ITGAV (Integrin alpha V)	**851.72**	**524.89**	**1.5×10^{-4}**	**1.64**
ITGB1 (Integrin beta 1)	**4691.45**	**3910.88**	**0.03**	**1.20**
ITGB2 (Integrin beta 2)	47.30	51.05	0.53	1.08
ITGB3 (Integrin beta 3)	45.74	36.88	0.25	1.24
ITGB4 (Integrin beta 4)	51.26	46.43	0.26	1.10
ITGB5 (Integrin beta 5)	**1927.06**	**1662.95**	**1×10^{-3}**	**1.16**
ITGB6 (Integrin beta 6)	6.52	12.10	0.11	1.86
ITGB7 (Integrin beta 7)	25.14	21.48	0.42	1.17
ITGB8 (Integrin beta 8)	17.36	16.89	0.82	1.03
ITGBL1 (Integrin beta-like 1)	36.32	34.09	0.39	1.07
IIK (Integrin-linked kinase)	796.20	756.35	0.38	1.05
IIKAP (Integrin-linked kinase-associated serine/threonine phosphatise 2C)	191.87	183.45	0.31	1.05
CD44 molecule (Indian blood group)	54.08	42.64	0.37	1.27
HAPLN3 (Hyaluronan and proteoglycan link protein 3)	87.09	78.79	0.05	0.90
HMMR (Hyaluronan-mediated motility receptor, RHAMM)	269.57	385.62	3×10^{-5}	1.43
HYAL2 (Hyaluronoglucosaminidase 2	415.54	519.13	9×10^{-3}	1.25

Chapter 4

Integrin sub-units which displayed significantly higher levels of expression in hESCs cultured in physiological normoxia (2% O_2) relative to hyperoxia (21% O_2) are shown in Figure 4.2. Expression levels were split into three different categories; (high expression >1500; medium expression > 250 but < 1500 and low expression < 250). Integrin sub-units expressed significantly at the highest levels in physiological normoxia (2% O_2) relative to hyperoxia (21% O_2) was observed by β1 and β5 followed by medium expression of β4 binding protein, α6, αV, β3 binding protein and αE, and low expression levels of β1 binding protein 1, α4, α8, α9 and αD.

Chapter 4
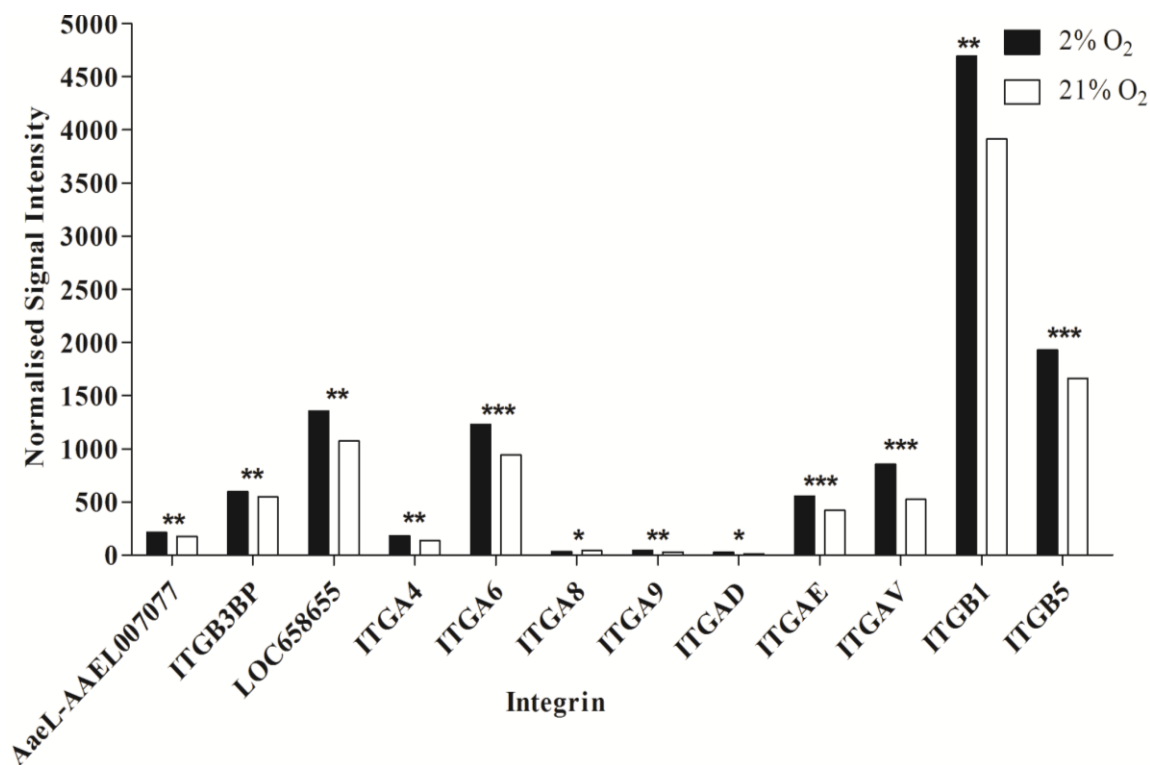
Figure 4.2 Selected relative expression levels of integrin subunits in hESCs. Microarray analysis of hESC cultured in both physiological normoxia (2% O_2) and hyperoxia (21% O_2) reveals significant expression differences for; AaeL-AAEL007077 (Integrin beta 1 binding protein 1), ITGB3BP (Integrin beta 3 binding protein, beta3-endonexin), LOC658655 (Integrin beta 4 binding protein), ITGA4 (Integrin alpha 4, antigen CD49D, alpha 4 subunit of VLA-4), ITGA6 (Integrin alpha 6), ITGA8 (Integrin alpha 8), ITGA9 (Integrin alpha 9), ITGAD (Integrin alpha D), ITGAE (Integrin alpha E), ITGAV (Integrin alpha V, vitronectin receptor, alpha polypeptide, antigen CD51), ITGB1 (Integrin beta 1, fibronectin receptor, beta polypeptide, antigen CD29 includes MDF2, MSK12) and ITGB5 (Integrin beta 5). No statistical significant difference was observed in CD44 gene expression between hESCs cultured in both 2% and 21% O_2. Values indicate mean normalised signal intensity as an indicator of relative abundance. $n=5$; * $p < 0.05$, ** $p < 0.01$, *** $p < 0.001$.

4.4.2 hESC Attachment after Post-Antibody Treatment

Integrin sub-units, α6, αE, αV and β5 (including the integrin αVβ5) as well as CD44 (Hyaluronan receptor; HA) which have the greatest significant change in expression between physiological normoxia (2% O_2) and hyperoxia (21% O_2), were selected for cell attachment studies. Receptor blocking using antibodies specific to the above integrin sub-units at various concentrations (0, 1 and 25 µg/ml) was performed to determine the effect on hESC adhesion in both physiological normoxia (2% O_2) and hyperoxia (21% O_2) after 24 hours, as demonstrated in Figure 4.3. Blocking of α6 sub-unit within hESCs expanded in both 2% O_2 and 21% O_2 demonstrated that with increasing antibody concentration there was a significant decrease in cell attachment when compared to the control (without antibody treatment) in 21% O_2 no significant differences were observed as shown in Figure 4.3A. Blocking of αE sub-unit demonstrated a decrease in cell attachment with increasing antibody concentration in both oxygen environments (2% O_2 and 21% O_2) as shown in Figure 4.3B. There were no significant differences observed in cell attachment when hESCs were blocked with αV or β5 sub-units in both oxygen concentrations (Figure 4.3C and 4.2D); the heterodimer αVβ5 demonstrated a significant decrease in cell attachment of hESCs in 2% O_2 when treated with 25 µg/ml of antibody blocking solution, relative to the control (without antibody treatment) (Figure 4.3E). Blocking of CD44 receptor within hESCs cultured in 2% O_2 or 21% O_2 demonstrated a significant reduction in cell attachment with increasing antibody concentration relative to the control (without antibody treatment) only in 21% O_2 (Figure 4.3F).
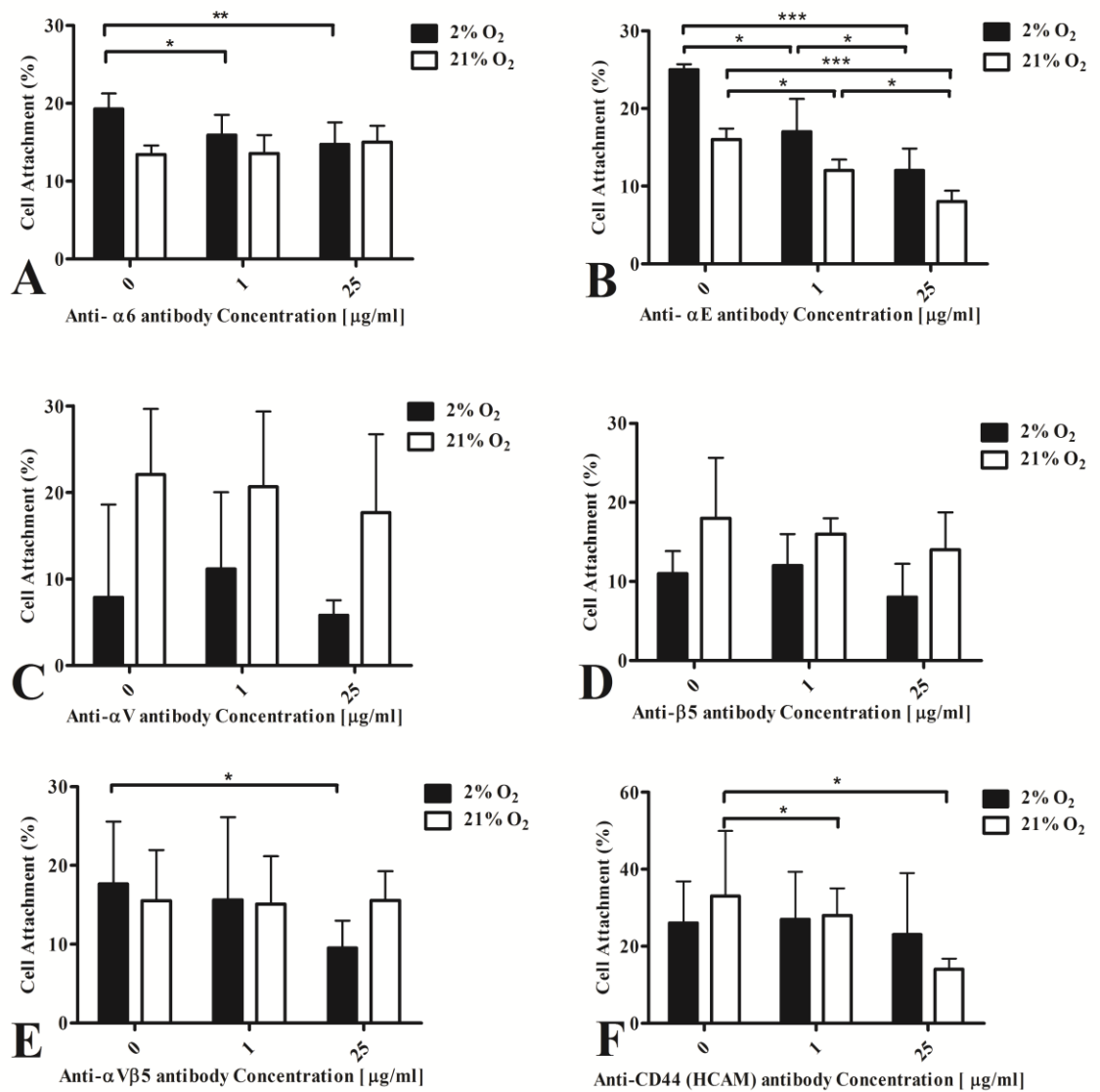
Figure 4.3 Effects of integrin blocking on the attachment of hESCs to Matrigel^{TM}. hESCs were cultured in; physiological normoxia (2% O_2) or hyperoxia (21% O_2) and treated with the following antibodies; (A) Anti-Alpha 6 (ITGA6) antibody, (B) Anti-Alpha E (ITGAE) antibody (C) Anti-Alpha V (ITGAV) antibody, (D) Anti-Beta 5 (ITGB5) antibody, (E) Anti-Alpha V beta 5 antibody and (F) Anti-CD44 antibody. Values indicate mean percentage of cell attachment and error bars indicate standard deviations (*n=6*); * $p < 0.05$, ** $p < 0.01$, *** $p < 0.001$.

Chapter 4

Due to substantial cell attachment variability with Matrigel™ control (hESCs without antibody treatment) wells difficulties arose when making direct comparisons of cell attachments between different integrin sub-unit blocking, at various concentrations, in both 2% O_2 and 21% O_2. To attempt to overcome this variation all integrin blocking data was normalised against the relevant Matrigel™ control (hESCs without antibody treatment), by dividing cell attachment value of treated samples by cell attachment value for that specific Matrigel™ control (hESCs without antibody treatment). Through this approach values greater than 1 indicated increased attachment whereas values less than 1 indicated reduced attachment (Figure 4.4).
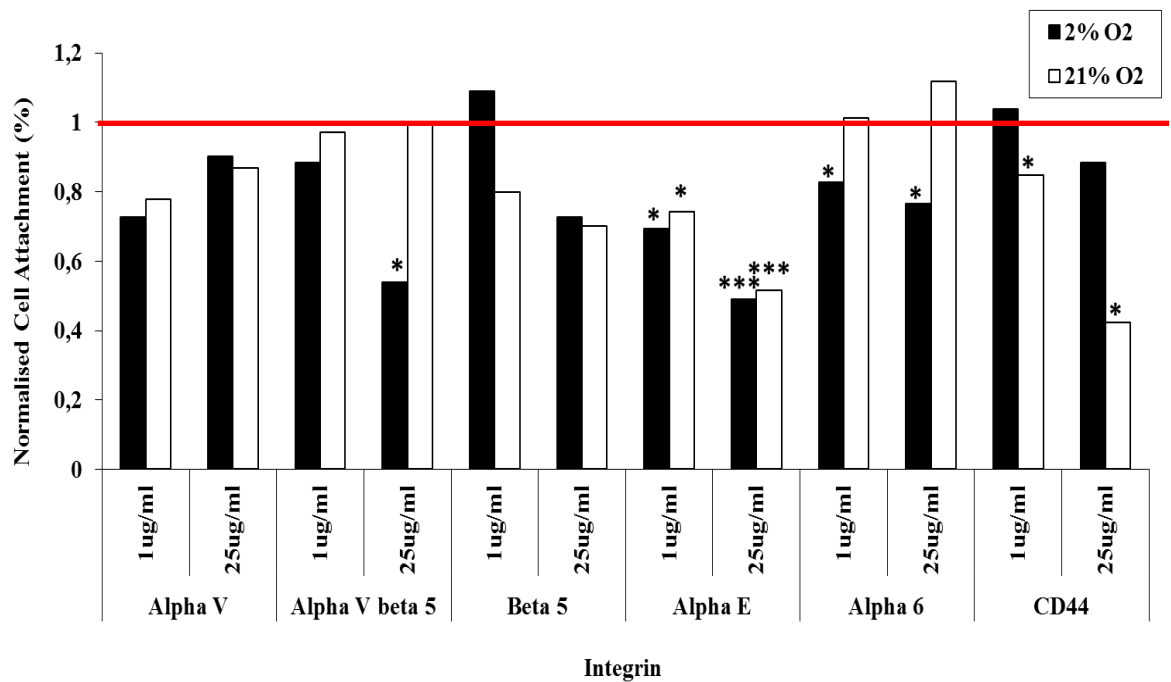
Figure 4.4 Normalised cell attachment values (%) of hESCs treated with anti-integrin antibodies at 1 μg/ml and 25 μg/ml concentrations, to the relevant control values for each integrin. Cell attachment evaluated after 24 hours of post-antibody treatment of hESCs cultured in either 2% O_2 or 21% O_2. Values indicate mean percentage of cell attachment ($n=6$); * $p < 0.05$, ** $p < 0.01$, *** $p < 0.001$.

4.4.3 Characterisation and Quantification of αVβ5 and CD44 Receptor Expression in hESCs

As the blocking of CD44 receptor hindered attachment of hESCs in hyperoxia (21% O_2) only and blocking of αVβ5 integrin and α6-subunit hindered attachment in physiological normoxia (2% O_2) only; CD44 receptor and αVβ5 integrin expression was characterised to visualise differences in expression patterns. Positive immunocytochemistry staining of these receptors confirmed surface expression within hESCs cultured in either oxygen environments but with differing levels and patterns. The expression pattern of αVβ5 in hESCs cultured in both 2% O_2 and 21% O_2 appeared broadly similar but with stronger staining being observed in 2% O_2 (Figure 4.5A). The expression of CD44 appeared predominantly membrane-bound with higher expression at cell-cell junctions but also present in the cytoplasmic and nuclear regions in 21% O_2 cultured hESCs (Figure 4.5B). Whereas, in 2% O_2 cultured hESCs, expression was predominantly visible in cytoplasmic and nuclear regions and less intense at cell-cell junctions when compared to 21% O_2 (Figure 4.5B).

Chapter 4
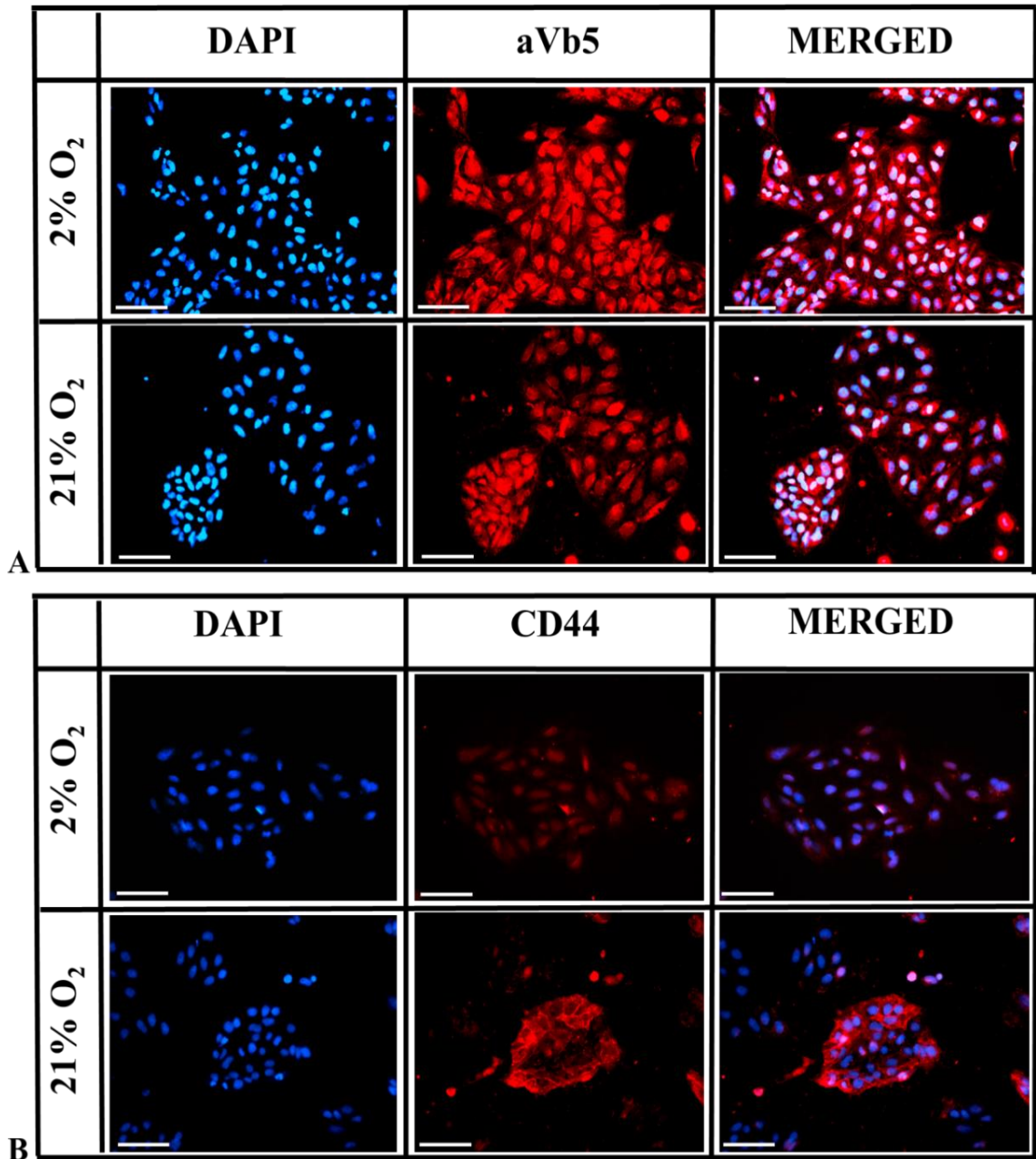
Figure 4.5 Representative immunostained images of (A) αVβ5 integrin and (B) CD44 receptor expression in hESCs cultured in both physiological normoxia (2% O_2) and hyperoxia (21% O_2) on Matrigel™ substrates. Scale bar = 100μm.

Chapter 4
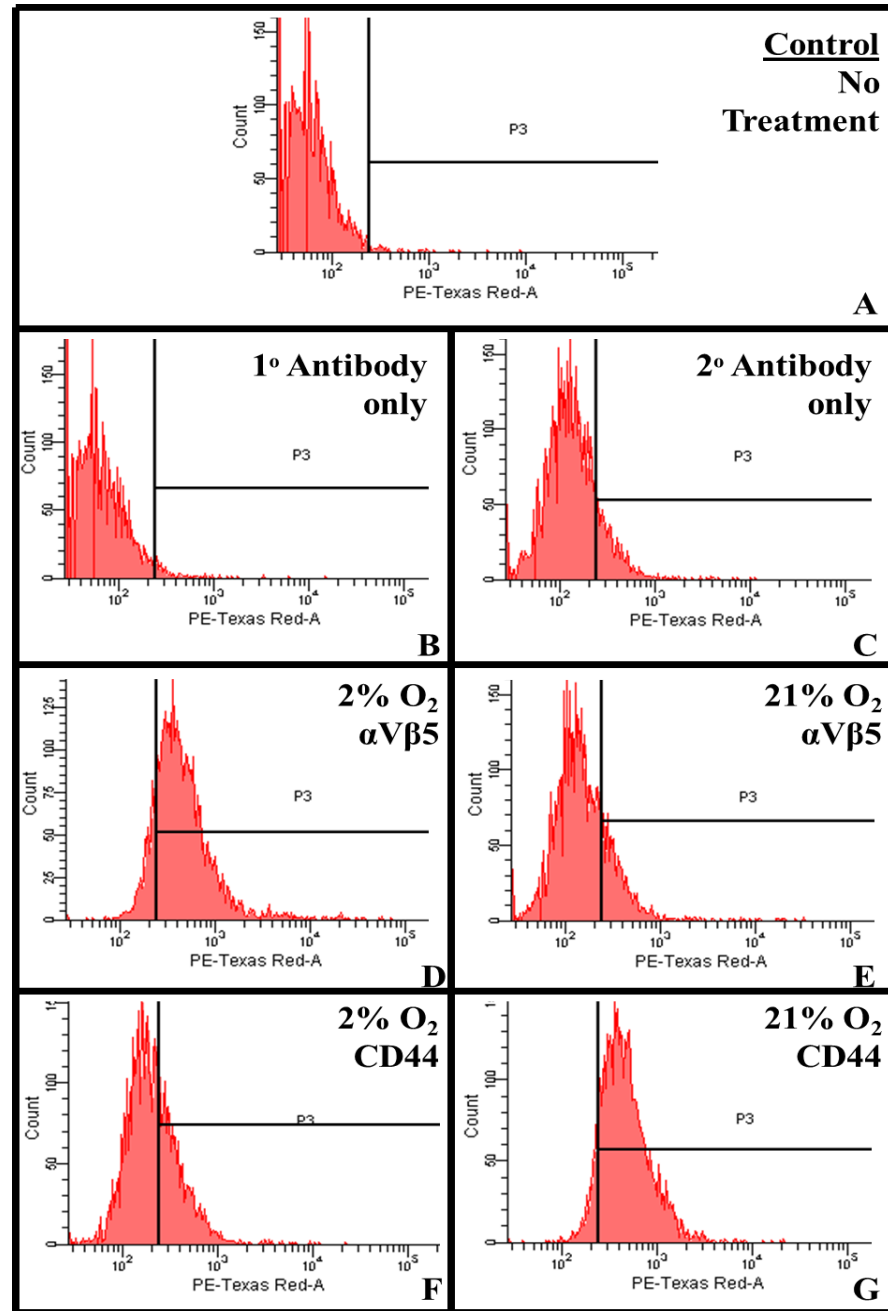
Figure 4.6 FACS analysis of αVβ5 expression in hESCs cultured in both physiological normoxia (2% O$_2$) and hyperoxia (21% O$_2$) conditions; (A) control – no treatment, (B) primary antibody treatment but no secondary antibody treatment, (C) no primary antibody treatment but secondary antibody treatment, (D) αVβ5 expression in hESCs cultured in 2% O$_2$, (E) αVβ5 expression in hESCs cultured in 21% O$_2$, (F) CD44 expression in hESCs cultured in 2% O$_2$ and (G) CD44 expression in 21% O$_2$.

Chapter 4

FACS analysis of αVβ5 and CD44 receptor expression in hESCs cultured in both 2% O_2 and 21% O_2 provided quantitative evaluation of expression activity. αVβ5 expression in hESCs cultured in 2% O_2 displayed a 2-fold increase (64.5 %) in expression levels vs. 21% O2 (32%) (p <0.029) (Figure 4.7A). Conversely, CD44 expression in hESCs cultured in 21% O_2 displayed a 1.38-fold increase (72.6%) in expression levels vs 2% O_2 (52.7%) (p < 0.037) (Figure 4.7B)
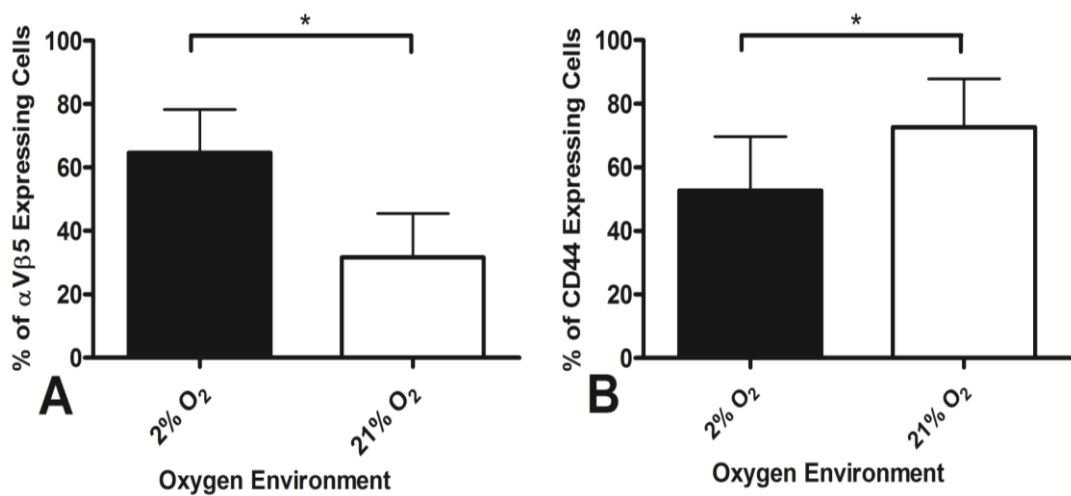
Figure 4.7 Quantitative analysis of FACS data representing: (A) αVβ5 integrin expression in hESCs cultured in both 2% and 21% O_2 environments, (B) CD44 (HCAM) integrin expression in hESCs cultured in both 2% O_2 and 21% O_2 environments. Values indicate mean percentage of cells that express the integrins (*n=5*); * $p < 0.05$.

Chapter 4

4.4.4 Pluripotent Marker Expression of hESCs with blocked αVβ5 and CD44 Receptors

Cultured hESCs which retained a substrate adhesion capacity 24 hours post-antibody blocking of the αVβ5 receptor were immunostained with a range of pluripotency markers. After αVβ5 blocking treatment (25 µg/ml), hESCs displayed a lack of nuclear localisation of Oct-3/4 and Nanog (Figure 4.8) and weak Alkaline phosphatase (ALP) and SSEA-4 labelling, in comparison to unblocked hESCs. Furthermore, this was only experienced in 2% O_2 whereas little effect on pluripotent marker expression was observed in 21% O_2. Additionally, CD44 receptor blocking (25 µg/ml) in hESCs cultured in 21% O_2, also resulted in an absence of Oct-3/4, and Nanog nuclear localisation (Figure 4.9) weaker stain for pluripotent markers, in comparison to untreated hESCs., shown in Figure 4.9. No effect on pluripotent marker expression was observed when hESCs were blocked with CD44 and cultured in 2% O_2 (Figure 4.9).

Quantification of Oct-3/4 and Nanog nuclear localisation demonstrated a 4-fold and 3.6-fold decrease respectively, relative to nuclear localisation in untreated hESCs after αVβ5 – receptor blocking in 2% O_2 only Additionally, blocking of the CD44 receptor in hESCs cultured in 21% O_2 only, resulted in a 4.33-fold decrease (Oct-3/4) and a 3.22-fold decrease (Nanog) in nuclear localisation, as shown in Figure 4.10.
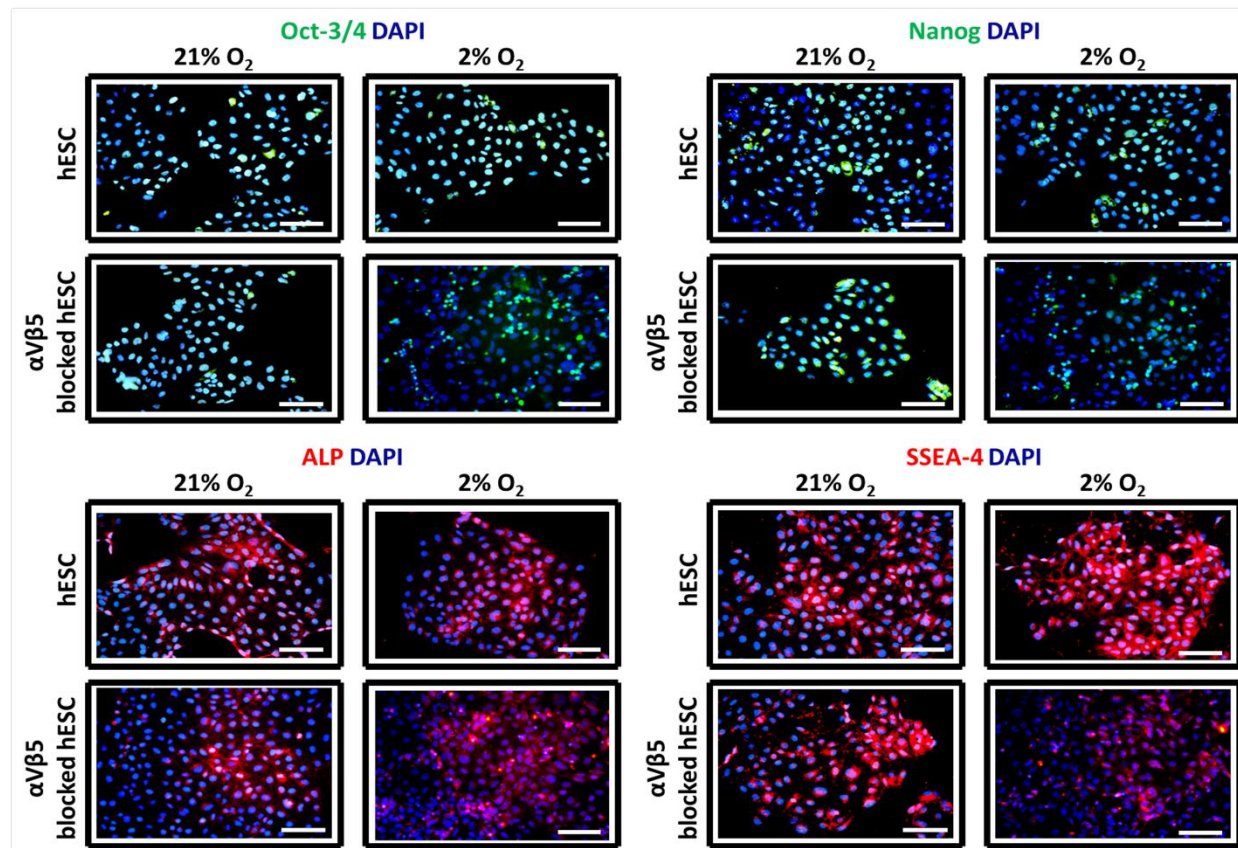
Figure 4.8 Evaluation of pluripotent marker (Oct 3/4, Nanog, ALP, SSEA-4) expression in hESCs treated with αVβ5 blocking antibody (25 μg/ml) and cultured in physiological normoxia (2% O_2). Scale bar = 100 μm.
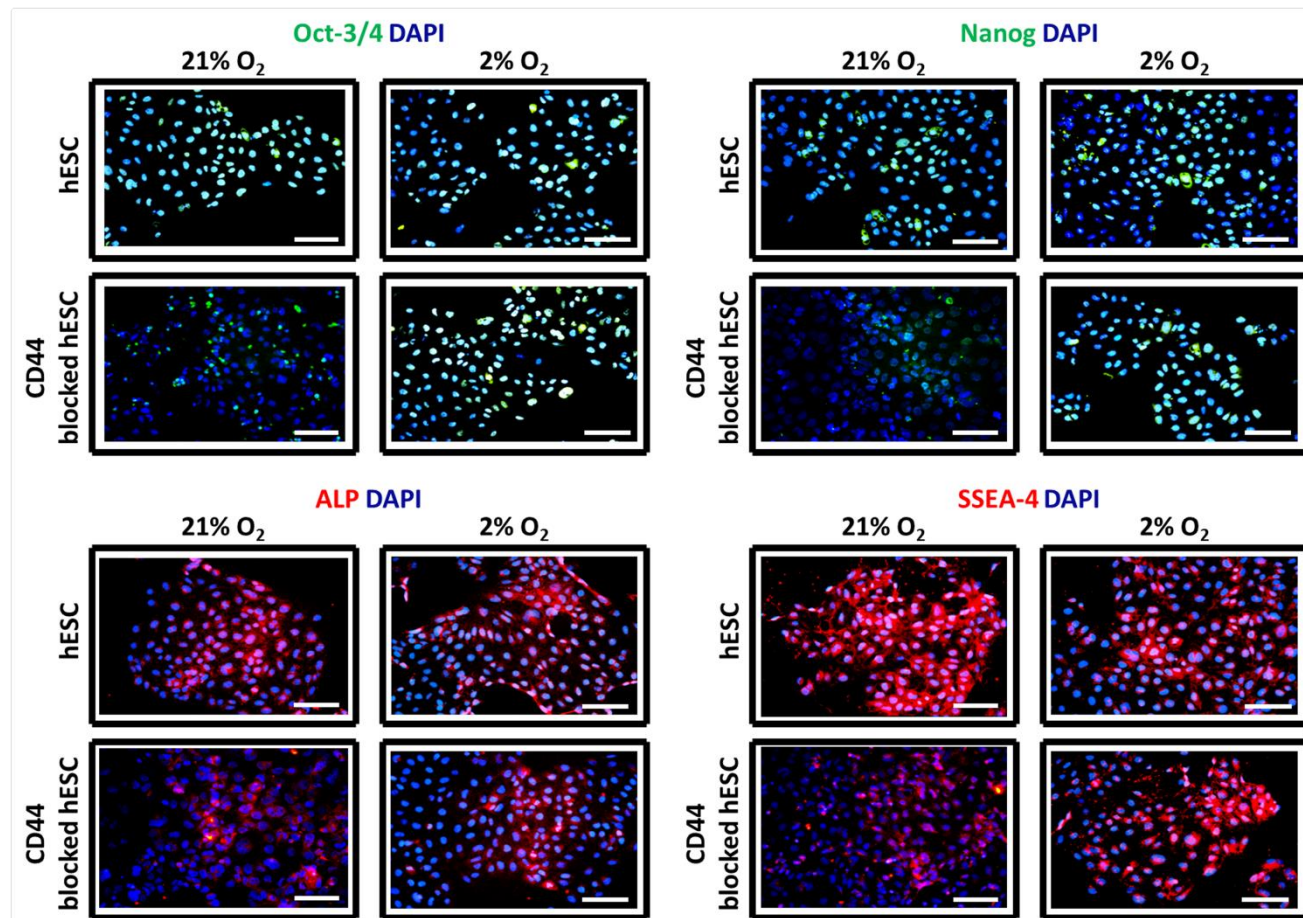
Chapter 4

Figure 4.9 Evaluation of pluripotent marker (Oct 3/4, Nanog, ALP, SSEA-4) expression in hESCs treated CD44 blocking antibody (25 µg/ml) and cultured in hyperoxia (21% O_2). Scale bar = 100 µm.
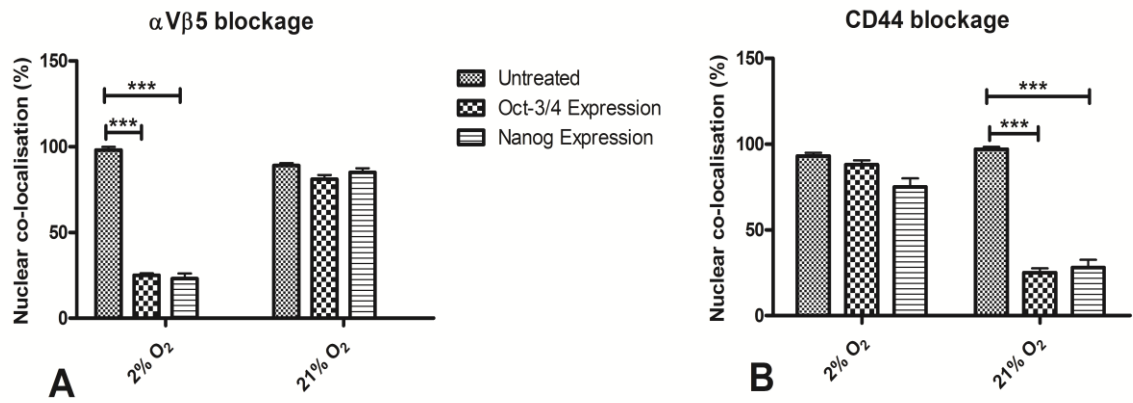
Figure 4.10 Oct-3/4 and Nanog nuclear localisation quantification: (A) αVβ5 (2% O_2) and (B) CD44 (21% O_2). Values indicate mean percentage of co-localisation of pluripotent genes expression; n=5, *** $p < 0.001$.

Chapter 4

4.4.5 Effect of Blocking αVβ5 Integrin Receptor in hESCs Cultured on Nanofibrous Substrates in Physiological Normoxia (2% O$_2$)

In physiological normoxia (2% O$_2$), αVβ5 was identified as a critical integrin receptor which hESCs utilised to adhere to Matrigel™ substrates. It was then hypothesised that the αVβ5 integrin may be the receptor through which hESCs are able to adhere to nanofibrous substrates when cultured in physiological normoxia.
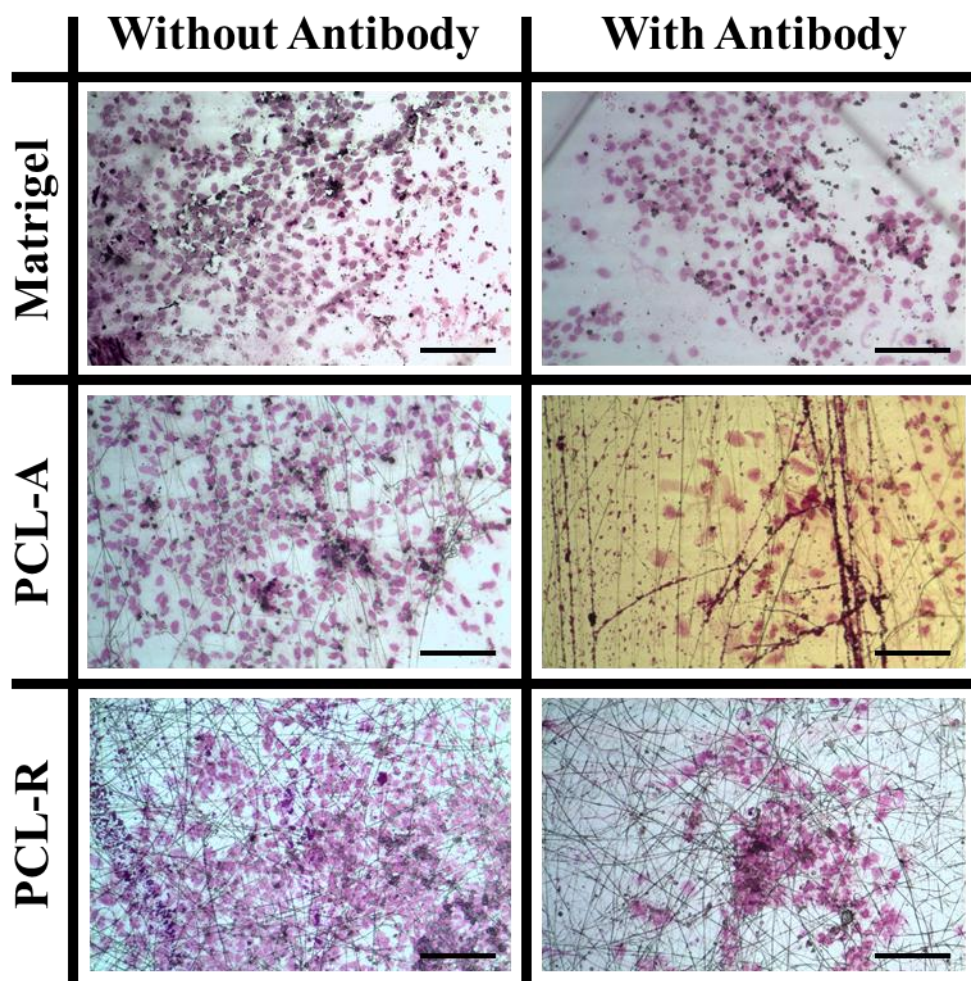
Figure 4.11 Characterisation of Giemsa stained hESC-CFU's expanded on Matrigel™ and PCL nanofibrous substrates (aligned and random) with and without anti-αVβ5 antibody blocking treatment at 25 µg/ml of hESCs before seeding and culturing onto nanofibrous substrates for 21 days in physiological normoxia (2% O$_2$). Scale Bar 200 µm.

Chapter 4

hESCs were treated with and without 25 µg/ml of antibody αVβ5 blocking solution before seeding onto electrospun PCL nanofibrous substrates (aligned and random) and cultured for 21 days in physiological normoxia (2% O_2). Characterisation of hESC CFUs formed without anti-αVβ5 treatment retained typical hESC colony morphology on Matrigel™, PCL-Aligned and PCL-Random nanofibrous substrates; shown by the dense, compact growth of hESCs together within a colony, in Figure 4.12. However, hESCs with anti-αVβ5 antibody blocked prior to seeding onto nanofibrous substrates generated colonies which were less compact with single hESCs spread out, particularly on the nanofibrous substrates, relative to Matrigel™.

Quantification of hESC CFUs recovered on nanofibrous substrates from hESCs treated with and without anti-αVβ5 antibody treatment revealed that Matrigel™ substrates supported significantly ($p < 0.05$) the greatest number of hESC colonies than any nanofibrous substrate (aligned and random) regardless of being treated with or without antibody blocking solution, before culturing onto these substrates Furthermore, there were significantly ($p < 0.05$) greater number of hESC CFUs recovered on non-treated Matrigel™ substrates compared to hESCs treated with αVβ5 antibody on Matrigel™ substrates. However, no significant differences were observed between untreated and treated hESCs cultured on PCL aligned and random nanofibrous substrates.
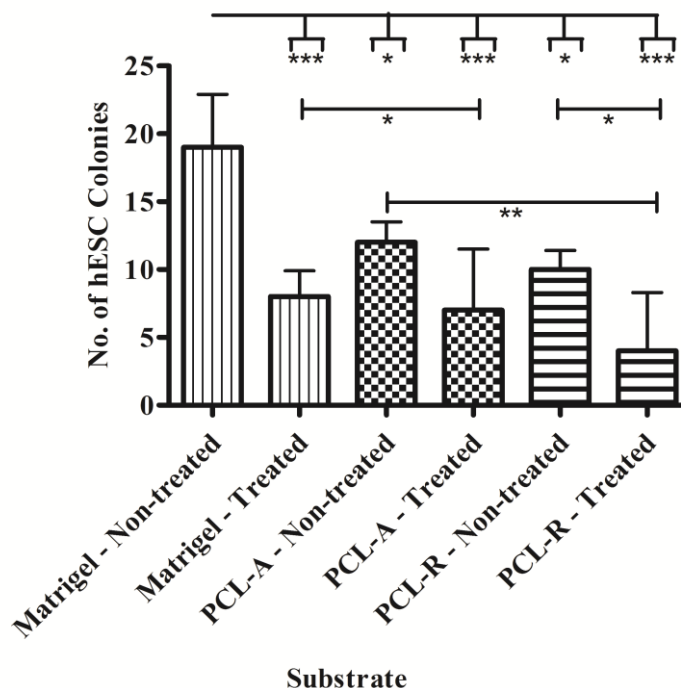
Figure 4.12 Quantification of colonies formed after the treatment of hESCs with and without anti-αVβ5 antibody blocking solution and cultured on nanofibrous substrates or Matrigel™ in physiological normoxia (2% O_2) for 21 days. Values indicate average number of hESC colonies; n=3, * $p < 0.05$, ** $p < 0.01$.

4.5 Discussion

In the previous chapter, we demonstrated a synergistic effect between nanofibrous substrates and oxygen environment. This chapter investigated the specific effects of oxygen on the attachment of hESCs on conventional substrates such as Matrigel™, cultured in physiological normoxia (2% O_2) and hyperoxia (21% O_2) to identify the critical integrins involved in the attachment of hESCs to Matrigel™. This study is the first to identify oxygen-responsive integrins/sub-units critical for initial attachment of hESCs to Matrigel™, followed by evaluation of pluripotency marker expression. These important

findings can potentially play a major role in the design and improvement of novel, synthetic substrates which would be tailored to support and interact with identified integrin receptors in hESCs, to enhance their attachment yield, scale up sufficient cell numbers for clinical applications and retention of pluripotency due to greater control on the mechanism pathways of hESCs leading to subsequent elimination of Matrigel^{TM} and any xenogenic contaminations driving hESCs into the regenerative medicine industry for the treatment of various diseases.

Significant upregulation of specific integrins in hESCs cultured on Matrigel^{TM} under physiological normoxia (2% O_2), relative to hyperoxia (21% O_2) were noted. Antibody inhibition of selected integrins/sub-units in hESCs, in both 2% and 21% O_2 was performed in order to evaluate their effects on initial attachment. Expression levels and patterns were characterised and quantified using immunostaining and FACS. The impact of blocking critical adhesion receptors in hESCs cultured in the most responsive oxygen environment was evaluated by testing the retention of pluripotent markers of hESCs that were able to adhere after post-antibody treatment.

Many studies have utilised Microarrays to analyse and investigate changes in pluripotent and differentiation markers within various hESC lines [Cai *et al.*, 2006; Lee *et al.*, 2010] Our research group has specifically explored the effects of expanding hESCs in various oxygen environments (21% O_2 and 2% O_2) on the transcriptional fingerprint [Forsyth *et al.*, 2008].This study analysed and detected changes in integrin expression levels and patterns in hESCs cultured in either 2% O_2 or 21% O_2, on Matrigel^{TM} substrates.

Chapter 4

Microarray analysis identified; β3 binding protein, β1 binding protein 1, β4 binding protein, α5, α6, α8, α9, αD, αE, αV, β1 and β5 to be significantly up regulated in hESCs expanded in physiological normoxia (2% O_2), relative to hESCs expanded in hyperoxia (21% O_2). Interestingly, we also noted the significant upregulation of HA-associated genes; Hyaluronan and proteoglycan link protein 3, Hyaluronan-mediated motility receptor and Hyaluronoglucosaminidase 2 in hyperoxia (21% O_2), instead of physiological normoxia (2% O_2); numerical values are stated in Table 4.2. CD44 is also an essential specific receptor and mediator for an ECM protein called Hyaluronic acid (HA), which promotes hESC proliferation and associated intracellular pathways [Bourguignon *et al.*, 2008; Gerecht *et al.*, 2007]. Similarly, a study by Saller *et al.*, 2012, also observed alteration in integrin expression in hMSCs as a result of changing the oxygen environment in which they were cultured. hMSCs expanded on various substrates (polystyrene, collagen I, fibronectin and laminin) significantly increased expression of α3 and α6 (laminin receptors), α1 and α11 (collagen receptors), α5 and αV (fibronectin receptors) and β1 and β5 sub-units in physiological normoxia (2% O_2), relative to normoxia (21% O_2). However, significant increase in α2 expression was observed in normoxia (21% O_2) relative to physiological normoxia (2% O_2). Furthermore, hMSCs cultured in physiological normoxia provided a more homogenous population of stem cells with increased stemness and better migration ability [Saller *et al.*, 2012].

Minimal research has been performed to identify and resolve which hESC integrin receptors mediate the initial attachment to Matrigel^{TM}, whilst also retaining their pluripotent nature during expansion. Integrins expressed by hESCs are reported and confirmed for: laminin (α6β1), vitronectin (αVβ5) and fibronectin (αVβ1, α5β1), collagen

Chapter 4

and laminin ($\alpha2\beta1$), nidogen, laminin, collagen I and fibronectin ($\alpha3\beta1$), collagen ($\alpha11\beta1$) [Braam *et al.*, 2008; Lee *et al.*, 2010; Miyazaki *et al.*, 2008]. These findings alongside the detection of oxygen-responsive integrins/sub-units encouraged the investigation of the effects in blocking integrin $\alpha V\beta5$ and sub-units; αV, $\beta5$, αE, $\alpha6$ and CD44 receptor in hESCs cultured in both physiological normoxia (2% O_2) and hyperoxia (21% O_2) on their initial attachment to Matrigel^{TM}.

Receptor blocking using antibodies specific to the integrin sub-units was performed to determine the effect on hESC adhesion to Matrigel^{TM} in 2% O_2 and 21% O_2. Results demonstrated that blocking of αE significantly reduced hESC attachment in both 2% O_2 and 21% O_2; interestingly inhibition of $\alpha6$ and $\alpha V\beta5$ receptors significantly reduced hESC attachment in 2% O_2. Though previous reports have detailed a reliance on $\alpha V\beta5$ and $\alpha6$ integrin sub-units for hESC attachment [Braam *et al.*, 2008; Meng *et al.*, 2010], these findings were observed in normal oxygen conditions only (21% O_2) and thus differ from the observations in this chapter where significant alterations in integrin gene expression and attachment rates were specifically witnessed in 2% O_2 only. Furthermore, blocking the CD44 receptor resulted in subsequent significant inhibition of hESC attachment in 21% O_2 conditions only. As mentioned earlier, CD44 is a specific receptor for HA. HA is secreted by MEFs into media at a concentration of approximately 840 ng/ml and plays a critical role in co-regulation of gene expression, signalling, proliferation, motility and adhesion of hESCs where levels are higher in undifferentiated hESCs and decrease with onset of differentiation [Bourguignon *et al.*, 2008; Gerecht *et al.*, 2007]. Our results provide validation and extension of recent reports in which antibody blocking of CD44 was described as reducing hESC clonogenicity in 21% O_2 [Bourguignon *et al.*, 2008; Gerecht

et al., 2007] Therefore, it is evident therefore that substantial redundancies exist across the signalling and cell-matrix interaction pathways that are associated with hESC adhesion and self-renewal. Taken together with our previous observations this collated data strongly suggests a strengthened statement that oxygen-signalling has a role in defining substrate adhesion mechanistic choice where a switch from CD44 reliance to αVβ5 and α6 is identified.

It is well documented that oxygen itself is a bioactive, signalling molecule which in conjunction with other regulatory factors can influence various cellular activities including cell attachment and proliferation as well as intracellular pathways which are involved in controlling stemness [Zachar *et al.*, 2010]. The exposure of hESCs to hypoxic environment is of no surprise, as these conditions are typical *in vivo*, where the trophoblast excludes any oxygenated material blood contact to the ICM up to a certain point [Ma *et al.*, 2009] and the uterine environment has oxygen levels reportedly in the range of 25 % - 5% O_2 [Chen *et al.*, 2010; Szablowska-Gadomska *et al.*, 2011]. Reductions in oxygen concentration regulate the expression of hypoxia inducible factors (HIFs), which are transcriptional factors composed of α and β sub-units, which can in turn also trigger the activation of various growth factors, integrins, cytokines and viral proteins. Thus, it can be speculated that HIFs may play a critical role in the expression levels and patterns of surface integrins which mediate hESC attachment to Matrigel™. Specifically, it is apparent that HIFs may be up regulating the expression of α6 and αVβ5 integrins in hESCs during hypoxic conditions and thus may be the mechanistic pathway for supporting hESC survival and attachment whilst retaining their pluripotency.

Chapter 4

HIFs interact with integrins and growth factors signalling; interestingly growth factor and integrin pathways are also strongly interlinked and the activation of these pathways are crucial in maintaining the pluripotency of hESCs. Interference with substrate adhesion mechanisms had an immediate role upon maintenance of the undifferentiated state in hESCs. Antibody blockage of $\alpha V\beta 5$ (in 2% O_2) and CD44 (in 21% O_2), significantly decreased the nuclear localisation of Oct-3/4 and Nanog. In addition to these a substantial decrease in Alkaline Phosphatase and SSEA-4 expression was noted in both. The consistency of response indicates that either $\alpha V\beta 5$ and CD44 are signalling via similar pathways; for instance interfering with the FGF-2 signalling pathway resulting in inactivation of pathways MAPK/ERK, PI3/AKT kinase and $NF_K\beta$, or through distinct, though mechanistically identical, self-renewal maintenance pathways [Armstrong *et al.*, 2006; Eiselleova *et al.*, 2009]. More specifically, in 2% O_2, HIFs are able to activate signalling pathways including FGF and Notch through up regulating the expression of transcriptional factors such as NF_kB, Activator protein-1 (AP-1), p53 and c-Myc [Ma *et al.*, 2009; Szablowska-Gadomska *et al.*, 2011]. Therefore, it is apparent that the inhibition of receptors $\alpha 6$ and $\alpha V\beta 5$ results in the outside-in signalling effect resulting in the inactivation of these intracellular pathways which cause the inactivation in the expression of pluripotent genes. Speculative mechanisms and the effects of blocking $\alpha V\beta 5$ (in 2% O_2) and CD44 (in 21% O_2), are illustrated in Figure 4.13

Chapter 4

Blocking αVβ5	Blocking CD44
↓	↓
Physiological normoxia (2 % O$_2$)	Hyperoxia (21 % O$_2$)
↓	↓
HIFs unable to up regulate transcriptional factors including NF$_K$B, AP-1, p53 and c-Myc	Interference of FGF-2 signalling
↓	↓
Inactivation of intracellular pathways FGF/Notch signalling	Inactivation of MAPK, ERK,PI3/AKT kinase and NF$_K$B pathways
↓	↓
Down regulation of pluripotent markers	Down regulation of pluripotent markers

Figure 4.13 Flow diagram representing the speculative mechanisms that may occur as a result of blocking the αVβ5 receptor in physiological normoxia (2% O$_2$) and CD44 receptor in hyperoxia (21% O$_2$) in hESCs cultured on Matrigel™.

As the αVβ5 receptor was significantly up regulated in hESCs cultured in physiological normoxia (2% O$_2$) and played a vital role in initial attachment to Matrigel™; it was hypothesised that the αVβ5 receptor may also play a crucial role in mediating the initial attachment of hESCs to nanofibrous substrates (PCL aligned and PCL random) when cultured in physiological normoxia (2% O$_2$). It was apparent that a decrease in the number

Chapter 4

of colonies formed and a decrease in cell density within those colonies was a result of blocking the αVβ5 receptor in hESCs before seeding and culturing onto nanofibrous substrates in physiological normoxia (2% O_2). Nanofibrous substrates can selectively adsorb ECM proteins from culture media onto their surfaces; hESC media contains many ECM proteins that are secreted by MEFs and hESCs which are able to adhere onto these substrates. However, the types of ECM proteins from hESC media which are able to adhere onto nanofibrous substrates (particularly PCL nanofibres) are relatively unknown. As blocking the αVβ5 integrin demonstrated a decrease in hESC CFU ability on PCL nanofibrous substrates in 2% O_2, it can be hypothesised that hESCs are strongly reliant on this receptor for attachment to nanofibrous substrates and that the corresponding ECM ligand (vitronectin) for the αVβ5 integrin receptor is selectively adsorbed onto nanofibrous substrates, thus permitting the critical connection between hESCs and nanofibrous substrates resulting in subsequent activation of intracellular pathways which encourage hESC adhesion and proliferation whilst retaining their undifferentiated state. This further leads to the speculation that: polymer material, fibre orientation and fibre diameter may dictate and select the types and amount of specific hESC ECM proteins which are able to adsorb onto nanofibrous substrates; adsorbed proteins on the surface provide recognition sites for corresponding hESC integrin receptors in order to support subsequent attachment and expansion in a pluripotent state. Therefore a combination of increased expression of critical integrin receptors in hESCs, cultured in physiological normoxia (2% O_2) and the selective ECM protein adsorption ability of nanofibrous substrates for corresponding ligands to these receptors provides a solid connection sufficient for hESC attachment and pluripotent expansion.

Chapter 4

Tailoring substrates to have integrin specific ligands for critical integrin receptors in hESCs that are known to play a crucial role in adhesion has not yet been performed; on the other hand attempts have been made using mESCs where a synthetic hydrogel fabricated from branched poly (ethylene glycol) was cross-linked with matrix metalloproteinase-sensitive peptides and functionalised with peptide adhesion ligands: RGDSP (specific for fibronectin and vitronectin), and TTSWSQ and AEIGIEL which were specific adhesion for integrins $\alpha5\beta1$ and $\alpha V\beta5$, $\alpha6\beta1$ and $\alpha9\beta1$ respectively. A combination of these peptide ligands on the synthetic hydrogel demonstrated the ability of mESCs to expand and form colonies and expressed key signal molecules that support stem cell self-renewal (β-catenin, smad-1/5/8 and Ant-1), expressed all pluripotent markers and encouraged the down regulation of differentiation markers [Lee *et al.*, 2010]. This technique may be applied in the future to the nanofibrous substrates used this study, where both PCL aligned and PCL random nanofibrous substrates could be functionalised with an adhesion peptide ligand that is specific for the critical integrin identified in this chapter as $\alpha V\beta5$ for enhancing hESC attachment and proliferation on nanofibrous substrates, when cultured in physiological normoxia (2% O_2).

4.6 Conclusion

This chapter has identified oxygen-responsive integrins/sub-units, which mediate the initial attachment of hESCs to Matrigel^{TM} coated substrates. *In silico* microarray data analysis revealed transcriptional level changes in a dozen oxygen-responsive integrin sub-units of which αV, $\beta5$, αE and $\alpha6$ were significantly elevated in 2% O_2 relative to 21% O_2. Concomitantly, HA-related receptor genes showed increased expression levels in 21% O_2, instead of 21% O_2. Cell attachment studies demonstrated that blocking of an essential

Chapter 4

ECM integrin αVβ5 and sub-unit α6 significantly hindered hESC attachment in 2% O_2 only and that CD44 inhibited cell attachment after 24 hours of post-antibody treatment, in 21% O_2 but not in 2% O_2. Furthermore, immunofluorescence staining confirmed the expression of αVβ5 and CD44 in both 2% O_2 and 21% O_2; αVβ5 receptor stained much stronger in 2% O_2 cultured hESCs, relative to 21% O_2 and CD44 was more membrane-bound and less predominant in cytoplasmic and nucleus regions in 21% O_2 cultured hESCs in comparison to 2% O_2. This was further confirmed by quantitative analysis by FACS which demonstrated a significantly higher percentage of αVβ5 expressing hESCs cultured in 2% O_2, relative to hESCs cultured in 21% O_2. Conversely, a greater number of 21% O_2 cultured hESCs expressed CD44; relative to 2% O_2 cultured hESCs. The effect of blocking αVβ5 in hESCs cultured in physiological normoxia (2% O_2) and blocking of CD44 (21% O_2) in hESCs cultured in hyperoxia (21% O_2) on hESC pluripotency was evaluated via immunofluorescence staining and demonstrated that upon blocking these receptors this decreased the expression of pluripotent markers such as Oct 3/4, Nanog, ALP and SSEA-4. Furthermore, blocking of the αVβ5 receptor in hESCs before seeding and culturing onto nanofibrous substrates in physiological normoxia revealed a decrease in the number of hESC colonies formed after 21 days; however no significant differences were found amongst the nanofibrous substrates although there was a significant difference found between hESC colonies formed from hESCs treated with or without anti-αVβ5 blocking solution and then cultured on Matrigel™ in physiological normoxia, for 21 days.

5. Characterisation of Protein Adsorption Activity on Electrospun Nanofibrous Substrates to Support hESC Attachment

5.1 Introduction

Current limitations associated with the use of human embryonic stem cells (hESCs) in clinical therapeutic applications includes: xenogenic exposure and the inability of large-scale manufacture which would provide consistency and repeatability in the production of a homogenous and high quality population of undifferentiated hESCs [Fadeev and Melkoumian, 2011]. To overcome these issues, the discovery and identification of the proteins which promote and enhance hESC attachment and pluripotent expansion may prove essential. This would permit the design and modification of suitable, synthetic biomaterial substrates to improve hESC attachment and expansion.

In this thesis, hESCs were cultured using the feeder-free method which involved Matrigel™ and MEF conditioned media. Matrigel™ is an ECM isolated from Engelbreth-Holm-Swarm mouse sarcoma and is a complex gel comprised of many ECM proteins (collagen IV, laminin, fibronectin and heparin proteoglycans), amongst others. Furthermore, MEF conditioned media has also been identified to contain many secreted ECM proteins (by MEFs) including; collagen I, collagen IV, laminin, fibronectin, heparin proteoglycans, entactin and nidogen, amongst others which are yet to be identified [Fadeev and Melkoumian, 2011; Xu *et al.*, 2001].

Chapter 5

ECM proteins are found in serum containing media and are critical in mediating a cells adhesion to a substrate (natural or synthetic). Ultimately this can dictate the biocompatibility of the substrate via formation of an interfacial layer of proteins that bridge materials and cells [Ma *et al.*, 2007]. During contact between media and a synthetic substrate the, initial adsorption of proteins from media onto the superficial layer of the substrate provides natural recognition sites for corresponding cell membrane receptors. These include integrins. These initial attachments promote filopodia interactions and cell-based secretion of proteins and carbohydrates essential for continued maintenance or modification of the interfacial layer [Ostuni *et al.*, 1999].

At lower protein solution concentrations, protein interaction with a biomaterial surface can be maximised (via orientation and unfolding), resulting in irreversible adsorption on the surface; at higher protein solution concentrations, there are less protein-surface interactions and hence are able to retain a stable conformation but can be easily detached [Nath *et al.*, 2004]. Proteins have a primary structure which is made up of a unique sequence of amino acids. In total, there are 20 amino acids and each amino acid differs in its chemical nature in terms of its side chain which gives rise to various physicochemical properties which also play a role in the overall properties of the protein itself [Patthy, 1999]

Furthermore, the structure of the protein can also determine the protein adsorption ability and conformational integrity on substrate surfaces; "hard" proteins (lysozyme and RNAse) adsorb voluntarily to hydrophobic surfaces and cause minimal structural changes whereas "soft" proteins (BSA and IgG) are able to adsorb onto most surfaces with subsequent changes in conformation [Nath *et al.*, 2004].The adsorbed protein interfacial layer (also referred as surface remodelling) is complex and dynamic, thus is constantly changing with

time. Initially, highly abundant serum proteins with low molecular weight adhere to the surface and are gradually replaced by less abundant, high molecular weight, cell adhesive proteins such as fibrinogen with time; this is known as the Vroman effect [Vroman, 1962]. Additionally, proteins that do adsorb onto substrate surfaces are likely to undergo unfolding at the surface with time resulting in subsequent alterations in conformation and thus changing the affinity status (wettability) of the biomaterial surface to permit cell attachment.

The amount and type of protein that is able to adhere to a biomaterial substrate is determined by several factors which consequently determine cell attachment and the ability to function appropriately. These factors include; polymer substrate chemistry, surface charge, wettability (polarity of the surface), functional groups and topography, all of which are known to have an impact on protein adsorption and conformation state of the protein (which determines the affinity for cell attachment) [Roach *et al.*, 2005; Stevens, 2008] Increasing surface roughness and introducing topography at the nanoscale with organised orientation enhanced cell attachment. Nanofibrous architecture through electrospun nanofibres is known to increase protein adsorption due to a greater surface area to volume ratio; essentially, nanofibrous architecture is able to closely mimic the natural ECM architecture resulting in a more desirable and recognisable environment for cell attachment. [Stevens and George, 2005; Woo *et al.*, 2003]. Furthermore, surface topography has a two-fold effect on cell attachment; it provides contact guidance, where cell integrin receptors in focal contact transfer the variable degrees of tension or compression into the cytoskeleton resulting in its reorganisation in accordance to the surface topography. The second effect is to induce changes in surface free energy due to edges and disruption effects [Ma *et al.*, 2007].

Chapter 5

Current methods of detecting and characterising proteins that have adsorbed onto a surface as well as being able to define the surface chemical structure of a polymeric biomaterial substrate include: Quartz crystal microbalance (QCM), surface plasmon resonance (SPR), ellipsometry, attenuated total reflectance Fourier transform infrared spectroscopy (ATR-FTIR), atomic force microscopy (AFM), X-ray photoelectron spectroscopy (XPS). A brief description of how these techniques operate and any associated limitations are summarised in Table 5.1. These are very powerful techniques and most of them are able to reveal qualitative and quantitative analysis; amongst them ATR-FTIR and XPS are the most widely used spectroscopic techniques in order to reveal the chemical structure of polymeric biomaterials [Ma *et al.*, 2007]. A critical parameter of a spectroscopic technique is surface sensitivity defined by the sampling depth which is important for interpreting results correctly [Ma *et al.*, 2007]. However, many of these techniques have limitations including; limited surface types that can be analysed issues with adsorption, inconsistent monitoring of reorganisation and desorption of proteins, and the inability to differentiate between proteins (as there are many similarities between most proteins) [Roach *et al.*, 2006; Wagner and Castner, 2001].

Table 5.1 A summary of various available techniques currently used to analyse and characterise protein adsorption.

Technique	Description
Quartz crystal microbalance (QCM)	Also known as the piezoelectric microbalance, allows the quantification of mass by measuring the change in frequency of a piezoelectric quartz crystal when it is disturbed by the addition of a tiny mass such as a protein. QCM measurements can be performed under vacuum and liquid environment, giving information regarding the approximate change in mass as well as the viscoelastic constant for the adsorbed layer of proteins on polymeric substrates by measuring frequency and dissipation (band width change or ring-down kinestics) respectively. [Ma *et al.*, 2007] **Limitations:** Measurements do not give direct information on adsorbing species – frequency and dissipation changes need to be modelled, giving only an indication of adsorbing species with errors brought into this dependant upon the validity of the model used.
Ellipsometry	Ellipsometry allows the characterisation of the surface protein thickness. This method focuses on the measurement of the changes in polarisation state of a reflected light from its incident light. A smooth surface will reflect a monochromatic linear polarised light and upon doing so changes its polarisation state; the protein layer thickness absorbed on the substrate surface further induces a change in the polarisation state of the reflected light which can be calculated. [Ma *et al.*, 2007] **Limitations:** Only limited to proteins adsorbed onto extremely smooth surfaces with strong reflective ability and with an obvious refractive index and hence is not practical for polymeric biomaterials surface analysis. [Ma *et al.*, 2007] This technique also heavily relies on fitting experiments to models, and so the validity of the model to fit the conditions under investigation are paramount.
Surface plasmon resonance (SPR)	An optical technique used to investigate biological interactions such as protein adsorption processes being capable of real time analysis to define protein adsorption and desorption rates. Calculates the relationship between resonance energy and mass concentration of proteins adsorbed onto a thin metal film. [Ma *et al.*, 2007]. Also a similar technique to ellipsometry. **Limitations:** as above with the model info
Attenuated total reflectance Fourier transform infrared spectroscopy (ATR-FTIR)	An evanescent wave (the incident radiation interacts with the sample with an exponentially decreasing penetration depth ranging from several nanometers to more than 1 μm, varying with respect to the wavelength. **Limitations**: a technique which does not allow a specific analysis of substrate surface as the signal is a combination of the surface and the substrate underneath. Is only practical for formed monomolecular layers on substrates such as silicate and inorganic crystals. Specifically for biodegradable polymers (PCL and PLA) bulk phase IR adsorption occurs therefore preventing the identification of immobilised proteins or polyacrylamide peaks.

Chapter 5

Atomic force microscopy (AFM)	A nano-scale resolution technique which requires no pre-preparation before imaging surface structure of insulating, semi-conductive or conductive samples. A sharp probe on a flexible lever allows the study of the structure of single biomolecules, native bio-membranes and the measurement of molecular forces at the single-molecule level. This technique has high force sensitivity, a high dynamic range (0.001-5000 nN) and a high positional accuracy (0.01 nm) with ability to operate in a physiological environment [Lee *et al.*, 2007] **Limitations:** AFM lacks the chemical specificity to identify adsorbed proteins unless the AFM tip is functionalised. [Wagner and Castner, 2001]
X-ray photoelectron spectroscopy (XPS)	XPS can provide information such as coverage and thickness of adsorbed proteins; specifically XPS determines whether the adsorbed layer is continuous or exists as a patchy film and has a much smaller sampling depth (< 10 nm) in comparison to ATR-FTIR. Amount of immobilised proteins on biomaterial surface can be measured by radio labelling using I^{125} and is highly sensitive. **Limitations**: XPS gathers information under high vacuum and thus may not be a true representation of the actual liquid-solid biomaterials surface. [Ma *et al.*, 2007]
Electron paramagnetic resonance (EPR)	Enables the evaluation in the behaviour of adsorbed proteins on biomaterial substrate surfaces. Adsorbed proteins are labelled with spin labels (nitroxide type); nitroxides have EPR spectra which especially sensitive to molecular mobility. By monitoring the changes in the EPR spectrum shape, one can clarify the behaviour of specific sites of proteins adsorbed on synthetic biomaterial surfaces. [Ma *et al.*, 2007]
Enzyme-linked immune sorbent assay (ELISA)	Allows the measurement and quantification of the bioactive state of immobilised proteins on biomaterials surfaces which can be characterised using a specific bio-recognition process between antibodies and antigens. [Ma *et al.*, 2007]. A similar technique to ELISA is circular dichroism spectroscopy (CD) which specifically studies the protein conformation of the secondary structure. **Limitations**: CD poses intrinsic inconsistency problems in absolute secondary structure [Roach *et al.*, 2006]

Recent improvement in instrument development which can be used to analyse protein adsorption onto surfaces and eliminate limitations associated with current techniques is Time of flight secondary ion mass spectrometry (Tof-SIMS). Tof-SIMS can analyse the chemical composition (or any protein adsorption) of substrate surfaces. It combines the analytical technique of SIMS and the Tof mass analyser; the Tof mass analyser gives a detailed mass resolution compared to other SIMS set-ups which reveals the detection of all elements and isotopes including the provision of chemical information. Tof-SIMS uses a

pulsed ion beam (incident particles such as Bismuth 3 [Bi^{3+}] cluster) to remove molecules from the very outermost surface of the substrate (10-20 Å). The particles are removed from atomic monolayers on the surface (secondary ions; positive and negative ions) and tend to be molecular compounds or fragments which are characteristic of specific amino acids or larger organic macromolecules; these particles/fragments are then accelerated into a flight tube and their mass is determined by measuring the exact time at which they reach the detector. A schematic of the Tof-SIMS set-up is demonstrated in Figure 5.1.

The advantages of using Tof-SIMS over existing tools is its extreme chemical specificity and high surface sensitivity, which provides specific molecular evaluation of composition, conformation, orientation and denaturation of proteins as well as being able to identify specific proteins adsorbed onto a substrate surface. Tof-SIMS provides greater chemical selection over XPS due to mass spectrometry and detailed molecular structure of the outermost layer (10-20 Å) of proteins adsorbed onto a substrate surface, including the orientation and degree of conformational changes (determines what amino acid fragment is exposed and thus detected by Tof-SIMS) resulting in a large number of quantity of peaks [Ma *et al.*, 2007]. A limitation with Tof-SIMS, is that the information obtained is under high vacuum and thus may not be a true representation of the actual liquid-solid biomaterials surface interface [Ma *et al.*, 2007]. Table 5.2 summarises the advantages and disadvantages of using Tof-SIMS.

Chapter 5
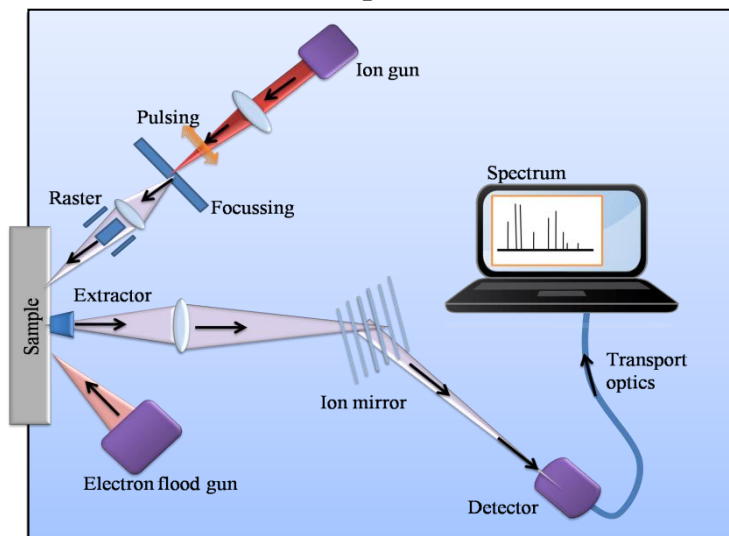
Figure 5.1 Schematic demonstrating the Tof-SIMS instrument set-up. Adapted from

http://www.ion-tof.com/

Table 5.2 Summary of the advantages and disadvantages associated with using Tof-SIMS.

Advantages	Disadvantages
Allows the survey of all masses on substrate surfaces	Not qualitative but is semi-quantitative
Mapping of elements and chemical groups on a sub-micron scale	Limited optical capabilities
High mass resolution	Image shift during a change in collection mode from positive ion to negative ion data
High sensitivity for trace elements/compounds	

As synthetic substrates (PCL aligned and random nanofibrous) substrates support the attachment and expansion of undifferentiated hESCs. It remains unknown which ECM proteins can adhere to these nanofibrous substrates and form an interfacial layer with structure and composition that is specifically able to support the attachment of hESCs. This may be through integrin-binding sites which have been identified to be expressed on hESC membranes in the previous chapter. In this chapter, Tof-SIMS in combination with principle component analysis (PCA) is used to attempt to identify key ECM protein fragments adsorbed onto PCL electrospun nanofibrous (aligned and random) substrates from pure protein solutions and partially defined ESC conditioned media.

Chapter 5

5.2 Aims and Objectives

We have determined that hESCs displayed significantly elevated expression of the $\alpha V\beta 5$ receptor and $\alpha 6$ and αE sub-units when cultured in physiological normoxia (2% O_2) vs hyperoxia (21% O_2) and played a crucial role in attachment to Matrigel™ substrates. These data argue that ECM proteins associated with these hESC integrin/sub-units will adsorb onto PCL electrospun nanofibrous substrates (aligned and random) in an active conformation state that allows hESCs to attach, spread and proliferate. It can be hypothesised that these may include ECM proteins such as: vitronectin, fibronectin, collagen and laminin. We have also demonstrated that decreasing the fibre diameter enhanced hESC-CFU ability in physiological normoxia (2% O_2); as smaller diameter fibres provides an increased surface area to volume ratio it can be hypothesised that this enhances the adsorption of proteins to the fibres with a subsequent increase in recognition sites for hESC integrin receptors.

The objectives of this chapter seek to test the above hypothesis and are as follows:

- Quantification of protein adsorption on PCL electrospun nanofibres (aligned and random) from pure protein solutions and MEF conditioned hESC media

- Using Tof-SIMS and PCA to determine variation of serum proteins adsorbed from pure protein solutions and hESC conditioned media (from MEFs) onto PCL electrospun nanofibrous substrates in both aligned and random conformations.

- To investigate the effect of varying fibre diameter of PCL nanofibrous substrates (aligned and random) on protein adsorption ability from pure protein solutions and hESC conditioned media.

Chapter 5

5.3 Materials and Methods

All nanofibrous substrates were fabricated using electrospinning. Aligned nanofibres were attained using the rotating mandrel technique, whereas random nanofibres were produced using the static copper plate collector. The operating parameters used to attain both aligned and random nanofibres onto 13 mm circular glass coverslips are stated in **Table 2.2-2.3, Section 2.13-2.1.4, Chapter 2.** Nanofibres on glass coverslips were further reinforced using silicone rubber strips and silicone glue to prevent their detachment whilst immersed in hESC conditioned media and pure protein solutions. All nanofibrous substrates were sterilised using 70% IMS for at least 1 hour. Fibre morphology, orientation and diameter were characterised using field emission scanning electron microscopy (FESEM).

Pure protein solutions of collagen I (Coll I), fibronectin (Fn), laminin (Ln) and vitronectin (Vn) prepared in PBS at a concentration of 50 µg/ml and hESC conditioned media were placed onto individual PCL electrospun nanofibrous substrates (aligned and random) as well as blank glass coverslip controls at a volume of 50 µl. Samples with protein solutions/hESC conditioned media were incubated for 2 hours in physiological normoxia (2% O_2). Substrates were then rinsed with PBS and water, dried and analysed using Tof-SIMS **Please refer to Section 2.5.3, Chapter 2**, schematic is also visible in Figure 5.2. All Tof-SIMS screening of samples was performed by Dr David Scurr at the University of Nottingham; data analysis/treatment (including PCA) was performed by Dr Paul Roach.
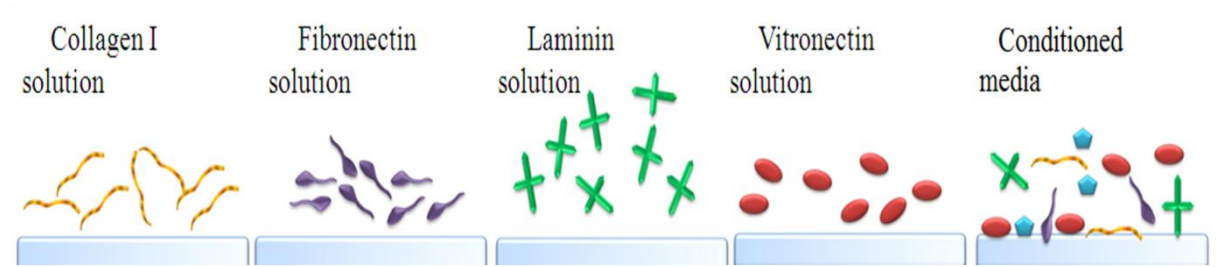
Figure 5.2 Protein adsorption protocol. Proteins from single protein solutions (50 µg/ml) and hESC conditioned media were allowed to adsorb onto substrates (glass, PCL-A and PCL-R) for 2 hours at 37 °C. Supernatant solution was removed; substrates were then washed with PBS and water, air dried and analysed using Tof-SIMS.

Quantification of protein absorption was performed using the fluorometric assay, NanoOrange®. Briefly, 50 µl of pure protein solutions of Coll I, Fn, Ln and Vn at 50 µg/ml, and hESC conditioned media were placed on PCL nanofibrous substrates/blank glass coverslips and incubated for 2 hours in physiological normoxia (2% O$_2$). Protein solution/media supernatant was collected and quantified using NanoOrange® and then subtracted from initial concentration of proteins/media solutions in order to calculate the amount of protein adsorbed onto PCL electrospun nanofibrous substrates/blank glass coverslips. **Detailed protocol stated in Section 2.5.4, Chapter 2.**

Chapter 5

5.4 Results

5.4.1 Characterisation of PCL Electrospun Nanofibrous Substrates

PCL was electrospun onto glass coverslips to attain nanofibres of large and small diameters, in both aligned and random conformations. Scanning electron microscopy (SEM) revealed nanofibrous substrate topography where all electrospun nanofibres had a similar morphology of uniform, linear fibres without any beading. SEM images allowed the measurement of fibre diameter (Figure 5.3); results demonstrated that 12.5% PCL provided smaller nanofibre diameters (aligned, 280 nm; random; 318 nm) whereas 15% PCL provided larger nanofibre diameters (aligned, 521 nm; random; 660 nm).
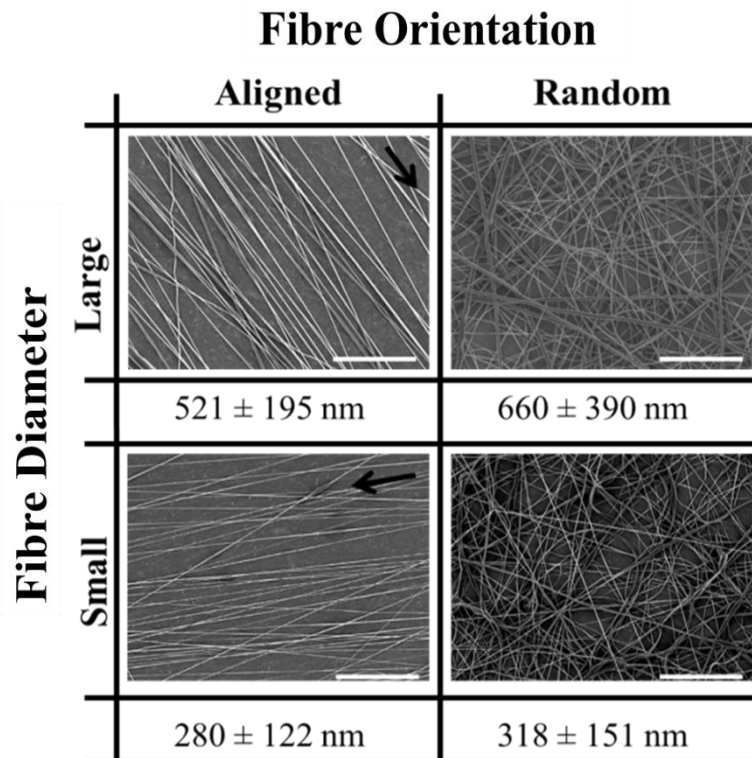
Figure 5.3 Representative FESEM images of PCL electrospun nanofibres in both aligned and random conformations, at various different fibre diameters. Scale bar = 200 μm.

Chapter 5

5.4.2 Quantification of Protein Adsorption on PCL Electrospun Nanofibrous Substrates in Physiological Normoxia (2% O_2)

A fluorometric assay, NanoOrange® was used to detect and quantify the amount of protein adsorbed/remained on PCL electrospun nanofibrous substrates (aligned and random) at the lower fibre diameter range. NanoOrange® is a highly sensitive assay which has the ability to detect small amounts (10 ng/ml) of proteins adsorbed on surfaces. PCL electrospun nanofibrous substrates (aligned and random) including blank glass coverslips (controls) were incubated with ES conditioned media (CM) as well as pure protein solutions of collagen I (Coll I), fibronectin (Fn), laminin (Ln) and vitronectin (Vn) at 50 µg/ml for 1 hour in physiological normoxia (2% O_2). After incubation, supernatant solutions of proteins and CM were collected and quantified using NanoOrange®; absorbance values were then deducted from initial protein solution/CM samples prior to placing on substrates, in order to calculate any adsorbed proteins onto substrates by mass balance.

As shown in Figure 5.4, NanoOrange® revealed that proteins from pure protein solutions and CM were able to adsorb onto all three substrates; PCL-A, PCL-R and glass coverslips. Statistical analysis revealed that there was a significantly greater adsorption of CM (total protein) on PCL-A (6.6 µg/ml) compared to glass (CTL; 5.8 µg/ml) ($p < 0.05$) and also significantly greater adsorption of Vn on PCL-A (2.2 µg/ml) compared to glass (CTL; 1.8 µg/ml) ($p < 0.01$). In other cases, despite differences in protein adsorption on nanofibrous substrates relative to glass (CTL) there was no real statistical differences between them.

Chapter 5
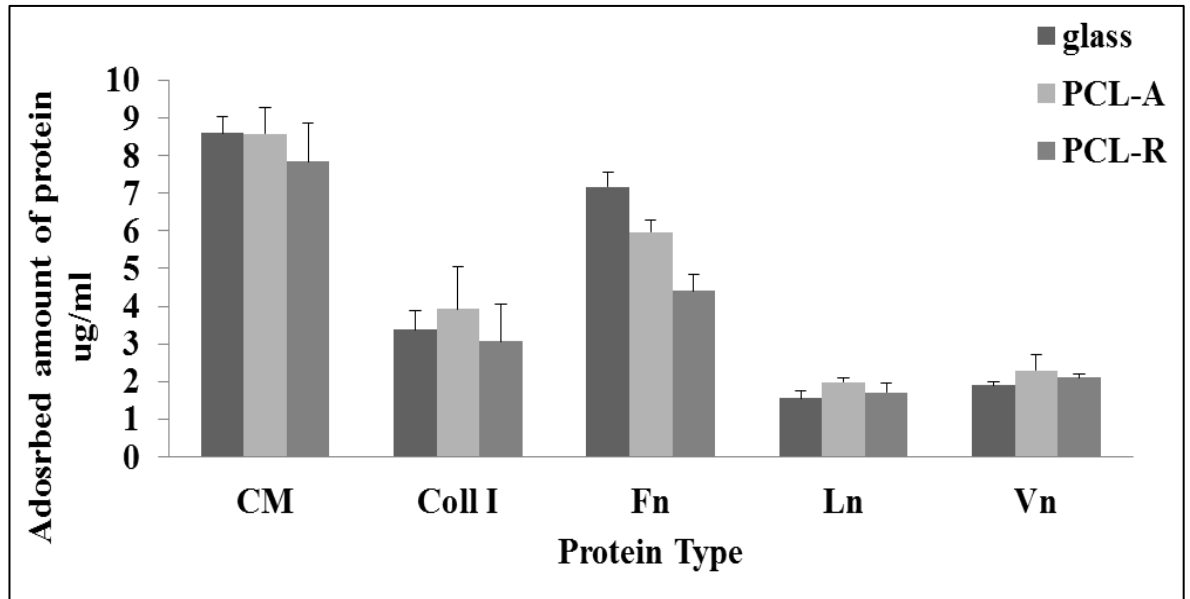
Figure 5.4 Quantification of protein adsorption from ES conditioned media (CM) and pure protein solutions; collagen I (Coll I), fibronectin (Fn), laminin (Ln) and vitronectin (Vn) at 50 μg/ml concentration, on PCL electrospun nanofibrous substrates in both aligned (A; 280 ± 122 nm) and random (R; 318 ± 151 nm) conformations as well as glass coverslips (control).$\Delta = I_c - F_c$ stands for the change in the initial protein concentration from final concentration. Values indicate mean adsorption of proteins and standard deviation of n=3; *$p < 0.05$, **$p < 0.01$.

5.4.3 Tof SIMS Analysis of Protein Adsorption on PCL Electrospun Nanofibrous Substrates in Physiological Normoxia (2% O_2)

Electrospun PCL nanofibrous substrates were fabricated with both small (280-318 nm) and large (518-660 nm) fibre diameter dimensions in both aligned and random conformations. All nanofibrous substrates including blank glass coverslips (control; CTL) were immersed in MEF-conditioned hESC media and pure protein solutions (Coll I, Fn, Ln and Vn) and incubated at 37 °C for 2 hours after which point media/protein solutions were removed and

Chapter 5

samples analysed in terms of the amount adsorbed and the identification of the adsorbed layer by Tof SIMS. After data treatment and PCA; score plots for both media and all pure proteins on substrates (nanofibres and controls) revealed distinct groups belonging to each of the proteins on each substrate in the positive ion fragment data set, as shown in Figure 5.5. PC1 and PC2 score plots of positive SIMS data indicated clustering of sample data into three distinct groups (cluster A, cluster B and cluster C; indicated by circles); however, a greater overlap between different samples were observed in cluster B and C particularly as shown in Figure 5.5 suggesting spectral similarities between several samples in terms of protein adsorption. The samples within each cluster are specified in Table 5.3.
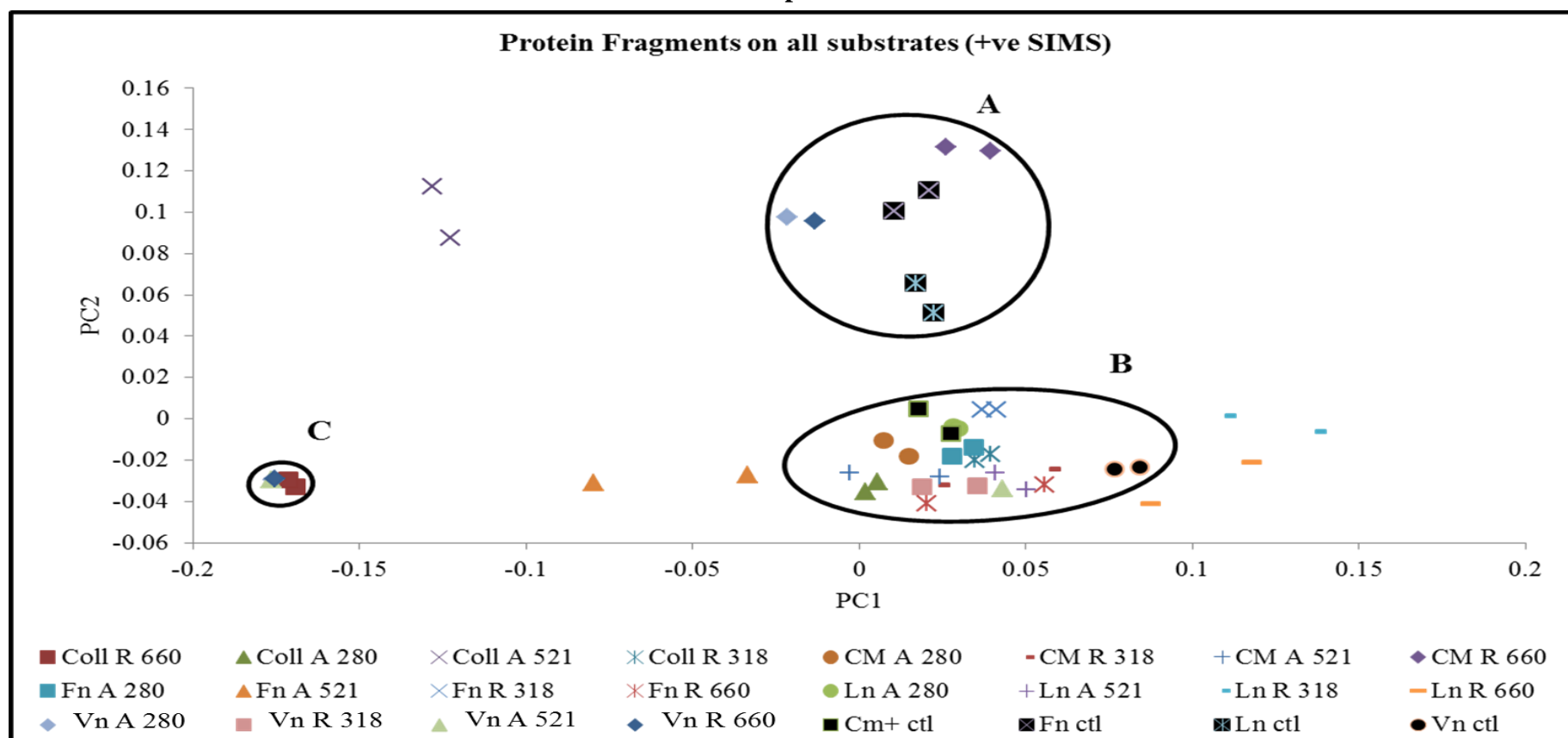
Figure 5.5 Scores plot on the first two multivariate axes from PCA of the Tof-SIMS spectra (positive ion data) of proteins adsorbed onto all electrospun nanofibrous substrates and control (blank glass coverslip). Definition of sample abbreviations: control (glass coverslip), A (aligned), R (random), Coll (collagen I), CM (conditioned media), Fn (fibronectin), Ln (laminin) and Vn (vitronectin). Circles indicating clustering of sample data with respect to PC1 and PC2.

Chapter 5

PCA score plots of positive SIMS data, of samples separated in terms of fibre diameter; (small Ø, 280-318 nm; large Ø 521-660 nm) further demonstrated spectral similarities between several samples. In Figure 5.6, PCA score plots of smaller fibre diameter samples revealed overlapping and clustering of various samples in cluster A (indicated by a circle). Larger fibre diameter samples also revealed spectral similarities and thus overlapping of various samples into two distinct clusters A and B, as shown in Figure 5.6. However, it can be visualised greater overlapping and clustering of samples within smaller fibre diameter samples (Figure 5.5) in comparison to larger fibre diameter samples (Figure 5.6). The samples identified within each cluster for both Figure 5.5and 5.6 are stated in Table 5.3.
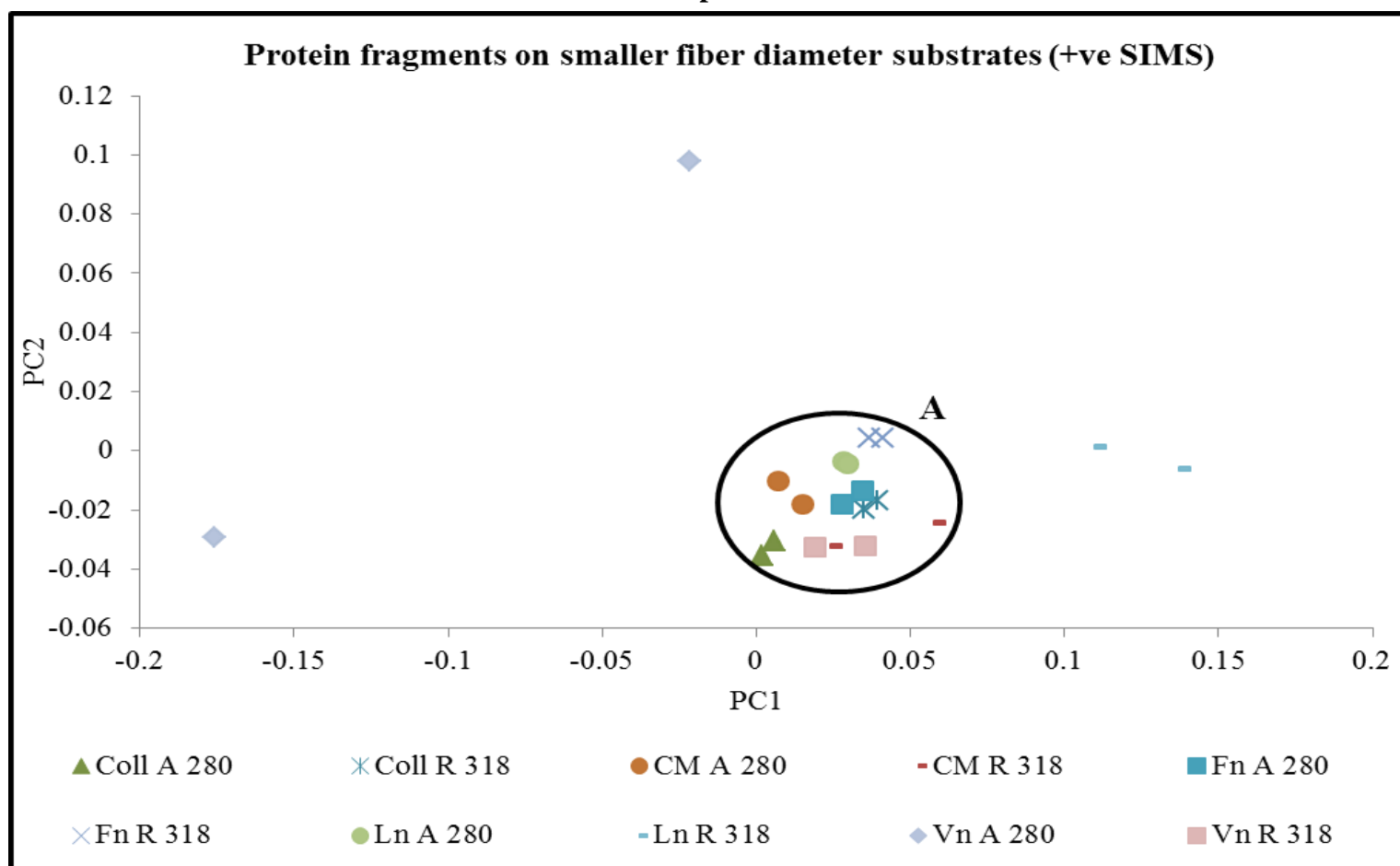
Figure 5.6 Scores plot on the first two multivariate axes from PCA of the Tof-SIMS spectra (positive ions data) of proteins adsorbed onto PCL nanofibrous substrates of smaller diameter (280 – 318 nm) and control (blank glass coverslip). Circles indicating clustering of sample data with respect to PC1 and PC2.
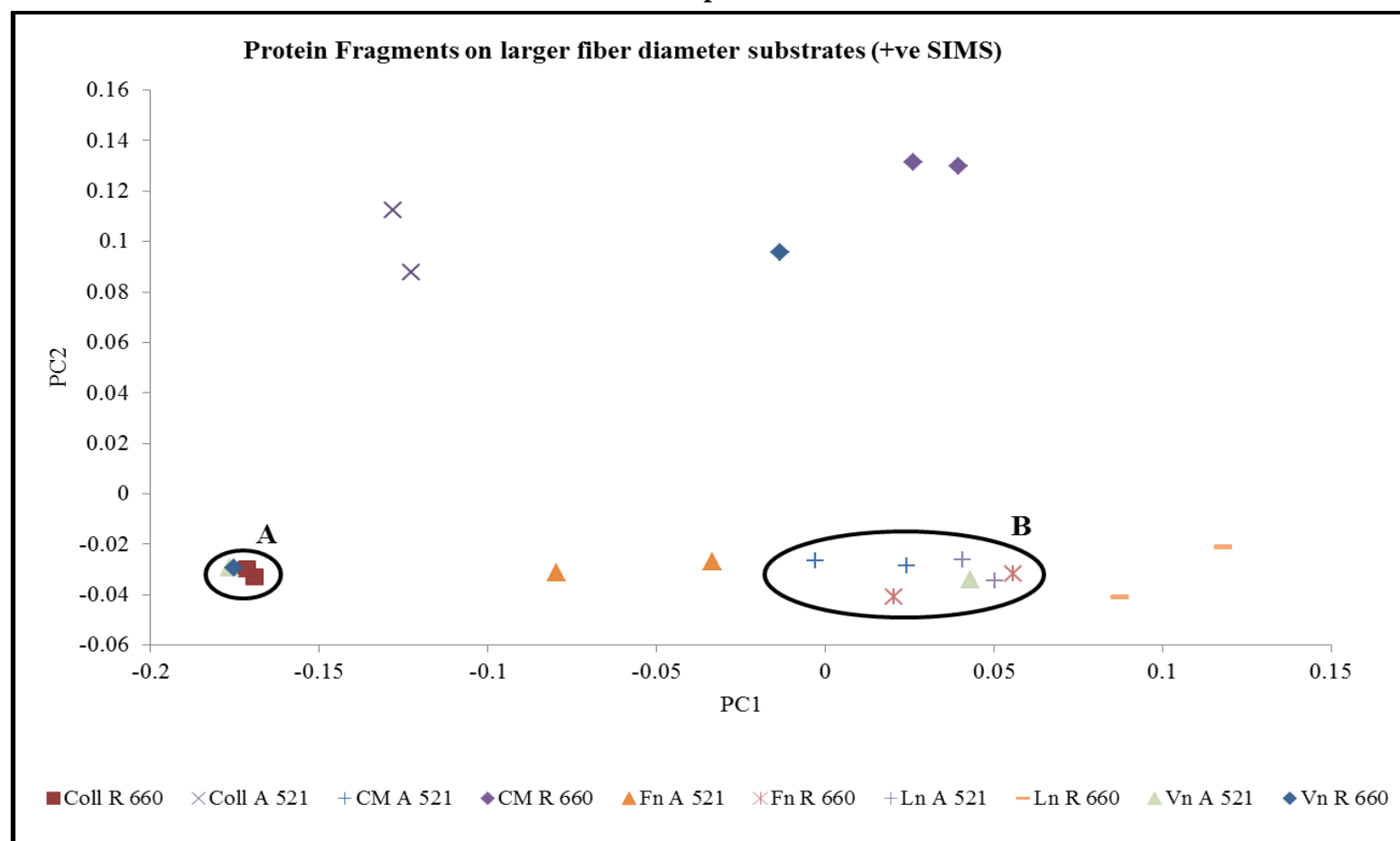
Figure 5.7 Scores plot on the first two multivariate axes from PCA of the Tof-SIMS spectra (positive ion data) of proteins adsorbed onto PCL nanofibrous substrates of larger diameter (521–660 nm) and control (blank glass coverslip). Circles indicating clustering of sample data with respect to PC1 and PC2.

Table 5.3 Definition of clusters observed in Figures 5.5-5.7 for protein fragments on all

substrates for all positive ion data

	Cluster	**Spectral similarities observed between proteins on various proteins (+ve SIMS)**
Figure 5.5	Cluster A	CM-R (660 nm), Fn ctl, Ln ctl, and Vn-R (660 nm)
	Cluster B	CM ctl, CM-A (280 nm), CM-A (521 nm), CM-R (318 nm), Coll-A (280 nm), Coll-R (318 nm), Coll-R (660 nm), Fn-A (280 nm), Fn-R (318 nm) and Fn-R (660 nm), Ln-A (280 nm), Ln-A (521 nm), Vn ctl and Vn-R (318 nm)
	Cluster C	Coll-R (660 nm), Vn-A (280 nm) and Vn-R (660 nm)
Figure 5.6	Cluster A	CM-R (660 nm), Fn ctl, Ln ctl, and Vn-R (660 nm)
Figure 5.7	Cluster A	Coll I-R (660 nm), Vn-R (660 nm), Vn-A (521 nm)
	Cluster B	CM-A (521 nm), Fn-R (660 nm), Ln-A (521 nm) and Vn-A (521 nm)

The score plots for PCA provided visualisation of spectral similarities between

multivariate data sets; they do not provide detailed information in terms of the original

variables such as the Tof-SIMS ion mass intensities and the exact difference in peak

intensities between the spectra of different proteins adsorbed onto various substrates.

However, the loading plots do provide this information; loading plots for PC1 and PC2

(Figure 5.8) for the positive ion fragments detected on substrates identified the following

amino acid fragments to be expressed at a higher normalised intensity: C_2H^+, C_2H_5,

CH_4N^+, $C_3H_3^+$, CNO^-, C_2H_5N, $C_2H_6N^+$, C_3H_3O, $C_4H_7^+$, $C_3H_6N^+$, CH_5N_3, $C_4H_6N^+$, C_4H_5O,

$C_4H_8N^+$, $C_6H_6^+$, SO_4^-, $C_4H_4NO_2^+$, $C_4H_{10}NS$, $C_8H_9NO^4$ and $C_{13}H_9^+$. For each of the positive

ion mass peaks identified, normalised intensity values were tabulated and categorised in

terms of the media/pure protein solutions in which they were detected (positive ion mass

tables; Table A1-A5 in Appendix). Furthermore, these values enabled the identification of

the samples on which normalised intensity peaks were the highest in terms of

media/protein type, substrate (glass, PCL-A, PCL-R) and fibre diameter (small Ø 280-318 nm; large Ø 521-660 nm). This information is summarised in Table 5.4.
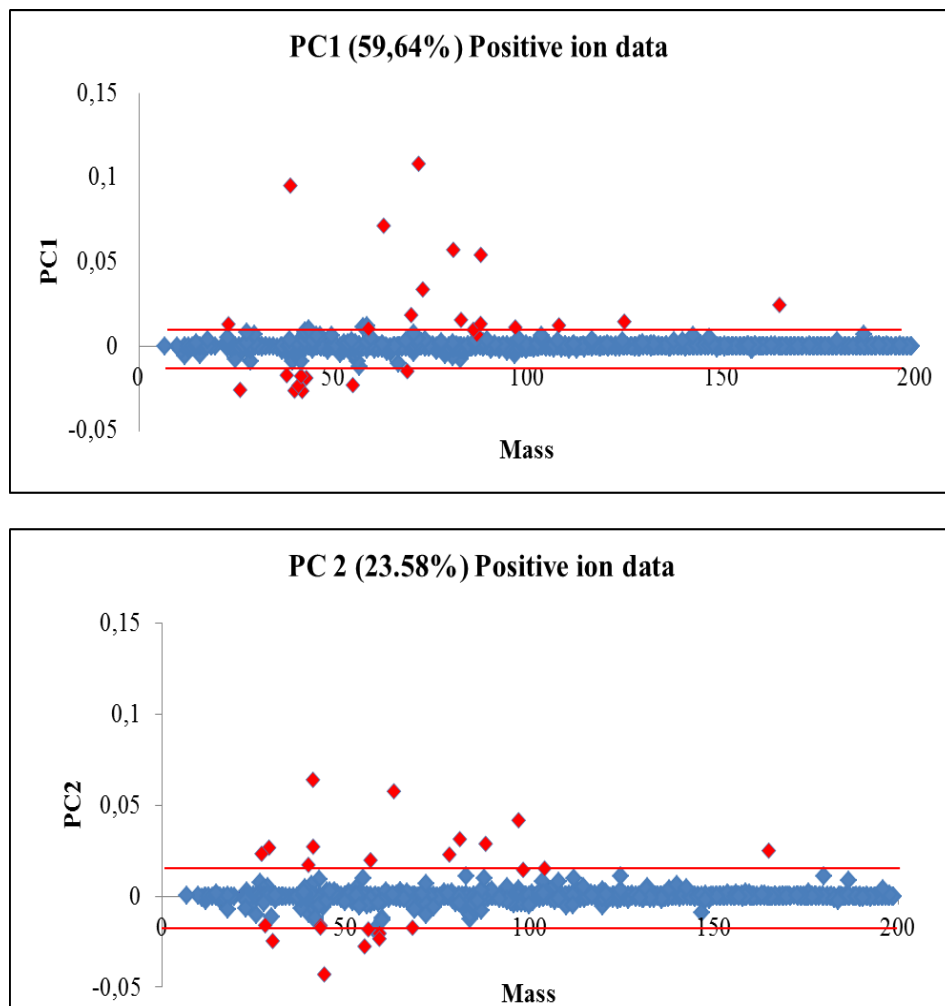
Figure 5.8 Loading plots for PC1 and PC2 from PCA of positive ions spectra of proteins adsorbed from CM and pure protein solutions (Coll I, Fn, Ln, and Vn) onto glass (control), PCL-A and PCL-R substrates of both small (Ø 280-318 nm) and large (Ø 521-660 nm) fibre diameter. Red line indicates the threshold set above which mass peaks are considered to be expressed at high intensity (indicated in red). Thresholds for PC1 (positive, 0.018; negative, -0.01469) and PC2 (positive, 0.0108; negative, -0.01594) were set at these values due to an obvious difference (plots) in PC values from the baseline when displayed on the loading plots.

Chapter 5

Table 5.4 Positive ion amino acid fragments identified from loading plots for PC1 and PC2 from PCA and the samples on which detected at the highest normalised intensity [Canavan *et al.*, 2006; Mahlstedt *et al.*, 2010; Wagner and Castner, 2001; Wagner *et al.*, 2002]

m/z (+ve ions)	Assignment	Proteins and Substrates on which greatest normalised intensity observed
25.9929	C_2H^+	Coll I-A (521 nm), Vn-A (280 nm)
27.9917	$C_2H_3^+$	Coll I-R (660 nm), Coll I CTL (glass), Coll I-A (521 nm), Fn CTL (glass), Vn-A (280 nm), Vn-R (660 nm), Vn CTL (glass)
29.0254	C_2H_5	Coll I-R (660 nm), Coll I CTL (glass), Coll I-A (280 nm), Fn-R (660 nm)
30.0112	CH_4N^+: Glycine	Coll I-R (660 nm), Coll I CTL (glass), Coll I-A (280 nm), Fn-R (660 nm)
39.7221	$C_3H_3^+$	Vn-A (280 nm)
41.0139	$C_3H_5^+$	Coll I-R (660 nm), Coll I-A (521 nm), Fn-A (521 nm), Vn-A (280 nm), Vn-A (521 nm), Vn-R (660 nm)
41.7003	$C_3H_5^+$	Coll I –R (660 nm), Coll I-A (521 nm), Fn-A (521 nm), Vn-A (521 nm)
41.9932	C_2H_4N: Alanine, Glycine	Coll I-A (521 nm)
42.9994	CNO^-; peptide backbone	Vn-A (521 nm)
43.0241	C_2H_5N	Coll I-R (660 nm), Coll I CTL (glass), Coll I-A (280 nm), Fn CTL (glass), Vn-R (318 nm), Vn CTL (glass)
43.0421	C_2H_5N	Coll I-R (660 nm), Coll I CTL (glass), Fn-R (660 nm)
44.0371	$C_2H_6N^+$ Alanine, Lysine, Asparagine	Coll I-R (660 nm), Coll I CTL (glass), Coll I-A (280 nm), Fn-R (660 nm), Vn-R (318 nm), Vn CTL (glass)
54.9998	C_3H_3O Tyrosine	Coll I-A (521 nm), Fn-A (521 nm), Vn-A (280 nm), Vn-R (318 nm), Vn-A (521 nm), Vn-R (660 nm), Vn CTL (glass)
55.0208	$C_4H_7^+$	Coll I-R (660 nm), Coll I CTL (glass)
56.0233	$C_3H_6N^+$	Coll I-R (660 nm), Coll I CTL (glass), Coll I-A (280 nm), Fn-R (660 nm)
56.6144	$C_3H_6N^+$	Vn-R (660 nm)
59.0496	CH_5N_3; Arginine	Coll I-R (660 nm), Coll I CTL (glass), Coll I-A (280 nm), Fn-R (660 nm), Vn-R (318 nm), Vn CTL (glass)
68.0263	$C_4H_6N^+$: Proline	Coll I-R (660 nm), Coll I CTL (glass), Coll I-A (280 nm), Fn-R (660 nm)
69.0374	C_4H_5O; Threonine	Coll I-R (660 nm), Coll I CTL (glass), Fn-R (660 nm)
70.0375	$C_4H_8N^+$: Arginine	Coll I-R (660 nm), Coll I CTL (glass), Coll I-A (270 nm), Fn-R (660 nm)
78.0441	$C_6H_6^+$	Coll I-R (660 nm), Coll I-A (521 nm), Fn-A (521 nm), Vn-A (280 nm), Vn-R (318 nm)
96.8582	SO_4^-	Vn-A (521 nm), Vn-R (660 nm)
98.1067	$C_4H_4NO_2^+$; asparagine	Coll I CTL (glass), Coll I-R (660 nm), Coll I-A (280 nm), Coll-A (521 nm), Coll-R (318 nm)
103.9236	$C_4H_{10}NS$: Methionine	Coll I CTL (glass), Fn-A (280 nm), Fn-R (660 nm), Vn-R (318 nm)
124.9131	$C_5H_{11}N_4$: Arginine	Fn CTL (glass) and Ln CTL (glass)
164.857	$C_{13}H_9^+$	Coll I-A (521 nm), Ln CTL (glass)

Chapter 5

However, of all positive ion mass peaks detected (stated in Table 5.4), the 11 positive ion fragments with the greatest normalised intensity values were selected as: 41.0139 ($C_3H_5^+$), 42.9994 (CNO^-, peptide backbone), 43.0241 (C_2H_5N), 43.0421 (C_2H_5N), 44.0371 ($C_2H_6N^+$; alanine, lysine or aspargine), 55.0208 ($C_4H_7^+$), 56.0233 ($C_3H_6N^+$), 59.0496 (CH_5N_3; arginine), 69.0374 (C_4H_5O; threonine), 70.0375 ($C_4H_8N^+$; arginine) and 124.9131 ($C_5H_{11}N_4$; arginine). (A description of how normalised intensity values were calculated is shown in Figure 5.9) These mass ion fragments were then plotted in terms of substrate type in order to distinguish any patterns in the proteins that are adsorbed and specificity in protein adsorption to substrates in terms of fibre orientation and diameter, as shown in Figure 5.10. Mass peaks detected at a higher normalised intensity value on each substrate type from pure protein solutions than from conditioned media in order to confirm the adsorption of these individual ECM proteins and their existence in conditioned media as well as to assess patterns of protein adsorption and fragmentation pattern to nanofibrous substrates are stated in Table 5.5.
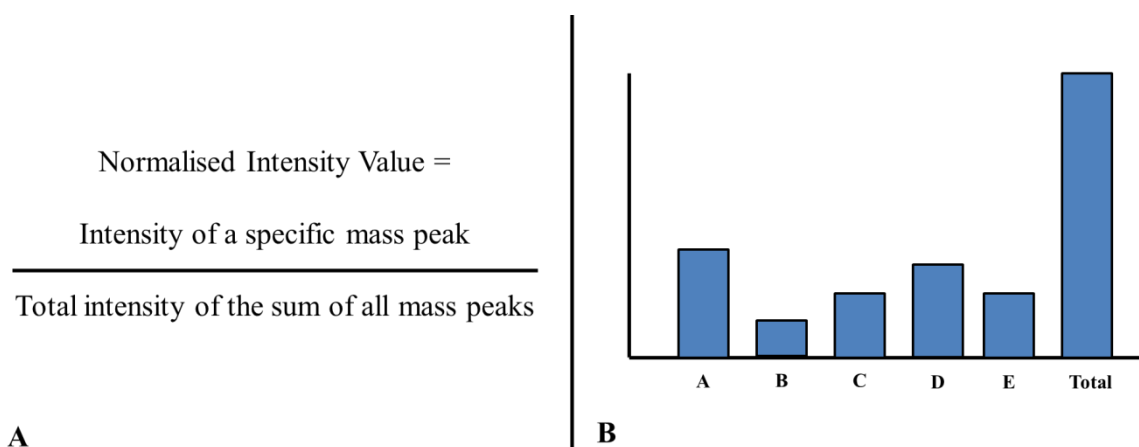
Figure 5.9 (A) Normalised intensity value is calculated by dividing the intensity of a specific mass peak by the total intensity of the sum of all mass peaks (B) Graph illustrating the intensity of a specific peak in comparison to the sum of all peaks (total) which would be calculation CM, Coll I, Fn, Ln and Vn.

Chapter 5

On glass coverslip substrates (control), many of the mass peaks with a higher intensity peak from pure protein solutions relative to conditioned media suggest that these amino acid fragments within these pure protein solutions are also present in conditioned media (Figure 5.10A and Table 5.5. However, it is apparent that Coll I is predominantly adsorbed onto glass coverslips. On PCL-A (280 nm) substrates, Coll I is also predominantly adsorbed onto these nanofibres, followed by Fn (Figure 5.10B). Interestingly by changing the fibre orientation; on PCL-R (318 nm) substrates, Coll I and Vn were predominantly being adsorbed instead (Figure 5.10C). By increasing the fibre diameter, PCL-A (521 nm) this changed the protein adsorption ability where in comparison to PCL-A (280 nm), not only did Coll I adsorb to the substrates but so did Fn and Ln (Figure 5.10D). On larger fibre diameter (660 nm) PCL-R substrates, Coll I, Fn and Ln were predominantly adsorbed with a greater number of mass peaks detected (Figure 5.10E). In terms of fibre diameter, there are less mass peaks detected at a higher intensity to conditioned media on smaller diameter fibres compared to larger fibres.
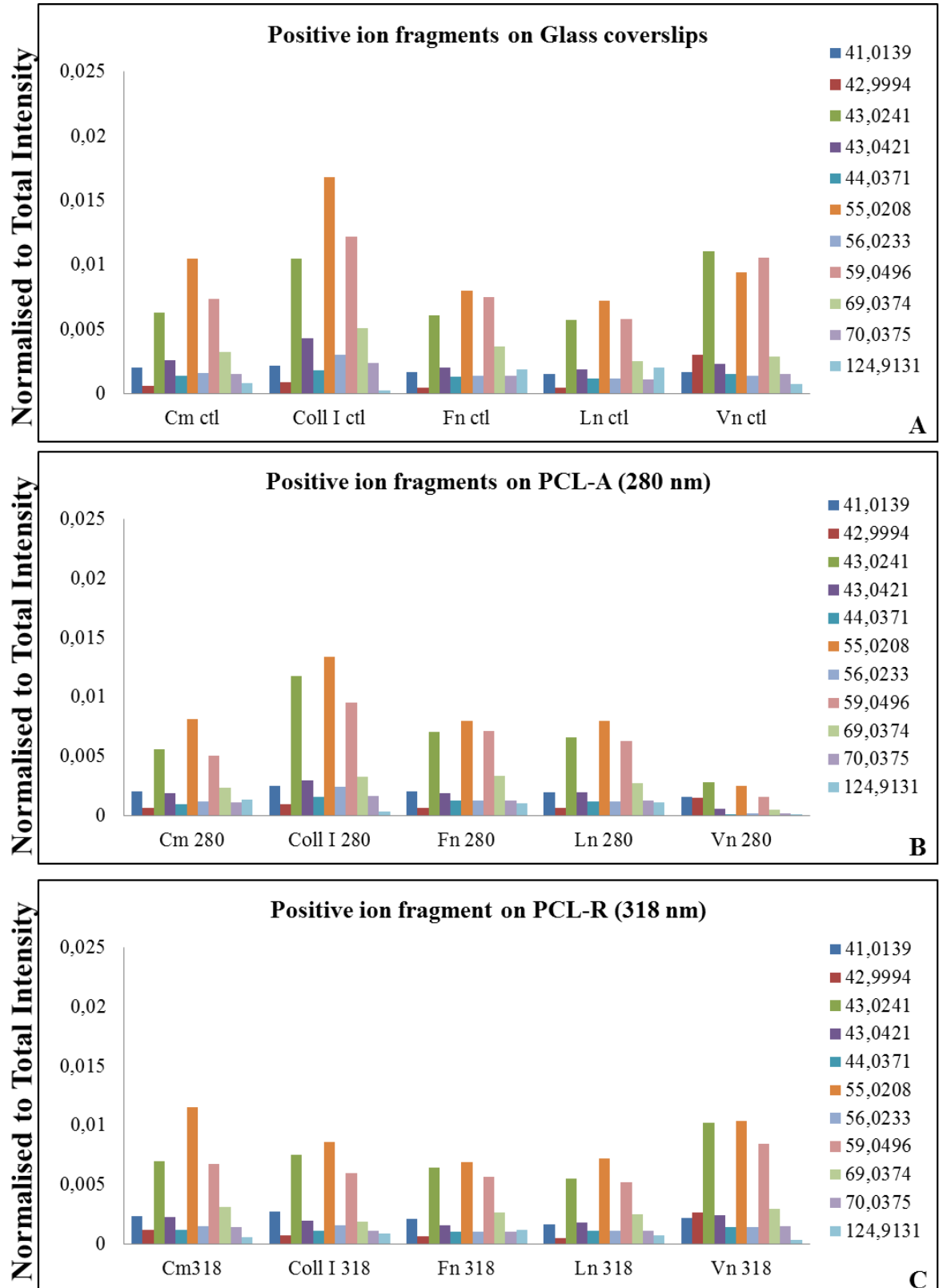
Chapter 5

Figure 5.10 Normalised intensity values of detected positive protein fragments from conditioned media (CM) and all pure protein solutions (Coll I, Fn, Ln and Vn) on: (A) glass coverslips (control), (B) PCL-A (280 nm), (C) PCL-R (318 nm), (D) PCL-A (521 nm) and (E) PCL-R (660 nm).

Table 5.5 Positive ion mass peaks detected at a higher normalised intensity value on each substrate type from each pure protein solution relative to conditioned media.

Substrate type	Pure protein solution	Positive ion fragments detected at a higher normalised intensity from pure protein solutions in comparison to conditioned media
Glass (control)	Coll I	43.0241, 43.0421, 55.0208, 56.0233, 59.0496, 69.0374 and 70.0375
	Fn	69.0374 and 124.9131
	Ln	124.9131
	Vn	43.0241 and 59.0496
PCL-A (280 nm)	Coll I	41.0139, 42.9994, 43.0421, 44.0371, 55.0208, 56.0233, 59.0496 and 69.0374
	Fn	42.9994, 59.0496 and 69.0374
	Ln	59.0496 and 69.0374
	Vn	Normalised intensity for all mass peaks equivalent to or less than conditioned media
PCL-R (318 nm)	Coll I	41.0139 and 43.0241
	Fn	124.9131
	Ln	Normalised intensity for all mass peaks equivalent to or less than conditioned media
	Vn	42.9994, 43.0241, 43.0421 and 59.0496
PCL-A (521 nm)	Coll I	41.0139 and 42.9994
	Fn	41.139, 43.0241, 55.0208 and 69.0374
	Ln	43.0241, 43.0421, 440.371, 55.0208, 59.0496 and 69.0374
	Vn	Normalised intensity for all mass peaks equivalent to or less than conditioned media
PCL-R (660 nm)	Coll I	41.0139, 43.0241, 43.0421, 44.0371, 55.0208, 56.0233, 59.0496, 69.0374 and 70.0375
	Fn	43.0241, 43.0421, 44.0371, 55.0208, 56.0233, 59.0496, 69.0374 and 70.0375
	Ln	43.0241, 43.0421, 44.0371, 55.0208, 56.0233, 59.0496, 69. 0374, 70.0375
	Vn	43.0241 and 55.0208

PCA analysis of the ***negative ion data set*** of media/pure protein solution adsorption on each substrate revealed distinct grouping of each data group, as shown in Figure 5.11. PC1 and PC2 score plots of negative SIMS data indicated clustering of sample data into four distinct groups (cluster A, cluster B, cluster C and cluster D; indicated by circles);

however, a greater overlap between different samples was observed in cluster A and cluster B thus suggesting spectral similarities between various sample in terms of protein adsorption, as shown in Figure 5.11. The samples within each cluster are specified in Table 5.6.

PCA score plots of negative SIMS data, of samples separated in terms of fibre diameter; (small Ø, 280-318 nm; large Ø 521-660 nm) further demonstrated spectral similarities between several samples. In Figure 5.12, PCA score plots of smaller fibre diameter samples revealed overlapping and clustering of various samples in cluster A and cluster B. Larger fibre diameter samples revealed no spectral similarities, as shown in Figure 5.13. This suggests that smaller fibre diameters support a greater overlapping and clustering samples within smaller fibre diameter samples in comparison to larger fibre diameter samples. The samples identified within each cluster for Figure 5.12 are stated in Table 5.6.
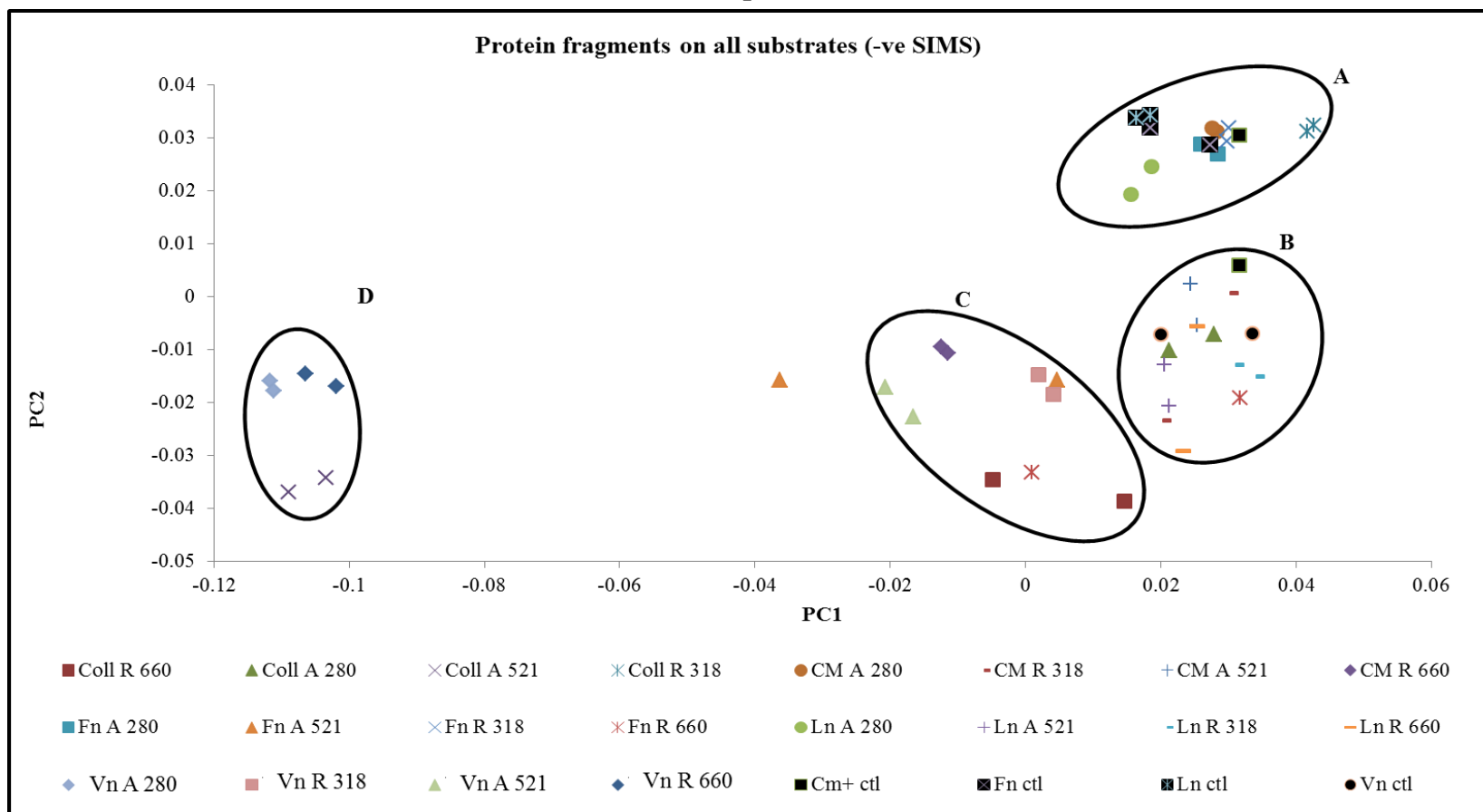
Figure 5.11 Scores plot on the first two multivariate axes from PCA of the Tof-SIMS spectra (negative ion data) of proteins adsorbed onto all electrospun nanofibrous substrates and control (blank glass coverslip). Circles indicating clustering of sample data with respect to PC1 and PC2.

Chapter 5
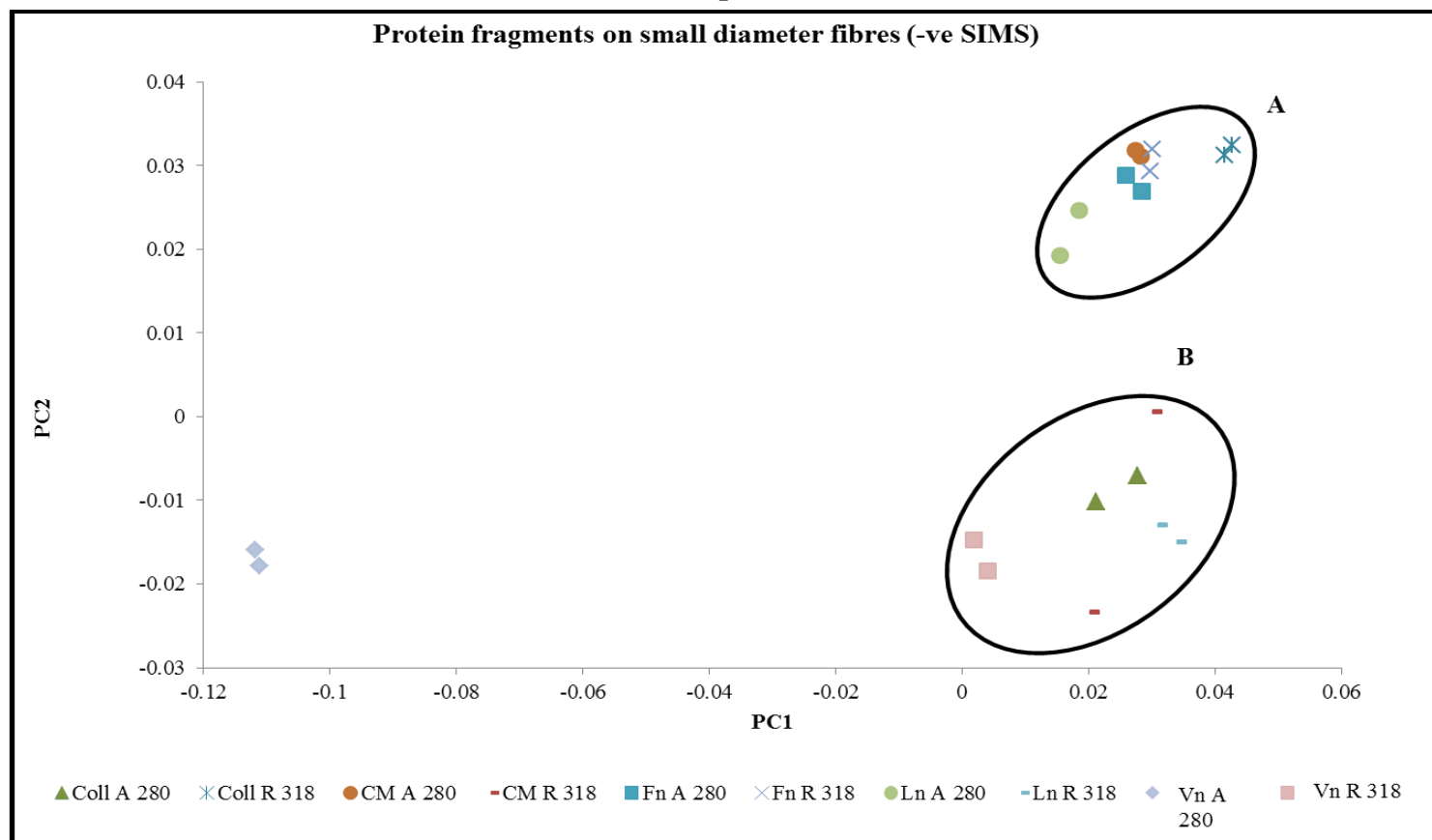
Figure 5.12 Scores plot on the first two multivariate axes from PCA of the Tof-SIMS spectra (negative ions data) of proteins adsorbed onto PCL nanofibrous substrates of smaller diameter (280 – 318 nm) and control (blank glass coverslip). Circles indicating clustering of sample data with respect to PC1 and PC2.
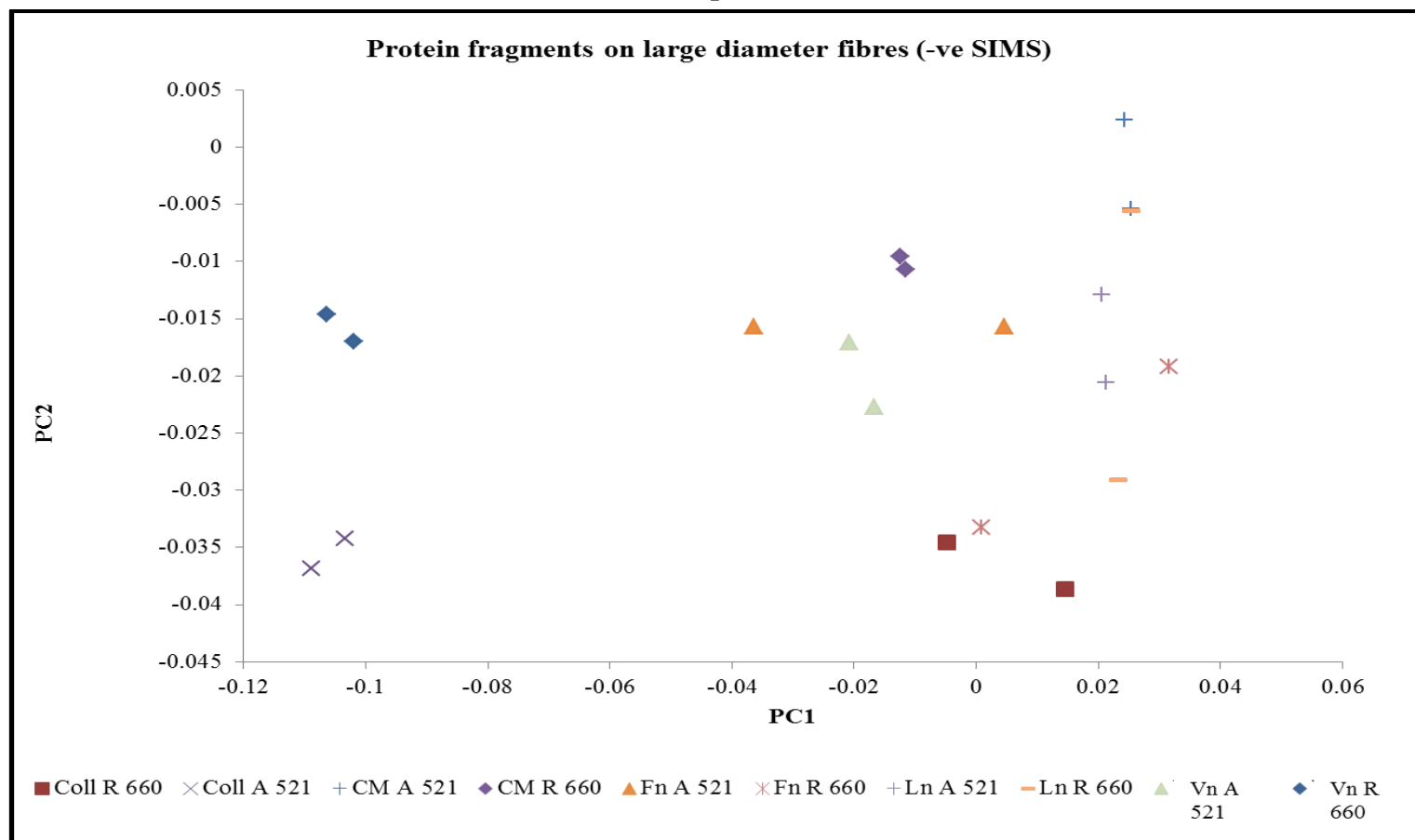
Figure 5.13 Scores plot on the first two multivariate axes from PCA of the Tof-SIMS spectra (negative ions data) of proteins adsorbed onto PCL nanofibrous substrates of smaller diameter (280 – 318 nm) and control (blank glass coverslip). Circles indicating clustering of sample data with respect to PC1 and PC2.

Table 5.6 Definition of clusters observed in Figures 5.11-5.13 for protein fragments on all substrates for all negative ion data.

	Cluster	Spectral similarities observed between proteins on various proteins
Figure 5.11	Cluster A	CM CTL, CM-A (280 nm), Coll I-R (318 nm), Fn CTL, Ln, CTL and Ln-A (280 nm)
	Cluster B	CM CTL, CM-A (521 nm), CM-R (318 nm), Coll I-A (280 nm), Fn-R (660 nm), Ln-A (521 nm), Ln-R (318 nm), Ln-R (660 nm) and Vn CTL
	Cluster C	CM-R (660 nm), Coll I-R (660 nm), Fn-R (660 nm), Vn-A (521 nm), Vn-R (318 nm)
	Cluster D	Coll I-A (521 nm), Vn-A (521 nm) and Vn-R (660 nm).
Figure 5.12	Cluster A	Coll I-R (660 nm), Vn-R (660 nm), Vn-A (521 nm)
	Cluster B	CM-A (521 nm), Fn-R (660 nm), Ln-A (521 nm) and Vn-A (521 nm)

The score plots for PCA provided visualisation of spectral similarities between multivariate data sets; they do not provide detailed information in terms of the original variables such as the Tof-SIMS ion mass peaks and the exact difference in peak intensities between the spectra of different proteins adsorbed onto various substrates. However, the loading plots do provide this information; loading plots for PC1 and PC2 (Figure 5.14) for the negative ion fragments detected on substrates identified the following amino acid fragments to be expressed at a higher normalised intensity: CN^-, SH^-, $C_3H_5^+$, CH_3N_2, C_2H_6NO, C_2H_5S, C_3H_8NO, C_2H_6NS, C_4H_6NO, $C_7H_7^+$, $C_4H_{10}N_3$ and $C_8H_{10}NO$. For each of the negative ion mass peaks identified, normalised intensity values were tabulated and categorised in terms of the media/pure protein solutions in which they were detected (negative ion mass tables; Table A6-A10, in Appendix). Furthermore, these values enabled the identification of the samples on which normalised intensity peaks were the highest in terms of media/protein type, substrate (glass, PCL-A, PCL-R) and fibre diameter (small Ø 280-318 nm; large Ø 521-660 nm). This information is summarised in Table 5.7.
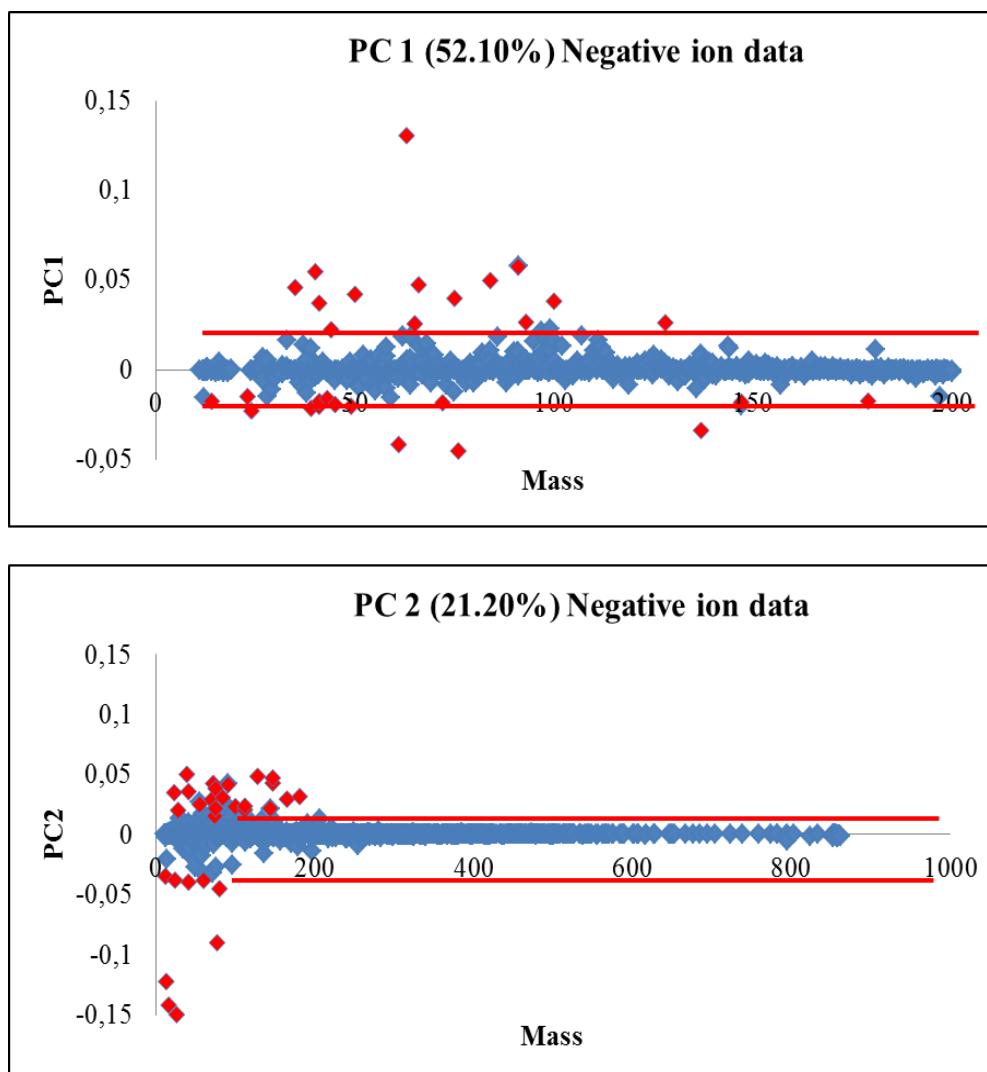
Figure 5.14 Loading plots for PC1 and PC2 from PCA of negative ions spectra of proteins adsorbed from CM and pure protein solutions (Coll I, Fn, Ln, and Vn) onto glass (control), PCL-A and PCL-R substrates of both small (Ø 280-318 nm) and large (Ø 521-660 nm) fibre diameter. Red line indicates the threshold set above which mass peaks are considered to be expressed at high intensity (indicated in red). Thresholds for PC1 (positive, 0.0265; negative, -0.0335) and PC2 (positive, 0.0294; negative, -0.0451) were set at these values due to an obvious difference (plots) in PC values from the baseline when display on the loading plots.

Chapter 5

Table 5.7 Negative ion amino acid fragments identified from loading plots for PC1 and PC2 from PCA and the samples on which detected at the highest normalised intensity. [Canavan *et al.*, 2006; Mahlstedt *et al.*, 2010; Wagner and Castner, 2001; Wagner *et al.*, 2002]

m/z (-ve ions)	Assignment	Proteins and Substrates on which greatest normalised intensity observed
25.0094	CN^-; peptide backbone	Coll I-A (521 nm), Fn-A (521 nm), Vn-A (280 nm), Vn-R (660 nm)
34.9712	SH^-; Cysteine	Coll I CTL (glass), Coll-A (280 nm), Fn CTL (glass), Ln CTL (glass), Ln-R (660 nm)
41.0453	$C_3H_5^+$	Coll I-R (660 nm), Fn-A (521 nm), Vn-A (280 nm), Vn-R (660 nm)
43.0017	CH_3N_2: Arginine (Kaivosoja et al., 2012)	Coll I-A (521 nm), Vn-A (280 nm), Vn-R (660 nm), Vn CTL (glass)
59.9676	C_2H_6NO: L-serine most prevalent in Fn	Coll I-A (521 nm), Vn-A (280 nm), Vn-R (660 nm), Vn CTL (glass)
62.9658	C_2H_5S: Methionine most prevalent in Coll	Coll I-A (521 nm), Vn-A (280 nm), Vn-R (660 nm)
74.9971	C_3H_8NO; Threonine most prevalent in Fn	Ln-A (280 nm), Ln-A (521 nm), Ln-R (318 nm), Ln-R (660 nm)
75.9611	C_2H_6NS; cysteine most prevalent in Fn	Coll I-A (521 nm), Vn-A (280 nm), Vn-R (660 nm)
76.9699	$C_2H_6NS^+$; cysteine	Coll I-A (521 nm), Vn-A (280 nm), Vn-R (660 nm)
83.9729	C_4H_6NO; glutamine	Fn CTL (glass), Ln-A (280), Ln-A (521 nm)
90.9943	C_7H_7; Phenylalanine or Tyrosine	Fn CTL (glass), Fn-A (280 nm), Ln-A (280 nm), Ln-A (521 nm), Ln-R (318 nm), Ln-R (660 nm)
90.9992	C_7H_7; Phenylalanine or Tyrosine	Fn CTL (glass), Fn-A (280 nm), Ln-A (280 nm), Ln-A (521 nm), Ln-R (280 nm)
99.9847	$C_4H_{10}N_3$; arginine	Fn CTL (glass), Fn-A (280 nm), Ln CTL (glass), Ln-A (280 nm), Ln-R (318 nm), Ln-R (660 nm)
127.9609	$C_8H_{10}NO$; arginine	Fn CTL (glass), Ln CTL (glass)
136.9337	$C_8H_{10}NO$; tyrosine	Coll I-A (521 nm), Fn CTL (glass), Ln CTL (glass), Vn-A (280 nm), Vn-R (660 nm)

Of all the negative ion mass peaks detected (stated in Table 5.7), 6 negative ions with the greatest normalised intensity values were selected as: 31.9712 (SH^-; cysteine), 62.9658

(C_2H_5S, methionine), 74.9971 (C_3H_3NO; threonine), 83.9729 (C_4H_6NO; glutamine), 90.9943 (C_7H_7; phenylalanine/tyrosine) and 90.9992 (C_7H_7; phenylalanine/tyrosine). These mass ion fragments were plotted in terms of substrate type in order to distinguish any protein adsorption patterns and specificity in protein adsorption to substrates in terms of fibre orientation and diameter (Figure 5.14). Mass peaks detected at a higher normalised intensity value on each substrate type from pure protein solutions than from conditioned media are stated in Table 5.8. Assessment of the presence of protein ions from individual pure proteins adsorbed onto substrates with high normalised intensities has been performed and fragment patterns of these proteins on various substrates identified. When comparing these patterns to samples where proteins were adsorbed from conditioned media; those peaks (amino acid fragments) at the same m/z suggest having arisen from the single protein with similar pattern of protein adsorption but does not definitely confirm which specific, individual protein the amino acid fragment is derived from (Figure 5.14A and Table 5.5). It was apparent that, Fn and Ln predominantly adsorbed onto glass coverslips, as evidently shown by similarities in spectral patterns for adsorption between Fn and Ln on glass coverslips (Cluster A, Figure 5.11). On PCL-A (280 nm) substrates, Fn and Ln again predominantly adsorbed onto these nanofibres (Figure 5.15B), further supported by similarities in protein adsorption. Interestingly by changing the fibre orientation; on PCL-R (318 nm) substrates, Coll I and Ln were predominantly being adsorbed instead (Figure 5.15C). However, it was observed that by increasing the fibre diameter resulted in a change in patterns of protein adsorption to substrates; both PCL-A (521 nm) and PCL-R (660 nm) predominantly absorbed Ln only, mostly to their surface whereas in the lower fibre diameter substrates (PCL-A, 280 nm; PCL-R, 318 nm), more than protein was being adsorbed.
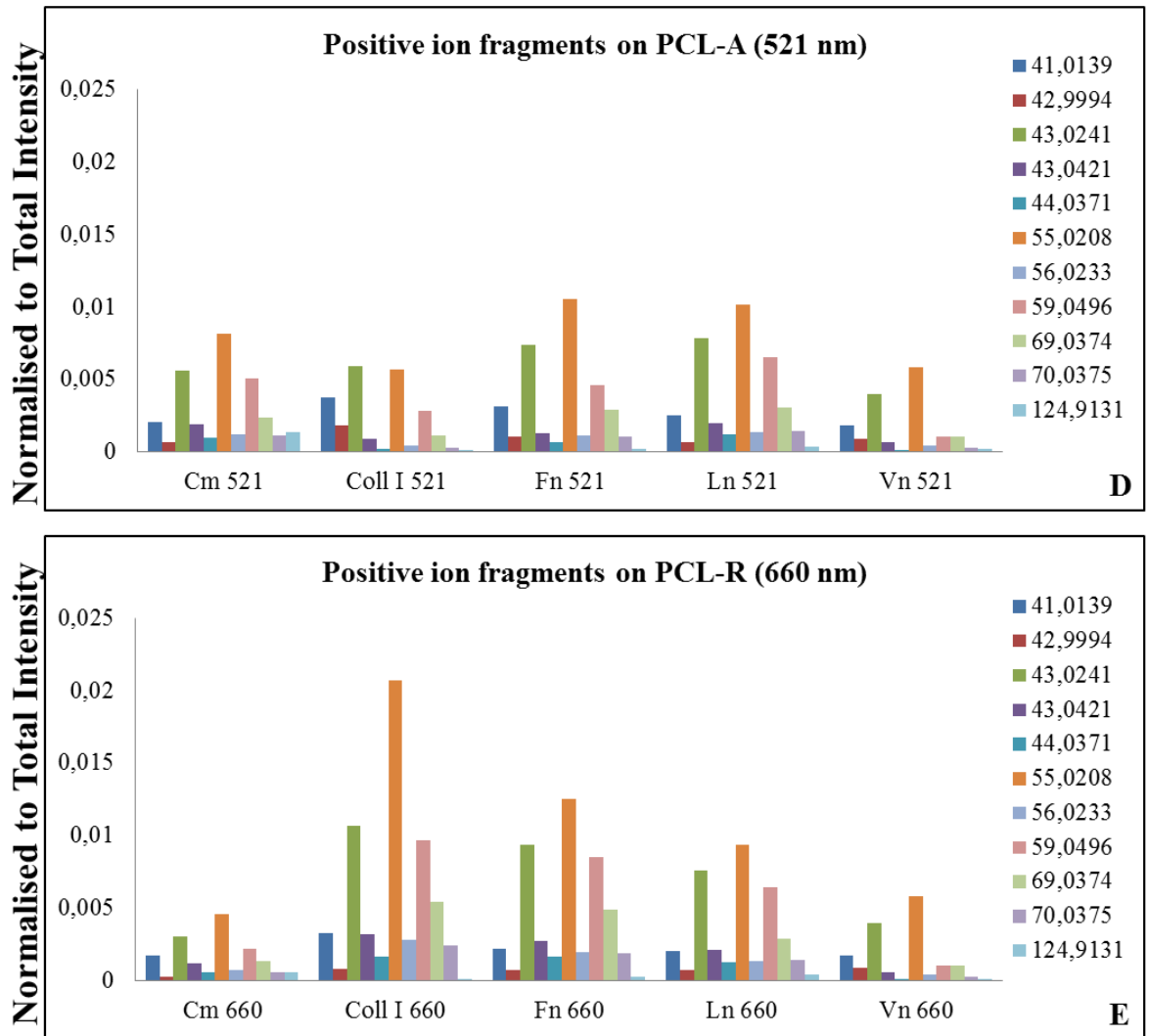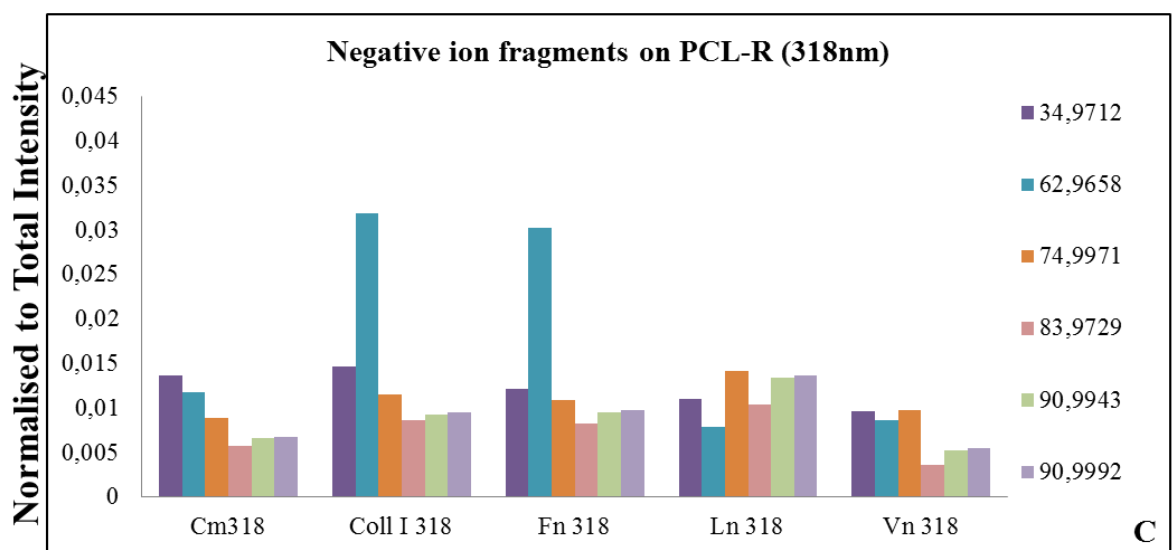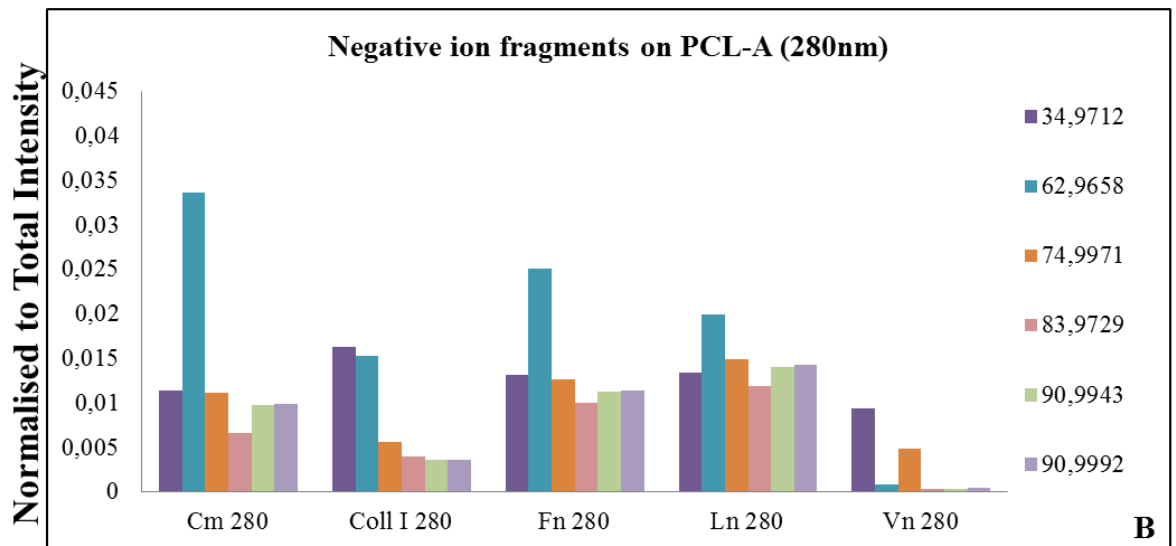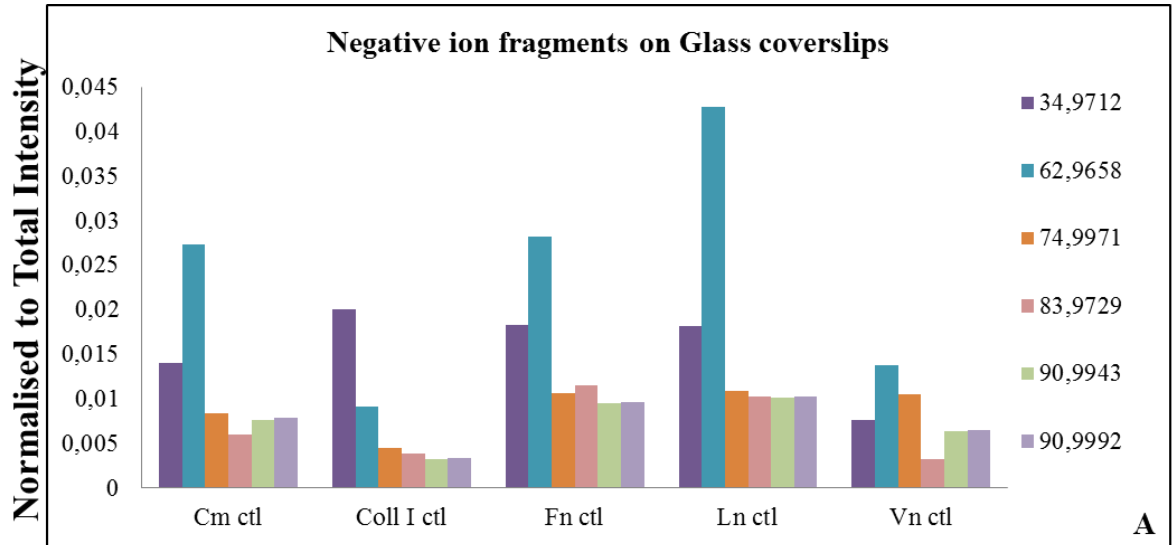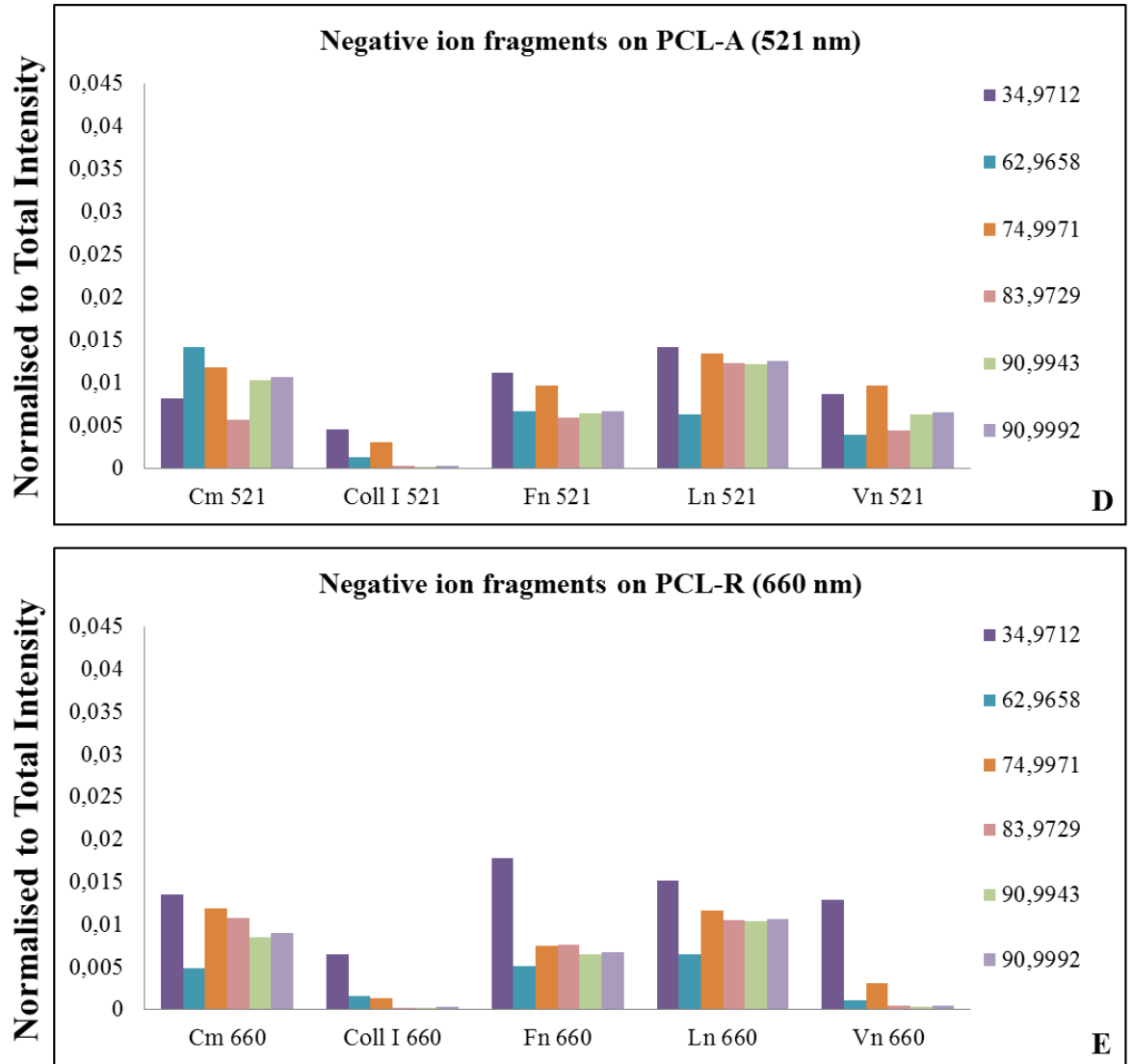
Figure 5.15 Normalised intensity values of negative ion mass peaks of protein fragments from conditioned media (CM) and all pure protein solutions (Coll I, Fn, Ln and Vn) on: (A) controls (glass coverslips), (B) PCL-A (280 nm), (C) PCL-R (318 nm), (D) PCL-A (521 nm) and (E) PCL-R (660 nm).

Chapter 5

Table 5.8 Negative ion mass peaks detected at a higher normalised intensity value on each

substrate type from each pure protein solution relative to conditioned media.

Substrate Type	Pure protein solution	Positive ion fragments detected at a higher normalised intensity from pure protein solutions in comparison to conditioned media
Glass (control)	Coll I	34.9712
	Fn	34.9712, 74.9971, 83.9729, 90.9943 and 90.9992
	Ln	34.9712, 62.9658, 74.9971, 83.9729 and 90.9943
	Vn	74.9971
PCL-A (280 nm)	Coll I	34.9712
	Fn	83.9729 and 90.9943
	Ln	74.9971, 83.9729, 90.9943 and 90.9992
	Vn	Normalised intensity for all mass peaks equivalent to or less than conditioned media
PCL-R (318 nm)	Coll I	62.9658, 74.9971, 83.9729, 90.9943 and 90.9992
	Fn	62.9658 and 90.9992
	Ln	74.9971, 83.9729, 90.9943 and 90.9992
	Vn	Normalised intensity for all mass peaks equivalent to or less than conditioned media
PCL-A (521 nm)	Coll I	Normalised intensity for all mass peaks equivalent to or less than conditioned media
	Fn	34.9712
	Ln	34.9712, 74.9971, 83.9729, 90.9943 and 90.9992
	Vn	Normalised intensity for all mass peaks equivalent to or less than conditioned media
PCL-R (660 nm)	Coll I	Normalised intensity for all mass peaks equivalent to or less than to conditioned media
	Fn	34.9712
	Ln	34.9712, 62.9658, 90.9943 and 90.9992
	Vn	Normalised intensity for all mass peaks equivalent to or less than conditioned media

Chapter 5

5.5 Discussion

Culture and expansion of undifferentiated hESCs *in vitro* is commonly performed using Matrigel™ and MEF-conditioned hESC media. Matrigel™ is a gel comprised of a complex of ECM proteins which provide the optimum composition and concentration required for the expansion of pluripotent hESCs. This protein complex acts as pivotal points which have suitable recognition sites for corresponding cell surface receptors such as integrins that are able to bind to these proteins, triggering a cascade of intracellular responses causing subsequent cell attachment and pluripotent expansion. This activity is further mediated and supported by the secretion of essential ECM proteins, growth factors and cytokines by hESCs themselves, crucial for their proliferation and maintenance of pluripotency. In the previous chapter (chapter 4), it was revealed that crucial hESC integrin receptors differed in their surface expression levels as a result of oxygen environment. Attachment of hESCs to Matrigel^{TM} was reliant on αVβ5, αE and α6 integrins/integrin sub-units in physiological normoxia (2% O_2); suggesting that their corresponding ECM proteins (collagen, fibronectin, laminin and vitronectin) must be present and make up the majority of the protein complex in Matrigel™. Furthermore, a novel, alternative method to culture and expand hESCs using synthetic electrospun nanofibrous substrates has also demonstrated the successful expansion of pluripotent hESCs with retention of differentiation capacity, but in physiological normoxia (2% O_2), only and thus was oxygen dependant. It is well accepted that cell attachment to biomaterial substrates usually occurs after the adsorption of a dynamic interfacial protein layer that is able to adsorb onto a substrate; therefore it can be hypothesised that the protein layer adsorbing onto these nanofibrous substrates must include collagen, fibronectin, laminin and vitronectin thus permitting hESC attachment and expansion. However, several factors can determine the type of protein, quantity, density, conformational state and orientation of the protein on a

substrate such as substrate chemistry and topography. This study investigated protein adsorption onto optimum electrospun nanofibrous substrates (PCL-A and PCL-R) for hESC expansion, from MEF conditioned hESC media and pure protein solutions (Coll I, Fn, Ln and Vn), in order to identify key ECM proteins and in detail, the critical amino acid fragments that may adsorb onto these substrates which mediate the initial attachment of hESCs. These important findings may play a crucial role in the design of novel, smart substrates, specifically tailored to increase the attachment and expansion rates of undifferentiated hESCs and also eliminating the use of xenogenic materials such as Matrigel™, resulting in their potential use for the regenerative medicine industry.

PCL was electrospun to fabricate nanofibres with different fibre diameters (small Ø, 280-318nm; large Ø, 521-660 nm) in both aligned and random conformations. Previously, it was observed that the smaller fibre diameter nanofibrous substrates supported the greatest number of hESC CFU formation and therefore these fibres were used to quantify the amount of protein adsorption to their surface. Quantification of protein adsorption from conditioned media and pure protein solutions (Coll I, Fn, Ln and Vn) onto PCL-A (280 nm), PCL-R (318 nm) and glass (control), in physiological normoxia (2% O_2) was determined using Nano Orange™. It was revealed statistically, that there was significantly increased adsorption of proteins from conditioned media on PCL-A compared to glass ($p<0.05$) and Vn adsorption on PCL-A compared to glass ($p<0.01$). Although, not the case in this study (demonstrated by Nano Orange™), surface topography at the nanoscale increases the surface area to volume ratio resulting in increased protein adsorption in comparison to a flat surface such as a glass coverslip. Decreasing substrate size topography and increasing surface roughness is known to increase protein adsorption ([Rechendorff *et*

al., 2006; Riedel *et al.*, 2001]. Although, it has been demonstrated that surface chemistry can also influence protein adsorption such as enhanced adsorption of albumin to hydrophilic substrates compared to hydrophobic surfaces, it has been reported topography alone can also enhance protein adsorption. For example, bovine serum albumin (BSA; a globular protein in shape) and fibrinogen (Fg; a larger protein with a rod-like shape) adsorbed in greater quantities on smaller particles (with a high surface curvature) [Roach *et al.*, 2006; Scopelliti *et al.*, 2010], also found that nano-scale morphology significantly increased adsorption of proteins BSA and fibrinogen on nanostructured TiO_x films (ranging from 15-30 nm surface morphology).

Protein adsorption ability can be affected by several factors including the characteristics of the protein itself (such as size, shape and conformational stability [Cai *et al.*, 2006]as well as substrate chemistry and topography[Roach, 2005]. Topography at the nano-scale (similar length scale to protein dimensions) can dictate and manipulate the protein shape resulting in orientation and conformational changes leading to changes in secondary structure and ordered state of the proteins [Roach, 2005]. Furthermore, some proteins may have weak internal bonds and hydrophobic interactions and therefore are easy to distort and induce conformational changes. However, others have strong internal bonds and hydrophobic interactions and are more difficult to distort and induce structural/conformational changes. These protein characteristics in combination with topography and surface chemistry determine the ability of a protein to unfold and interact with a substrate in such a way which can consequently affect the active state of the protein and its ability to mediate cell attachment.

Chapter 5

In this chapter, the effect of fibre diameter (small Ø 280-318 nm; large Ø 521-660 nm) of PCL-A and PCL-R nanofibrous substrates was investigated in terms of protein adsorption from MEF-conditioned hESC media and pure protein solutions (Coll I, Fn, Ln and Vn). Score plots from PCA of both positive and negative ion Tof-SIMS data sets revealed that fibre diameter influenced protein adsorption; positive ion data set showed clustering for large diameter fibres (521-660 nm) and even greater clustering and overlapping of various samples on small diameter fibres (Ø 280-318 nm) suggesting spectral similarities between various substrates and conditioned media samples (Table 5.3). Whereas, negative ion data set revealed clustering and overlapping of samples amongst small fibre diameter substrates and no clustering of samples amongst large fibre diameter samples (Table 5.6). Interpretation of Tof-SIMS data revealed that proteins from various pure proteins solutions (Coll I, Fn, Ln and Vn) and conditioned media were able to adsorb to nanofibrous substrates, as demonstrated by spectral similarities in patterns of protein adsorption. To pin point and identify the exact amino acid fragments within those adsorbed proteins on substrates which were being exposed, loading plots were formulated. This further identified the ion intensity of amino acid fragments (positive and negative) on the various substrates and fragmentation patterns of these proteins in comparison to protein adsorption patterns to conditioned media. Also, the key amino acid fragments detected on the substrates were identified.

Loading plots (for positive ion data) revealed a fragmentation pattern of mass peaks for ion fragments to be the following: 41.0139 ($C_3H_5^+$), 42.9994 (CNO^-, peptide backbone), 43.0241 (C_2H_5N), 43.0421 (C_2H_5N), 44.0371 ($C_2H_6N^+$; alanine, lysine or aspargine), 55.0208 ($C_4H_7^+$), 56.0233 ($C_3H_6N^+$), 59.0496 (CH_5N_3; arginine), 69.0374 (C_4H_5O;

threonine), 70.0375 ($C_4H_8N^+$; arginine) and 124.9131 ($C_5H_{11}N_4$; arginine) all had higher intensity peaks on various nanofibrous substrates (of different fibre diameter and orientation) adsorbed from pure protein solutions (Coll I, Fn, Ln and Vn) than proteins adsorbed from conditioned media onto substrates. Similarly, loading plots (for negative ion data) revealed that mass peaks for ion fragments: 31.9712 (SH^-; cysteine), 62.9658 (C_2H_5S, methionine), 74.9971 (C_3H_3NO; threonine), 83.9729 (C_4H_6NO; glutamine), 90.9943 (C_7H_7; phenylalanine/tyrosine) and 90.9992 (C_7H_7; phenylalanine/tyrosine) all had higher intensity peaks on various nanofibrous substrates (of different fibre diameter) adsorbed from pure protein solutions (Coll I, Fn, Ln and Vn) than from proteins adsorbed from conditioned media onto substrates. This suggests that not only are these pure proteins present in conditioned media but infact these identified amino acid fragments are exposed on the substrate which may facilitate hESC attachment by providing recognisable attachment sites. However, limitations of this data are that no control substrates (nanofibrous substrates without any protein/media adsorption) were analysed which could have eliminated CH populations containing ion mass peaks that could be arising from the polymer material itself rather than proteins.

A similar study performed by [Mahlstedt *et al.*, 2010] also identified a significant increase in 14 ions (including m/z 41.0397, 55.0217, 69.0007, 83.061 and 123.0505), using Tof-SIMS, on plasma treated PE-TCPS (oxygen plasma etched tissue culture polystyrene) in comparison to TCPS. Radio frequency plasma etching alone displayed an increase in 14 ions on the substrate in comparison to standard TCPS; molecular species on PE-TCPS, played an important role in the pluripotent expansion of hESCs with consistent proliferation during continuous passage whilst retaining their differentiation capacity

[Mahlstedt *et al.*, 2010]. Five of these molecular species were also identified by the data in this thesis on the nanofibrous substrates which were: 41.0139, 43.0421, 55.0208, 69.0374 and 70.0375.

The data in this chapter has suggested obvious clustering and overlapping of various samples in PCA score plots, in terms of fibre diameter size and proteins adsorbed from pure protein solutions and conditioned media. These highlighted, spectral similarities between various samples, giving an indication of similarities in fragmentation patterns between samples as well as identifying key protein fragments exposed on each substrate type. This protein adsorption behaviour may be a result of a multiple number of reasons. Proteins differ in terms of size and shape. Protein adsorption can increase with an increase in surface area by increasing surface curvature/roughness (when normalised to surface area). In this case, surface roughness was introduced by nanofibrous features (changing fibre diameter also) in comparison to a flat glass coverslip. Furthermore, proteins are flexible chains that have been coiled, folded and bent to form a particular conformation; however, this can be modified upon interaction with a substrate. Substrate chemistry (is the same, as PCL was used for all nanofibrous substrates) and topography can influence the way a protein unfolds onto a substrate and effects its orientation Furthermore, PCL is a hydrophobic material; hydrophobic materials bind more proteins as they are more energetically favourable and also bind them tightly by causing greater distortion of the protein in order to maximise surface interactions [Roach *et al.*, 2005; Roach *et al.*, 2006]; this is further maximised with increasing surface area (decreasing fibre diameter). Hence, it can be hypothesised that each protein has individual characteristics and thus interacts differently with substrates (in terms of fibre diameter) as a result of orientation and unfolding which reveals different amino acid fragments due to difference in

conformational changes. On smaller fibre diameters, positive ion data revealed amino acid fragmentation patterns being similar to a range of proteins (Coll I, Fn, Ln and Vn), whereas negative ion data indicated fragmentation patterns similar to Fn and Ln but not from Vn. On larger fibre diameter substrates, positive ion data revealed amino acid fragmentation patterns predominantly similar to Fn and Ln and this was also witnessed in negative ion data. Difference in the orientation of PCL nanofibres (aligned and random) demonstrated to show a difference in colony forming unit number, where PCL-A substrates provided a greater number of CFUs relative to PCL-R. Cell attachment occurs after the adsorption of proteins to biomaterials, which then provides recognisable attachment sites for hESC attachment. Nano Orange™ demonstrated significant increase in conditioned media and Vn adsorption to PCL-A nanofibrous substrates in comparison to glass coverslips (control); however, score plots of PCA, of aligned and random substrates separately, demonstrated no real clustering between samples of proteins adsorbed from pure protein solutions and conditioned media, with no spectral similarities. This suggests that generally topography at the nano-scale enhances protein adsorption but the conformation of the fibres i.e. aligned or random, causes no difference in protein adsorption or the intensity of key amino acid fragments presented on the substrates for hESC attachment. However, the difference in hESC CFU formation between aligned and random nanofibrous substrates may be a result of, changes in the orientation of the protein and the way the proteins adsorb onto the substrates (aligned or random), which could encourage the unfolding of proteins and conformational changes on aligned nanofibrous substrates in such a way, which is favourable and better for hESC attachment in comparison to random fibre orientation. Therefore, it may be that the aligned nanofibrous substrates cause a specific change in the secondary structure of certain proteins which either exposes a certain amino acid fragment which hESCs prefer on a multiple number of proteins, or that the specific amino acid

fragments are arising from a specific protein which could be Vn (suggested by Nano Orange™ due to the greatest abundance of Vn witnessed on aligned nanofibres). However, this would have to be confirmed by further experimental investigations such as infrared spectroscopy for an in depth view of the secondary structure of adsorbed proteins. It can also be hypothesised that there may be a threshold in the quantity of each of the proteins adsorbed onto the nanofibrous substrates and that, as shown by Nano Orange™, the increased adsorption (substrate concentration) of Vn on aligned nanofibrous substratres causes a greater number of specific amino acid fragments to be exposed, which are essentially relevant for mediating hESC attachment and proliferation.

The use of Tof-SIMS has allowed the investigation of protein adsorption from pure protein solutions and conditioned media to electrospun nanofibrous substrates. Specifically, score plots of PCA (positive and negative ion data) demonstrated spectral similarities between adsorption of proteins from pure protein solutions to nanofibrous substrates and proteins adsorbing from conditioned media onto nanofibrous substrates thus confirming the presence on Coll I, Fn, Ln and Vn in conditioned media. Furthermore, smaller diameter fibres (280-318 nm) displayed a closer clustering and overlapping of numerous samples in comparison to larger fibre diameter substrates (521-660 nm). Loading plots identified the exact ion mass fragments where differences were observed in terms of peak intensity which not only confirmed their existence in conditioned media but also stated the fact that these may be critical mediators involved in hESC attachment and proliferation. However, Nano Orange™ suggested that only a significant increase in adsorption of Vn and conditioned media on PCL-A compared to glass coverslip controls. Coll I, Fn, Ln and Vn all share various similarities in their primary structure and thus the exact origin of the

Chapter 5

identified key amino acid fragment mediators is still unknown. Future work would include investigating the secondary structure of the proteins adsorbed onto the nanofibrous substrates in order to confirm the exact protein from which it has originated and also to determine its conformational state and orientation.

The overall findings in this chapter have demonstrated the successful conditioning of electrospun nanofibrous substrates by conditioned media which supports the adsorption of critical proteins and the exposure of key amino acid fragments as well as the effect of fibre diameter on fragmentation patterns which all influence and mediate the attachment of hESCs. Furthermore, fibre diameter also influenced adsorption of proteins from conditioned media and pure protein solutions. The discovery of critical amino acid fragments detected on the nanofibrous substrates provides exciting opportunities for the design and tailoring of novel substrates to enhance the characteristics of synthetic substrates such as nanofibres for hESC culture.

<div align="center">Chapter 5</div>

5.6 Conclusion

Electrospun PCL nanofibrous substrates (aligned and random) have successfully supported undifferentiated hESC CFU expansion, in 2% O_2. This is mediated by conditioning of nanofibre substrates by proteins present in conditioned media which adsorb from conditioning media. Nano Orange™ quantified the adsorption of proteins from pure protein solutions (Coll I, Fn, Ln and Vn) and total protein from MEF-conditioned hESC media; a significant increase in conditioned media and Vn was apparent on PCL-A substrates in comparison to glass coverslips (control). Identification of the characteristics of the nanofibrous substrates was performed using Tof-SIMS. Score plots of PCA (positive and negative ion data), revealed clustering and thus spectral similarities between various nanofibrous substrates to conditioned media samples confirming the presence of the pure proteins (Coll I, Fn, Ln and Vn) in MEF-conditioned hESC media. Furthermore, a difference in protein adsorption was also detected with varying fibre diameter, where smaller fibre diameter substrates (280-318 nm) demonstrated a closer clustering of various samples in comparison to larger fibre diameter substrates (521-660 nm). Loading plots (PC1 and PC2) identified the exact ion mass peaks which had a higher normalised intensity peak than conditioned media, on various substrates. These ion mass fragments appear to be the key mediators for hESC attachment and many of them suggested have adsorbing from either a predominant protein or from a range of proteins adsorbing onto substrates, which was also different depending on fibre diameter. Identification of characteristics of nanofibrous substrates provides the opportunity to further modify and enhance electrospun nanofibrous substrate biocompatibility to increase hESC attachment, increase proliferation, maintain pluripotency, and retain differentiation capacity which would drive the use of hESCs towards stem cell therapies and regenerative medicine.

Chapter 6

6 General Discussion, Future Work and Conclusions

6.1 Discussion

Limitations associated with current techniques used to culture and expand hESCs *in vitro* have encouraged research towards alternative substrates and techniques. In this thesis, a novel substrate in the form of electrospun nanofibrous substrates has been developed and investigated for the appropriate use in hESC expansion. This substrate provides the opportunity to elimination the use of Matrigel™ and feeder layers which have limitations including direct xenogenic exposure to hESCs, poor attachment resulting in low expansion rates and scale-up issues, difficulty in controlling and maintaining hESC behaviour and finally a substrate which only limits expansion to a 2D *in vitro* environment and resulting in difficulty to transport and translate towards a clinical setting. Furthermore, this thesis is the first to report the use of purely synthetic FDA approved polymers to expand undifferentiated hESCs without the use of natural polymers and the co-culture of feeder layers, whilst also investigating the synergistic effects of oxygen and nanofibre technology.

Various polymers (PCL, PLGA and PLLA) were investigated in both aligned and random nanofibre conformations; the optimal performance was witnessed by PCL-aligned substrates. Furthermore, it was apparent that the synergistic effect of oxygen environment and nanofibre technology had dictated the expansion of hESCs. It was revealed that hESCs cultured under hyperoxic conditions (21% O_2), were unable to adhere to substrates resulting in the formation of EBL features, after 21 days of culture despite using hESC conditioned media. However, in physiological normoxia (2% O_2) hESCs cultured on electrospun nanofibrous substrates (in combination with hESC conditioned media)

demonstrated the ability to attach and expand, to form typical undifferentiated CFUs as would be expected on Matrigel™. Further evaluation revealed that recovered hESCs on nanofibrous substrates maintained pluripotency and their differentiation capacity when cultured under 2% O_2. Furthermore, it is reported in literature that physiological normoxic conditions enhance clonogenicity, decrease *in vitro* spontaneous differentiation and maintain greater pluripotency of hESCs on Matrigel™ in comparison to hESCs cultured in 21% O_2 [Forsyth *et al.*, 2006; Westfall *et al.*, 2008]. This is a result of mimicking the *in vivo* oxygen environment of hESCs to which they are exposed. Furthermore, this thesis revealed increased clonogenicity with decreasing fibre diameter of nanofibrous substrates (fabricated from PCL; aligned and random) in combination with physiological normoxic culture conditions. This lies in agreement with a previous study where HUVECs also demonstrated the same observations [Keun Kwon, 2005]}. The general dogma is that fibre diameters below 500 nm promote cell adhesion and encourage greater cell attachment due to mimicking the similar nano-scale features and topography of native ECM [Ma *et al.*, 2008; Ravichandran *et al.*, 2009]. Hence, by mimicking a combination of both the nano-scale ECM architecture and the oxygen environment this may further create an environment which resembles the *in vivo* hESC conditions as accurately as possible dictating their natural behaviour and function *in vitro*.

Discovering the change in hESC activity on nanofibrous substrates by altering the oxygen environment (2% O_2 and 21% O_2), encouraged investigations into the integrin expression patterns of hESCs (Matrigel™) cultured in 2% or 21% O_2 environments. These findings contributed to understand and identify the mechanisms of action and critical interactions associated with hESCs, which are yet to be fully elucidated. Microarrays have previously

been used to investigate changes in pluripotent and differentiation markers within various hESC lines [Cai *et al.*, 2006; Lee *et al.*, 2010] as well as the alterations in integrin expression for hMSCs as a result of changing the oxygen environment when cultured on various substrates (polystyrene, collagen I, fibronectin and laminin) [Saller *et al.*, 2012]. In this thesis, analysis of microarray data revealed for the first time that integrin expression levels and patterns changed in hESCs as a result in the change of oxygen environment. It was found that β3 binding protein, β1 binding protein 1, β4 binding protein, α5, α6, α8, α9, αD, αE, αV, β1 and β5 were significantly up regulated in hESCs cultured in 2% O_2 in comparison to 21% O_2. Furthermore, many of these subunits corresponded to the integrins which have been previously identified in literature to be expressed by hESCs for corresponding ECM proteins; laminin (α6β1), vitronectin (αVβ5) and fibronectin (αVβ1, α5β1), collagen and laminin (α2β1), nidogen, laminin, collagen I and fibronectin (α3β1), collagen (α11β1) [Braam *et al.*, 2008; Lee *et al.*, 2010; Miyazaki *et al.*, 2008]. Therefore we selected the following integrins/sub-units to investigate the initial attachment of hESCs to Matrigel™ when cultured under 2% or 21% O_2: αVβ5, αV, β5, αE, α6 and CD44 (CD44, a receptor for HA, which is secreted by MEFs in hESC media).

Receptor blocking of these integrin sub-units revealed that inhibition of αE receptor significantly reduced hESC attachment in both 2% O_2 and 21% O_2 on Matrigel™; whereas inhibition of α6 and αVβ5 receptors significantly reduced hESC attachment in 2% O_2 only. Although it has been previously identified that hESCs rely on αVβ5 and α6 on hESC attachment [Braam *et al.*, 2008; Meng *et al.*, 2010], this thesis was the first to examine attachment in different oxygen environments. In 21% O_2, only blockage of CD44 significantly reduced initial hESC attachment. This provides further validation and

extension of previous reports where blocking of CD44 demonstrated reduction in hESC clonogenicity; also witnessed in 21% O_2 [Bourguignon *et al.*, 2008; Gerecht *et al.*, 2007]. Observations from this thesis and from previous reports collated together strongly suggest that oxygen-signalling has a role in defining substrate adhesion mechanistic choices where a switch from CD44 reliance to αVβ5 and α6 was identified. Oxygen is a bioactive, signalling molecule which can influence various cellular activities including cell attachment, proliferation and related intracellular pathways for controlling stemness [Zachar *et al.*, 2010]. In particular, reduced oxygen concentrations regulate the expression of HIFs and it can be speculated that HIFs may be promoting the expression of α6 and αVβ5 integrins in hESCs during 2% O_2 culture, permitting the attachment of hESCs to Matrigel™.

The interlink between HIFs, integrins and growth factors all appear to have an effect on activation pathways of maintaining pluripotency of hESCs. Interference with substrate adhesion mechanism had an instant role upon the maintenance of pluripotency in hESCs. Antibody blocking αVβ5 (2% O_2) and CD44 (21% O_2), significantly decreased the nuclear localisation of pluripotent markers Oct 3/4, Nanog, Alkaline Phosphatase and SSEA-4. Specifically, in 2% O_2 it was apparent that blocking αVβ5 prevents HIFs to upregulate transcriptional factors (N_KB, AP-1, p53 and c-Myc) resulting in inactivation of intracellular pathways (FGF/Notch signalling) which are known to directly affect expression of pluripotent markers [Armstrong *et al.*, 2006; Eiselleova *et al.*, 2009]. Whereas in 21% O_2, it can be speculated that blocking CD44 caused an interference in FGF-2 signalling resulting in inactivation of MAPK, ERK, PI3/AKT kinase and NF_KB pathways with subsequent effects on pluripotency [Ma *et al.*, 2009; Szablowska-Gadomska *et al.*, 2011]

Chapter 6

Identification of the critical integrin receptor (αVβ5) which was not only significantly up regulated in 2% O$_2$ but also played a vital role in the initial attachment of hESCs to Matrigel™, lead to the hypothesis of its potential role and importance in mediating the attachment of hESCs to electrospun nanofibrous substrates (PCL aligned and random) under 2% O$_2$. It was revealed for the first time that hESCs with blocked αVβ5 receptors decreased their clonogenicity ability on electrospun nanofibrous substrates in comparison to hESCs without blocked αVβ5 receptors. As integrins interact with corresponding ECM proteins which contain peptides such as the RGD sequence, which they are able to bind to; it was important to cross-validate the importance of these identified hESC integrins by evidently proving the existence of these corresponding proteins (collagen I, IV, fibronectin and laminin secreted from MEFs into hESC conditioned media) on electrospun nanofibrous substrates.

Interaction of cells with synthetic substrates is a subsequent result of the initial adsorption of proteins from media to form an interfacial layer on substrates which provide natural recognition sites for corresponding integrins [Ma *et al.*, 2007]. This ultimately dictates the biocompatibility of the substrate. Furthermore, the amount and type of protein adsorbed to substrates can be determined by various factors including polymer chemistry, topography and fibre diameter [Roach, 2005; Stevens and George, 2005]. This thesis was the first to investigate protein adsorption behaviour of individual, important ECM proteins (collagen I, fibronectin, laminin and vitronectin) identified in hESC conditioned media as well as conditioned media as a total protein solution, on electrospun nanofibrous substrates (PCL aligned and random) using Tof-SIMS. Furthermore, the effect of changing fibre diameter

Chapter 6

on protein adsorption was also investigated as earlier; decreasing fibre diameter displayed an increase in hESC CFUs when cultured in 2% O_2.

NanoOrange was able to quantify the adsorption of proteins from pure protein solutions and conditioned media on nanofibrous substrates (PCL aligned and random) and glass coverslips; significant increases in conditioned media and vitronectin were apparent on PCL aligned substrates in comparison to glass coverslips. Tof-SIMS analysis confirmed the adsorption of ECM proteins from conditioned media as well as the existence of collagen I, fibronectin, laminin and vitronectin in conditioned media. PCA score plots of Tof-SIMS data (positive and negative ions) revealed spectral similarities between proteins adsorbed onto substrates from pure protein solutions and conditioned media. Specifically, smaller fibre diameter substrates revealed greater overlapping and clustering of samples and thus greater spectral similarities in comparison to larger fibre diameter samples. Loading plots further revealed fragmentation patterns of adsorbed proteins to substrates from pure protein solutions and conditioned media and contributed to identifying the exact amino acid fragments present on each substrate type and the intensity of expression on each substrate in comparison to conditioned media.

For the first time, the following ion fragments were identified on the nanofibrous substrates from pure protein solutions and conditioned media with the highest intensity values: (*positive ions*) 41.0139 ($C_3H_5^+$), 42.9994 (CNO^-, peptide backbone), 43.0241 (C_2H_5N), 43.0421 (C_2H_5N), 44.0371 ($C_2H_6N^+$; alanine, lysine or aspargine), 55.0208 ($C_4H_7^+$), 56.0233 ($C_3H_6N^+$), 59.0496 (CH_5N_3; arginine), 69.0374 (C_4H_5O; threonine), 70.0375

($C_4H_8N^+$; arginine) and 124.9131 ($C_5H_{11}N_4$; arginine); (*negative ions*) 31.9712 (SH^-; cysteine), 62.9658 (C_2H_5S, methionine), 74.9971 (C_3H_3NO; threonine), 83.9729 (C_4H_6NO; glutamine), 90.9943 (C_7H_7; phenylalanine/tyrosine) and 90.9992 (C_7H_7; phenylalanine/tyrosine). However, the intensity of these ion fragments differed depending on substrate type, in the context of fibre diameter which could be a result of the way in which the protein interacts, unfolds and changes it conformational state causing changes in secondary structure with subsequent exposure of specific amino acid fragments. However, it is yet to be fully elucidated the exact origin of the identified amino acid fragments as all proteins used in this investigation (Coll I, Fn, Ln and vn) share similarities in their primary structure; hence future work would include unveiling the secondary structure and locating the origin of the protein from which it has occurred from as well as the conformational state and orientation of the protein. This would have to be further investigated in detail using infrared spectroscopy.

Nonetheless, the ion fragments detected had all adsorbed from proteins (Coll I, Fn, Ln and Vn) which appear to be present in conditioned media. Furthermore, this confirmed the adsorption of corresponding ECM proteins for critical integrins expressed in hESCs (cultured in 2% O_2) identified, to play a critical role in initial attachment. αVβ5 is the corresponding and preferred integrin receptor for vitronectin; which was confirmed to adsorb to nanofibrous substrates. However, the two individual sub-units αV and β5 including α6 are all also able to adhere to a range of ECM proteins, as many of these proteins (Coll I, Fn, Ln and Vn) share similarities in their primary structure (such as the RGD peptide).

Chapter 6

So why were hESCs able to adhere to electrospun nanofibrous substrates in 2% O_2 and form pluripotent CFUs whereas in 21% O_2 embryoid body like features were formed instead; whilst maintaining all other parameters consistent? It appears that this is a result of integrin expression levels and the availability of critical hESC integrins which are required to be at a specific threshold, relevant for permitting and mediating hESC attachment. In combination to this, the relative concentration and availability of corresponding ion fragments exposed (further determined by how the protein unfolds with conformational changes) and available on a substrate determine the chances of interaction and connection between the integrin and adsorbed ECM protein on the nanofibrous substrates. Therefore, there also maybe a threshold in the quantity of each of the proteins adsorbed onto the nanofibrous substrates relevant for hESC attachment and their maintenance in pluripotency. Furthermore, it appears the relative ratio of ion fragments may also play an important factor in determining the exposure and availability of critical amino acid fragments to corresponding integrins, as it was witnessed that the ratio in the intensity of each of the ion peaks changed depending on the substrate and fibre diameter. This was particularly found on PCL aligned nanofibrous substrates (smaller fibre diameter) where the ratio between certain ion fragments was far less in comparison to larger fibre diameter substrates (PCL aligned or random) and conditioned media. This may therefore expose the critical ion fragments on which are perhaps overpowered by the high expression of fragments which perhaps are not as critical or important in mediating the initial attachment of hESCs. However, further investigations would be required to further narrow down and pin point the exact ion fragments which are crucial for mediating hESC attachment.

Chapter 6

Anyhow, the identification of these ion fragments provides an opportunity to further explore these mass fragments and their importance in hESC attachment in greater detail, as well as tailor and modify the electrospun nanofibrous substrates with these identified ion fragments in order to further enhance and improve the attachment and expansion efficiency of hESCs whilst retaining their pluripotency. However, optimisation of various parameters would be required such as the exact ion fragments; their concentration and whether a combination of ion fragments tailored onto the substrates would enhance attachment, expansion rates as well as hESC stemness.

This thesis has developed and investigated the applicability of a novel application of electrospun nanofibrous substate for the use in the expansion of undifferentiated hESCs. The beauty of this substrate is the elimination of limitations currently associated with the expansion and culture of hESCs *in vitro*. The novel substrate has the potential to replace Matrigel™ and the use of feeder layers which excludes xenogenic contact. This novel substrate is FDA approved and can act as a 3D carrier substrate for the delivery of differentiated hESCs into various tissue specific sites *in vivo* and thus encourages their drive towards a clinical setting without the need to remove the substrate due to its biodegradability, which would be the ultimate purpose. This thesis has set the fundamental foundations for expanding pluripotent hESCs which provides the opportunity to differentiate them towards countless lineages of the three germ layers, which in theory they are able to produce. The key findings of this thesis are summarised in Figure 6.1.

Chapter 6
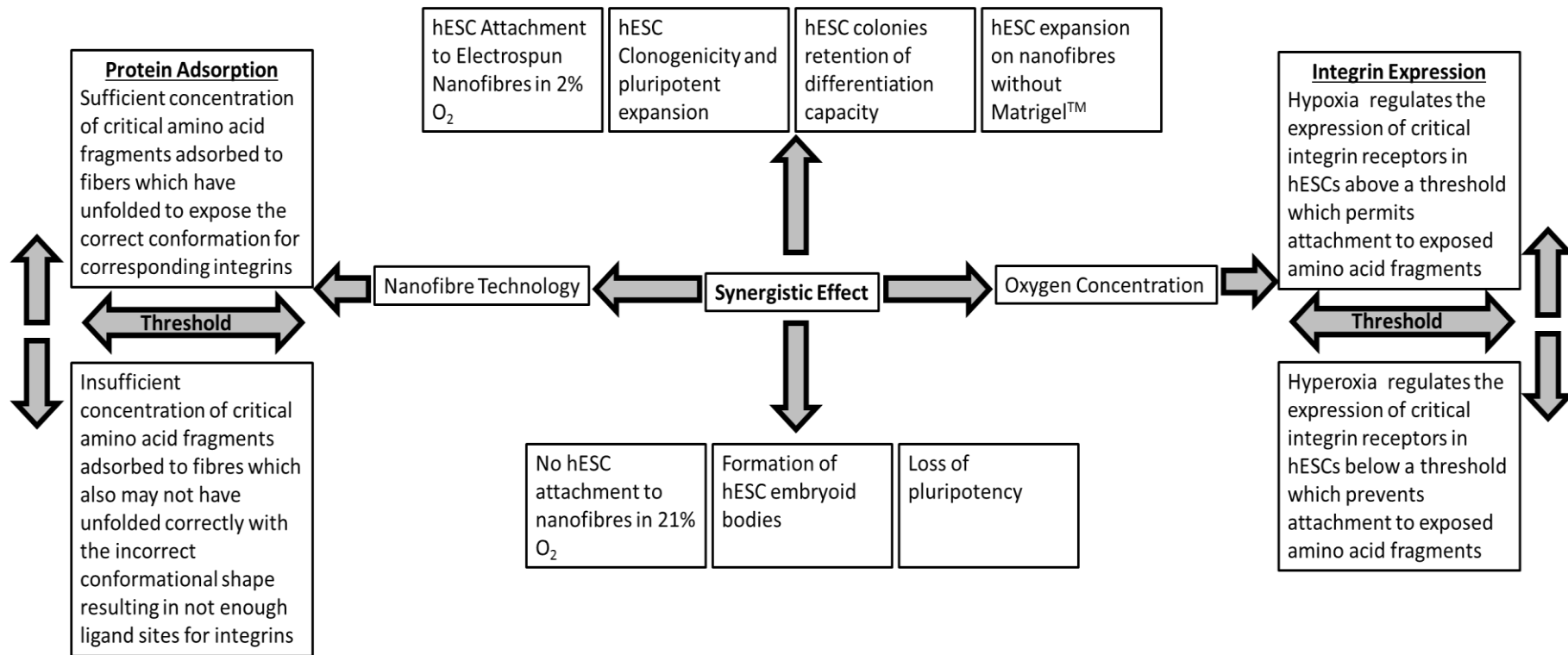
Figure 6.1 An overriding schematic which describes the key, novel findings identified in this thesis, collating together the results from Chapter 3, 4 (Integrin mechanisms) and 5 (Protein adsorption to nanofibrous substrates).

Chapter 6

6.2 Future Work

This thesis has laid down the foundation of a suitable substrate which eliminates the use of Matrigel™ which currently limits the use of hESCs to 2D structures only. Due to poor attachment and expansion rates of hESCs to Matrigel™, this has prevented and hindered the use of hESCs in tissue engineering and regenerative medicine applications to the best of their ability. These electrospun nanofibrous substrates can be further improved by further tailoring and modification with identified amino acid fragments in this thesis. It would be hoped that these improvements would further enhance the biocompatibility of these substrates resulting in improved attachment, expansion rates, enhanced scale-up whilst maintaining their stemness. Additional improvements could also include the incorporation of growth factors into the electrospun nanofibrous substrates, required for specific lineage differentiation which would be released over time as the fibres degraded in order to continually provide the relevant chemical cues to differentiate hESCs.

These substrates provide the opportunity to act as a 3D substrate which then allows the all tissue engineering principles to be applied such as 3D spatial environment, substrate topography, chemical environment and mechanical stimulation. The combinatory effects all these optimised parameters allows the opportunity to mimic and create countless *in vivo* environments encouraging their differentiation into many different cell types of interest of all three germ layers (mesoderm, endoderm and ectoderm). Therefore, future work could include the use of bioreactors to create this multi-environment and attempt to differentiate hESCs towards lineages such as bone, cartilage and tendon tissue. Differentiated hESCs and secreted matrix on substrates then have the potential to be implanted into *in vivo* models to investigate their ability to repair and regenerate tissue-specific defect sites.

6.3 Concluding Remarks

This thesis has shown that electrospun nanofibrous substrates have the potential to function as an appropriate, alternative substrate for the culture and expansion of hESCs *in vitro*, thus potentially eliminating the use of Matrigel™ and xenogenic contaminations. From the investigations reported in this thesis, this was dependant upon the synergistic effect between electrospun nanofibrous substrates and oxygen environment, where hESC CFU expansion with maintenance of pluripotency and retention of differentiation capacity was only possible in 2% O_2. The key issues highlighted here were that oxygen environment changes expression levels of key hESC integrins which mediate attachment to Matrigel™ and influence their pluripotency. Furthermore, it has been demonstrated that corresponding ECM proteins for those crucial hESC integrins adsorb to electrospun nanofibrous substrates and that this adsorption activity can be influenced by fibre diameter resulting in fragmentation patterns; as well as the exposure and intensity of critical ion fragments at significantly higher levels with the appropriate conformation facilitating hESC attachment. Armed with this knowledge this allows further modification and tailoring of the substrates with critical amino acid fragments in order to enhance the biocompatibility of these substrates to ensure maximum hESC attachment and enhance expansion rates whilst maintaining pluripotency.

Chapter 7

7. References

Abeyta MJ, Clark AT, Rodriguez RT, Bodnar MS, Pera RAR and Firpo MT. Unique gene expression signatures of independently-derived human embryonic stem cell lines. Human Molecular Genetics 2004;13(6):601-608.

Agarwal S, Wendorff JH and Greiner A. Use of electrospinning technique for biomedical applications. Polymer 2008;49(26):5603-5621.

Amit M, Carpenter MK, Inokuma MS, Chiu C-P, Harris CP, Waknitz MA, Itskovitz-Eldor J and Thomson JA. Clonally Derived Human Embryonic Stem Cell Lines Maintain Pluripotency and Proliferative Potential for Prolonged Periods of Culture. Developmental Biology 2000;227(2):271-278.

Amit M, Chebath J, Margulets V, Laevsky I, Miropolsky Y, Shariki K, Peri M, Blais I, Slutsky G, Revel M and Itskovitz-Eldor J. Suspension Culture of Undifferentiated Human Embryonic and Induced Pluripotent Stem Cells. Stem Cell Reviews and Reports 2010;6(2):248-259.

Amit M, Margulets V, Segev H, Shariki K, Laevsky I, Coleman R and Itskovitz-Eldor J. Human Feeder Layers for Human Embryonic Stem Cells. Biology of Reproduction 2003;68(6):2150-2156.

Amit M, Shariki C, Margulets V and Itskovitz-Eldor J. Feeder Layer and Serum-Free Culture of Human Embryonic Stem Cells. Biology of Reproduction 2004;70(3):837-845.

Armstrong L, Hughes O, Yung S, Hyslop L, Stewart R, Wappler I, Peters H, Walter T, Stojkovic P, Evans J, Stojkovic M and Lako M. The role of PI3K/AKT, MAPK/ERK and NFkb signalling in the maintenance of human embryonic stem cell pluripotency and viability highlighted by transcriptional profiling and functional analysis. Human Molecular Genetics 2006;15(11):1894-1913.

Ashammakhi N, Wimpenny I, Nikkola L and Yang Y. Electrospinning: methods and development of biodegradable nanofibers for drug release. Journal of Biomedical Nanotechnology 2009;5(1):1-19.

Axelrod HR. Embryonic stem cell lines derived from blastocysts by a simplified technique. Developmental Biology 1984;101(1):225-228.

Azarin SM and Palecek SP. Matrix Revolutions: A Trinity of Defined Substrates for Long-Term Expansion of Human ESCs. Cell Stem Cell 2010;7(1):7-8.

Badami AS, Kreke MR, Thompson MS, Riffle JS and Goldstein AS. Effect of fiber diameter on spreading, proliferation, and differentiation of osteoblastic cells on electrospun poly(lactic acid) substrates. Biomaterials 2006;27(4):596-606.

Bajada S, Mazakova I, Ashton BA, Richardson JB and Ashammakhi N. Stem Cells in Regenerative Medicine. In: Ashammakhi N, Reis R and Chiellini F, editors. Topics in Tissue Engineering. Volume 4; 2008a.

Chapter 7

Bajada S, Mazakova I, Richardson JB and Ashammakhi N. Updates on stem cells and their applications in regenerative medicine. Journal of Tissue Engineering and Regenerative Medicine 2008b;2(4):169-183.

Baksh D, Song L and Tuan RS. Adult mesenchymal stem cells: characterization, differentiation, and application in cell and gene therapy. Journal of Cellular and Molecular Medicine 2004;8(3):301-316.

Barber RD, Harmer DW, Coleman RA and Clark BJ. GAPDH as a housekeeping gene: analysis of GAPDH mRNA expression in a panel of 72 human tissues. Physiol. Genomics 2005;21(3):389-395.

Barnes CP, Sell SA, Boland ED, Simpson DG and Bowlin GL. Nanofiber technology: Designing the next generation of tissue engineering scaffolds. Advanced Drug Delivery Reviews 2007;59(14):1413-1433.

Bauwens C, Yin T, Dang S, Peerani R and Zandstra PW. Development of a perfusion fed bioreactor for embryonic stem cell-derived cardiomyocyte generation: Oxygen-mediated enhancement of cardiomyocyte output. Biotechnology and Bioengineering 2005;90(4):452-461.

Beachley V and Wen X. Effect of electrospinning parameters on the nanofiber diameter and length. Materials Science and Engineering: C 2009;29(3):663-668.

Beltrami AP, Barlucchi L, Torella D, Baker M, Limana F, Chimenti S, Kasahara H, Rota M, Musso E, Urbanek K, Leri A, Kajstura J, Nadal-Ginard B and Anversa P. Adult Cardiac Stem Cells Are Multipotent and Support Myocardial Regeneration. Cell 2003;114(6):763-776.

Benoit DSW, Schwartz MP, Durney AR and Anseth KS. Small functional groups for controlled differentiation of hydrogel-encapsulated human mesenchymal stem cells. Nat Mater 2008;7(10):816-823.

Bianco A, Di Federico E, Moscatelli I, Camaioni A, Armentano I, Campagnolo L, Dottori M, Kenny JM, Siracusa G and Gusmano G. Electrospun poly(e-caprolactone)/Ca-deficient hydroxyapatite nanohybrids: Microstructure, mechanical properties and cell response by murine embryonic stem cells. Materials Science and Engineering: C 2009;29(6):2063-2071.

Bielby RC, Boccaccini AR, Polak JM and Buttery LD. In vitro differentiation and in vivo mineralization of osteogenic cells derived from human embryonic stem cells. Tissue Eng 2004;10(9-10):1518-1525.

Biggs MJP, Richards RG and Dalby MJ. Nanotopographical modification: a regulator of cellular function through focal adhesions. Nanomedicine: Nanotechnology, Biology and Medicine 2010;6(5):619-633.

Chapter 7

Bini TB, Gao S, Wang S and Ramakrishna S. Poly(l-lactide-co-glycolide) biodegradable microfibers and electrospun nanofibers for nerve tissue engineering: an in vitro study J Mater Sci Mater Med 2006;41:6453-6459.

Boland E, Telemeco T, DG S, Wnek G and Bowlin G. Utilizing acid pretreatment and electrospinning to improve biocompatibility of poly(glycolic acid) for tissue engineering. Journal of Biomedical Materials Research Part B: Applied Biomaterials 2004;71B(1):144-152.

Bourguignon LYW, Peyrollier K, Xia W and Gilad E. Hyaluronan-CD44 Interaction Activates Stem Cell Marker Nanog, Stat-3-mediated MDR1 Gene Expression, and Ankyrin-regulated Multidrug Efflux in Breast and Ovarian Tumor Cells. Journal of Biological Chemistry 2008;283(25):17635-17651.

Braam SR, Zeinstra L, Litjens S, Ward-van Oostwaard D, van den Brink S, van Laake L, Lebrin F, Kats P, Hochstenbach R, Passier R, Sonnenberg A and Mummery CL. Recombinant Vitronectin Is a Functionally Defined Substrate That Supports Human Embryonic Stem Cell Self-Renewal via αVβ5 Integrin. STEM CELLS 2008;26(9):2257-2265.

Brafman DA, Chang CW, Fernandez A, Willert K, Varghese S and Chien S. Long-term human pluripotent stem cell self-renewal on synthetic polymer surfaces. Biomaterials 2010;31(34):9135-9144.

Brännvall K, Bergman K, Wallenquist U, Svahn S, Bowden T, Hilborn J and Forsberg-Nilsson K. Enhanced neuronal differentiation in a three-dimensional collagen-hyaluronan matrix. Journal of Neuroscience Research 2007;85(10):2138-2146.

Cai J, Chen J, Liu Y, Miura T, Luo Y, Loring JF, Freed WJ, Rao MS and Zeng X. Assessing Self-Renewal and Differentiation in Human Embryonic Stem Cell Lines. STEM CELLS 2006;24(3):516-530.

Canavan HE, Graham DJ, Cheng X, Ratner BD and Castner DG. Comparison of Native Extracellular Matrix with Adsorbed Protein Films Using Secondary Ion Mass Spectrometry€ Langmuir 2006;23(1):50-56.

Carlberg B, Axell MZ, Nannmark U, Liu J and Kuhn HG. Electrospun polyurethane scaffolds for proliferation and neuronal differentiation of human embryonic stem cells. Biomedical Materials 2009;4(4):7.

Chadwick K, Wang L, Li L, Menendez P, Murdoch B, Rouleau A and Bhatia M. Cytokines and BMP-4 promote hematopoietic differentiation of human embryonic stem cells. Blood 2003;102(3):906-915.

Chan CK, Liao S, Li B, Lareu RR, Larrick JW, Ramakrishna S and Raghunath M. Early adhesive behavior of bone-marrow-derived mesenchymal stem cells on collagen electrospun fibers. Biomedical Materials 2009;4(3):035006.

Chapter 7

Chen HF, Kuo HC, Lin SP, Chien CL, Chiang MS and Ho HN. Hypoxic culture maintains self-renewal and enhances embryoid body formation of human embryonic stem cells. Tissue Eng Part A 2010;16(9):2901-2913.

Choi JS, Lee SJ, Christ GJ, Atala A and Yoo JJ. The influence of electrospun aligned poly(e-caprolactone)/collagen nanofiber meshes on the formation of self-aligned skeletal muscle myotubes. Biomaterials 2008;29(19):2899-2906.

Chong EJ, Phan TT, Lim IJ, Zhang YZ, Bay BH, Ramakrishna S and Lim CT. Evaluation of electrospun PCL/gelatin nanofibrous scaffold for wound healing and layered dermal reconstitution. Acta Biomaterialia 2007;3(3):321-330.

Conley BJ, Young JC, Trounson AO and Mollard R. Derivation, propagation and differentiation of human embryonic stem cells. The International Journal of Biochemistry & Cell Biology 2004;36(4):555-567.

Cooper HM, Tamura RN and Quaranta V. The major laminin receptor of mouse embryonic stem cells is a novel isoform of the alpha 6 beta 1 integrin. The Journal of Cell Biology 1991;115(3):843-850.

Coppolino MG and Dedhar S. Bi-directional signal transduction by integrin receptors. The international journal of biochemistry & cell biology 2000;32(2):171-188.

Csete M. Oxygen in the Cultivation of Stem Cells. Annals of the New York Academy of Sciences 2005;1049(1):1-8.

D'Ippolito G, Diabira S, Howard GA, Menei P, Roos BA and Schiller PC. Marrow-isolated adult multilineage inducible (MIAMI) cells, a unique population of postnatal young and old human cells with extensive expansion and differentiation potential. Journal of Cell Science 2004;117(14):2971-2981.

Danen EHJ, Sonneveld P, Brakebusch C, Fassler R and Sonnenberg A. The fibronectin-binding integrins a5b1 and avb3 differentially modulate RhoA-GTP loading, organization of cell matrix adhesions, and fibronectin fibrillogenesis. The Journal of Cell Biology 2002;159(6):1071-1086.

De Coppi P, Bartsch G, Siddiqui MM, Xu T, Santos CC, Perin L, Mostoslavsky G, Serre AC, Snyder EY, Yoo JJ, Furth ME, Soker S and Atala A. Isolation of amniotic stem cell lines with potential for therapy. Nat Biotech 2007;25(1):100-106.

De Filippis L and Delia D. Hypoxia in the regulation of neural stem cells. Cellular and Molecular Life Sciences 2011;68(17):2831-2844.

Dee KC, Puleo DA and Bizios R. Protein-Surface Interactions. An Introduction To Tissue-Biomaterial Interactions. Hoboken, NJ, USA: John Wiley & Sons, Inc.; 2003. p 37-52.

Derda R, Li L, Orner BP, Lewis RL, Thomson JA and Kiessling LL. Defined Substrates for Human Embryonic Stem Cell Growth Identified from Surface Arrays. ACS Chemical Biology 2007;2(5):347-355.

Chapter 7

Dhandayuthapani B, Yoshida Y, Maekawa T and Kumar DS. Polymeric Scaffolds in Tissue Engineering Application: A Review. International Journal of Polymer Science 2011;2011:1-19.

Doran MR, Frith JE, Prowse ABJ, Fitzpatrick J, Wolvetang EJ, Munro TP, Gray PP and Cooper-White JJ. Defined high protein content surfaces for stem cell culture. Biomaterials 2010;31(19):5137-5142.

Dua HS and Azuara-Blanco A. Limbal Stem Cells of the Corneal Epithelium. Survey of Ophthalmology 2000;44(5):415-425.

Eiselleova L, Matulka K, Kriz V, Kunova M, Schmidtova Z, Neradil J, Tichy B, Dvorakova D, Pospisilova S, Hampl A and Dvorak P. A Complex Role for FGF-2 in Self-Renewal, Survival, and Adhesion of Human Embryonic Stem Cells. STEM CELLS 2009;27(8):1847-1857.

Ellis S and Tanentzapf G. Integrin-mediated adhesion and stem-cell-niche interactions. Cell and Tissue Research 2010;339(1):121-130.

Engler AJ, Sen S, Sweeney HL and Discher DE. Matrix Elasticity Directs Stem Cell Lineage Specification. Cell 2006;126(4):677-689.

Erickson GR, Gimble JM, Franklin DM, Rice HE, Awad H and Guilak F. Chondrogenic Potential of Adipose Tissue-Derived Stromal Cells in Vitro and in Vivo. Biochemical and Biophysical Research Communications 2002;290(2):763-769.

Evans ND, Minelli C, Gentleman E, LaPointe V, Patankar SN, Kallivretaki M, Chen X, Roberts CJ and Stevens MM. Substrate stiffness affects early differentiation events in embryonic stem cells. Eur Cell Mater 2009;18:1-13; discussion 13-14.

Ezashi T, Das P and Roberts RM. Low O2 tensions and the prevention of differentiation of hES cells. Proceedings of the National Academy of Sciences of the United States of America 2005;102(13):4783-4788.

Fadeev AG and Melkoumian Z. Synthetic Surfaces for Human Embryonic Stem Cell Culture: InTech; 2011.

Feng L, Li S, Li H, Zhai J, Song Y, Jiang L and Zhu D. Super-hydrophobic surface of aligned polyacrylonitrile nanofibers. Angewandte Chemie International Edition 2002;41(7):1221-1223.

Finkemeier CG. Bone-grafting and bone-graft substitutes. Journal of Bone and Joint Surgery - Series A 2002;84(3):454-464

Fong H, Chun I and Reneker DH. Beaded nanofibers formed during electrospinning. Polymer 1999;40:4585-4592.

Chapter 7

Forristal CE, Wright KL, Hanley NA, Oreffo ROC and Houghton FD. Hypoxia inducible factors regulate pluripotency and proliferation in human embryonic stem cells cultured at reduced oxygen tensions. Reproduction 2010;139(1):85-97.

Forsyth NR, Kay A, Hampson K, Downing A, Talbot R and McWhir J. Transcriptome alterations due to physiological normoxic (2% O2) culture of human embryonic stem cells. Regenerative Medicine 2008;3(6):817-833.

Forsyth NR and McWhir J. Human embryonic stem cell telomere length impacts directly on clonal progenitor isolation frequency. Rejuvenation Res 2008;11(1):5-17.

Forsyth NR, Musio A, Vezzoni P, Simpson AH, Noble BS and McWhir J. Physiologic oxygen enhances human embryonic stem cell clonal recovery and reduces chromosomal abnormalities. Cloning Stem Cells 2006;8(1):16-23.

Franco SJ, Rodgers MA, Perrin BJ, Han J, Bennin DA, Critchley DR and Huttenlocher A. Calpain-mediated proteolysis of talin regulates adhesion dynamics. Nat Cell Biol 2004;6(10):977-983.

Friedenstein AJ, Chailakhyan RK and Gerasimov UV. Bone marrow osteogenic stem cells: in vitro cultivation and transplantation in diffusion chambers. Cell Proliferation 1987;20(3):263-272.

Furue MK, Na J, Jackson JP, Okamoto T, Jones M, Baker D, Hata R-I, Moore HD, Sato JD and Andrews PW. Heparin promotes the growth of human embryonic stem cells in a defined serum-free medium. Proceedings of the National Academy of Sciences 2008;105(36):13409-13414.

Galbraith CG and Sheetz MP. Forces on adhesive contacts affect cell function. Current Opinion in Cell Biology 1998;10(5):566-571.

Galli R, Pagano SF, Gritti A and Vescovi AL. Regulation of Neuronal Differentiation in Human CNS Stem Cell Progeny by Leukemia Inhibitory Factor. Developmental Neuroscience 2000;22(1-2):86-95.

Gao SY, Lees JG, Wong JCY, Croll TI, George P, Cooper-White JJ and Tuch BE. Modeling the adhesion of human embryonic stem cells to poly(lactic-co-glycolic acid) surfaces in a 3D environment. Journal of Biomedical Materials Research Part A 2010;92A(2):683-692.

Gauthaman K, Venugopal JR, Yee FC, Peh GSL, Ramakrishna S and Bongso A. Nanofibrous substrates support colony formation and maintain stemness of human embryonic stem cells. Journal of Cellular and Molecular Medicine 2009;13(9B):3475-3484.

Gearhart JD and Mintz B. Contact-mediated myogenesis and increased acetylcholinesterase activity in primary cultures of mouse teratocarcinoma cells. Proceedings of the National Academy of Sciences 1974; 71: 1734-1738.

Chapter 7

Gerecht S, Burdick JA, Ferreira LS, Townsend SA, Langer R and Vunjak-Novakovic G. Hyaluronic acid hydrogel for controlled self-renewal and differentiation of human embryonic stem cells. Proceedings of the National Academy of Sciences 2007;104(27):11298-11303.

Godier AFG, Marolt D, Gerecht S, Tajnsek U, Martens TP and Vunjak-Novakovic G. Engineered microenvironments for human stem cells. Birth Defects Research Part C: Embryo Today: Reviews 2008;84(4):335-347.

Goldmann WH. Kinetic Determination of Focal Adhesion Protein Formation. Biochemical and Biophysical Research Communications 2000;271(2):553-557.

Grayson WL, Zhao F, Izadpanah R, Bunnell B and Ma T. Effects of hypoxia on human mesenchymal stem cell expansion and plasticity in 3D constructs. Journal of Cellular Physiology 2006;207(2):331-339.

Greiner A and Wendorff JH. Electrospinning: A Fascinating Method for the Preparation of Ultrathin Fibers. Angewandte Chemie International Edition 2007;46(30):5670-5703.

Griffith LG and Swartz MA. Capturing complex 3D tissue physiology in vitro. Nat Rev Mol Cell Biol 2006;7(3):211-224.

Gunatillake PA and Adhikari R. Biodegradable synthetic polymers for tissue engineering. Eur Cell Mater 2003;5:1-16; discussion 16.

Halvorsen YD, Franklin D, Bond AL, Hitt DC, Auchter C, Boskey AL, Paschalis EP, Wilkison WO and Gimble JM. Extracellular matrix mineralization and osteoblast gene expression by human adipose tissue-derived stromal cells. Tissue Eng 2001;7(6):729-741.

Hashemi SM, Soleimani M, Zargarian SS, Haddadi-Asl V, Ahmadbeigi N, Soudi S, Gheisari Y, Hajarizadeh A and Mohammadi Y. In vitro Differentiation of Human Cord Blood-Derived Unrestricted Somatic Stem Cells into Hepatocyte-Like Cells on Poly(e-Caprolactone) Nanofiber Scaffolds. Cells Tissues Organs 2009;190(3):135-149.

Hewitt Z, Forsyth NR, Waterfall M, Wojtacha D, Thomson AJ and McWhir J. Fluorescence-activated single cell sorting of human embryonic stem cells. Cloning Stem Cells 2006;8(3):225-234.

Higuchi O, Okabe M, Yoshida T, Fathy M, Saito S, Miyawaki T and Nikaido T. Stemness of Human Wharton's Jelly Mesenchymal Cells Is Maintained by Floating Cultivation. Cell Reprogram 2012:In press.

Horbett TA, Schway MB and Ratner BD. Hydrophilic-hydrophobic copolymers as cell substrates: Effect on 3T3 cell growth rates. Journal of Colloid and Interface Science 1985;104(1):28-39.

Horwitz A, Duggan K, Buck C, Beckerle MC and Burridge K. Interaction of plasma membrane fibronectin receptor with talin - a transmembrane linkage. Nature 1986;320(6062):531-533.

Chapter 7

Howard D, Buttery LD, Shakesheff KM and Roberts SJ. Tissue engineering: strategies, stem cells and scaffolds. Journal of Anatomy 2008;213(1):66-72.

Howell JC and Yoder MC. Adult Stem Cell Plasticity Defined. NeoReviews 2003;4(7):e181-e186.

Humphries JD, Byron A and Humphries MJ. Integrin ligands at a glance. Journal of Cell Science 2006;119(19):3901-3903.

Hynes RO. Integrins: Bidirectional, Allosteric Signaling Machines. Cell 2002;110(6):673-687.

Irwin EF, Gupta R, Dashti DC and Healy KE. Engineered polymer-media interfaces for the long-term self-renewal of human embryonic stem cells. Biomaterials 2011;32(29):6912-6919.

Ivanović, Bartolozzi, Bernabei, Cipolleschi, Rovida, Milenković, Praloran and Sbarba. Incubation of murine bone marrow cells in hypoxia ensures the maintenance of marrow-repopulating ability together with the expansion of committed progenitors. British Journal of Haematology 2000;108(2):424-429.

Jacobson L, Kahan B, Djamali A, Thomson J and Odorico JS. Differentiation of endoderm derivatives, pancreas and intestine, from rhesus embryonic stem cells. Transplantation Proceedings 2001;33(1â€"2):674.

Jaiswal N, Haynesworth SE, Caplan AI and Bruder SP. Osteogenic differentiation of purified, culture-expanded human mesenchymal stem cells in vitro. Journal of Cellular Biochemistry 1997;64(2):295-312.

Jiang Y, Jahagirdar BN, Reinhardt RL, Schwartz RE, Keene CD, Ortiz-Gonzalez XR, Reyes M, Lenvik T, Lund T, Blackstad M, Du J, Aldrich S, Lisberg A, Low WC, Largaespada DA and Verfaillie C. Pluripotency of mesenchymal stem cells derived from adult marrow. 2002

Jin H-J, Chen J, Karageorgiou V, Altman GH and Kaplan DL. Human bone marrow stromal cell responses on electrospun silk fibroin mats. Biomaterials 2004;25(6):1039-1047.

Jones LJ, Haugland RP and Singer VL. Development and characterization of the NanoOrange protein quantitation assay: a fluorescence-based assay of proteins in solution. Biotechniques 2003;34(4):850-854, 856, 858 passim.

Jones MB, Chu CH, Pendleton JC, Betenbaugh MJ, Shiloach J, Baljinnyam B, Rubin JS and Shamblott MJ. Proliferation and pluripotency of human embryonic stem cells maintained on type I collagen. Stem Cells Dev 2010;19(12):1923-1935.

Kang X, Xie Y, Powell HM, James Lee L, Belury MA, Lannutti JJ and Kniss DA. Adipogenesis of murine embryonic stem cells in a three-dimensional culture system using electrospun polymer scaffolds. Biomaterials 2007;28(3):450-458.

Chapter 7

Karner E, Unger C, Sloan AJ, Ahrlund-Richter L, Sugars RV and Wendel M. Bone matrix formation in osteogenic cultures derived from human embryonic stem cells in vitro. Stem Cells Dev 2007;16(1):39-52.

Kasemo B. Biological surface science. Current Opinion in Solid State & Materials Science 1998;3(5):451-459.

Kasemo B. Biological surface science. Surface Science 2002;500(1-3):656-677.

Keun Kwon I, Kidoaki S and Matsuda T. Electrospun nano- to microfiber fabrics made of biodegradable copolyesters: structural characteristics, mechanical properties and cell adhesion potential. Biomaterials 2005;26(18):3929-3939.

Khademhosseini A, Ling Y, Karp JM and Langer R. Micro- and Nanoscale Control of Cellular Environment for Tissue Engineering. Nanobiotechnology II: Wiley-VCH Verlag GmbH & Co. KGaA; 2007. p 347-364.

Kim S, Ahn SE, Lee JH, Lim D-S, Kim K-S, Chung H-M and Lee S-H. A Novel Culture Technique for Human Embryonic Stem Cells Using Porous Membranes. STEM CELLS 2007;25(10):2601-2609.

Koay EJ, Hoben GMB and Athanasiou KA. Tissue Engineering with Chondrogenically Differentiated Human Embryonic Stem Cells. STEM CELLS 2007;25(9):2183-2190.

Kogler G, Radke TF, Lefort Al, Sensken S, Fischer J, Sorg RdV and Wernet P. Cytokine production and hematopoiesis supporting activity of cord blood-derived unrestricted somatic stem cells. Experimental Hematology 2005;33(5):573-583.

Kothapalli R, Yoder S, Mane S and Loughran T. Microarray results: how accurate are they? BMC Bioinformatics 2002;3(1):1-10.

Krampera M, Pizzolo G, Aprili G and Franchini M. Mesenchymal stem cells for bone, cartilage, tendon and skeletal muscle repair. Bone 2006;39(4):678-683.

Kruegel J and Miosge N. Basement membrane components are key players in specialized extracellular matrices. Cellular and Molecular Life Sciences 2010;67(17):2879-2895.

Kumar D, Gittings JP, Turner IG, Bowen CR, Bastida-Hidalgo A and Cartmell SH. Polarization of hydroxyapatite: Influence on osteoblast cell proliferation. Acta Biomaterialia 2010;6(4):1549-1554.

Kweon H, Yoo MK, Park IK, Kim TH, Lee HC, Lee H-S, Oh J-S, Akaike T and Cho C-S. A novel degradable polycaprolactone networks for tissue engineering. Biomaterials 2003;24(5):801-808.

Labat-Robert J. Cell-Matrix interactions, the role of fibronectin and integrins. A survey. Pathologie Biologie 2012;60(1):15-19.

Lakshmipathy U and Verfaillie C. Stem cell plasticity. Blood reviews 2005;19(1):29-38.

Le Clainche C and Carlier M-F. Regulation of Actin Assembly Associated With Protrusion and Adhesion in Cell Migration. Physiological Reviews 2008;88(2):489-513.

Lee C-K, Wang Y-M, Huang L-S and Lin S. Atomic force microscopy: Determination of unbinding force, off rate and energy barrier for protein-ligand interaction. Micron 2007;38(5):446-461.

Lee KH, Kim HY, Khil MS, Ra YM and Lee DR. Characterization of nano-structured poly(Îμ-caprolactone) nonwoven mats via electrospinning. Polymer 2003;44(4):1287-1294.

Lee S, Kim J, Park TJ, Shin Y, Lee SY, Han Y-M, Kang S and Park H-S. The effects of the physical properties of culture substrates on the growth and differentiation of human embryonic stem cells. Biomaterials 2011;32(34):8816-8829.

Lee ST, Yun JI, Jo YS, Mochizuki M, van der Vlies AJ, Kontos S, Ihm JE, Lim JM and Hubbell JA. Engineering integrin signaling for promoting embryonic stem cell self-renewal in a precisely defined niche. Biomaterials 2010;31(6):1219-1226.

Levenberg S, Huang NF, Lavik E, Rogers AB, Itskovitz-Eldor J and Langer R. Differentiation of human embryonic stem cells on three-dimensional polymer scaffolds. Proceedings of the National Academy of Sciences 2003;100(22):12741-12746.

Li HY, Liao CY, Lee KH, Chang HC, Chen YJ, Chao KC, Chang SP, Cheng HY, Chang CM, Chang YL, Hung SC, Sung YJ and Chiou SH. Collagen IV significantly enhances migration and transplantation of embryonic stem cells: involvement of alpha2beta1 integrin-mediated actin remodeling. Cell Transplant 2011;20(6):893-907.

Li J, Bardy Ja, Yap L, Chen A, Victor N, Cool S, Oh S and Birch W. Impact of vitronectin concentration and surface properties on the stable propagation of human embryonic stem cells. Biointerphases 2010;5(3):FA132-FA142.

Li L, Wang S, Jezierski A, Moalim-Nour L, Mohib K, Parks RJ, Francesco Retta S and Wang L. A Unique Interplay Between Rap1 and E-Cadherin in the Endocytic Pathway Regulates Self-Renewal of Human Embryonic Stem Cells. STEM CELLS 2009;28(2):247-257.

Li W-J, Tuli R, Okafor C, Derfoul A, Danielson KG, Hall DJ and Tuan RS. A three-dimensional nanofibrous scaffold for cartilage tissue engineering using human mesenchymal stem cells. Biomaterials 2005;26(6):599-609.

Li WJ, Laurencin CT, Caterson EJ, Tuan RS and Ko FK. Electrospun nanofibrous structure: a novel scaffold for tissue engineering. J Biomed Mater Res 2002;60(4):613-621.

Liao S, Chan CK and Ramakrishna S. Stem cells and biomimetic materials strategies for tissue engineering. Materials Science and Engineering: C 2008;28(8):1189-1202.

Lim SH and Mao H-Q. Electrospun scaffolds for stem cell engineering. Advanced Drug Delivery Reviews 2009;61(12):1084-1096.

Chapter 7

Lin X. Functions of heparan sulfate proteoglycans in cell signaling during development. Development 2004;131(24):6009-6021.

Liu S, Calderwood DA and Ginsberg MH. Integrin cytoplasmic domain-binding proteins. Journal of Cell Science 2000;113(20):3563-3571.

Ludwig TE, Levenstein ME, Jones JM, Berggren WT, Mitchen ER, Frane JL, Crandall LJ, Daigh CA, Conard KR, Piekarczyk MS, Llanas RA and Thomson JA. Derivation of human embryonic stem cells in defined conditions. Nat Biotech 2006;24(2):185-187.

Ma K, Chan CK, Liao S, Hwang WYK, Feng Q and Ramakrishna S. Electrospun nanofiber scaffolds for rapid and rich capture of bone marrow-derived hematopoietic stem cells. Biomaterials 2008;29(13):2096-2103.

Ma PX and Zhang R. Synthetic nano-scale fibrous extracellular matrix. Journal of Biomedical Materials Research Part A 1999;46(1):60-72.

Ma T, Grayson WL, Fröhlich M and Vunjak-Novakovic G. Hypoxia and stem cell-based engineering of mesenchymal tissues. Biotechnology Progress 2009;25(1):32-42.

Ma Z, Mao Z and Gao C. Surface modification and property analysis of biomedical polymers used for tissue engineering. Colloids and Surfaces B: Biointerfaces 2007;60(2):137-157.

Ma ZW. Modification and cytocompatibility of poly-l-lactic acid (PLLA) scaffold for cartilage tissue engineering. Hangzhou: Zhejiang University, China; 2003.

Mackay AM, Beck SC, Murphy JM, Barry FP, Chichester CO and Pittenger MF. Chondrogenic differentiation of cultured human mesenchymal stem cells from marrow. Tissue Eng 1998;4(4):415-428.

Mahlstedt MM, Anderson D, Sharp JS, McGilvray R, Barbadillo Muñoz MD, Buttery LD, Alexander MR, Rose FRAJ and Denning C. Maintenance of pluripotency in human embryonic stem cells cultured on a synthetic substrate in conditioned medium. Biotechnology and Bioengineering 2010;105(1):130-140.

Mallon BS, Park K-Y, Chen KG, Hamilton RS and McKay RDG. Toward xeno-free culture of human embryonic stem cells. The International Journal of Biochemistry & Cell Biology 2006;38(7):1063-1075.

Mano JoF, Sousa RA, Boesel LF, Neves NM and Reis RL. Bioinert, biodegradable and injectable polymeric matrix composites for hard tissue replacement: state of the art and recent developments. Composites Science and Technology 2004;64(6):789-817.

Martin MJ, Muotri A, Gage F and Varki A. Human embryonic stem cells express an immunogenic nonhuman sialic acid. Nat Med 2005;11(2):228-232.

Mason C and Dunnill P. A brief definition of regenerative medicine. Regenerative Medicine 2008;3(1):1-5.

Chapter 7

Matthews JA, Wnek GE, Simpson DG and Bowlin GL. Electrospinning of Collagen Nanofibers. Biomacromolecules 2002;3(2):232-238.

McHale G, Shirtcliffe NJ and Newton MI. Contact-Angle Hysteresis on Super-Hydrophobic Surfaces. Langmuir 2004;20(23):10146-10149.

Meng Y, Eshghi S, Li YJ, Schmidt R, Schaffer DV and Healy KE. Characterization of integrin engagement during defined human embryonic stem cell culture. The FASEB Journal 2010;24(4):1056-1065.

Millward-Sadler SJ and Salter DM. Integrin-Dependent Signal Cascades in Chondrocyte Mechanotransduction. Annals of Biomedical Engineering 2004;32(3):435-446.

Mitchell KE, Weiss ML, Mitchell BM, Martin P, Davis D, Morales L, Helwig B, Beerenstrauch M, Abou-Easa K, Hildreth T and Troyer D. Matrix Cells from Wharton's Jelly Form Neurons and Glia. STEM CELLS 2003;21(1):50-60.

Miyazaki T, Futaki S, Hasegawa K, Kawasaki M, Sanzen N, Hayashi M, Kawase E, Sekiguchi K, Nakatsuji N and Suemori H. Recombinant human laminin isoforms can support the undifferentiated growth of human embryonic stem cells. Biochemical and Biophysical Research Communications 2008;375(1):27-32.

Mohyeldin A, Garzon-Muvdi T and Quinones-Hinojosa A. Oxygen in Stem Cell Biology: A Critical Component of the Stem Cell Niche. Cell Stem Cell 2010;7(2):150-161.

Moro L, Venturino M, Bozzo C, Silengo L, Altruda F, Beguinot L, Tarone G and Defilippi P. Integrins induce activation of EGF receptor: role in MAP kinase induction and adhesion-dependent cell survival. EMBO J 1998;17(22):6622-6632.

Mostafavi-Pour Z, Keihani S, Talaei-Khozani T, Mokaram P, Fardaei M, Rohani L, Ebadat S and Sardarian A. Expression of $\alpha2$, $\alpha5$ and $\alpha6$ subunits of integrin in de-differentiated NIH3T3 cells by cell-free extract of embryonic stem cells. Molecular Biology Reports 2012;39(7):7339-7346.

Mummery C, Ward-van Oostwaard D, Doevendans P, Spijker R, van den Brink S, Hassink R, van der Heyden M, Opthof T, Pera M, de la Riviere AB, Passier R and Tertoolen L. Differentiation of Human Embryonic Stem Cells to Cardiomyocytes. Circulation 2003;107(21):2733-2740.

Nagaoka M, Si-Tayeb K, Akaike T and Duncan S. Culture of human pluripotent stem cells using completely defined conditions on a recombinant E-cadherin substratum. BMC Developmental Biology 2010;10(1):60.

Nain A, Wong J, Amon C and Sitti M. Drawing suspended polymer micro/nanofibers using glass micropipettes. Applied Physics Letters 2006;89(18):183105-183107.

Nath N, Hyun J, Ma H and Chilkoti A. Surface engineering strategies for control of protein and cell interactions. Surface Science 2004;570(1-2):98-110.

Chapter 7

Nistor GI, Totoiu MO, Haque N, Carpenter MK and Keirstead HS. Human embryonic stem cells differentiate into oligodendrocytes in high purity and myelinate after spinal cord transplantation. Glia 2005;49(3):385-396.

Nur-E-Kamal A, Ahmed I, Kamal J, Schindler M and Meiners S. Three-dimensional nanofibrillar surfaces promote self-renewal in mouse embryonic stem cells. Stem Cells 2006;24(2):426-433.

Odorico JS, Kaufman DS and Thomson JA. Multilineage Differentiation from Human Embryonic Stem Cell Lines. STEM CELLS 2001;19(3):193-204.

Olivier EN, Rybicki AC and Bouhassira EE. Differentiation of Human Embryonic Stem Cells into Bipotent Mesenchymal Stem Cells. STEM CELLS 2006;24(8):1914-1922.

Osafune K, Caron L, Borowiak M, Martinez RJ, Fitz-Gerald CS, Sato Y, Cowan CA, Chien KR and Melton DA. Marked differences in differentiation propensity among human embryonic stem cell lines. Nat Biotech 2008;26(3):313-315.

Ostuni E, Yan L and Whitesides GM. The interaction of proteins and cells with self-assembled monolayers of alkanethiolates on gold and silver. Colloids and Surfaces B: Biointerfaces 1999;15(1):3-30.

Otey CA, Pavalko FM and Burridge K. An interaction between alpha-actinin and the beta 1 integrin subunit in vitro. The Journal of Cell Biology 1990;111(2):721-729.

Paikal D, Zhang G, Cheng QI and Lee DA. The Effect of Integrin Antibodies on the Attachment and Proliferation of Human Tenon's Capsule Fibroblasts. Experimental Eye Research 2000;70(4):393-400.

Parsons JT. Focal adhesion kinase: the first ten years. Journal of Cell Science 2003;116(8):1409-1416.

Patthy L. Protein Evolution. Oxford, UK: Blackwell Science Ltd; 1999. 228 p.

Phanstiel DH, Brumbaugh J, Wenger CD, Tian S, Probasco MD, Bailey DJ, Swaney DL, Tervo MA, Bolin JM, Ruotti V, Stewart R, Thomson JA and Coon JJ. Proteomic and phosphoproteomic comparison of human ES and iPS cells. Nature Methods 2012; 8(10): 821-827.

Pittenger MF, Mackay AM, Beck SC, Jaiswal RK, Douglas R, Mosca JD, Moorman MA, Simonetti DW, Craig S and Marshak DR. Multilineage Potential of Adult Human Mesenchymal Stem Cells. Science 1999;284(5411):143-147.

Polak JM and Bishop AE. Stem Cells and Tissue Engineering: Past, Present, and Future. Annals of the New York Academy of Sciences 2006;1068(1):352-366.

Poschl E, Schlotzer-Schrehardt U, Brachvogel B, Saito K, Ninomiya Y and Mayer U. Collagen IV is essential for basement membrane stability but dispensable for initiation of its assembly during early development. Development 2004;131(7):1619-1628.

Chapter 7

Prabhakaran M, Venugopal J, Ghasemi-Mobarakeh L, Kai D, Jin G, Ramakrishna S, Jayakumar R and Nair S. Stem Cells and Nanostructures for Advanced Tissue Regeneration Biomedical Applications of Polymeric Nanofibers. Advances in Polymer Science: Springer Berlin / Heidelberg; 2012. p 21-62.

Price PJ, Goldborough MD and Tilkins ML; Embryonic Stem Cell Serum Replacement. US. 1998.

Prowse ABJ, Chong F, Gray PP and Munro TP. Stem cell integrins: Implications for ex-vivo culture and cellular therapies. Stem Cell Research 2011;6(1):1-12.

Ramakrishna S, Fujihara K, Teo W, Lim T and Ma Z. An Introduction to Electrospinning and Nanofibers. Singapore: World Scientific Publishing Co.; 2005. 1-380.

Ramakrishna S, Fujihara K, Teo W, Yong T, Ma Z and Ramaseshan R. Electrospun nanofibers: solving global issues. Materials Today 2006;9(3):40-50.

Ravichandran R, Liao S, Ng C, Chan CK, Raghunath M and Ramakrishna S. Effects of nanotopography on stem cell phenotypes. World J Stem Cells 2009;1(1):55-66.

Rechendorff K, Hovgaard MB, Foss M, Zhdanov VP and Besenbacher F. Enhancement of Protein Adsorption Induced by Surface Roughness. Langmuir 2006;22(26):10885-10888.

Ren H, Cao Y, Zhao Q, Li J, Zhou C, Liao L, Jia M, Zhao Q, Cai H, Han ZC, Yang R, Chen G and Zhao RC. Proliferation and differentiation of bone marrow stromal cells under hypoxic conditions. Biochemical and Biophysical Research Communications 2006;347(1):12-21.

Richards M, Fong C-Y, Chan W-K, Wong P-C and Bongso A. Human feeders support prolonged undifferentiated growth of human inner cell masses and embryonic stem cells. Nat Biotech 2002;20(9):933-936.

Riedel M, Müller B and Wintermantel E. Protein adsorption and monocyte activation on germanium nanopyramids. Biomaterials 2001;22(16):2307-2316.

Roach P. Measurement of Surface-Protein Interactions on Novel Surfaces. Nottingham: Nottingham Trent University; 2005. 142 p.

Roach P, Farrar D and Perry CC. Interpretation of Protein Adsorption: Surface-Induced Conformational Changes. Journal of the American Chemical Society 2005;127(22):8168-8173.

Roach P, Farrar D and Perry CC. Surface Tailoring for Controlled Protein Adsorption: Effect of Topography at the Nanometer Scale and Chemistry. Journal of the American Chemical Society 2006;128(12):3939-3945.

Rodesch F, Simon P, Donner C and Jauniaux E. Oxygen Measurements in Endometrial and Trophoblastic Tissues During Early Pregnancy. Obstetrics & Gynecology 1992;80(2)

Chapter 7

Rodin S, Domogatskaya A, Strom S, Hansson EM, Chien KR, Inzunza J, Hovatta O and Tryggvason K. Long-term self-renewal of human pluripotent stem cells on human recombinant laminin-511. Nat Biotech 2012;28(6):611-615.

Rose FRAJ and Oreffo ROC. Bone Tissue Engineering: Hope vs Hype. Biochemical and Biophysical Research Communications 2002;292(1):1-7.

Ross AM, Nandivada H, Ryan AL and Lahann J. Synthetic substrates for long-term stem cell culture. Polymer 2012;53(13):2533-2539.

Rowland TJ, Miller LM, Blaschke AJ, Doss EL, Bonham AJ, Hikita ST, Johnson LV and Clegg DO. Roles of integrins in human induced pluripotent stem cell growth on Matrigel and vitronectin. Stem Cells Dev 2010;19(8):1231-1240.

Rozen S and Skaletsky H. Primer3 on the WWW for General Users and for Biologist Programmers In: Misener S and Krawetz SA, editors. Bioinformatics Methods and Protocols. Totowa, New Jersey: Humana Press Inc.; 1999. p 365-386.

Safford KM, Hicok KC, Safford SD, Halvorsen Y-DC, Wilkison WO, Gimble JM and Rice HE. Neurogenic differentiation of murine and human adipose-derived stromal cells. Biochemical and Biophysical Research Communications 2002;294(2):371-379.

Saller MM, Prall WC, Docheva D, Schonitzer V, Popov T, Anz D, Clausen-Schaumann H, Mutschler W, Volkmer E, Schieker M and Polzer H. Increased stemness and migration of human mesenchymal stem cells in hypoxia is associated with altered integrin expression. Biochemical and Biophysical Research Communications 2012;423(2):379-385.

Schaller MD, Otey CA, Hildebrand JD and Parsons JT. Focal adhesion kinase and paxillin bind to peptides mimicking beta integrin cytoplasmic domains. The Journal of Cell Biology 1995;130(5):1181-1187.

Schindler M, Ahmed I, Kamal J, Nur-E-Kamal A, Grafe TH, Young Chung H and Meiners S. A synthetic nanofibrillar matrix promotes in vivo-like organization and morphogenesis for cells in culture. Biomaterials 2005;26(28):5624-5631.

Schlaepfer DD and Hunter T. Evidence for in vivo phosphorylation of the Grb2 SH2-domain binding site on focal adhesion kinase by Src-family protein-tyrosine kinases. Molecular and Cellular Biology 1996;16(10):5623-5633.

Schnell E, Klinkhammer K, Balzer S, Brook G, Klee D, Dalton P and Mey J. Guidance of glial cell migration and axonal growth on electrospun nanofibers of poly-e-caprolactone and a collagen/poly-e-caprolactone blend. Biomaterials 2007;28(19):3012-3025.

Schoenwaelder SM and Burridge K. Bidirectional signaling between the cytoskeleton and integrins. Current Opinion in Cell Biology 1999;11(2):274-286.

Schvartz I, Seger D and Shaltiel S. Vitronectin. The International Journal of Biochemistry & Cell Biology 1999;31(5):539-544.

Chapter 7

Schwartz MA. Integrin signaling revisited. Trends in Cell Biology 2001;11(12):466-470.

Scopelliti PE, Borgonovo A, Indrieri M, Giorgetti L, Bongiorno G, Carbone R, Podestà A and Milani P. The Effect of Surface Nanometre-Scale Morphology on Protein Adsorption. PLoS ONE 2010;5(7):e11862.

Seo MJ, Suh SY, Bae YC and Jung JS. Differentiation of human adipose stromal cells into hepatic lineage in vitro and in vivo. Biochemical and Biophysical Research Communications 2005;328(1):258-264.

Shabani I, Haddadi-Asl V, Seyedjafari E, Babaeijandaghi F and Soleimani M. Improved infiltration of stem cells on electrospun nanofibers. Biochemical and Biophysical Research Communications 2009;382(1):129-133.

Shih YR, Chen CN, Tsai SW, Wang YJ and Lee OK. Growth of mesenchymal stem cells on electrospun type I collagen nanofibers. Stem Cells 2006;24(11):2391-2397.

Sill TJ and von Recum HA. Electrospinning: Applications in drug delivery and tissue engineering. Biomaterials 2008;29(13):1989-2006.

Silva MMCG, Cyster LA, Barry JJA, Yang XB, Oreffo ROC, Grant DM, Scotchford CA, Howdle SM, Shakesheff KM and Rose FRAJ. The effect of anisotropic architecture on cell and tissue infiltration into tissue engineering scaffolds. Biomaterials 2006;27(35):5909-5917.

Siti-Ismail N, Bishop AE, Polak JM and Mantalaris A. The benefit of human embryonic stem cell encapsulation for prolonged feeder-free maintenance. Biomaterials 2008;29(29):3946-3952.

Slaughter BV, Khurshid SS, Fisher OZ, Khademhosseini A and Peppas NA. Hydrogels in Regenerative Medicine. Advanced Materials 2009;21(32-33):3307-3329.

Smith LA, Liu X, Hu J and Ma PX. The influence of three-dimensional nanofibrous scaffolds on the osteogenic differentiation of embryonic stem cells. Biomaterials 2009;30(13):2516-2522.

Spangrude GJ, Heimfeld S and Weissman IL. Purification and characterization of mouse hematopoietic stem cells. Science 1988;241(4861):58-62.

Stalder AF, Kulik G, Sage D, Barbieri L and Hoffmann P. A snake-based approach to accurate determination of both contact points and contact angles. Colloids and Surfaces A: Physicochemical and Engineering Aspects 2006;286(1-3):92-103.

Stevens MM. Biomaterials for bone tissue engineering. Materials Today 2008;11(5):18-25.

Stevens MM and George JH. Exploring and Engineering the Cell Surface Interface. Science 2005;310(5751):1135-1138.

Chapter 7

Streuli CH and Akhtar N. Signal co-operation between integrins and other receptor systems. Biochemical Journal 2009;418(3):491-506.

Sundberg C and Rubin K. Stimulation of beta(1) integrins on fibroblasts induces PDGF independent tyrosine phosphorylation of PDGF beta-receptors. Journal of Cell Biology 1996;132(4):741-752.

Symes K, Smith EM, Mitsi M and Nugent MA. Sweet cues: How heparan sulfate modification of fibronectin enables growth factor guided migration of embryonic cells. Cell Adhesion & Migration 2010;4(4):507-510.

Szablowska-Gadomska I, Zayat V and Buzanska L. Influence of low oxygen tensions on expression of pluripotency genes in stem cells. Acta Neurobiol Exp (Wars) 2011;71(1):86-93.

Taborelli M, Eng L, Descouts P, Ranieri JP, Bellamkonda R and Aebischer P. Bovine serum albumin conformation on methyl and amine functionalized surfaces compared by scanning force microscopy. Journal of Biomedical Materials Research 1995;29(6):707-714.

Taylor G. Disintegration of water drops in an electric field Proceedings of the Royal Society of London 1964;A A280:383-397.

Teo W and Ramakrishna S. Electrospun fibre bundle made of aligned nanofibres over two fixed points. Nanotechnology 2005;16:1878-1884.

Teo WE and Ramakrishna S. A review on electrospinning design and nanofibre assemblies. Nanotechnology 2006;17(14):R89.

Thomson JA, Itskovitz-Eldor J, Shapiro SS, Waknitz MA, Swiergiel JJ, Marshall VS and Jones JM. Embryonic Stem Cell Lines Derived from Human Blastocysts. Science 1998;282(5391):1145-1147.

Toh Y-C, Ng S, Khong YM, Zhang X, Zhu Y, Lin P-C, Te C-M, Sun W and Yu H. Cellular responses to a nanofibrous environment. Nano Today 2006;1(3):34-43.

Trounson A. The Production and Directed Differentiation of Human Embryonic Stem Cells. Endocrine Reviews 2006;27(2):208-219.

van der Flier A and Sonnenberg A. Function and interactions of integrins. Cell and Tissue Research 2001;305(3):285-298.

van Wachem PB, Hogt AH, Beugeling T, Feijen J, Bantjes A, Detmers JP and van Aken WG. Adhesion of cultured human endothelial cells onto methacrylate polymers with varying surface wettability and charge. Biomaterials 1987;8(5):323-328.

Vasita R and Katti DS. Nanofibers and their applications in tissue engineering. Int J Nanomedicine 2006;1(1):15-30.

Chapter 7

Vogler EA. Structure and reactivity of water at biomaterial surfaces. Advances in Colloid and Interface Science 1998;74(1-3):69-117.

Vroman L. Effect of Adsorbed Proteins on the Wettability of Hydrophilic and Hydrophobic Solids. Nature 1962;196(4853):476-477.

Wagers AJ and Weissman IL. Plasticity of Adult Stem Cells. Cell 2004;116(5):639-648.

Wagner MS and Castner DG. Characterization of Adsorbed Protein Films by Time-of-Flight Secondary Ion Mass Spectrometry with Principal Component Analysis. Langmuir 2001;17(15):4649-4660.

Wagner MS, Tyler BJ and Castner DG. Interpretation of Static Time-of-Flight Secondary Ion Mass Spectra of Adsorbed Protein Films by Multivariate Pattern Recognition. Analytical Chemistry 2002;74(8):1824-1835.

Wang J, Rao S, Chu J, Shen X, Levasseur DN, Theunissen TW and Orkin SH. A protein interaction network for pluripotency of embryonic stem cells. Nature 2006;444(7117):364-368.

Watt FM and Hogan BL. Out of Eden: stem cells and their niches. Science 2000;287(5457):1427-1430.

Westfall SD, Sachdev S, Das P, Hearne LB, Hannink M, Roberts RM and Ezashi T. Identification of oxygen-sensitive transcriptional programs in human embryonic stem cells. Stem Cells Dev 2008;17(5):869-881.

Wiesner S, Legate KR and Fässler R. Integrin-actin interactions. Cellular and Molecular Life Sciences 2005;62(10):1081-1099.

Wimpenny I, Hampson K, Yang Y, Ashammakhi N and Forsyth NR. One-step recovery of marrow stromal cells on nanofibers. Tissue Eng Part C Methods 2010;16(3):503-509.

Wobus AM and Boheler KR. Embryonic Stem Cells: Prospects for Developmental Biology and Cell Therapy. Physiological Reviews 2005;85(2):635-678.

Wong SSY and Bernstein HS. Cardiac regeneration using human embryonic stem cells: producing cells for future therapy. Regenerative Medicine 2010;5(5):763-775.

Woo KM, Chen VJ and Ma PX. Nano-fibrous scaffolding architecture selectively enhances protein adsorption contributing to cell attachment. Journal of Biomedical Materials Research Part A 2003;67A(2):531-537.

Xie J, Willerth SM, Li X, Macewan MR, Rader A, Sakiyama-Elbert SE and Xia Y. The differentiation of embryonic stem cells seeded on electrospun nanofibers into neural lineages. Biomaterials 2009;30(3):354-362.

Chapter 7

Xu CH, Inokuma MS, Denham J, Golds K, Kundu P, Gold JD and Carpenter MK. Feeder-free growth of undifferentiated human embryonic stem cells. Nature Biotechnology 2001;19(10):971-974.

Xu R-H, Peck RM, Li DS, Feng X, Ludwig T and Thomson JA. Basic FGF and suppression of BMP signaling sustain undifferentiated proliferation of human ES cells. Nat Meth 2005;2(3):185-190.

Yang F, Murugan R, Wang S and Ramakrishna S. Electrospinning of nano/micro scale poly(L-lactic acid) aligned fibers and their potential in neural tissue engineering. Biomaterials 2005;26(15):2603-2610.

Yang J, Rose FRAJ, Gadegaard N and Alexander MR. A High-Throughput Assay of Cell-Surface Interactions using Topographical and Chemical Gradients. Advanced Materials 2009;21(3):300-304.

Yla-Outinen L, Mariani C, Skottman H, Suuronen R, Harlin A and Narkilahti S. Electrospun poly (L, D-lactide) scaffolds support the growth of human embryonic stem cell-derived neuronal cells. The Open Tissue Engineering and Regenerative Medicine Journal 2010;3:1-9.

Young H and Carpentar MK. Characterisation of human embryonic stem cells. In: Atala A and Lanza RP, editors. Methods of tissue engineering: Essentials of Stem Cell Biology. London: Elsevier Academic Press; 2002. p 265-268.

Young HE and Black AC. Adult stem cells. The Anatomical Record Part A: Discoveries in Molecular, Cellular, and Evolutionary Biology 2004;276A(1):75-102.

Zachar V, Prasad S, Weli S, Gabrielsen A, Petersen K, Petersen M and Fink T. The effect of human embryonic stem cells (hESCs) long-term normoxic and hypoxic cultures on the maintenance of pluripotency. In Vitro Cellular & Developmental Biology - Animal 2010;46(3):276-283.

Zhang Y, Ouyang H, Lim CT, Ramakrishna S and Huang Z-M. Electrospinning of gelatin fibers and gelatin/PCL composite fibrous scaffolds. Journal of Biomedical Materials Research Part B: Applied Biomaterials 2005;72B(1):156-165.

Zhang Z, Vuori K, Reed JC and Ruoslahti E. The alpha 5 beta 1 integrin supports survival of cells on fibronectin and up-regulates Bcl-2 expression. Proceedings of the National Academy of Sciences 1995;92(13):6161-6165.

Zhu Y, Gao C, Liu X and Shen J. Surface Modification of Polycaprolactone Membrane via Aminolysis and Biomacromolecule Immobilization for Promoting Cytocompatibility of Human Endothelial Cells. Biomacromolecules 2002;3(6):1312-1319.

Zuk PA, Zhu M, Ashjian P, De Ugarte DA, Huang JI, Mizuno H, Alfonso ZC, Fraser JK, Benhaim P and Hedrick MH. Human Adipose Tissue Is a Source of Multipotent Stem Cells. Molecular Biology of the Cell 2002;13(12):4279-4295.

Chapter 7

Zuo WW, Zhu MF, Yang W, Yu H, Chen YM and Zhang Y. Experimental study on relationship between jet instability and formation of beaded fibers during electrospinning. Polymer Engineering and Science 2005;45(5):704-709.

Zussman E, Theron A and Yarin AL. Formation of nanofiber crossbars in electrospinning. Applied Physics Letters 2003;82(6):973-975.

Appendix

Table A1 Normalised intensity values of positive ion amino acid fragments identified by Tof-SIMS on PCL electrospun nanofibrous substrates, in both aligned (280 ± 122 nm) and random (318 ± 151 nm) conformations when incubated in conditioned media.

m/z	Potential Assignment	CM+ CTL	CM+ A (280 nm)	CM+ A (521 nm)	CM+ R (318nm)	CM+R (660 nm)
22,9718	Na (Wagner *et al*., 2001)	1,23E-04	8,74E-05	8,74E-05	1,08E-04	1,25E-04
25,9929	C_2H^- (Wagner *et al*., 2001)	2,40E-05	1,83E-05	1,83E-05	1,88E-05	1,98E-05
26.995	CN^- (peptide backbone) (Wagner *et al*., 2001)	1,59E-04	1,41E-04	1,41E-04	1,60E-04	1,11E-04
27,9917	$C_2H_3^+$ (Wagner et al 2002) (Mahlstedt *et al*., 2009)	7,18E-05	4,32E-05	4,32E-05	5,23E-05	3,49E-05
29,0254	C_2H_5 (Mahlstedt *et al.,* 2009)	7,92E-04	6,72E-04	6,72E-04	7,47E-04	4,26E-04
30,0112	CH_4N^+: Glycine (Wagner *et al.,*2001).	8,64E-05	7,38E-05	7,38E-05	8,51E-05	5,22E-05
37,9999	No assignment identified	3,82E-05	2,87E-05	2,87E-05	2,39E-05	1,75E-05
39,7221	$C_3H_3^+$ (Wagner *et al.,* 2002)	1,47E-04	1,13E-04	1,13E-04	1,31E-04	1,73E-04
40,0167	No assignment identified	3,10E-04	2,46E-04	2,46E-04	2,49E-04	1,87E-04
40,9458	No assignment identified	1,03E-04	1,21E-04	1,21E-04	1,18E-04	9,73E-05
41,0139	$C_3H_5^+$ (Wagner *et al*., 2002) (Mahlstedt *et al*., 2009)	2,03E-03	2,02E-03	2,02E-03	2,34E-03	1,77E-03
41,7003	$C_3H_5^+$ (Wagner *et al*., 2002)	2,85E-04	3,19E-04	3,19E-04	3,64E-04	1,91E-04
41,9932	$C_3H_5^+$ (Wagner *et al*., 2002)	2,27E-04	2,25E-04	2,25E-04	3,02E-04	1,06E-04
42,9994	CNO^-: peptide backbone (Wagner *et al*., 2001)	5,92E-04	6,20E-04	6,20E-04	1,18E-03	2,50E-04
43,0241	$CH_3N_2^+$ (Argenine: laminin (Wagner *et al*., 2002) .	6,29E-03	5,59E-03	5,59E-03	6,98E-03	3,08E-03
43,0421	C_2H_5N (Hazen *et al.,* 2006)	2,60E-03	1,86E-03	1,86E-03	2,29E-03	1,21E-03

44,0371	$C_2H_6N^+$ (Wagner *et al*., 2002)	1,40E-03	9,95E-04	9,95E-04	1,23E-03	5,45E-04
54,9998	No assignment identified	2,49E-04	2,33E-04	2,33E-04	3,37E-04	1,49E-04
55,0208	$C_4H_7^+$ (Wagner *et al*., 2002)	1,05E-02	8,17E-03	8,17E-03	1,16E-02	4,60E-03
56,0233	$C_3H_6N^+$ (Wagner *et al*., 2002)	1,64E-03	1,16E-03	1,16E-03	1,53E-03	7,17E-04
56,6144	$C_3H_6N^+$ (Wagner *et al*., 2002)	2,18E-04	2,11E-04	2,11E-04	2,42E-04	1,11E-04
58,0392	C_2H_4NO: Glycine; collagen (Cannnan *et al*., 2007)	8,52E-04	1,03E-03	1,03E-03	8,73E-04	5,12E-04
59,0118	$C_3H_7O^+$ (Wagner *et al*., 2002)	2,12E-04	1,50E-04	1,50E-04	2,30E-04	8,14E-05
59,0496	CH_5N_3: Arginine; laminin (Cannnan *et al*., 2007)	7,36E-03	5,09E-03	5,09E-03	6,76E-03	2,20E-03
68,0263	$C_4H_6N^+$ (Wagner *et al*., 2002)	1,28E-03	9,28E-04	9,28E-04	1,23E-03	5,84E-04
69,0374	C_4H_5O: threonine; fibronectin (Cannnan *et al*., 2007)	3,26E-03	2,37E-03	2,37E-03	3,14E-03	1,36E-03
70,0375	$C_4H_8N^+$ (Wagner *et al*., 2002)	1,56E-03	1,08E-03	1,08E-03	1,41E-03	6,05E-04
78,0441	$C_6H_6^+$ Toporski *et al.,* 2002	9,61E-04	1,03E-03	1,03E-03	1,04E-03	5,33E-04
87,9004	$C_4H_9O_2^+$ Cheng *et al*., 2008	6,68E-05	8,51E-05	8,51E-05	5,25E-05	1,10E-04
96,8582	SO_4^- (Alexander & Jones *et al.,* 1995)	2,65E-05	2,39E-05	2,39E-05	2,59E-05	4,91E-05
98,1067	$C_4H_4NO_2^+$: asparagine (Wagner *et al*., 2001)	4,74E-04	3,82E-04	3,82E-04	5,15E-04	3,51E-04
103,9236	No assignment identified	1,70E-04	1,32E-04	1,32E-04	1,22E-04	3,13E-03
124,9131	$C_8H_9NO^4$ (125 m/z) (Mahlstedt *et al*., 2009)	8,45E-04	1,35E-03	1,35E-03	5,63E-04	5,41E-04
164.857	$C_{13}H_9^+$ (165 m/z) (Delcorte	1,34E-04	2,67E-04	2,67E-04	1,31E-04	1,60E-04

	et al., 1997)				
180,0851	No assignment identified	1,22E-04	1,12E-04	1,12E-04	1,17E-04	9,01E-05

Table A2 Normalised intensity values of positive ion amino acid fragments identified by Tof-SIMS on PCL electrospun nanofibrous substrates, in both aligned (280 ± 122 nm) and random (318 ± 151 nm) conformations when incubated in pure collagen I protein solution (50 µg/ml).

m/z	Potential Assignment	Coll I CTL	Coll I +A (280nm)	Coll I +A (521nm)	Coll I +R (318nm)	Coll I +R (660nm)
22,9718	Na (Wagner *et al.*, 2001)	8,37E-05	5,45E-05	3,10E-05	1,30E-04	8,90E-06
25,9929	C_2H^- (Wagner *et al.*, 2001)	2,25E-05	2,15E-05	7,46E-05	2,25E-05	2,16E-05
26.995	CN^- (peptide backbone) (Wagner *et al.*, 2001)	1,68E-04	1,87E-04	4,99E-04	2,18E-04	2,41E-04
27,9917	$C_2H_3^+$ (Wagner et al 2002) (Mahlstedt *et al.*, 2009)	1,03E-04	7,41E-05	1,49E-04	5,67E-05	7,73E-05
29,0254	C_2H_5 (Mahlstedt *et al.,* 2009)	1,16E-03	9,22E-04	6,08E-04	7,39E-04	1,10E-03
30,0112	CH_4N^+: Glycine (Wagner *et al.,*2001).	1,41E-04	1,02E-04	4,36E-05	7,59E-05	1,29E-04
37,9999	No assignment identified	3,18E-05	2,64E-05	3,09E-05	2,78E-05	1,54E-05
39,7221	$C_3H_3^+$ (Wagner *et al.,* 2002)	1,16E-04	1,39E-04	4,70E-04	1,46E-04	1,58E-04
40,0167	No assignment identified	4,12E-04	3,31E-04	2,85E-04	2,78E-04	3,01E-04
40,9458	No assignment identified	9,77E-05	1,12E-04	2,97E-04	1,42E-04	1,70E-04
41,0139	$C_3H_5^+$ (Wagner *et al.*, 2002) (Mahlstedt *et al.*,	2,17E-03	2,48E-03	3,76E-03	2,72E-03	3,28E-03

	2009)					
41,7003	$C_3H_5^+$ (Wagner *et al*., 2002)	2,92E-04	4,32E-04	1,03E-03	4,78E-04	6,62E-04
41,9932	$C_3H_5^+$ (Wagner *et al*., 2002)	3,15E-04	2,95E-04	6,44E-04	2,42E-04	3,27E-04
42,9994	CNO^-: peptide backbone (Wagner *et al*., 2001)	9,00E-04	9,99E-04	1,84E-03	7,25E-04	8,09E-04
43,0241	$CH_3N_2^+$ (Argenine: laminin (Wagner *et al*., 2002) .	1,05E-02	1,18E-02	5,93E-03	7,53E-03	1,07E-02
43,0421	C_2H_5N (Hazen *et al.,* 2006)	4,32E-03	2,95E-03	9,14E-04	1,96E-03	3,24E-03
44,0371	$C_2H_6N^+$ (Wagner *et al*., 2002)	1,79E-03	1,58E-03	2,04E-04	1,14E-03	1,63E-03
54,9998	No assignment identified	3,33E-04	3,61E-04	9,45E-04	2,79E-04	4,75E-04
55,0208	$C_4H_7^+$ (Wagner *et al*., 2002)	1,68E-02	1,34E-02	5,64E-03	8,63E-03	2,07E-02
56,0233	$C_3H_6N^+$ (Wagner *et al*., 2002)	3,05E-03	2,44E-03	4,50E-04	1,57E-03	2,79E-03
56,6144	$C_3H_6N^+$ (Wagner *et al*., 2002)	3,01E-04	2,94E-04	5,22E-04	2,62E-04	5,30E-04
58,0392	C_2H_4NO: Glycine; collagen (Cannnan *et al*., 2007)	8,55E-04	6,73E-04	2,13E-04	4,96E-04	8,28E-04
59,0118	$C_3H_7O^+$ (Wagner *et al*., 2002)	3,53E-04	2,82E-04	9,41E-05	1,80E-04	3,22E-04

59,0496	CH$_5$N$_3$: Arginine; laminin (Cannnan *et al*., 2007)	1,22E-02	9,53E-03	2,81E-03	5,95E-03	9,68E-03
68,0263	C$_4$H$_6$N$^+$ (Wagner *et al*., 2002)	2,28E-03	1,89E-03	4,30E-04	1,27E-03	2,33E-03
69,0374	C$_4$H$_5$O: threonine; fibronectin (Cannnan *et al*., 2007)	5,12E-03	3,26E-03	1,13E-03	1,91E-03	5,45E-03
70,0375	C$_4$H$_8$N$^+$ (Wagner *et al*., 2002)	2,41E-03	1,64E-03	2,64E-04	1,10E-03	2,42E-03
78,0441	C$_6$H$_6$$^+$ Toporski *et al.,* 2002	1,23E-03	1,25E-03	2,08E-03	1,03E-03	1,69E-03
87,9004	C$_4$H$_9$O$_2$$^+$ Cheng *et al*., 2008	4,35E-05	3,68E-05	3,14E-05	6,38E-05	3,55E-05
96,8582	SO$_4$$^-$ (Alexander & Jones *et al.,* 1995)	3,64E-05	2,80E-05	2,25E-05	2,33E-05	3,73E-05
98,1067	C$_4$H$_4$NO$_2$$^+$: asparagine (Wagner *et al*., 2001)	8,05E-04	8,72E-04	7,16E-04	8,68E-04	8,37E-04
103,9236	No assignment identified	6,91E-05	6,93E-05	1,54E-04	1,24E-04	4,43E-05
124,9131	C$_8$H$_9$NO^4 (125 m/z) (Mahlstedt *et al*., 2009)	2,43E-04	3,22E-04	1,14E-04	8,85E-04	1,12E-04
164.857	C$_{13}$H$_9$$^+$ (165 m/z) (Delcorte *et al*., 1997)	8,05E-05	9,67E-05	2,36E-04	2,19E-04	9,70E-05
180,0851	No assignment identified	1,43E-04	1,29E-04	1,30E-04	1,18E-04	1,29E-04

Table A3 Normalised intensity values of positive ion amino acid fragments identified by Tof-SIMS on PCL electrospun nanofibrous substrates, in both aligned (280 ± 122 nm) and random (318 ± 151 nm) conformations when incubated in pure fibronectin protein solution (50 µg/ml).

m/z	Potential Assignment	Fn CTL	Fn +A (280nm)	Fn +A (521nm)	Fn +R (318nm)	Fn +R (660nm)
22,9718	Na (Wagner *et al.*, 2001)	7,58E-05	1,07E-04	7,49E-05	7,43E-05	1,35E-04
25,9929	C_2H^- (Wagner *et al.*, 2001)	1,92E-05	2,25E-05	1,52E-05	2,30E-05	2,53E-05
26.995	CN^- (peptide backbone) (Wagner *et al.*, 2001)	9,71E-05	1,62E-04	2,06E-04	1,71E-04	1,79E-04
27,9917	$C_2H_3^+$ (Wagner et al 2002) (Mahlstedt *et al.*, 2009)	5,35E-05	5,16E-05	3,39E-05	4,06E-05	7,87E-05
29,0254	C_2H_5 (Mahlstedt *et al.,* 2009)	7,72E-04	6,93E-04	5,93E-04	6,23E-04	9,33E-04
30,0112	CH_4N^+: Glycine (Wagner *et al.,*2001).	7,92E-05	6,10E-05	3,89E-05	5,49E-05	9,77E-05
37,9999	No assignment identified	3,50E-05	3,43E-05	1,16E-05	2,56E-05	3,06E-05
39,7221	$C_3H_3^+$ (Wagner *et al.*, 2002)	1,66E-04	1,17E-04	1,64E-04	1,35E-04	1,19E-04
40,0167	No assignment identified	3,44E-04	3,12E-04	1,67E-04	2,57E-04	3,39E-04
40,9458	No assignment identified	7,45E-05	8,68E-05	2,26E-04	1,10E-04	8,05E-05
41,0139	$C_3H_5^+$ (Wagner *et al.*, 2002) (Mahlstedt *et al.*,	1,65E-03	2,03E-03	3,12E-03	2,14E-03	2,20E-03

	2009)				
41,7003	$C_3H_5^+$ (Wagner *et al*., 2002)	1,41E-04	3,38E-04	8,43E-04	3,54E-04	3,07E-04
41,9932	$C_3H_5^+$ (Wagner *et al*., 2002)	1,53E-04	1,82E-04	2,83E-04	1,77E-04	2,13E-04
42,9994	CNO^-: peptide backbone (Wagner *et al*., 2001)	4,88E-04	6,47E-04	1,01E-03	6,26E-04	7,11E-04
43,0241	$CH_3N_2^+$ (Argenine: laminin (Wagner *et al*., 2002) .	6,06E-03	7,06E-03	7,34E-03	6,43E-03	9,36E-03
43,0421	C_2H_5N (Hazen *et al.,* 2006)	2,05E-03	1,87E-03	1,25E-03	1,60E-03	2,70E-03
44,0371	$C_2H_6N^+$ (Wagner *et al*., 2002)	1,35E-03	1,31E-03	6,42E-04	1,08E-03	1,68E-03
54,9998	No assignment identified	2,14E-04	2,31E-04	3,81E-04	2,16E-04	3,23E-04
55,0208	$C_4H_7^+$ (Wagner *et al*., 2002)	8,03E-03	7,96E-03	1,06E-02	6,92E-03	1,26E-02
56,0233	$C_3H_6N^+$ (Wagner *et al*., 2002)	1,36E-03	1,24E-03	1,14E-03	1,02E-03	1,94E-03
56,6144	$C_3H_6N^+$ (Wagner *et al*., 2002)	1,95E-04	2,66E-04	6,37E-04	2,43E-04	2,83E-04
58,0392	C_2H_4NO: Glycine; collagen (Cannnan *et al*., 2007)	3,53E-04	3,43E-04	4,54E-04	3,30E-04	4,64E-04
59,0118	$C_3H_7O^+$ (Wagner *et al*., 2002)	2,09E-04	2,07E-04	1,63E-04	1,78E-04	2,57E-04
59,0496	CH_5N_3: Arginine; laminin	7,47E-03	7,14E-03	4,58E-03	5,68E-03	8,53E-03

	(Cannnan *et al*., 2007)				
68,0263	$C_4H_6N^+$ (Wagner *et al*., 2002)	1,16E-03	1,13E-03	1,05E-03	9,80E-04	1,71E-03
69,0374	C_4H_5O: threonine; fibronectin (Cannnan *et al*., 2007)	3,65E-03	3,36E-03	2,89E-03	2,68E-03	4,87E-03
70,0375	$C_4H_8N^+$ (Wagner *et al*., 2002)	1,41E-03	1,28E-03	1,03E-03	1,06E-03	1,91E-03
78,0441	$C_6H_6^+$ Toporski *et al.,* 2002	5,97E-04	8,77E-04	1,48E-03	8,15E-04	1,14E-03
87,9004	$C_4H_9O_2^+$ Cheng *et al*., 2008	9,06E-05	8,29E-05	4,50E-05	7,20E-05	5,37E-05
96,8582	SO_4^- (Alexander & Jones *et al.,* 1995)	3,22E-05	2,30E-05	2,82E-05	2,23E-05	2,96E-05
98,1067	$C_4H_4NO_2^+$: asparagine (Wagner *et al*., 2001)	3,30E-04	3,97E-04	7,36E-04	4,07E-04	6,17E-04
103,9236	No assignment identified	1,00E-03	1,32E-04	7,72E-05	2,27E-04	8,90E-05
124,9131	$C_8H_9NO^4$ (125 m/z) (Mahlstedt *et al*., 2009)	1,87E-03	1,02E-03	1,82E-04	1,23E-03	2,37E-04
164.857	$C_{13}H_9^+$ (165 m/z) (Delcorte *et al*., 1997)	2,49E-04	2,27E-04	9,67E-05	2,68E-04	9,48E-05
180,0851	No assignment identified	9,10E-05	1,19E-04	1,07E-04	1,13E-04	1,81E-04

Table A4 Normalised intensity values of positive ion amino acid fragments identified by Tof-SIMS on PCL electrospun nanofibrous substrates, in both aligned (280 ± 122 nm) and random (318 ± 151 nm) conformations when incubated in pure laminin protein solution (50 µg/ml).

m/z	Potential Assignment	Ln CTL	Ln +A (280nm)	Ln +A (521nm)	Ln +R (318nm)	Ln +R (660nm)
22,9718	Na (Wagner *et al*., 2001)	8,91E-05	1,06E-04	1,32E-04	1,26E-04	1,98E-04
25,9929	C_2H^- (Wagner *et al*., 2001)	1,84E-05	2,29E-05	2,03E-05	2,12E-05	2,14E-05
26.995	CN^- (peptide backbone) (Wagner *et al*., 2001)	1,08E-04	1,59E-04	1,82E-04	1,19E-04	1,65E-04
27,9917	$C_2H_3^+$ (Wagner et al 2002) (Mahlstedt *et al*., 2009)	4,96E-05	4,70E-05	4,02E-05	3,69E-05	4,69E-05
29,0254	C_2H_5 (Mahlstedt *et al.,* 2009)	6,79E-04	6,70E-04	7,35E-04	5,80E-04	7,08E-04
30,0112	CH_4N^+: Glycine (Wagner *et al.,*2001).	7,39E-05	6,42E-05	6,95E-05	5,10E-05	7,41E-05
37,9999	No assignment identified	3,94E-05	3,26E-05	2,23E-05	2,67E-05	2,30E-05
39,7221	$C_3H_3^+$ (Wagner *et al*., 2002)	9,98E-05	1,09E-04	1,29E-04	9,01E-05	1,05E-04
40,0167	No assignment identified	3,04E-04	3,11E-04	2,77E-04	2,69E-04	2,75E-04
40,9458	No assignment identified	7,79E-05	8,69E-05	1,24E-04	6,25E-05	8,28E-05
41,0139	$C_3H_5^+$ (Wagner *et al*., 2002) (Mahlstedt *et al*.,	1,54E-03	1,98E-03	2,53E-03	1,62E-03	2,06E-03

	2009)				
41,7003	$C_3H_5^+$ (Wagner *et al*., 2002)	1,34E-04	3,11E-04	4,88E-04	1,87E-04	3,70E-04
41,9932	$C_3H_5^+$ (Wagner *et al*., 2002)	1,56E-04	1,94E-04	2,05E-04	1,25E-04	1,89E-04
42,9994	CNO^-: peptide backbone (Wagner *et al*., 2001)	4,64E-04	6,81E-04	6,67E-04	4,88E-04	7,18E-04
43,0241	$CH_3N_2^+$ (Argenine: laminin (Wagner *et al*., 2002) .	5,71E-03	6,57E-03	7,80E-03	5,50E-03	7,61E-03
43,0421	C_2H_5N (Hazen *et al.,* 2006)	1,87E-03	1,94E-03	1,98E-03	1,81E-03	2,16E-03
44,0371	$C_2H_6N^+$ (Wagner *et al*., 2002)	1,19E-03	1,21E-03	1,20E-03	1,12E-03	1,29E-03
54,9998	No assignment identified	1,87E-04	2,23E-04	2,69E-04	1,85E-04	2,49E-04
55,0208	$C_4H_7^+$ (Wagner *et al*., 2002)	7,19E-03	7,98E-03	1,01E-02	7,19E-03	9,39E-03
56,0233	$C_3H_6N^+$ (Wagner *et al*., 2002)	1,15E-03	1,23E-03	1,33E-03	1,11E-03	1,35E-03
56,6144	$C_3H_6N^+$ (Wagner *et al*., 2002)	1,17E-04	2,01E-04	3,42E-04	1,43E-04	2,46E-04
58,0392	C_2H_4NO: Glycine; collagen (Cannnan *et al*., 2007)	3,43E-04	3,97E-04	4,25E-04	3,26E-04	4,69E-04
59,0118	$C_3H_7O^+$ (Wagner *et al*., 2002)	1,58E-04	1,88E-04	2,08E-04	1,51E-04	2,11E-04

59,0496	CH$_5$N$_3$: Arginine; laminin (Cannnan *et al*., 2007)	5,80E-03	6,27E-03	6,50E-03	5,24E-03	6,47E-03
68,0263	C$_4$H$_6$N$^+$ (Wagner *et al*., 2002)	8,97E-04	1,02E-03	1,13E-03	9,25E-04	1,11E-03
69,0374	C$_4$H$_5$O: threonine; fibronectin (Cannnan *et al*., 2007)	2,51E-03	2,72E-03	3,02E-03	2,49E-03	2,92E-03
70,0375	C$_4$H$_8$N$^+$ (Wagner *et al*., 2002)	1,12E-03	1,25E-03	1,40E-03	1,16E-03	1,41E-03
78,0441	C$_6$H$_6^+$ Toporski *et al.,* 2002	5,64E-04	8,09E-04	1,18E-03	6,68E-04	8,73E-04
87,9004	C$_4$H$_9$O$_2^+$ Cheng *et al.,* 2008	1,01E-04	1,18E-04	9,69E-05	8,26E-05	8,60E-05
96,8582	SO$_4^-$ (Alexander & Jones *et al.,* 1995)	3,06E-05	2,48E-05	2,46E-05	2,03E-05	2,61E-05
98,1067	C$_4$H$_4$NO$_2^+$: asparagine (Wagner *et al*., 2001)	2,80E-04	3,74E-04	4,54E-04	3,13E-04	4,40E-04
103,9236	No assignment identified	5,07E-04	2,26E-04	1,21E-04	4,92E-04	1,63E-04
124,9131	C$_8$H$_9$NO[4] (125 m/z) (Mahlstedt *et al*., 2009)	2,05E-03	1,09E-03	3,77E-04	7,25E-04	4,45E-04
164.857	C$_{13}$H$_9^+$ (165 m/z) (Delcorte *et al*., 1997)	4,29E-04	2,67E-04	1,15E-04	1,45E-04	1,33E-04
180,0851	No assignment identified	7,72E-05	1,09E-04	1,21E-04	1,01E-04	1,18E-04

Table A5 Normalised intensity values of positive ion amino acid fragments identified by Tof-SIMS on PCL electrospun nanofibrous substrates, in both aligned (280 ± 122 nm) and random (318 ± 151 nm) conformations when incubated in pure vitronectin protein solution (50 µg/ml).

m/z	Potential Assignment	Vn CTL	Vn +A (280nm)	Vn +A (521nm)	Vn +R (318nm)	Vn +R (660nm)
22,9718	Na (Wagner *et al*., 2001)	3,59E-04	9,07E-05	1,68E-04	2,93E-04	1,01E-04
25,9929	C_2H^- (Wagner *et al*., 2001)	1,76E-05	2,37E-05	2,05E-05	1,91E-05	2,06E-05
26.995	CN^- (peptide backbone) (Wagner *et al*., 2001)	1,49E-04	2,29E-04	2,01E-04	1,80E-04	2,01E-04
27,9917	$C_2H_3^+$ (Wagner et al 2002) (Mahlstedt *et al*., 2009)	9,01E-05	7,06E-05	5,88E-05	7,59E-05	5,88E-05
29,0254	C_2H_5 (Mahlstedt *et al*., 2009)	6,10E-04	1,08E-04	2,77E-04	6,83E-04	2,76E-04
30,0112	CH_4N^+: Glycine (Wagner *et al*.,2001).	9,10E-05	1,33E-05	3,09E-05	8,03E-05	3,05E-05
37,9999	No assignment identified	2,53E-05	1,39E-03	3,41E-05	2,13E-05	9,95E-06
39,7221	$C_3H_3^+$ (Wagner *et al*., 2002)	9,61E-05	2,06E-03	2,17E-04	1,08E-04	5,03E-04
40,0167	No assignment identified	2,37E-04	9,80E-05	1,20E-03	2,42E-04	1,49E-04
40,9458	No assignment identified	7,80E-05	9,62E-05	3,19E-04	9,13E-05	1,40E-04
41,0139	$C_3H_5^+$ (Wagner *et al*., 2002) (Mahlstedt *et al*.,	1,69E-03	1,57E-03	1,79E-03	2,23E-03	1,75E-03

	2009)					
41,7003	$C_3H_5^+$ (Wagner *et al.*, 2002)	2,19E-04	3,36E-04	4,21E-04	3,14E-04	4,40E-04
41,9932	$C_3H_5^+$ (Wagner *et al.*, 2002)	5,37E-04	3,31E-04	1,22E-03	4,97E-04	2,86E-04
42,9994	CNO^-: peptide backbone (Wagner *et al.*, 2001)	2,99E-03	1,52E-03	8,91E-04	2,65E-03	8,58E-04
43,0241	$CH_3N_2^+$ (Argenine: laminin (Wagner *et al.*, 2002) .	1,11E-02	2,79E-03	4,00E-03	1,02E-02	3,98E-03
43,0421	C_2H_5N (Hazen *et al.*, 2006)	2,32E-03	5,62E-04	6,19E-04	2,42E-03	6,15E-04
44,0371	$C_2H_6N^+$ (Wagner *et al.*, 2002)	1,50E-03	7,58E-05	1,01E-04	1,43E-03	1,01E-04
54,9998	No assignment identified	3,65E-04	3,55E-04	3,48E-04	4,29E-04	3,24E-04
55,0208	$C_4H_7^+$ (Wagner *et al.*, 2002)	9,42E-03	2,47E-03	5,85E-03	1,04E-02	5,81E-03
56,0233	$C_3H_6N^+$ (Wagner *et al.*, 2002)	1,40E-03	1,88E-04	4,26E-04	1,43E-03	4,29E-04
56,6144	$C_3H_6N^+$ (Wagner *et al.*, 2002)	1,62E-04	1,30E-04	2,17E-04	1,99E-04	2,71E-03
58,0392	C_2H_4NO: Glycine; collagen (Cannnan *et al.*, 2007)	5,62E-04	2,89E-04	1,64E-04	5,58E-04	1,68E-04
59,0118	$C_3H_7O^+$ (Wagner *et al.*, 2002)	3,09E-04	6,82E-05	6,69E-05	2,66E-04	7,25E-05

59,0496	CH_5N_3: Arginine; laminin (Cannnan et al., 2007)	1,06E-02	1,57E-03	1,03E-03	8,42E-03	1,05E-03
68,0263	$C_4H_6N^+$ (Wagner et al., 2002)	1,23E-03	1,88E-04	4,85E-04	1,25E-03	4,56E-04
69,0374	C_4H_5O: threonine; fibronectin (Cannnan et al., 2007)	2,92E-03	4,80E-04	1,03E-03	2,98E-03	1,05E-03
70,0375	$C_4H_8N^+$ (Wagner et al., 2002)	1,54E-03	1,65E-04	2,71E-04	1,47E-03	2,74E-04
78,0441	$C_6H_6^+$ Toporski et al., 2002	1,07E-03	7,48E-04	6,90E-04	1,56E-03	7,28E-04
87,9004	$C_4H_9O_2^+$ Cheng et al., 2008	1,31E-04	1,60E-05	1,42E-04	7,73E-05	2,70E-04
96,8582	SO_4^- (Alexander & Jones et $al.,$ 1995)	2,62E-05	3,52E-04	1,66E-05	2,42E-05	3,86E-05
98,1067	$C_4H_4NO_2^+$: asparagine (Wagner et al., 2001)	3,64E-04	1,09E-04	1,41E-04	4,48E-04	5,61E-04
103,9236	No assignment identified	1,77E-04	1,11E-04	4,11E-04	1,30E-04	1,46E-04
124,9131	$C_8H_9NO^4$ (125 m/z) (Mahlstedt et al., 2009)	7,25E-04	1,48E-04	1,54E-04	3,42E-04	4,98E-05
164.857	$C_{13}H_9^+$ (165 m/z) (Delcorte et al., 1997)	1,85E-04	7,37E-05	9,65E-05	1,79E-04	6,66E-05
180,0851	No assignment identified	1,19E-04	5,62E-05	7,40E-05	1,71E-04	4,13E-05

Table A6 Normalised intensity values of negative ion amino acid fragments identified by Tof-SIMS on PCL electrospun nanofibrous substrates, in both aligned (280 ± 122 nm) and random (318 ± 151 nm) conformations when incubated in pure collagen I protein solution.

m/z	Potential Assignment	CM+ CTL	CM+ A (280 nm)	CM+ A (521 nm)	CM+ R (318nm)	CM+R (660 nm)
13.0086	No assignment identified	1,06E-02	1,01E-02	1,33E-02	1,30E-02	9,75E-03
15.9954	No assignment identified	1,59E-02	1,12E-02	8,24E-03	1,52E-02	1,13E-02
17.0034	No assignment identified	1,47E-02	1,17E-02	1,01E-02	1,38E-02	1,27E-02
25.0094	CN^- (m/z of 26) peptide backbone (Wagner *et al*., 2001)	2,24E-06	2,36E-06	3,10E-06	3,04E-06	2,14E-06
34.9712	SH^- (m/z of 33) cysteine (Wagner *et al*., 2001)	1,40E-02	1,14E-02	8,17E-03	1,37E-02	1,35E-02
41.0453	$C_3H_5^+$ (m/z of 41) (Wagner *et al*., 2002)	7,32E-04	7,74E-04	1,03E-03	9,94E-04	9,63E-04
43.0017	CH_3N_2 (m/z of 43.0296) Glycine most prevalent in coll (Canavan *et al*., 2007)	4,34E-03	3,19E-03	2,59E-03	3,00E-03	1,85E-03
59.9676	C_2H_6NO (m/z of 60.0449) L-serine most prevalent in Fn (Canavan *et al*., 2007)	1,50E-03	9,70E-04	9,62E-04	1,58E-03	6,15E-04
60.9755	C_2H_5S (m/z of 61.011) methionine most prevalent in Coll (Canavan *et al*., 2007)	1,56E-03	1,05E-03	1,08E-03	1,58E-03	4,87E-04
62.9658	No assignment identified	2,74E-02	3,36E-02	1,42E-02	1,18E-02	4,89E-03

74.9971	C_3H_8NO (m/z of 74.061) threonine most prevalent in Fn (Canavan *et al*., 2007)	8,43E-03	1,12E-02	1,18E-02	8,95E-03	1,19E-02
75.9611	C_2H_6NS (76.022) cysteine most prevalent in Fn (Canavan *et al*., 2007)	7,68E-04	3,48E-04	2,60E-04	3,98E-04	9,49E-05
76.9699	$C_2H_6NS^+$ (m/z of 76) cysteine (Wagner *et al*., 2001)	4,36E-03	2,26E-03	2,16E-03	2,84E-03	8,26E-04
78.9615	No assignment identified	7,17E-02	8,21E-02	4,50E-02	3,58E-02	1,55E-02
79.9609	No assignment identified	4,92E-03	4,81E-03	5,44E-03	5,62E-03	2,30E-03
83.9729	C_4H_6NO (m/z of 84.0449) glutamine; most prevalent in Fn (Canavan *et al*., 2007)	5,97E-03	6,63E-03	5,73E-03	5,78E-03	1,08E-02
90.9943	No assignment identified	7,68E-03	9,74E-03	1,04E-02	6,60E-03	8,58E-03
90.9992	$C_7H_7^+$ (m/z of 91) (Wagner *et al*., 2002)	7,84E-03	9,92E-03	1,07E-02	6,81E-03	8,97E-03
92.944	No assignment identified	3,80E-03	2,96E-03	1,99E-03	3,31E-03	5,28E-03

99.9847	$C_4H_{10}N_3$(m/z of 100.0875) arginine; most prevalent in Ln (Canavan *et al*., 2007)	2,97E-03	5,98E-03	2,71E-03	2,14E-03	1,31E-03
127.9609	$C_5H_{11}N_4$ (m/z of 127.0984) arginine; most prevalent in Ln (Canavan *et al*., 2007)	3,60E-04	4,52E-04	4,59E-04	3,91E-04	6,17E-04
136.9337	$C_8H_{10}NO$ (m/z of 136.076) tyrosine; most prevalent in Fn (Canavan *et al*., 2007)	9,58E-04	2,27E-03	6,63E-04	6,96E-04	3,26E-04
164.9226	No assignment identified	1,44E-03	3,19E-03	8,48E-04	9,25E-04	2,51E-04
180.904	No assignment identified	1,06E-02	1,01E-02	1,33E-02	1,30E-02	9,75E-03

Table A7 Normalised intensity values of negative ion amino acid fragments identified by Tof-SIMS on PCL electrospun nanofibrous substrates, in both aligned (280 ± 122 nm) and random (318 ± 151 nm) conformations when incubated in pure collagen I protein solution.

m/z	Potential Assignment	Coll I CTL	Coll I +A (280nm)	Coll I +A (521nm)	Coll I +R (318nm)	Coll I +R (660nm)
13.0086	No assignment identified	1,29E-02	1,50E-02	3,35E-02	1,29E-02	2,16E-02
15.9954	No assignment identified	2,27E-02	1,88E-02	4,61E-02	1,03E-02	1,82E-02
17.0034	No assignment identified	1,84E-02	1,87E-02	6,35E-02	1,33E-02	1,90E-02
25.0094	CN^-(26) peptide backbone (Wagner *et al*., 2001)	2,27E-06	2,48E-06	7,57E-06	2,98E-06	2,67E-06
34.9712	SH^- (33) cysteine (Wagner *et al*., 2001)	2,01E-02	1,64E-02	4,58E-03	1,47E-02	6,55E-03
41.0453	$C_3H_5^+$ (41) (Wagner *et al*., 2002)	6,32E-04	6,79E-04	4,71E-04	7,64E-04	1,13E-03
43.0017	CH_3N_2 (43.0296) Glycine most prevalent in coll (Canavan *et al*., 2007)	3,15E-03	2,25E-03	1,56E-02	2,31E-03	1,96E-03
59.9676	C_2H_6NO (60.0449) L-serine most prevalent in Fn (Canavan *et al*., 2007)	1,80E-03	2,14E-03	1,51E-02	1,36E-03	1,34E-03

60.9755	C_2H_5S (61.011) methionine most prevalent in Coll (Canavan *et al.*, 2007)	1,99E-03	2,26E-03	1,26E-02	1,41E-03	1,72E-03
62.9658	No assignment identified	9,09E-03	1,53E-02	1,31E-03	3,19E-02	1,60E-03
74.9971	C_3H_8NO (74.061) threonine most prevalent in Fn (Canavan *et al.*, 2007)	4,54E-03	5,64E-03	3,10E-03	1,15E-02	1,37E-03
75.9611	C_2H_6NS (76.022) cysteine most prevalent in Fn (Canavan *et al.*, 2007)	7,90E-04	9,16E-04	1,22E-02	5,93E-04	4,44E-04
76.9699	$C_2H_6NS^+$ (76) cysteine (Wagner *et al.*, 2001)	5,43E-03	5,95E-03	3,78E-02	3,38E-03	4,34E-03
78.9615	No assignment identified	2,15E-02	4,44E-02	2,94E-03	9,30E-02	6,33E-03
79.9609	No assignment identified	5,59E-03	1,45E-02	1,81E-03	7,59E-03	4,53E-03

83.9729	C_4H_6NO (84.0449) glutamine; most prevalent in Fn (Canavan *et al.*, 2007)	3,82E-03	3,97E-03	3,31E-04	8,67E-03	2,80E-04
90.9943	No assignment identified	3,27E-03	3,56E-03	1,95E-04	9,27E-03	2,43E-04
90.9992	$C_7H_7^+$ (91) (Wagner *et al.*, 2002)	3,35E-03	3,68E-03	2,76E-04	9,47E-03	3,06E-04
92.944	No assignment identified	2,33E-03	3,72E-03	1,37E-04	4,81E-03	9,94E-05
99.9847	$C_4H_{10}N_3$(100.0875) arginine; most prevalent in Ln (Canavan *et al.*, 2007)	1,10E-03	1,28E-03	1,69E-04	4,33E-03	1,29E-04
127.9609	$C_5H_{11}N_4$ (127.0984) arginine; most prevalent in Ln (Canavan *et al.*, 2007)	2,25E-04	2,17E-04	2,10E-04	2,63E-04	2,24E-04
136.9337	$C_8H_{10}NO$ (136.076) tyrosine; most prevalent in Fn (Canavan *et al.*, 2007)	6,56E-04	5,93E-04	3,28E-04	2,31E-03	2,32E-04

| 164.9226 | No assignment identified | 1,20E-03 | 1,07E-03 | 8,43E-04 | 3,71E-03 | 3,57E-04 |
| 180.904 | No assignment identified | 1,29E-02 | 1,50E-02 | 3,35E-02 | 1,29E-02 | 2,16E-02 |

Table A8 Normalised intensity values of negative ion amino acid fragments identified by Tof-SIMS on PCL electrospun nanofibrous substrates, in both aligned (280 ± 122 nm) and random (318 ± 151 nm) conformations when incubated in pure fibronectin protein solution.

m/z	Potential Assignment	Fn CTL	Fn +A (280nm)	Fn +A (521nm)	Fn +R (318nm)	Fn +R (660nm)
13.0086	No assignment identified	7,64E-03	9,27E-03	1,58E-02	1,08E-02	1,43E-02
15.9954	No assignment identified	1,46E-02	1,10E-02	7,89E-03	9,56E-03	1,89E-02
17.0034	No assignment identified	1,23E-02	1,14E-02	9,76E-03	1,14E-02	1,66E-02
25.0094	CN^- (26) peptide backbone (Wagner *et al*., 2001)	1,90E-06	2,43E-06	5,81E-06	3,32E-06	2,33E-06
34.9712	SH^- (33) cysteine (Wagner *et al*., 2001)	1,83E-02	1,32E-02	1,12E-02	1,22E-02	1,78E-02
41.0453	$C_3H_5^+$ (41) (Wagner *et al*., 2002)	6,58E-04	7,45E-04	1,19E-03	7,78E-04	8,97E-04
43.0017	CH_3N_2 (43.0296) Glycine most prevalent in coll (Canavan *et al*., 2007)	2,80E-03	2,64E-03	2,22E-03	2,17E-03	2,61E-03
59.9676	C_2H_6NO (60.0449) L-serine most prevalent in Fn (Canavan *et al*., 2007)	8,31E-04	9,34E-04	1,67E-03	9,28E-04	1,12E-03
60.9755	C_2H_5S (61.011) methionine most prevalent in Coll (Canavan *et al*., 2007)	8,22E-04	9,05E-04	1,86E-03	9,24E-04	1,11E-03

62.9658	No assignment identified	2,82E-02	2,51E-02	6,73E-03	3,03E-02	5,14E-03
74.9971	C_3H_8NO (74.061) threonine most prevalent in Fn (Canavan *et al*., 2007)	1,07E-02	1,26E-02	9,77E-03	1,10E-02	7,54E-03
75.9611	C_2H_6NS (76.022) cysteine most prevalent in Fn (Canavan *et al*., 2007)	2,68E-04	3,22E-04	3,36E-04	3,11E-04	4,30E-04
76.9699	$C_2H_6NS^+$ (76) cysteine (Wagner *et al*., 2001)	1,79E-03	1,87E-03	2,81E-03	1,86E-03	2,58E-03
78.9615	No assignment identified	7,66E-02	7,77E-02	1,32E-02	8,30E-02	1,42E-02
79.9609	No assignment identified	2,91E-03	4,72E-03	6,40E-03	5,43E-03	2,67E-03
83.9729	C_4H_6NO (84.0449) glutamine; most prevalent in Fn (Canavan *et al*., 2007)	1,15E-02	1,00E-02	5,93E-03	8,29E-03	7,62E-03
90.9943	No assignment identified	9,50E-03	1,13E-02	6,43E-03	9,48E-03	6,53E-03
90.9992	$C_7H_7^+$ (91) (Wagner *et al*., 2002)	9,70E-03	1,15E-02	6,67E-03	9,72E-03	6,71E-03
92.944	No assignment identified	7,79E-03	4,59E-03	2,37E-03	4,34E-03	4,34E-03
99.9847	$C_4H_{10}N_3$(100.0875) arginine; most prevalent	7,17E-03	5,76E-03	1,15E-03	5,81E-03	1,46E-03

	in Ln (Canavan *et al.*, 2007)					
127.9609	$C_5H_{11}N_4$ (127.0984) arginine; most prevalent in Ln (Canavan *et al.*, 2007)	2,81E-04	2,73E-04	2,51E-04	2,64E-04	2,74E-04
136.9337	$C_8H_{10}NO$ (136.076) tyrosine; most prevalent in Fn (Canavan *et al.*, 2007)	3,15E-03	2,19E-03	5,96E-04	2,86E-03	5,86E-04
164.9226	No assignment identified	4,57E-03	3,19E-03	7,07E-04	4,01E-03	8,09E-04
180.904	No assignment identified	7,64E-03	9,27E-03	1,58E-02	1,08E-02	1,43E-02

Table A9 Normalised intensity values of negative ion amino acid fragments identified by Tof-SIMS on PCL electrospun nanofibrous substrates, in both aligned (280 ± 122 nm) and random (318 ± 151 nm) conformations when incubated in pure laminin protein solution.

m/z	Potential Assignment	Ln CTL	Ln +A (280nm)	Ln +A (521nm)	Ln +R (318nm)	Ln +R (660nm)
13.0086	No assignment identified	8,45E-03	9,05E-03	1,15E-02	8,90E-03	9,86E-03
15.9954	No assignment identified	1,38E-02	1,01E-02	7,90E-03	1,10E-02	9,62E-03
17.0034	No assignment identified	1,30E-02	1,05E-02	9,21E-03	1,03E-02	9,71E-03
25.0094	CN^- (26) peptide backbone (Wagner *et al*., 2001)	1,82E-06	2,53E-06	2,56E-06	2,09E-06	2,10E-06
34.9712	SH^- (33) cysteine (Wagner *et al*., 2001)	1,82E-02	1,35E-02	1,42E-02	1,10E-02	1,52E-02
41.0453	$C_3H_5^+$ (41) (Wagner *et al*., 2002)	6,71E-04	7,84E-04	9,22E-04	8,13E-04	8,33E-04
43.0017	CH_3N_2 (43.0296) Glycine most prevalent in coll (Canavan *et al*., 2007)	2,26E-03	2,15E-03	1,93E-03	1,86E-03	2,08E-03
59.9676	C_2H_6NO (60.0449) L-serine most prevalent in Fn (Canavan *et al*., 2007)	7,10E-04	8,69E-04	7,47E-04	5,62E-04	7,82E-04
60.9755	C_2H_5S (61.011) methionine most prevalent in Coll (Canavan *et al*., 2007)	7,20E-04	8,12E-04	6,31E-04	4,85E-04	6,93E-04
62.9658	No assignment identified	4,29E-02	1,99E-02	6,38E-03	7,88E-03	6,48E-03

74.9971	C_3H_8NO (74.061) threonine most prevalent in Fn (Canavan *et al.*, 2007)	1,09E-02	1,50E-02	1,35E-02	1,42E-02	1,17E-02
75.9611	C_2H_6NS (76.022) cysteine most prevalent in Fn (Canavan *et al.*, 2007)	1,62E-04	2,21E-04	1,12E-04	9,18E-05	1,14E-04
76.9699	$C_2H_6NS^+$ (76) cysteine (Wagner *et al.*, 2001)	1,02E-03	1,24E-03	7,41E-04	5,84E-04	8,03E-04
78.9615	No assignment identified	7,41E-02	6,48E-02	2,01E-02	2,85E-02	2,17E-02
79.9609	No assignment identified	3,45E-03	4,80E-03	5,35E-03	3,62E-03	5,76E-03
83.9729	C_4H_6NO (84.0449) glutamine; most prevalent in Fn (Canavan *et al.*, 2007)	1,03E-02	1,19E-02	1,23E-02	1,04E-02	1,06E-02
90.9943	No assignment identified	1,01E-02	1,40E-02	1,23E-02	1,34E-02	1,04E-02
90.9992	$C_7H_7^+$ (91) (Wagner *et al.*, 2002)	1,03E-02	1,43E-02	1,26E-02	1,37E-02	1,07E-02
92.944	No assignment identified	8,41E-03	5,08E-03	5,62E-03	3,88E-03	5,36E-03
99.9847	$C_4H_{10}N_3$(100.0875) arginine; most prevalent in Ln (Canavan *et al.*, 2007)	9,57E-03	6,25E-03	2,22E-03	3,63E-03	2,68E-03
127.9609	$C_5H_{11}N_4$ (127.0984) arginine; most prevalent in Ln (Canavan *et al.*, 2007)	2,83E-04	3,45E-04	3,47E-04	3,48E-04	3,14E-04

136.9337	$C_8H_{10}NO$ (136.076) tyrosine; most prevalent in Fn (Canavan *et al.*, 2007)	5,20E-03	2,28E-03	5,82E-04	8,74E-04	8,28E-04
164.9226	No assignment identified	7,93E-03	2,91E-03	6,13E-04	1,03E-03	9,64E-04
180.904	No assignment identified	8,45E-03	9,05E-03	1,15E-02	8,90E-03	9,86E-03

Table A10 Normalised intensity values of negative ion amino acid fragments identified by Tof-SIMS on PCL electrospun nanofibrous substrates, in both aligned (280 ± 122 nm) and random (318 ± 151 nm) conformations when incubated in pure vitronectin protein solution.

m/z	Potential Assignment	Vn CTL	Vn +A (280nm)	Vn +A (521nm)	Vn +R (318nm)	Vn +R (660nm)
13.0086	No assignment identified	1,02E-02	2,50E-02	1,29E-02	1,39E-02	2,28E-02
15.9954	No assignment identified	1,76E-02	3,05E-02	8,97E-03	1,62E-02	3,13E-02
17.0034	No assignment identified	1,31E-02	3,79E-02	1,02E-02	1,29E-02	3,71E-02
25.0094	CN^- (26) peptide backbone (Wagner *et al.*, 2001)	2,69E-06	9,60E-06	4,77E-06	3,70E-06	6,05E-06
34.9712	SH^- (33) cysteine (Wagner *et al.*, 2001)	7,70E-03	9,34E-03	8,65E-03	9,67E-03	1,29E-02
41.0453	$C_3H_5^+$ (41) (Wagner *et al.*, 2002)	6,40E-04	1,11E-03	9,94E-04	8,34E-04	1,46E-03
43.0017	CH_3N_2 (43.0296) Glycine most prevalent in coll (Canavan *et al.*, 2007)	3,53E-03	1,06E-02	2,72E-03	2,72E-03	8,72E-03
59.9676	C_2H_6NO (60.0449) L-serine most prevalent in Fn (Canavan *et al.*, 2007)	2,54E-03	9,81E-03	1,76E-03	2,37E-03	7,98E-03
60.9755	C_2H_5S (61.011) methionine most prevalent in Coll (Canavan *et al.*, 2007)	2,26E-03	8,25E-03	1,86E-03	2,13E-03	6,54E-03
62.9658	No assignment identified	1,38E-02	9,00E-04	3,93E-03	8,70E-03	1,12E-03

74.9971	C$_3$H$_8$NO (74.061) threonine most prevalent in Fn (Canavan *et al*., 2007)	1,05E-02	4,89E-03	9,71E-03	9,76E-03	3,08E-03
75.9611	C$_2$H$_6$NS (76.022) cysteine most prevalent in Fn (Canavan *et al*., 2007)	6,15E-04	7,85E-03	3,59E-04	2,87E-04	6,86E-03
76.9699	C$_2$H$_6$NS$^+$ (76) cysteine (Wagner *et al*., 2001)	3,33E-03	2,36E-02	2,56E-03	2,05E-03	1,99E-02
78.9615	No assignment identified	4,26E-02	2,35E-03	7,11E-03	2,21E-02	2,94E-03
79.9609	No assignment identified	1,84E-02	9,80E-03	2,02E-02	1,75E-02	1,36E-02
83.9729	C$_4$H$_6$NO (84.0449) glutamine; most prevalent in Fn (Canavan *et al*., 2007)	3,30E-03	3,62E-04	4,41E-03	3,66E-03	5,00E-04
90.9943	No assignment identified	6,34E-03	3,36E-04	6,35E-03	5,28E-03	3,47E-04
90.9992	C$_7$H$_7^+$ (91) (Wagner *et al*., 2002)	6,51E-03	4,78E-04	6,55E-03	5,47E-03	4,39E-04
92.944	No assignment identified	1,26E-03	3,13E-04	1,20E-03	1,57E-03	4,10E-04
99.9847	C$_4$H$_{10}$N$_3$(100.0875) arginine; most prevalent in Ln (Canavan *et al*., 2007)	1,68E-03	1,37E-04	4,95E-04	9,13E-04	1,64E-04
127.9609	C$_5$H$_{11}$N$_4$ (127.0984) arginine; most prevalent in Ln (Canavan *et al*., 2007)	3,06E-04	3,03E-04	4,08E-04	3,29E-04	3,50E-04

136.9337	C$_8$H$_{10}$NO (136.076) tyrosine; most prevalent in Fn (Canavan *et al*., 2007)	7,95E-04	4,71E-04	4,66E-04	4,68E-04	4,33E-04
164.9226	No assignment identified	9,05E-04	8,81E-04	3,96E-04	4,96E-04	7,99E-04
180.904	No assignment identified	1,02E-02	2,50E-02	1,29E-02	1,39E-02	2,28E-02